

UNIVERSITÄT
BAYREUTH

Faculty of Biology, Chemistry and Geosciences

Department of Organic Chemistry I.

advised by Prof. Rainer Schobert

**Biochemical studies of targeted and bimodal
analogues of the natural anticancer compounds
combretastatin A-4 and illudin M**

Miroslava Zoldakova

*A thesis submitted in fulfillment
of the requirements for the degree of
Rerum Naturalis Doctor*

Bayreuth, 2011

Die vorliegende Arbeit wurde in der Zeit von August 2006 bis März 2011 am Lehrstuhl für Organische Chemie der Universität Bayreuth unter der Betreuung von Herrn Prof. Dr. R. Schobert angefertigt.

Vollständiger Abdruck der von der Fakultät für Biologie, Chemie und Geowissenschaften der Universität Bayreuth genehmigten Dissertation zur Erlangung des akademischen Grades Doktor der Naturwissenschaften (Dr. rer. nat.).

Amtierender Dekan:

Prof. Dr. Stephan Clemens

Tag des Einreichens der Dissertation: 28. 03. 2011

Tag des wissenschaftlichen Kolloquiums: 04. 07. 2011

Prüfungsausschuß:

Prof. Dr. Rainer Schobert (Erstgutachter)

Dr. Emília Madarász (Zweitgutachter)

Prof. Dr. Franz X. Schmid (Vorsitzender)

Prof. Dr. Olaf Stemmann

Erklärung

Hiermit erkläre ich, dass ich die Arbeit selbständig verfasst und keine anderen als die von mir erklärte Quellen und Hilfsmittel benutzt habe.

Ferner erkläre ich, dass ich anderweitig mit oder ohne Erfolg nicht versucht habe, diese Dissertation einzureichen. Ich habe keine gleichartige Doktorprüfung an einer anderen Hochschule endgültig nicht bestanden.

Bayreuth, 28.03.2011

.....
Miroslava Zoldakova

For Gabriel

Acknowledgment

This work has been carried out in the Laboratory of Organic Chemistry, University of Bayreuth, Bayreuth, Germany.

I would like to thank Prof. Dr. Rainer Schobert for giving me this great opportunity.

His encouragement, valuable advice, constructive comments and suggestions have all been of inestimable value for the presentation of this thesis in its present form. My time in his group was spent under a discretionary trust that I could perform many new techniques, and I have learned to solve many types of problems – work-related, administrative and personal. I am especially grateful to Dr. Bernhard Biersack for his precision and patience during my study, for very carefully reading my thesis, and for his great help with the writing and editing of our manuscripts.



My special thanks belong to Silvia Kastner for showing good will and helping me fight with all the bureaucracy. Thank you!

I am indebted to Dr. Emília Madarász DrSc. (Budapest, Hungary) for introducing me to the world of neural science, which turned into fascinating work. I



am grateful for her support and trust during my short-time fellowship (two months). I always admired her scientific enthusiasm, which was so inspirational for me during that time in her laboratory. I would also like to thank her for help with authorship of our manuscript. In her laboratory, all of the members were excellent co-workers and I was especially very happy to work with Dr. Zsuzsanna Környei, who introduced me to neuron isolation and helped me plan many crucial experiments.

I would like to thank Prof. Dr. Viktor Brabec (Brno, Czech Republic). He is one of the foremost specialists in the field of platinum antitumor drugs and the



biophysical chemistry of DNA. I am grateful he accepted me in his laboratory for a short, four months fellowship. I would also like to thank him for his help with authoring our manuscript. I would also like to thank all members of his group for their valuable advice and support. I am especially indebted to Prof. Dr. Jana Kašpárková, Dr. Olga Nováková, and Dr. Hana Kostrhúnová, who were always present to help me solve all kinds of

problems and discuss the results. This work was supported by a scholarship for the advancement of women by the University of Bayreuth (01.09. - 31.12.2010).



My special thanks belong to Dr. Stefan Geimer for granting all access to electron microscope and expert help as well as his students, Dirk Scholz (for special assistance) and Melina Fischer (for taking several pictures of my samples).

I would like to thank Prof. Dr. Olaf Stemmann for granting my access to flow cytometer and his PhD-student Andreas Brown for excellent help with the cell cycle and western-blot analysis.



I want to thank all my *colleagues* with whom it was a pleasure to share a laboratory, and all my *students* with whom together we solved professional and personal challenges. Our works are listed in Chapter 8 under the name “Zoldakova” for simplicity.

I will never forget the prayers of my *parents and family* back home, which have been a constant source of encouragement throughout my life. Special thanks are due to them as well. There are a number of *people who have helped me* during the course of my research; however, it is impossible to mention them all here. I hope that they accept my *sincere thanks and appreciation*.

My greatest debt of gratitude and appreciation is to my husband Gabriel, whose help, courage and support made my achievement possible. I appreciate his forbearance and patience during the course of my research and for his very precise reading of my thesis. The support I received from him has made my life easier and happier; I cannot imagine my life without him.



Table of Contents

Introduction	1.1-1
1.1 Novel chemotherapeutic drugs based on scaffolds designed by nature	1.1-1
1.1.1 Combretastatin A-4 analogue – chalcone (1)	1.1-2
1.1.2 Natural alkylation agent - illudin M (4).....	1.1-3
1.1.3 Activity of all trans retinoic acid	1.1-4
1.2 Drugs uptake and efflux	1.2-5
1.3 Cisplatin and chemoresistance	1.3-8
1.4 The aim of this study	1.4-11
Material and Methods	2.1-12
2.1 Materials	2.1-12
2.1.1 Instruments	2.1-12
2.1.2 Chemicals	2.1-12
2.1.3 Solutions and buffers	2.1-13
2.1.4 Cell cultures	2.1-16
2.1.5 Cell counting using Neubauer chamber.....	2.1-17
2.2 Methods	2.2-18
2.3 Cytotoxicity - MTT assay	2.3-18
2.4 Cellular drug uptake	2.4-20
2.4.1 Temperature effect.....	2.4-20
2.4.2 ICP-MS measurement of Pt-content	2.4-21
2.4.3 Western blot analysis	2.4-21
2.5 Sub-cellular microscopy methods	2.5-21
2.5.1 Time-lapse microscopy	2.5-21
2.5.2 Immunocytochemistry	2.5-22
2.5.3 ELISA - <i>In situ</i> detection of neural β -tubulin level	2.5-22
2.5.4 Microscopic observations of the cells by Giemsa staining	2.5-22
2.5.5 Transmission electron microscopy	2.5-23
2.6 Apoptosis - DNA degradation	2.6-24
2.6.1 Alkaline single cell gel electrophoresis	2.6-24
2.6.2 Cell cycle analysis	2.6-25
2.6.3 DNA fragmentation	2.6-26
2.7 Interaction of complex with DNA in vitro	2.7-27
2.7.1 Electrophoretic mobility shift assay with native agarose gel	2.7-27
2.7.2 Circular dichroism - secondary structure of DNA-complex.....	2.7-27
2.7.3 Melting temperature of DNA-complex adducts	2.7-28
2.7.4 Mono- and bifunctional adduct study	2.7-28
2.7.5 Radioactive 3'-ends labelling of plasmid DNA.....	2.7-28
2.7.6 Interstrand cross-links study in denatured agarose gel	2.7-29
2.7.7 Inhibition of RNA synthesis	2.7-30
2.7.8 Measurement of DNA-Pt content	2.7-31
2.8 Apoptotic signals	2.8-32
2.8.1 Colorimetric caspase assay	2.8-32
2.8.2 Intracellular concentration of Ca^{2+}	2.8-33
2.9 Drug resistance	2.9-33
2.9.1 Activity of P-gp transporters in KBv1 cells - calcein assay	2.9-33
2.9.2 Activity of BCRP transporters in MCF-7 cells - mitoxantrone assay	2.9-34
2.9.3 Repair DNA synthesis by human cell extracts	2.9-34
2.9.4 Reaction of Pt-complex with glutathione	2.9-35
Results and Discussion	
Effects of chalcone (1)	3.1-36
3.1 Inhibition of cell growth - MTT assay	3.1-36

Table of Contents

3.1.1 Neural cells	3.1-36
3.1.2 Cancer cells expressing ABC-transporters	3.1-38
3.1.3 518A2 melanoma and HL60 leukemia cells	3.1-39
3.2 Cellular uptake of chalcone (1)	3.2-40
3.2.1 Inhibition of endocytosis by temperature change	3.2-40
3.2.2 Inhibition of the uptake of chalcone (1) with specific inhibitors	3.2-40
3.3 Cellular and sub-cellular observations	3.3-43
3.3.1 Inhibition of drug uptake monitored <i>via</i> time-lapse recording	3.3-43
3.3.2 Altered cell shapes in cells treated with chalcone (1)	3.3-43
3.3.3 Actin re-distribution induced by chalcone (1)	3.3-49
3.3.4 Microscopic observations of 518A2 cells by Giemsa staining	3.3-51
3.3.5 Transmission electron microscopy	3.3-53
3.4 DNA degradation of chalcone (1) during apoptosis	3.4-55
3.4.1 Cell cycle analysis	3.4-55
3.4.2 DNA fragmentation from isolated cells	3.4-56
3.5 Characterization of DNA-chalcone interactions	3.5-57
3.5.1 Electrophoretic mobility shift assay of plasmid DNA	3.5-58
3.5.2 Secondary structure study of DNA-chalcone (1) interactions	3.5-58
3.5.3 Melting temperatures of DNA-chalcone (1) adducts	3.5-60
3.6 Activation of caspases after chalcone (1)	3.6-61
3.7 Interference with ABC transporters	3.7-61
3.7.1 Chalcone (1) efflux <i>via</i> P-glycoproteins	3.7-62
3.7.2 Chalcone (1) efflux <i>via</i> BCRP proteins	3.7-63
3.8 Conclusion	3.8-64
Effects of chalcone-Pt (2)	4.1-65
4.1 Inhibition of cell growth - MTT assay	4.1-65
4.1.1 Neural cells	4.1-65
4.1.2 Tumor cells expressing ABC-transporters	4.1-66
4.1.3 Cancer cells	4.1-66
4.2 Cellular uptake of chalcone-Pt (2)	4.2-68
4.2.1 Inhibition of endocytosis by temperature change	4.2-68
4.2.2 Inhibition of drug uptake with specific inhibitors	4.2-69
4.2.3 Western blot analysis of OCT1/2 in melanoma 518A2 cells	4.2-70
4.2.4 Platinum contents of 518A2 cells treated with 2 (<i>via</i> ICP-MS)	4.2-71
4.3 Cellular and sub-cellular observations	4.3-72
4.3.1 Inhibition of drug uptake monitored by time-lapse microscopy	4.3-72
4.3.2 Altered cell shapes of cells treated with chalcone-Pt (2)	4.3-73
4.3.3 Actin distribution induced by chalcone-Pt (2)	4.3-74
4.3.4 Microscopic observations of 518A2 cells by Giemsa staining	4.3-75
4.3.5 Transmission electron microscopy	4.3-77
4.4 Activation of caspase-3 after chalcone-Pt (2) treatment	4.4-80
4.5 The role of DNA degradation during apoptosis	4.5-80
4.5.1 Effects of conjugate 2 on chromosomal DNA	4.5-80
4.5.2 Cell cycle analysis	4.5-81
4.6 DNA interaction with conjugate 2	4.6-83
4.6.1 Electrophoretic mobility shift assay of plasmid DNA	4.6-83
4.6.2 Kinetic of DNA binding by chalcone-Pt (2)	4.6-84
4.6.3 DNA secondary structure changes	4.6-85
4.6.4 Melting temperatures of DNA-chalcone-Pt (2) adducts	4.6-86
4.7 Drug resistance	4.7-86
4.7.1 Interference with ABC transporters	4.7-86
4.7.2 Interaction of chalcone-Pt (2) with glutathione	4.7-88
4.8 Conclusion	4.8-90

Effects of chalcone-DAP-Pt (3)	5.1-91
5.1 Inhibition of cell growth - MTT assay	5.1-91
5.1.1 Tumor cells expressing ABC-transporters.....	5.1-91
5.1.2 Cancer cells.....	5.1-92
5.2 Microscopic observations of 518A2 cells by Giemsa staining	5.2-93
5.3 DNA degradation of chalcone-DAP-Pt (3) during apoptosis.....	5.3-95
5.4 Characterization of DNA-chalcone-DAP-Pt interactions	5.4-96
5.4.1 Electrophoretic mobility shift assay of plasmid DNA.....	5.4-96
5.4.2 Kinetic of chalcone-DAP-Pt (3) DNA binding	5.4-97
5.4.3 Changes of the DNA secondary structure	5.4-97
5.4.4 Melting temperatures of DNA modified with complex (3)	5.4-98
5.4.5 Mono- or bi-functional character of DNA-(3) adducts.....	5.4-99
5.4.6 Interstrand-crosslink ability of chalcone-DAP-Pt (3)	5.4-102
5.4.7 Inhibition of RNA synthesis	5.4-103
5.5 Chalcone-DAP-Pt (3) resistance	5.5-104
5.5.1 Interference with ABC transporter	5.5-104
5.5.2 DNA repair	5.5-106
5.5.3 Reaction of chalcone-DAP-Pt (3) with glutathione.....	5.5-107
5.6 Conclusion	5.6-108
Effects of retinoic acid conjugate of illudin M (5).....	6.1-109
6.1 Inhibition of cell growth - MTT assay	6.1-109
6.1.1 Neural derived cell lines	6.1-109
6.1.2 Tumor cells expressing ABC-transporters.....	6.1-110
6.1.3 Cancer cells.....	6.1-111
6.2 Cellular and sub-cellular observations	6.2-112
6.2.1 Altered cell-shape in neural cells.....	6.2-112
6.2.2 Altered cell-shape in cancer cells	6.2-114
6.2.3 Microscopic observations of 518A2 cells by Giemsa staining.....	6.2-116
6.2.4 Immunostaining of β -tubulin in treated neurons	6.2-117
6.3 Single cell DNA damage monitoring by comet-assay	6.3-120
6.4 Intracellular calcium concentration	6.4-121
6.5 Interference with ABC transporters.....	6.5-122
6.5.1 Illudin efflux <i>via</i> P-glycoproteins	6.5-122
6.5.2 Illudin efflux <i>via</i> BCRP proteins	6.5-123
6.6 Conclusion	6.6-124
Summary.....	7.1-125
7.1 Chalcone (1) and its Pt-derivatives (2, 3).....	7.1-125
7.2 Illudin M (4) and its retinoate (5).....	7.2-126
Zusammenfassung	7.2-127
7.3 Chalkon (1) und seine Pt-Derivate (2, 3)	7.3-127
7.4 Illudin M (4) und sein Retinoat (5)	7.4-129
References	8-130
Publications and conference activities	9-144

Abbreviations

°C	degree Celsius
ABC transporter	ATP-binding cassette transporters
bp	base pair
Bq	Becquerel
BSA	bovine serum albumin
CFE	cell-free extract
chalcone (1)	(2E)-3-(3-hydroxy-4-methoxyphenyl)-1-(3,4,5-trimethoxyphenyl)prop-2-en-1-one; <i>m</i> -hydroxychalcone
chalcone-Pt (2)	
chalcone-DAP-Pt (3)	<i>cis</i> -{(E)-2-Methoxy-5-[3'-oxo-3'-(3,4,5-trimethoxyphenyl)prop-1'-enyl]phenyl(D,L)-(2,3)-diaminopropionate}dichloridoplatinum(II); chalconyl dichlorido(2,3-diaminopropionate)Pt(II)
cisplatin (CDDP)	<i>cis</i> -diamminedichloroplatinum(II)
CLs	cross-links
colchicine	(N- [(7 <i>S</i>)- 1, 2, 3, 10- tetramethoxy- 9- oxo- 5, 6, 7, 9-tetrahydrobenzo [<i>a</i>] heptalen- 7- yl] acetamide)
ctDNA	calf thymus DNA
Ctr1	Copper related transporter 1
CuCl ₂	Copper (II) chloride
DMS	dimethyl sulfate
DMF	N,N-dimethylformamid
DNase	Deoxyribonuclease I
DTT	dithiothreitol
EC ₅₀	half maximal effective concentration
EMSA	electrophoretic mobility shift assay
FAAS	flameless atomic absorption spectrophotometry
GSH	glutathione
GST	glutathione-S-transferase
IC ₅₀	half maximal inhibitory concentration
ICP-MS	inductively coupled plasma mass spectrometry
IEC	interstrand cross-link
JNK	c-Jun N-terminal kinase
KF ⁻	Klenow fragment of <i>E. coli</i> DNA polymerase I (exonuclease minus)
MTT	3-(4,5-Dimethylthiazol-2-yl)-2,5-diphenyltetrazolium bromide
nic-Pt	dichloridoplatinum(II)(6-aminomethylnicotinate)
nucleosomes	protein-containing structures that occur in chromatin at ~200-bp intervals
oc	open circular
OCT	organic cation transporter
PAA	polyacrylamide
PAGE	polyacrylamide gel electrophoresis
pDNA	plasmid DNA
PI	propidium iodide
PNK	T4 polynucleotide kinase
RA-Illudin 5	retinoic acid illudinyll M ester
r _b	molar ratio of platinum bound to nucleotides
r _i	molar ratio of input drug/DNA
sc(DNA)	super helical covalently closed plasmid DNA
SDS	sodium dodecyl sulphate
TEA	tetra-ethyl-ammonium
TRIS	tris(hydroxymethyl)aminomethane(2-Amino-2-hydroxymethyl-propane-1,3-diol)

Introduction

The history of empirical preparation changed when the first isolation of active drugs (alkaloids such as morphine) arrived in the hospitals during the early 19th century. Soon, the first derivatives were synthesized (e.g. heroine from morphine) and natural products became preferable lead structures for synthetic drugs. Major pharmaceutical companies have been eagerly searching for naturally designed drugs worldwide possessing potentially interesting pharmaceutical effects. A small series of these fascinating compounds is mentioned below.

1.1 Novel chemotherapeutic drugs based on scaffolds designed by nature

Fruits of *Schisandra chinensis* (Turcz.) Baill (*Schisandraceae*) belong to the most widely used plants in traditional Chinese, Japanese and Russian herbal medicine due to their hepatoprotective, antiasthmatic, antidiabetic, sedative and tonic properties (Chang et al., 2005). Monoester derivatives of schisandrol A (Figure 1- 1) inhibited the P-gp drug transporters of multidrug-resistant human KBv1^{+Vbl} cervix carcinoma cells better than the natural benzoate and comparable to the clinical sensitizer verapamil (Schobert et al., 2008). A novel schisandroxy(methyl)titanocene complex reached single-digit micromolar IC₅₀ values against cells of leukemia HL-60, melanoma 518A2, multi-drug resistant cervix carcinoma KBv1^{+Vbl} and breast carcinoma MCF-7^{+Top} (Gmeiner et al., 2010).

Simple terpenes ((+)-menthol Figure 1- 1, thymol, perillyl alcohol, limonene, linalyl acetate) can affect the permeability of cell membranes as well as membrane-anchored and down-stream proteins crucial for proliferation-related signalling (Hardcastle et al., 1999; Trombetta et al., 2005; Yuri et al., 2004). Antiproliferative effects of various terpene alcohols esterified with [6-(aminomethyl)nicotinate]dichlorideplatinum(II) complex (**nic-Pt**) were demonstrated on different cancer cell lines (Bernhardt et al., 2008; Schobert et al., 2007).

The combretastatins are natural compounds extracted from the tree *Combretum caffrum* (Pettit et al., 1989) and were the first microtubule depolymerizing agents identified to have tumor vascular disrupting activity at well tolerated doses (Chaplin et al., 1996; Dark et al., 1997). Combretastatin A-4 phosphate (CA-4-P or Zybrestat) (<http://www.oxigene.com>), a soluble pro-drug of the natural parent CA-4 molecule in

1. Introduction

Figure 1- 1 (Pettit et al., 1995), is by far the most widely studied VDA of the microtubule depolymerizing family and was the first such agent to enter clinical trial (Dowlati et al., 2002). It specifically binds to the colchicine binding site of tubulin and exhibits distinct anticancer activity *in vitro* and *in vivo* (Hinnen and Eskens, 2007).

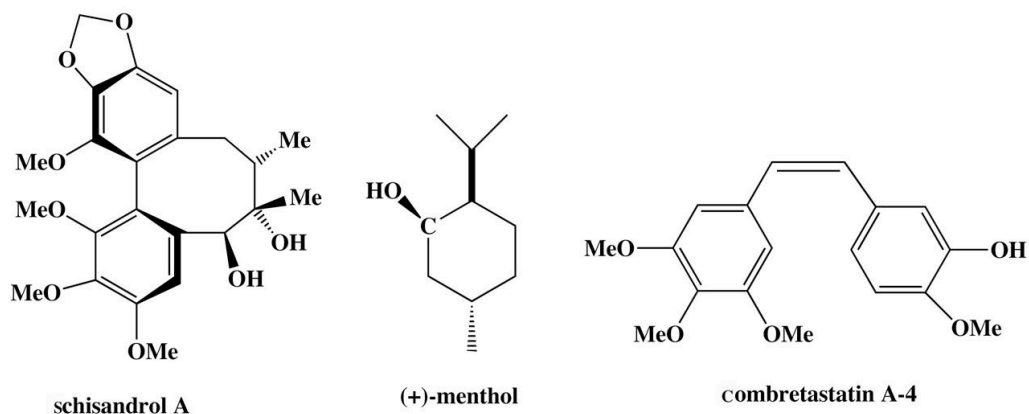


Figure 1- 1 Structures of schisandrol A, (+)-menthol and combretastatin A-4.

1.1.1 Combretastatin A-4 analogue – chalcone (1)

Trimethoxyphenyl chalcones like **1** are structurally related to combretastatin (Lawrence et al., 2006). Chalcones, which are classified under polyphenolic compounds, are basically flavonoids, ubiquitously presented in plants, especially in fruits and vegetables (Calliste et al., 2001). A cursory look at the recent literature cited in relation to chalcones indicates that there is a growing interest in evaluating the pharmaceutically important biological activities of chalcones, presuming their role in the prevention of various degenerative diseases and other human ailments (Batovska and Todorova, 2010). Some chalcones were reported with significant anticancer activities originating from other modes of action such as the inhibition of resistance-relevant ABC-transporters (Hirschmann-Jax et al., 2004; Liu et al., 2008). Recently, fluorinated 2'-hydroxychalcones of the garcinol type were shown to owe their increased anticancer activity in a pancreas tumor to an up-regulated COX-2 expression (Padhye et al., 2010), and a chlorambucil conjugate of combretastatin A-4 was found far more efficacious against neuroblastoma cells than combretastatin A-4 alone (Coggiola et al., 2005).

Recently, chalcone (**1**) and its dichloridoplatinum(II)(6-aminomethylnicotinate) complex (Figure 1- 2) inhibited the polymerization of tubulin when applied *in vitro* (Schobert et al., 2009). Morphologically, both test compounds led to a rounding and detachment of 518A2 cells and an enhancement of their motility and cell shrinking

dynamic. This behaviour is in line with the generally accepted mechanisms of tubulin binding agents (TBAs) (Lippert, 2007) involving activation of RhoA/RhoA kinase, an intracellular coordinator of cytoskeletal rearrangement of microtubules and actin (Zoldakova et al., 2010).

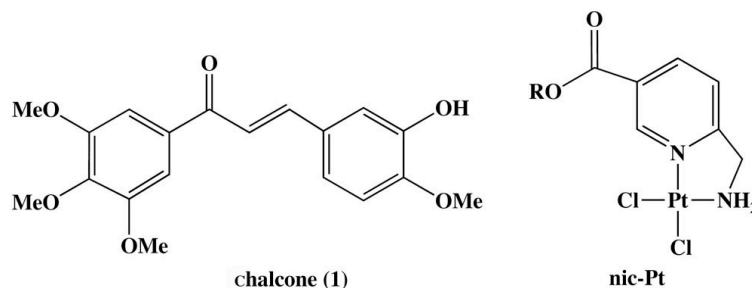


Figure 1- 2 Structure of studied chalcone (1) and dichloridoplatinum(II)(6-aminomethylnicotinate; nic-Pt).

The tumoral vascular network is characterized by peculiar irregularities and thus has been identified early on as a promising drug target. Vascular disrupting agents (VDAs) have been intensively investigated and some already went on clinical trials, mostly as combination with DNA-targeting drugs (Kanthou and Tozer, 2009; Lippert, 2007). The majority of VDAs shows a pronounced affinity for tubulin and interferes with the delicate mitotic machinery of dynamic microtubule formation and destruction. The microtubule cytoskeleton fibers are crucial to mitosis and cell division, for the maintenance of cell shape and for the transport of vesicles (Vantard et al., 2000). Moreover, they are essential structural components of dendrites. In the brain, the formation of dendrites is dependent on neural activity and is mediated in part by the modulation of microtubule stability (Vaillant et al., 2002).

1.1.2 Natural alkylation agent - illudin M (4)

Illudin M and its close congener illudin S are natural sesquiterpenes of the bioluminescent Jack o'Lantern mushroom (*Omphalotus olearius*, formerly *Clitocybe illudens*) growing in the east of North America, which were discovered by Anchel *et al.* in the course of their search for fungal antibiotics in 1950 (Anchel et al., 1950). The unique chemical structures of these sesquiterpenes displaying a tricyclic spirocyclopropylindane core were determined by McMorris and Anchel in 1963 (McMorris and M., 1963). Their mode of action was soon discovered to be a special sort of triggered alkylation. Initially attacked at their enone moiety by naturally occurring sulfur nucleophiles, both compounds alkylate nucleic acid and protein targets by ring opening of the spirocyclopropane (Figure 1- 3). Alkylation of the DNA leads to apoptotic cell death (McMorris et al., 1990).

1. Introduction

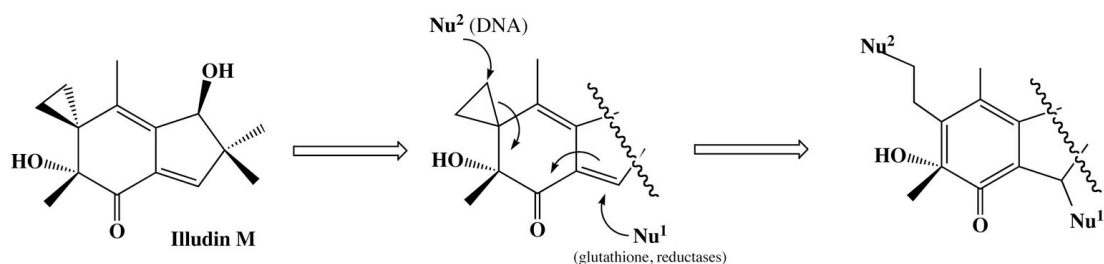


Figure 1- 3 Proposed mechanism of the illudin M action. After a pre-activating reduction of its enone by NADPH-dependent oxido-reductases or glutathione (Nu¹), illudin M can alkylate DNA, RNA and proteins (Nu²) via opening of the spirocyclopropane and so induce apoptotic cell death.

Although both illudin M and illudin S showed high cytotoxic activity in various cancers they turned out to be too toxic for any clinical application (Kelner et al., 1987). However, due to their unique mechanisms of action many efforts to synthesize novel and improved illudin derivatives have been carried out (Schobert et al., 2011). Indeed, less reactive semi-synthetic illudin derivatives were discovered with diminished toxicity and improved therapeutic indices.

1.1.3 Activity of all *trans* retinoic acid

Retinoids are naturally occurring or synthetic compounds related to vitamin A (retinol). They have significant effect on many cell functions including differentiation and apoptosis (Aebi et al., 1997; Tavares et al., 2008). Retinoic acid (RA, Figure 1- 4) induces differentiation of various types of stem cells, including cancer stem cells and neural stem cells, making it a useful tool for the treatment of cancer (Matthay et al., 2009; Schlett and Madarasz, 1997; Tang and Gudas, 2011). RA is mainly involved in the induction of neural differentiation, motor axon outgrowth and neural patterning. These effects are mediated by nuclear retinoic acid receptors, usually heterodimers of RAR and RXR proteins (Chambon, 1996; Mey, 2006). Thus, RA could be used as a therapeutic molecule for the induction of axon regeneration and the treatment of neurodegeneration (Maden, 2007).

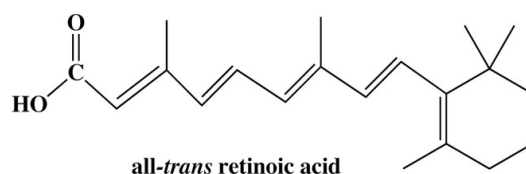


Figure 1- 4 Structure of all-*trans* retinoic acid (RA).

In addition, interactions with other signaling pathways like estrogen signaling were discovered (Hua et al., 2009). Retinoids induce differentiation and stop proliferation combination with classical anticancer drugs like cisplatin (Aebi et al., 1997).

Mechanisms of all *trans* retinoic acid (RA)-induced differentiation are also covered but not fully understood. RA is a potent inducer of HL60 cell differentiation and when used as a single agent it can induce complete remission in patients with acute promyelocytic leukemia (APL). While one mechanism of the effect of RA involves RA nuclear receptors, retinoylation (a posttranslational modification of proteins by RA) may be a new non-genomic mechanism by which RA acts on cells (Takahashi, 2002).

Cell differentiation is essential for normal growth and homeostasis, and drug-induced differentiation of tumor cells into benign or normal cells is an important approach for anticancer chemotherapy. Studies of induction mechanisms for cell differentiation and discovery of differentiation-inducing factors are thus critical components of drug development.

1.2 Drugs uptake and efflux

The cell membrane is often overlooked in drug development. However, the membrane is not a passive or necessarily benign solvent and directly impacts on the protein molecules and complexes it contains. Various membrane transporters and carriers mediate cellular uptake and efflux of drugs Figure 1- 5. The uptake may involve the carriers or channels as well as various endocytotic routes.

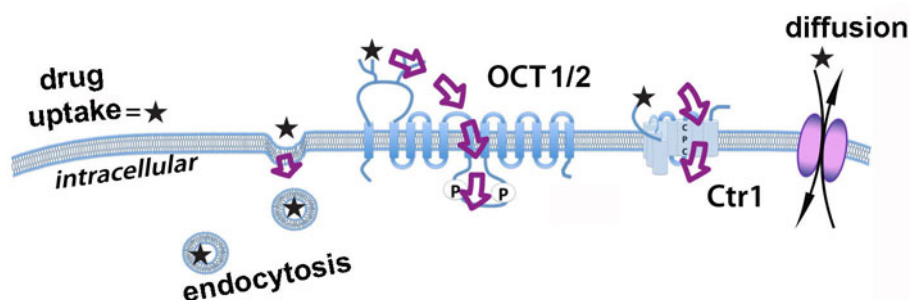


Figure 1- 5 Scheme of drug transport through cell membranes. Passive transport is represented by simple diffusion (as well as channel-mediated or carrier mediated diffusion). Endocytosis plays a specific role in drug uptake and here the clathrine-dependent endocytosis is shown. Positively charged drugs are actively transported via organic cation transporters (OCT = SLC22A1/2), which pump the compounds against the concentration gradient. The copper-related transporter (Ctr1) was found to transport platinum complexes (Safaei and Howell, 2005).

The existence of different endocytotic mechanisms is interesting; for instance in relation to growth and differentiation, cell adhesion, regulation of the activity of signalling receptors and drug delivery. There are several endocytotic mechanisms. The clathrin-dependent one and mechanisms, which operate without clathrin, are based on different requirements (dynamin, small GTP-binding proteins of the Rho-family and specific lipids). One of the most studied examples of a clathrin-

1. Introduction

independent endocytic mechanism that is based on actin polymerization is macropinocytosis, a major fluid-phase uptake pathway (Sandvig et al., 2008).

Macropinocytosis differs from other types of endocytosis by its unique susceptibility to inhibitors of Na^+/H^+ exchange. However, the functional relationship between Na^+/H^+ exchange and macropinosome formation remains obscure. Recently, submembranous acidification was found to play a crucial role in the elimination of macropinosomes formation (Koivusalo et al., 2010).

The Na^+/K^+ -ATPase, sometimes called Na^+/K^+ pump, is a transmembrane enzyme acting as an electrogenic ion transporter in the plasma membrane of all mammalian cells. Each cycle of Na^+/K^+ -ATPase activity extrudes three Na^+ ions from a cell, moves two K^+ ions into the cell and utilizes the energy from the hydrolysis of one ATP molecule (Rakowski et al., 1989). The primary role of the Na^+/K^+ -ATPase is therefore to maintain high intracellular K^+ and low intracellular Na^+ (Robinson and Flashner, 1979).

Like other P-type ATPases, proteins utilize the energy of ATP hydrolysis to transport Cu^{2+} across the vesicular membrane *via* a process that involves the formation of a transient acylphosphate intermediate (Solioz and Vulpe, 1996). The major Cu^{2+} uptake transporter is the copper transporter receptor 1 (Ctr1) (Culotta et al., 1999). Recent data indicate that the Cu^{2+} homeostasis system also regulates the uptake, intracellular compartmentalization and efflux of cisplatin (Katano et al., 2003; Safaei and Howell, 2005).

The majority of drugs for therapeutic use including many antihistaminics, antacids, antiarrhythmics, antihypertensives and anticholinergics are organic cations or weak bases, i.e. molecules with a transient or permanent positive net charge (Muller et al., 2005). The main membrane transporters for cationic drugs are the organic cation transporters (OCT) of the SLC22 family (Cetinkaya et al., 2003; Koepsell et al., 2007). The OCTs play a pivotal role in the distribution and excretion of cationic drugs. They mediate electrogenic translocation of cations in both directions. OCTs are poly-specific transporters (Koepsell, 2011; Koepsell et al., 2007). They mediate intracellular uptake of a broad range of structurally diverse organic cations with molecular masses generally < 400 Da (Wright, 2005; Zhang et al., 2006).

There are many genes encoding major human transporters such as:

- Solute-linked carrier organic anion transporter family: *SLCO1B1* (OATP1B1, OATP-C, OATP2), *SLCO1B3* (OATP1B3, OATP8), *SLCO2B1*, *SLC21A9* (OATP-B).
- Solute-linked carrier transporter family: *SLC10A1* (NTCP - sodium taurocholate co-transporting polypeptide), *SLC10A2* (ASBT- apical sodium-dependent bile salt transporter), *SLC15A1* (PEPT1); *SLC15A2* (PEPT2), *SLC22A1* (OCT-1 - organic cation transporter), *SLC22A2* (OCT2), *SLC22A3* (OCT3), *SLC22A4* (OCTN1), *SLC22A5* (OCTN2), *SLC22A6* (OAT1 - organic anion transporter), *SLC22A7* (OAT2), *SLC22A8* (OAT3).

Interactions between exogenous, amphiphilic compounds and the membrane can be critically damaging to the cell and affecting its structural integrity. This may produce a desirable outcome concerning tumor treatment. Resistance of cancer cells is a main problem for a successful treatment. ATP-binding cassette (ABC) transporters represent a family of proteins that mediate multi-drug resistance (MDR) (Figure 1- 6). The ABC superfamily is probably the largest and most diverse family of proteins that mediate the selective movement of solutes across biological membranes (Higgins, 1995, 2007).

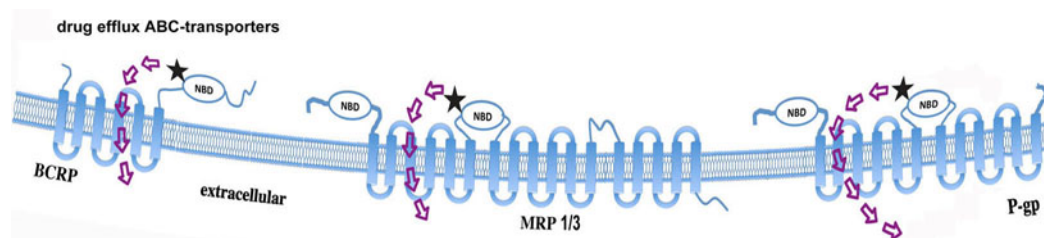


Figure 1- 6 Relevant ABC-transporters responsible for drug efflux and multi-drug resistance.

Cells may become drug-resistant by several different mechanisms. One major type of MDR is linked to the over-expression of a 170 kDa plasma membrane glycoprotein known as the P-glycoprotein (P-gp) (Sharom, 1997). This protein functions as an ATP-dependent efflux pump for hydrophobic drugs, including the *Vinca* alkaloids, anthracyclines, epipodophyllotoxins, and taxanes. P-gp expression in tumors *in vivo* is often associated with poor overall prognosis and response to chemotherapy (Goldstein, 1996).

Over-expression of the member G (white) subfamily of ABC transporters was found in MCF-7 human breast carcinoma cells, and this transporter was termed breast cancer resistance protein (BCRP) (Doyle and Ross, 2003). Unlike P-glycoprotein and

1. Introduction

MRP1, which are arranged in 2 repeated halves, BCRP (ABCG2) is a half-transporter consisting of just one nucleotide binding domain connected to a single membrane-spanning domain (Rocchi et al., 2000). The strategic and substantial localization of BCRP in the placenta, in the small intestine, and in the liver suggests that BCRP functions as a protective efflux pump in the placenta and has the potential to limit oral absorption and increase biliary elimination of toxic xenobiotics that are BCRP substrates (Mao, 2008; Mao and Unadkat, 2005).

The multidrug resistance-associated protein (MRP) is a 190-kDa membrane-bound glycoprotein. Similar to P-gp, the MRP gene product contains two nucleotide-binding motifs localized in the intracellular domains and thus appears to be another member of the ATP-binding cassette transporter superfamily (ABC-C) (Wada et al., 1999). P-glycoprotein transports unmodified drugs, whereas MRP1 can transport drugs either conjugated to anionic ligands such as glutathione (GSH), glucuronide, or sulfate, or in an unmodified form, possibly together with GSH. Concerning all MRP family members, MRP3 is closest to MRP1 (58% amino acid identity) and able to confer resistance to many anti-cancer drugs (as methotrexate, etoposide, and teniposide) (Kool et al., 1999).

The main transporters associated with mammalian drug resistance in the ABC superfamily are once more listed below:

- **ABCB1** (P-gp- P-glycoprotein, MDR1 - multi-drug resistance).
- **ABCB4** (MDR3).
- **ABCB11** (BSEP - bile salt export pump).
- **ABCC1** (MRP1: multi-drug resistance related protein).
- **ABCC2** (MRP2, CMOAT).
- **ABCC3** (MRP3, CMOAT2); **ABCC4** (MRP4); **ABCC5** (MRP5); **ABCC6** (MRP6).
- **ABCG2** (BCRP: breast cancer resistance protein).

1.3 Cisplatin and chemoresistance

Cisplatin has a central role in cancer chemotherapy, especially for testicular cancer, for which the overall cure rate exceeds 90%, and reaches nearly 100% for early stage cancers (Bach et al., 2001). The treatment is limited, however, by side effects including nephrotoxicity, emetogenesis and neurotoxicity (Wang and Lippard, 2005).

A profound understanding of the mechanism by which cells process cisplatin (CDDP) provides important insights for the design of more efficient platinum-based drugs.

The mechanism of cellular uptake and efflux of cisplatin is still not fully understood. Early studies suggested that cisplatin enters the cell mainly by passive diffusion but recently growing body of evidence revealed a direct link with the copper related protein (Ctr1) (Binks and Dobrota, 1990; Ishida et al., 2002). Several reports already suggested that Na⁺/K⁺-ATPase mediates the uptake of CDDP (Andrews et al., 1991; Kishimoto et al., 2006). Recent data indicate that the Cu²⁺ homeostasis system likewise regulates the efflux of CDDP (Ahmed et al., 2009; Katano et al., 2003; Safaei and Howell, 2005).

Cisplatin is usually administered in chloride-containing solution as short intravenous infusion. In the bloodstream cisplatin encounters a relatively high concentration of chloride ions (100 mM) that suppresses hydrolysis (Figure 1- 7).

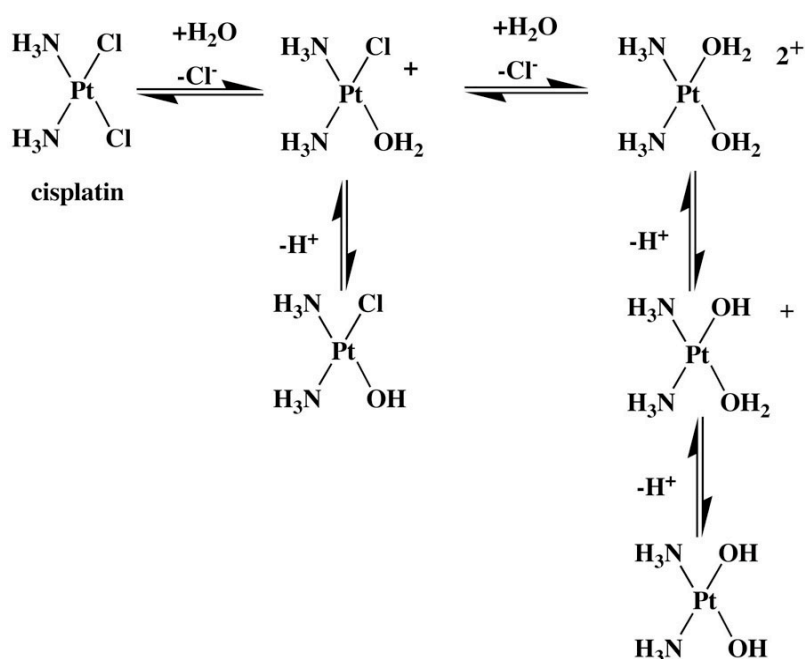


Figure 1- 7 Hydrolysis of cisplatin in aqueous solution. The chloride ligands are hydrolysed, which results in reactive compounds.

After entering the cell, the diminished chloride concentration (~20mM) facilitates the hydrolysis of cisplatin resulting in activated positively charged mono- and di-aqua species (Jennerwein and Andrews, 1995). The hydrolysis reaction is the rate-limiting step for DNA-binding (Carte et al., 2000).

There is convincing evidence that the cytotoxic properties of cisplatin are a consequence of DNA-adduct formation, which affects DNA-dependent cellular functions. Cisplatin reacts with DNA preferentially by coordination to the N-7 atoms

1. Introduction

of purines, which are exposed in the major groove of the double helix and are not involved in base-pair hydrogen bonding (Balcarova et al., 1992; Brabec and Kasparkova, 2002; Zoldakova et al., 2011). Up to 90% of platinum-DNA adducts comprise of 1,2-intrastrand CLs (Figure 1- 8) involving adjacent bases, and 1,2-d(GpG) CL involving two adjacent guanine is two to three times more frequent than 1,2-d(ApG) CL involving adenine adjacent to guanine (Poirier et al., 1992).

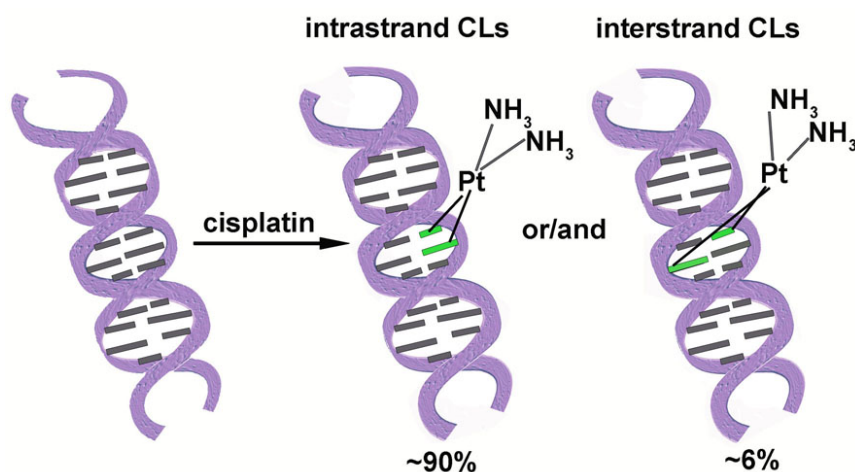


Figure 1- 8 Cisplatin-DNA adducts comprise of 1,2d(GdG)-intrastrand (90%) or interstrand cross-links (6%).

The Schobert's group synthesized large number of platinum- or ruthenium based conjugates (Bernhardt et al., 2008; Biersack et al., 2010; Schobert and Biersack, 2005). Several of them displayed cytotoxicity at nanomolar concentrations and were specific against various cancer cells. Recently, chalcone (**1**) and its Pt(II)-dichlorido-(6-aminomethyl)-nicotinate ester presented remarkable combinatorial effects on DNA and tubulin and inhibited the growth of certain cisplatin-resistant tumor cell lines (Schobert et al., 2009). Conjugate (**2**) is accumulated in cancer cells mainly *via* cell-controlled transporters and induces apoptosis by triggering multiple targets (Zoldakova et al., 2010).

1.4 The aim of this study

The molecular mechanism of chalcone (**1**) deals with microtubules. However, its vascular disrupting effects are yet not fully understood. Moreover, the breach of cisplatin resistance is crucial for future oncological research.

In the presented study of complexes based on *m*-hydroxychalcone (**1**) and cisplatin a focus was set on mechanisms of action and effects in living cells and *in vitro*. Novel conjugates **2** and **3** of the combretastatin A-4 analogous chalcone (**1**) were tested for antitumor activity, altered cell shapes and sub-cellular compartments, apoptotic signals, DNA-binding and glutathione-binding properties.

Furthermore, the selective impact of illudin M and its new retinoate (**5**) on glioma and stem cell rich astrocytoma cells was tested and compared with that on normal neurons, astrocytes and cancer cells.

Material and Methods

2.1 Material

Flasks 75 cm² (Nunc, Wiesbaden, Germany), 96-well filtration plates HTS (Millipore), 50 mL falcon type tubes (Greiner bio-one), 10 mL falcon type tubes (VWR), glass slides (round) AL; Ø 1.5 cm, microscope slides AL; ca. 76 × 26 mm, petri dishes Ø 13.5 cm (Roth), sterile filter pore size: 0.25 – 0.45 µm (NALGENE), FACS tubes (Becton Dickinson), 18×18 mm Aclar-fovia (Ted Pella), slot grids (Plano), Maco EM-Film EMS, 8.3×10.2 cm (Maco), imaging plate BAS-IP MS 2040 – 20x40 cm (Cat. No: 08000097-Fujifilm).

2.1.1 Instruments

Microplate reader (MWG-BIOTECH/BioRad), TECAN Infinite F200 plate reader, autoclave H+P (Varioklav), centrifuge (Eppendorf), miniSpin Centrifuge (UNIEQUIP), UNIVAPO 150 H Centrifuge (Heraeus); Varifuge 20 RS -Rotor: 5148, fluorescence spectrometer Inc. LS 50 B (Perkin Elmer), gel-documentation apparatus (LTF Labortechnik), heater (Eppendorf), thermomixer 5436, hemocytometer - Neubauer improved (Brand), horizontal gel electrophoresis apparatus C.B.S Model #SGU-020T-02, Incubator (Heraeus), Laminar-Flow-Box aura Vertical S.D. 4 (Nunc), Optical Microscope Axiovert 135 and AxioCam MRc5 (Zeiss), UV-Transilluminator (Vilber Lourmat), Vacuum centrifuge - Vacuum Concentrator BA-VC-300H (Saur), Mini 900rate meter (Thermo), FPLC was carried out on a Waters FPLC system consisting of Waters 262 Pump, Waters 2487 UV detector and Waters 600S Controller with MonoQ HR 5/5 column. Autoradiograph reader and Eraser – Raytest (Fujifilm BSA-2500).

2.1.2 Chemicals

Antibiotics antimycotics from Gibco, 3-(4,5-dimethylthiazol-2-yl)-2,5-diphenyltetrazolium bromide (MTT; ABCR), acetic acid (Fluka), agarose (Roth, Serva), BSA – bovine serum albumin (Roth), cimetidine (CalBiochem), wortmannin (CalBiochem), chlorpromazine (CalBiochem), amiloride (CalBiochem), ouabaine (CalBiochem), mitoxantrone (Ralenova), CaCl₂ · 2 H₂O – calcium chloride dihydrate (Merck), digitonin (CalBiochem), Pluronic F127, propidium iodide (Sigma), calcein-

AM, fumitremorgin C, 100 bp DNA ladder Plus (0.5 mg DNA/mL), (PeQlab), DNA ladder loading buffer (6×) (PeQlab); EDTA – ethylene diamine tetraacetic acid (VWR), EGTA – ethylene glycol tetraacetic acid (CalBiochem), EtdBr – ethidium bromide (Merck), ethanol (100 %) (VWR), Fura-2/AM – Fura-2-acetoxymethyl ester (SIGMA), Giemsa dye (Roth), glucose (water-free) (Riedel de Haen), HEPES – 4-(2-hydroxyethyl)-1-piperazineethanesulfonic acid (Roth), PIPES -piperazine-N,N'-bis(2-ethanesulfonic acid) (VWR), DTT - dithiothreitol (VWR), CHAPS - 3-[(3-cholamidopropyl)-dimethyl-ammonio]-1-propanesulfonate (Roth), K₂HPO₄ – dipotassium hydrogen phosphate (Merck), KCl – potassium chloride (Merck), methanol (Fluka), MgCl₂ · 6 H₂O – magnesium chloride hexahydrate (Merck), Na₂HPO₄ - disodium hydrogen phosphate (Fluka), NaCl – sodium chloride (Grüssing), SDS – sodium dodecyl sulfate (Roth), Tris (Roth), Trypsin-EDTA 0.5% (Gibco), NaOH – sodium hydroxide (Roth), proteinase K (≥ 30 U/mg) (Roth), Ribonuclease A (RNase A; 90 U/mg) (Roth) and for FACS analysis - RNase 10 mg/L (Qiagen), 18% formaldehyde (Riedel-de Haen), glycine, 1% OsO₄ in H₂O, Pb(NO₃)₂ (Merck), 25% glutaraldehyde, Glycider 100, propylene oxide, 2,4,6-tris(dimethylaminomethyl)phenol (Epon; Serva), 0.5% tannic acid (Mallinckrodt), polioform powder, uranyl acetate (Plano). Dr. Bernhard Biersack synthesized all test compounds according to literature procedures (Lawrence, Patterson et al. 2006; Schobert, Biersack et al. 2009), illudin M was purified by Sebastian Knauer (Schobert, Biersack et al. 2008; Knauer, Biersack et al. 2009).

Antibodies: glial fibrillary acidic protein (GFAP; Invitrogen), streptavidin-conjugated horseradish peroxidase (HRP; Sigma A8924), phalloidin-biotin, anti-mouse IgG Alexa 594 (A11005), anti-rabbit Alexa 594 chicken, and 4'-6-diamidino-2-phenylindole (Invitrogen), anti-mouse neuron specific βIII-tubulin (SDL3D10) and goat anti-mouse streptavidin Alexa Fluor 488 conjugate (S32354) (Sigma).

2.1.3 Solutions and buffers

Antibiotics-antimycotic solution Penicillin G (Na-Salt) 10 000 units/mL,
Streptomycin-Sulfat 10 000 µg/mL,
Amphotericin B 25 µg/mL in 0,85 % PBS buffer

MTT solution 0.5mg/mL MTT solved in PBS buffer

DMSO solution 10 % SDS in 99.4 % DMSO / 0.6 % acetic acid

2. Material and Methods

PBS buffer	8 g NaCl, 0.2 g KCl, 1.44 g Na ₂ HPO ₄ •12H ₂ O,
pH = 7.4	0.24 g KH ₂ PO ₄ per 1 L
Caspase buffer	20 mM PIPES, 100 mM NaCl, 10 mM DTT
pH = 7.2	freshly prepared, 1 mM EDTA, 0.1% (w/v) CHAPS, 10% (w/v) sucrose, in 1 L of dH ₂ O
Ca-buffer	120 mM NaCl, 5 mM KCl, 2 mM MgCl ₂ •6H ₂ O,
pH 7.4	1.5 mM CaCl ₂ •2H ₂ O, 125 mM HEPES, 10 mM glucose for 1 L; stored at 4 °C
Cs-buffer	2% BSA in 1 mL Ca buffer, 5 µL of Pluronic F127 (20% in DMSO)
-for Ca ²⁺ assay	+ 0.8 µL Fura-2/AM (5 mM in DMSO)
EtdBr staining solution	250 mL 0.5 × TAE buffer, 100 µL of 1 % EtBr solution
EtdBr washing solution	250 mL 0.5×TAE buffer
DNA-lysis-buffer	10 mM Tris-HCl (pH 8.5), 5 mM EDTA, 200 mM NaCl, 0.2 % SDS
PBS (for DNA isolation)	137 mM NaCl, 27 mM KCl, 100 mM Na ₂ HPO ₄ ,
pH 7.4	2 mM K ₂ HPO ₄
1×TAE	40 mM Tris-HCl, 20 mM Acetic Acid, 10 mM EDTA
pH 8.18-8.29	
50xTAE	2 M Tris-acetate, 0.05 M EDTA [242 g Tris + 57,1 mL ice-cold acetic acide + 100 mL 0.5 M EDTA in 1000 mL H ₂ O
pH 8.0	
1xTBE	0.09 M Trizma-Base, 0.002 M EDTA
pH 8.3	
1×TE	10 mM Tris-HCl, 1 mM EDTA; 37 °C
pH 8.0	
FPLC/Buffer A	10 mL 1M Tris-HCl pH 7.4, 12.4 mL 4 M NaCl, add to 1 L dH ₂ O

FPLC/Buffer B	10 mL 1M Tris-HCl pH 7.4, 250 mL 4 M NaCl, add to 1 L dH ₂ O
Denatured 1% agarose gel	1 g agarose, 100 mL dd H ₂ O boiled with 1 minute in microwave, 0.03 M NaCl, 1 mM EDTA
Denaturation buffer	0.03 M NaOH, 1 mM EDTA
DNA-Loading-buffer	6 mL Glycerol, 20 mg Xylenecyanol, 1 mL 5x TBE, 3 mL H ₂ O
5x[γ]ATP buffer	0.18 M MgCl ₂ , 0.5M imidazol, 1 mM spermidin, 1mM EDTA, 1 mM ADP, 0.05 M DTT in H ₂ O
10x Klenow buffer	0.5 M Tris-Cl (pH 7.2), 0.1 M MgSO ₄ , 0.001 M DTT
5xTranscription buffer	0.2 M Tris-HCl (pH 7.5), 0.05 M NaCl, 0.03 M MgCl ₂ , 0.01 M spermidin
Stock solution of 40% acrylamide	38% AA + 2% bis-AA [38 g Acrylamide + 2 g N,N'-methylenebisacrylamide] in 100 mL H ₂ O
Stock solution of 30% acrylamide	29% AA + 1% bis-AA [38 g Acrylamide + 2 g N,N'-methylenebisacrylamide] in 100 mL H ₂ O
Blue-loading buffer	40% (w/v) Sacharose in H ₂ O, 0.1% (w/v) Bromphenol-blue, 0.1% (w/v) Xylencyanol
Lysis buffer I	10 mM Tris-base (0.6057g); 60 mM KCl (2.235g); 1.2 mM EDTA (0.1791g); 1 mM DTT (1 μL 1M), add 500 mL dH ₂ O
Lysis buffer II	10 mM 1 μL 1 M DTT
5xNER buffer	0.22 M HEPES (pH 7.8 with KOH), 0.035 M MgCl ₂ , 2.5 mM DTT, 100 μM dNTP (except that used to label the reaction – 20 μM), 200 mM phosphocreatine, 17% glycerol, 1.5 mg/mL bovine serum albumin (BSA)

2. Material and Methods

Media and supplements

MEM and E-MEM (Eagle's minimum essential) media were purchased from Sigma. Ham's 12, D-MEM (Dulbecco's modified eagle medium), NeuroBasal media, Insulin-Transferin-Selenium (ITS) were bought from Gibco, Invitrogen, B27 supplement, fetal calf serum (FCS), antibiotic-antimycotic solution, gentamycin, 3 mM retinoic acid, 10% poly-lysine, and glutamine from Gibco-BRL-Life.

2.1.4 Cell cultures

The cells were cultured as "monolayer cultures" or growth as "suspension" in 75 cm², 125 cm² flasks resp. Ø 15 cm Petri dish. The cell cultures were incubated at 37°C / 5% CO₂ in different culture media.

Cancer cells:

Human melanoma 518A2 cells were obtained from the department of oncology and hematology of the Martin-Luther-University, Halle, and cultured in D-MEM with 10% FBS, 0.55% antibiotic-antimycotic solution and 0.3% gentamycin. The cells were continuously passaged once a week by 0.05% trypsin solution and new flask was seeded with 10⁵ cells.

Human leukemia HL60 cells were obtained from the department of oncology and hematology of the Martin-Luther-University, Halle, and cultured as "suspension" in RPMI medium supplemented with 5% FBS, 0.55% antibiotic-antimycotic solution and 0.3% gentamycin.

Human cervix carcinoma (KBv1^{+Vbl}) and breast carcinoma (MCF-7^{+Top}) cells were a gift from the department of pharmacy, University of Regensburg (Kuhnle, Egger et al. 2009). The cells were passaged each 3rd - 4th day and ¼ was used for new flask (~2×10⁶ cells/mL). The KBv1/KBv1^{+Vbl} cells were cultured in D-MEM with 10% FBS, 0.55% antibiotic-antimycotic solution and 0.3% gentamycin, without/with 340 nM vinblastine. The MCF-7/MCF-7^{+Top} cells were grown in E-MEM supplemented with 5% FBS, without/with 550 nM topotecane.

Human colon adenocarcinoma cells (HT-29/HT-29^{+Colc}) were obtained from the Institute for Surgical Research, Philipps University Marburg and were cultured in RPMI medium supplemented with 5% FBS, without/with 62.5 nM colchicine (Kok, Veldman et al. 2000).

Neural cells:

Neuroectodermal stem cells NE-4C, primary mouse astrocytes (Schlett and Madarasz 1997; Kornyei, Szlavik et al. 2005), glioma cell lines: rat glioma C6 [ATCC No.: CCL-107] and human astroglioma U87 [ATCC No.: HTB-14], non-neural mouse fibrosarcoma cells WEHI 164 (Huszti and Madarasz 2002). Cells were maintained under a moisture-saturated atmosphere (95% humidity, 5% CO₂) at 37 °C in 75 mL culture flasks (Nunc, Germany). They were serially passaged using 0.05% trypsin / 0.02% EDTA (PAA Laboratories, Cölbe, Germany).

2.1.5 Cell counting using Neubauer chamber

Trypsinated cells in suspension were centrifuged, repipetted in a fresh media and 10-fold volume dilution was prepared ($V_f = 270 \mu\text{L}$ of PBS + $30 \mu\text{L}$ of cell suspension). The counting grid pattern in Neubauer chamber is designed to allow the standard cell counting procedure to be followed. About 10 to 15 μL of cell-containing sample was pipetted into the counting chamber through one of the ports. Liquid spread inside the chamber and replaced air. The volume of the counting chamber, which has dimensions of 1 mm \times 1 mm \times 0.1 mm (in depth) and the volume is given in cubic centimeters ($\text{cm}^3 = \text{mL}$). The cell counting chamber was placed under a microscope with a typical magnification of 100. The microscope was focused onto the grid pattern and the cell particles (Figure 2- 1). The counted cell number was multiplied by dilution factor (V_f) and by the volume of the counting chamber. The cell concentration was recalculated according to the following equation (Equation 2- 1).

Equation 2- 1 Calculation of the cell concentration

$$\text{cell number / mL} = \frac{\text{total cell number}}{\text{number of quadrats}} \times V_f \times 10^4$$

2. Material and Methods

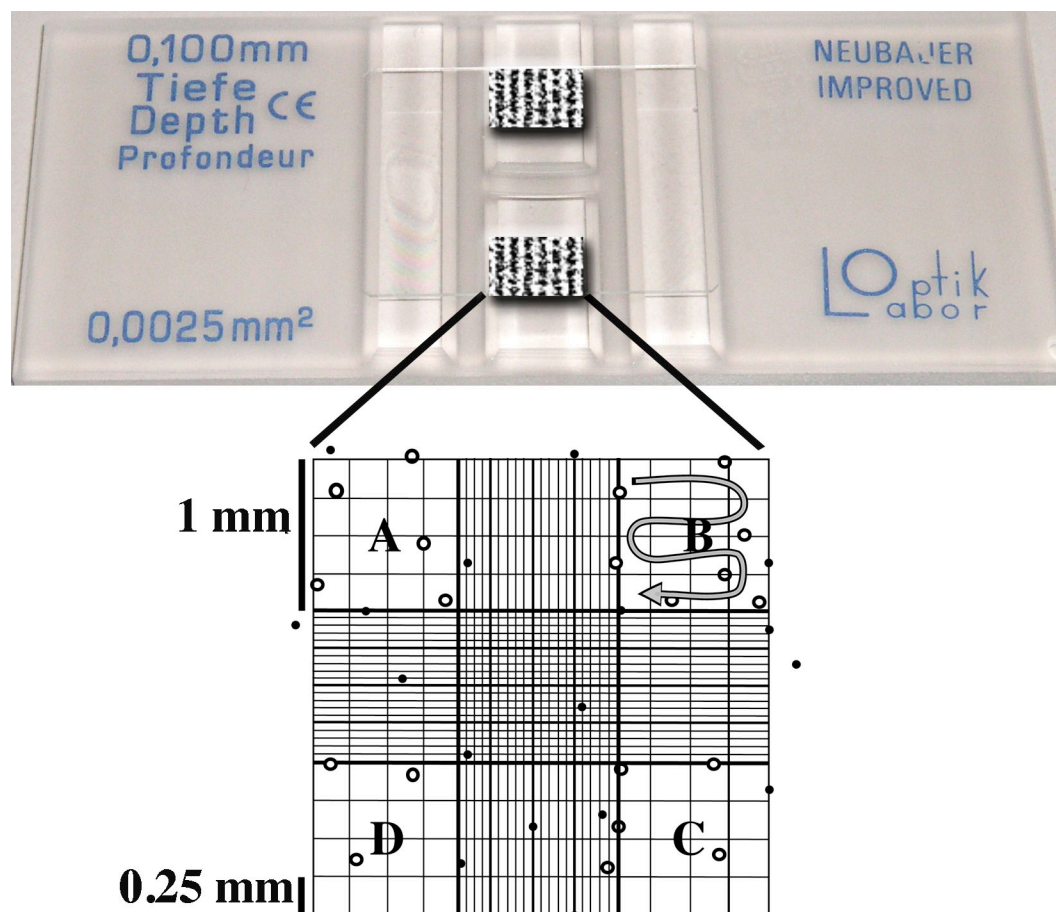


Figure 2- 1. The Neubauer chamber cell counting. The counting chamber consists from two pattern grids. Detail from one of them is cartooned below. The cells, animated as open rings, in the corners A-D are counted (in direction of gray arrow); black points represent the cells aside of counted area.

2.2 Methods

2.3 Cytotoxicity - MTT assay

MTT (3-[4,5-dimethylthiazol-2-yl]-2,5-diphenyl-tetrazolium bromide) was used to estimate the amount of viable cells, which are able to reduce it to a violet formazan dye (Mosmann 1983). Many factors could affect the final result and therefore reproducibility of the established IC_{50} concentrations has to be proved.

The MTT assay was performed according to literature (Grotemeier 2006). The cells ($1 - 0.5 \times 10^5$ cells/mL) were cultured for 12-24 hours depending on the growth progress. Cell incubation (5% CO_2 , 95% humidity, 37 °C) was followed by treatment with test compounds. Stock solutions of the complexes were dissolved in DMF. Dilutions were prepared using PBS buffer. DMF (and DMSO) belong to the group of water-miscible organic solvents.

In the mixture, the solubility of the drug is changed, hence, precipitation can occur and non-homogeneous suspension sometimes appears. Despite of this

behaviour all dilutions were prepared in media, required for certain cell types, and precipitation occurred rarely. As shown in the dilutions scheme in Table 2- 1, test substances at varying dilutions (200 – 0.5 μM) were prepared in a 96-well microplate. Plates with grown cells were modified, 50 μL of old media was removed and 50 μL of new media were pipetted from the plate containing the different drug concentrations (Table 2- 1). Blank and solvent controls were treated identically. After 24 or 48 hours 50 μL of media was discarded and 5.5 μL of MTT 0.5 % solution was added. After formation of the formazan crystals inside the cells (Figure 2- 2; after ~1-2 hours), the precipitate was dissolved with 100 μL of the DMSO solution. In the case of the neural cells formazan was dissolved in acidified (0.08 M HCl) isopropanol and measured immediately.

Table 2- 1 Test-substances dilutions scheme

Dilutions of different substances													
Row	1	2	3	4	5	6	7	8	9	10	11	12	
Substance	Media [μL]												
A	6	294	150									X	X
B													
C													
D													
E													
F													
G													
H													
Dilution with 150 μL	Series of dilutions from column 1 to 2; from 3 to 4; ...										X	X	
μM	200	100	50	25	12.5	6.5	3.75	1.9	0.9	0.47	-	-	
Dilutions are placed (50 μL) into a cell-plate with final concentration													
Row	1	2	3	4	5	6	7	8	9	10	11	12	
final	100	50	25	12.5	6.5	3.75	1.9	0.9	0.47	0.26	ctrl*	ctrl*	

* Control cells used as blank and solvent controls

The absorbance at 570 nm and 630 nm was measured with an automatic microplate reader. All experiments were carried out at least in triplicate; the percentage of viable cells was calculated as the mean \pm SD relative to controls set to 100%. Final IC_{50} values were calculated using the GraFit 3.0 program (Equation 2- 2),

2. Material and Methods

Equation 2- 2 Calculation of IC_{50}

$$y = \frac{A}{1 + \left(\frac{x}{IC_{50}}\right)^s}$$

where A are percentage of the recalculated absorbance, y is Y range, x is concentration of the substance on the x axis and s is slope factor of the curve

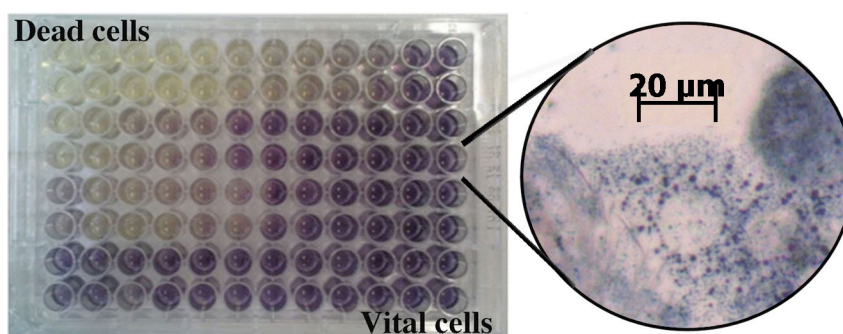


Figure 2- 2 Example of the MTT test plate with melanoma 518A2 cells. Metabolically active 518A2 cells reduced yellowish MTT solution onto the violet formazan (crystals are solved in DMSO solution inside of the wells).

2.4 Cellular drug uptake

2.4.1 Temperature effect

Cells (5×10^5 cells/mL) were grown on 96-well (filtration) plates. First, endocytosis was tested parallel in two identical plates by temperature change. Two plates were identically pipetted with test compounds in various concentrations ranging from $50 \mu\text{M}$ to $300 \mu\text{M}$. One plate was kept under $\sim 4^\circ\text{C}$; another at 37°C in the dark. After 3.5 h and/or 5 h vitality of the cells in both plates was analysed by MTT test described in chapter 2.3. After 24 hours inhibitors were applied to final concentrations of 0.5 mM cimetidine, 0.1 mM tetraethylammonium (TEA), 10 nM wortmannin, $14 \mu\text{M}$ chlorpromazine, $10 \mu\text{M}$ amiloride, or $5 \mu\text{M}$ ouabaine. The 518A2 cells were pre-incubated with these inhibitors for 15 minutes and then treated with the required concentration of the test substance or reference compounds. After 3.5 hours / 5 hours cell vitality was measured by MTT tests. The insoluble formazan crystals were washed with distilled water, dissolved in DMSO and the absorbance of the resulting filtered solution was measured. The difference of absorbance at 570 and 630 nm was calculated relative to the controls (untreated cells) and to the cells treated with the inhibitors.

The cytotoxicities of the test compounds were cross validated by comparison with their effects on cells which were not incubated with an inhibitor and with the net effect of the respective inhibitor in cells not exposed to any test compounds.

2.4.2 ICP-MS measurements of Pt-content

The cells were seeded in 6-well plates and grown for 24 hours, then optionally treated with the respective inhibitor for 15 minutes. Complex **2** (100 μ M) was added and incubation continued for 3.5 hours. The cells were trypsinized, centrifuged (800 rpm, 5 minutes) and washed with PBS. Samples were dissolved in 10 mL of pure water and measured by Inductively Coupled Plasma Mass Spectrometry ICPMS (Agilent 7500ce, Cetac ASX-510). Concentrations were calculated in μ g/L. For samples pre-incubated with inhibitors, a relative inhibition of uptake was calculated with respect to the platination of inhibitor-free cells, which were set to 100%.

2.4.3 Western blot analysis

This experiment was performed in the laboratory of Prof. Olaf Stemmann, Genetics Department - University Bayreuth by his PhD student Andreas Brown. Cells were collected by centrifugation, suspended in a SDS-PAGE sample buffer, sonificated to shear genomic DNA and boiled at 95 °C for 15 minutes. The resulting cell suspension was passed through a 27-gauge needle. The combined extracts were separated on a gradient SDS-PAGE gel and transferred to a PVDF membrane. The individual proteins were detected by means of anti-goat polyclonal OCT-1 (N-12) (sc-19809), anti-goat polyclonal OCT-2 (C-13) (sc-19814) and anti-alpha-tubulin (12G10 mouse monoclonal from hybridoma supernatant) primary antibodies and appropriate secondary antibodies conjugated with HRP (Sigma Aldrich).

2.5 Sub-cellular microscopy methods

2.5.1 Time-lapse microscopy

This work I performed in the Laboratory of Dr. Emília Madarasz with introduction and special assistance help of Dr. Környei. Cells were grown on IBIDI dishes in a customary microscope stage incubator (37 °C, 5% CO₂). Time-lapse recording was performed (in the laboratory of Dr. Madarász) with a computer-controlled Zeiss Axiovert 200M microscope equipped with 10- and 20-fold objectives and an AxioCam MRm digital camera.

2. Material and Methods

2.5.2 Immunocytochemistry

This work I performed in the Laboratory of Dr. Emília Madarasz with introduction and special assistance help of Dr. Környei. The cells (518A2 melanoma, astroglia) grown on poly-*L*-lysine-coated optical-glass cover slips were X-crossed (Környei, Czirik et al. 2000) before treatment and then fixed with 4% paraformaldehyde in PBS for 20 minutes at room temperature. The cells were permeabilised with Triton X-100 (0.1% v/v in PBS; 5 minutes). Nonspecific antibodies were blocked by incubation with 3% FBS in PBS (room temperature, 1 h). α -GFAP antibody (rabbit, DAKO) was used in a dilution of 1:2000 and was visualized by anti-rabbit IgG Alexa 594 (1:1000). Phalloidin-biotin was applied in a 1:1000 dilution followed by avidin-Alexa 488 (1:800). Fluorescence images were captured manually on a Zeiss Axiovert 200M microscope fitted with 20–60 fold zoom and a Zeiss AxioCam MRm digital camera.

2.5.3 ELISA - *In situ* detection of neural β -tubulin level

This work I performed in the Laboratory of Dr. Emília Madarasz with introduction and special assistance help of Dr. Környei. The neurons, grown in 24-well plates, were incubated for 24 hours with test compounds. After incubation neurons were washed with PBS containing 0.5% TritonX 100 for 10 minutes. Specific biotin-conjugated anti-mouse β III-tubulin antibody (1:1000) was incubated for 1 hour at room temperature. After washing step avidin-peroxidase (Sigma) diluted in PBS was applied and used in 1:1000 dilution. The antibody binding was visualized by 3,3'-diaminobenzidine (DAB, Sigma). Percentage of β III-tubulin was recalculated regarding to untreated control neurons.

2.5.4 Microscopic observations of the cells by Giemsa staining

A 6-well-plate was prepared by attaching round optical-glass slides (\varnothing 1.5 cm) to the bottom of the wells. A confluent cell layer in a Petri dish was trypsinized and diluted with medium giving a concentration of 0.75×10^5 cells/mL. A volume of 2 mL of this diluted suspension was added to each well, so that the round optical-glass slides were completely covered. The cells were incubated at 37 °C and 5 % CO₂ for about 24 hours. Subsequently to this pre-incubation, an X-cross was performed with 10 μ L tip (Környei, Czirik et al. 2000) and test compounds were added to the wells

(one substance per well). Moreover, DMF were added to a further well (1:1000 dilution of DMF), while another well contained just the plain cell culture as a negative control. Then the cells were incubated (5 % CO₂ and 95 % humidity, 37 °C). The assay was carried out after various incubation periods. Afterwards, the medium was discarded and the adherent cells were washed with PBS, followed by a washing step with a mixture of PBS and methanol (1:1.5). In order to fix the cells on the surface of the glass plates, they were covered with methanol for 15 minutes. Subsequently, the methanol was discarded and the cells were washed with fresh methanol. In order to stain the melanoma cells, the glass plates were completely covered with a 1:15 dilution of Giemsa dye for 5 minutes. The Giemsa dilution was prepared from a mixture of methanol and demineralized H₂O (7:3). After adding tap water to the wells (about twice the volume of the Giemsa dilution) and another two minutes of incubation, the aqueous Giemsa solution was discarded. The cells were carefully washed with demineralized H₂O before they were fixed and dried on the microscope slides. Pictures of the different cell samples were taken by using an optical microscope (320× magnification) and the software Axio Vision (AxioVs 40 V 4.5.0.0; Carl Zeiss Imaging Solutions GmbH). The analysis of the pictures was performed by AxioVision program.

2.5.5 Transmission electron microscopy

This work I performed in the Electron Microscopy Laboratory (University of Bayreuth) under guidance of Dr. Geimer and his student Dirk Scholz (introduction and special assistance help). I appreciate the help of Melina Fischer for taking the micrographs: Fig 3-20 a,d,f,g,i and Fig 4-13 d,e,h during analysis of my prepared TEM samples. My TEM samples were also used for her bachelor work (Geimer and Fischer 2008). Melanoma 518A2 cells were plated on pieces of aclar film, incubated for 24 hours, exposed to 100 μM of compound **1** or **2** for 20 minutes and flat-embedded for transmission electron microscopy. For this reason cells were fixed in 0.1 M HEPES, 4 mM CaCl₂ containing 2.5% glutaraldehyde, pH 7.2, for 4 hours at room temperature. After three rinses with 0.1 M HEPES, 4 mM CaCl₂, pH 7.2, cells were postfixed with 1% osmium tetroxide in distilled water for 45 minutes at 4 °C, rinsed three times in distilled water and incubated in 1% uranyl acetate in distilled water for 1 hour at 4 °C. Dehydration of the samples in an ethanol series, infiltration with Epon, and flat embedding was performed according to standard procedures. Dr

2. Material and Methods

Stefan Geimer / Rita Grotjahn performed ultrathin sectioning (60–70 nm) cut and mounted onto pioloform-coated copper grids. Sections were stained with uranyl acetate and lead citrate (Reynolds 1963) and viewed with a Zeiss CEM 902 transmission electron microscope at 80 kV. Micrographs were taken using EMS EM film.

2.6 Apoptosis - DNA degradation

2.6.1 Alkaline single cell gel electrophoresis

The bottom agar was prepared from an already prepared 1 % normal melting point (A-NMP) agarose gel (Zoldakova and Rymarczyk 2009). It was boiled in a microwave oven and then diluted with TAE of the same volume (total volume ~13 mL). The middle layer agar consisted of 1 % of low melting point agarose (A-LMP, 15 mg per 1.5 mL) and was prepared in an Eppendorf tube using a heat block (95 °C) to dissolve the agarose. After dilution in order to obtain 0.5 % LMP agarose gels were refrigerated until usage.

Treatment: Drug dose response was conducted either without direct light or in the dark. Aliquots of 200 μ L were taken from the suspension culture of HL60 cells and pipetted into Eppendorf tubes. Then, 2 μ L of illudin M (0.1 mM diluted in RPMI medium) were added to reach a final concentration of 1 μ M illudin M in the cell suspension. The control sample was treated without illudin M. Then the samples were put in the incubator over a period of 10 minutes or 5 minutes, respectively.

Repair: For measuring the rate of DNA repair the samples were centrifuged (5 minutes, 800 rpm) after incubation with illudin M. The pellet was resuspended in fresh RPMI (same volume as the supernatant) and then the samples were incubated experimentally for 2 hours or 1.5 hours, allowing repair of the DNA.

Preparation of the microgels: The gel for the bottom layer was prepared in a glass Petri dish, with the latter having been previously washed with 70 % ethanol and dried in an oven. Then, 5 mL of hot liquid 0.5 % NMP agarose were pipetted into the Petri dish and evenly distributed. It solidified at room temperature. From this gel the first layer was cut out (3.8 x 1.8 cm) and carefully placed on a microscope slide (washed and oven dried to prevent residual fibres). When the gel in the Petri dish was not needed anymore, it was stored in TAE buffer in order to avoid desiccation.

Depending on the cell number in the incubated samples, 10 - 17 μL cell suspension was mixed with 75 to 90 μL 0.5 % LMP agarose, so that the mixture contained approximately 10,000 cells. Immediately after mixing, 10 μL of the cell agarose mixture were pipetted onto one half of the bottom layer. While the first sample was left to solidify at room temperature the second one was prepared in a similar manner and pipetted onto the other half of the bottom layer.

After solidification the cell layer was covered with a second layer of 0.5 % LMP agarose. The prepared 0.5 % LMP agarose was melted in the heat block and approximately 200 to 300 μL were pipetted on top of the cell layer. The microgel was kept at 4 °C for 5 minutes to allow for the solidification of the agarose.

Lysis and Electrophoresis: The microgel was placed in a small glass Petri dish and immersed in a prechilled lysing solution and kept for 1 h on ice in the dark. This procedure was used to lyse the cells and permit the DNA to unfold (Singh, McCoy et al. 1988). Before the microgel was placed into the horizontal electrophoretic unit, it was rinsed in bidistilled water. The short sides of the microgel were in contact with the walls of the platform unit in a way that the cell dots were not lined up one after the other concerning the direction of current flow. Then, the buffer reservoirs were filled with chilled electrophoresis buffer until the liquid completely covered the gel. The microgel was allowed to equilibrate in the buffer for 20 minutes in order to facilitate unwinding of the DNA. The equilibration was followed by a 20-minute electrophoresis at 25 V and \sim 200 mA using an electrophoresis compact power supply. Before and during electrophoresis the unit was kept on ice and in the dark.

The visualisation of DNA damage was performed with an Axiovert 135 microscope, equipped with an excitation filter of 515 – 560 nm and an emission filter of 590 nm. The stained gels were illuminated with a blue-light transilluminator. Images were taken at 200 and 320 magnifications using an AxioCam MRc5 camera, which was attached to the microscope and the image analysis software AxioVision Rel. 4.6. For estimation of DNA damage, a minimum of 50 cells from each sample was scored using TriTek CometScoreTM version 1.5 (free software program).

2.6.2 Cell cycle analysis

518A2 melanoma cells (10^6) were treated with the test compounds, positive (250 $\mu\text{g}/\text{mL}$ nocodazole) / negative (DMF) controls and then harvested at certain time intervals (12, 18 and 24 hours). The cells were washed, re-suspended in 200 μL PBS,

2. Material and Methods

and incubated with 8 mL of 70% ice-cold ethanol for fixation. They were centrifuged, washed with PBS, and re-suspended in 1 mL of a PBS solution of 3.8 mM sodium citrate and 50 $\mu\text{g}/\text{mL}$ propidium iodide with freshly added RNase A (Krishan 1975). After 1 hour incubation at 37 °C the concentration of double-stranded DNA in the samples was determined by measuring (The FACS analysis was performed in the laboratory of Prof. Olaf Stemmann, Genetics Department - University Bayreuth with special assistance of his PhD student Andreas Brown) the emission (570 nm) of its fluorescent adducts excited at 488 nm, using a Beckman CYTOMICS FC 500 cytometer.

2.6.3 DNA fragmentation

The DNA of cancer cells was isolated after the cells have been treated with several test compounds. In order to detect whether the applied chemical compounds caused a DNA fragmentation agarose gel electrophoresis was carried out with the isolated DNA samples. After incubation for 24 hour (5 % CO₂, 95 % humidity, 37 °C) the negative control and the treated cell cultures were trypsinized. Then, the cell suspensions of the samples were transferred into falcon type tubes (50 mL). Following a centrifugation step (800 rpm, 5 minutes), the supernatant was discarded and the pellets were washed twice with 2 mL of PBS. During these washing steps the cell suspensions were transferred into 2 mL Eppendorf reaction tubes. Subsequently, the cell pellets were frozen at -20 °C and melted again in a 37 °C water bath. This freezing/melting-process was repeated three times. Cell pellets were resuspended in 1 mL of lysis buffer and incubated at 60 °C for 5 minutes. Before incubation at 60 °C for 1 hours, RNase A (5 μL) and Proteinase K (2.5 μL) were added to each sample. In order to precipitate proteins after cell lysis, 250 μL of 5 M NaCl were pipetted to the lysis buffer and the suspension was mixed carefully by inverting the reaction tubes several times, which were then kept on ice for 15 minutes. Following a centrifugation at 10,000 rpm for 15 minutes the supernatants with the solved DNA were collected and transferred into a new tube (2 mL), while the pellets of proteins were thrown away. To precipitate the DNA, ice-cold ethanol (100 %) was filled into the tube up to a total volume of 2 mL. The samples were carefully mixed by inversion of the reaction tubes and kept at -20 °C overnight to increase the DNA yield. The tubes were centrifuged (10,000 rpm, 10 minutes) and after washing twice with 70 % ethanol, the DNA pellets were dried using a vacuum centrifuge. The DNA was solved in 1× TE

buffer (10-20 μL depending on the amount of DNA) and the samples were stored at 4 $^{\circ}\text{C}$. For gel electrophoresis the DNA samples were heated (50 $^{\circ}\text{C}$, \sim 20 minutes), 3 μL of loading buffer was added to 7.5 μL of each sample and the DNA was applied to a 1.5 % agarose gel. The 100 - 3000 bp-DNA ladder was mixed with 1 μL of its own loading buffer as well as 5 μL of ddH₂O according to the manufacturer protocol. The electrophoresis was carried out at 85 V and 25 mA in 1 \times TAE buffer for 3 hours. To visualize the DNA bands, the gel was stained with an ethidium bromide staining solution and examined under UV light. Pictures of the stained DNA gels were taken using the software BioCapt (Version 11.02 for Windows).

2.7 Interaction of complex with DNA *in vitro*

2.7.1 Electrophoretic mobility shift assay with native agarose gel

The interaction of test compounds with pBR322 plasmid DNA was studied by agarose gel electrophoresis according to the literature (Chowdhury, Huq et al. 2005). Briefly, 6 μL aliquots of pBR322 plasmid DNA (conc. 73.5 mg/mL) solved in TE buffer were incubated in the presence of increasing complex concentrations (0, 5, 20, 40, 60 μM) dissolved in DMSO. Incubation was carried out in the dark at 37 $^{\circ}\text{C}$ for 24 h. Samples containing 1.5 mg of plasmid DNA were loaded onto a 1% agarose gel, and electrophoresis was carried out in 1 \times TEA buffer for 4 h at 66 V. The gel was then stained in the same buffer containing ethidium bromide (1 mg/mL) and visualized with a transilluminator. The band intensities were analyzed using Image Tools software.

2.7.2 Circular dichroism - secondary structure of DNA-complex

This work I performed in the Laboratory of Prof. Viktor Brabec, introduced by Dr. Kostrhúnová. The circular dichroism (CD) method is applied for the study of optical activity of (macro) molecules in solution (Alison Rodger and Nordén, 1997). Circular dichroism is the difference in absorption of left and right circularly polarized light, which could be changed after interaction with reactive Pt complexes. All measurements were performed on a Jasco Spectropolarimeter. The concentration of Pt-complexes covalently bound to DNA was established after DNA dialysis in 0.01 M NaClO₄. After reaction of calf thymus DNA with the corresponding Pt complex for 24 hours CD spectra were measured under following conditions: Start wavelength 450 nm; End wavelength 220 nm; Step resolution 0.5; Speed 200; Accumulation 3;

2. Material and Methods

Response 0.25 s; Band Width 2; Sensitivity 20 millidegrees. CD spectra were measured in ellipticity $\Delta\epsilon$ [$M^{-1}\cdot cm^{-1}$]. Blank, 0.01M NaClO₄, was measured for each spectrum. Spectrum maxima at wavelength 246 nm and 278 nm were read and compared with spectra of untreated DNA.

2.7.3 Melting temperature of DNA-complex adducts

This work I performed in the Laboratory of Prof. Viktor Brabec, introduced by Dr. Kostrhúnová, Dr. Malina. Samples for measurements of T_m curves were taken from the CD experiments. The absorbance was measured in a mono-block of a spectrophotometer (Varian Cary 4000).

2.7.4 Mono- and bifunctional adduct study

This work I performed in the Laboratory of Prof. Viktor Brabec, introduced by Dr. Kostrhúnová. The oligonucleotide 5'-CCT CTC CTT **GGT** CTC CTT CTC-3' was synthesized on an Applied Biosystems solid-phase synthesizer and purified by ion-exchange FPLC. The single-stranded DNA was allowed to react with a stoichiometric amount of the platinum complex (1:1 ratio). The platinated oligonucleotides were purified by FPLC. It was verified by platinum FAAS and by optical density measurements that the modified oligonucleotide contained just one platinum atom. It was also verified using DMS footprinting (Brabec and Leng 1993; Leng and Brabec 1994) that in the platinated top strands the N7 position of both neighbouring guanines was not accessible for reaction with DMS. DMS methylates the N7 position of guanine residues in DNA, producing alkali-labile sites (Maxam and Gilbert 1980). However, if N7 is covalently bound to platinum, it cannot be methylated. The oligonucleotides were then treated with hot piperidine and analyzed by denaturing polyacrylamide gel electrophoresis. For the nonmodified oligonucleotides, shortened fragments due to the cleavage of the strand at the two methylated guanine residues were observed in the gel. The platinated strands were allowed to anneal with nonplatinated complementary strands in 50 mM NaCl plus 1 mM Tris-HCl with 0.1 mM EDTA, pH 7.4. FPLC purification and FAAS measurements were carried out on a Pharmacia Biotech FPLC System with a MonoQ HR 5/5 column and a Unicam 939 AA spectrometer equipped with a graphite furnace, respectively.

2.7.5 Radioactive 3'-ends labelling of plasmid DNA

This work I performed in the Laboratory of Prof. Viktor Brabec, introduced by Dr. Kostrhúnová, Dr. Zerzánková.

Incorporation of [γ - ^{32}P]dATP: an aliquot of linear plasmid DNA ($\sim 1 \mu\text{g}$) was dissolved in a total volume of $10 \mu\text{L}$ with $2 \mu\text{L}$ of $5\times[\gamma]$ ATP buffer, $2 \mu\text{L}$ of 24% aqueous polyethylene glycol (PEG). One of the last components were $1 \mu\text{L}$ of [γ - ^{32}P]ATP and $1 \mu\text{L}$ of T4 polynucleotide kinase. Reaction mixture was incubated for 30 minutes at 37°C and loaded into pre-prepared sephadex G-50 column in total volume of $100 \mu\text{L}$. Radioactively labeled pSP 73 KB was collected and used in the experiment.

Incorporation of [α - ^{32}P]dATP: An aliquot of linear plasmid DNA ($\sim 1 \mu\text{g} \approx 3 \mu\text{L}$ of $c = 334.9 \mu\text{g/mL}$) was solved in the total volume of $10 \mu\text{L}$ with $1 \mu\text{L}$ of Neb II buffer, $1 \mu\text{L}$ of enzyme Klenow fragment and $5 \mu\text{L}$ of water. After all components $1 \mu\text{L}$ of [α - ^{32}P]dATP was placed. Reaction mixture was incubated for 30 minutes at 37°C and $1 \mu\text{L}$ of Klenow fragment was added and incubated for additional 30 minutes. After loading onto the pre-prepared Sephadex G-50 column in a total volume of $100 \mu\text{L}$, radioactively labeled plasmid DNA was collected and used for the next experiments.

2.7.6 Interstrand cross-links study in denatured agarose gel

This work I performed in the Laboratory of Prof. Viktor Brabec, introduced by Dr. Kostrhúnová, Dr. Zerzánková. Plasmid DNA pSP 73 (2464 bp) was cleaved using restriction enzyme EcoRI (5'-G•AATTC-3'). Linear DNA was deproteinised (phenol:chloroform mixture), precipitated (2 x 100% ethanol; 1/10 of sodium acetate) and dissolved in dH_2O .

For ethidium bromide staying: Linear pSP73 KB was incubated with test compounds at various r_b values and incubated in the dark for 24 hours at 37°C (after dialysis the Pt-content was verified by FAAS or ICP). A denatured 1% agarose gel was kept in denaturation buffer overnight. Samples with loading buffer (6x) and 0.03 M NaOH were loaded onto the gel in freshly prepared denaturation buffer. The gel was running overnight with 0.5 V/cm. After neutralization the gel was kept in 1xTBE at 4°C for 30 minutes. After ethidium bromide staining the gel was visualised on a transilluminator.

2. Material and Methods

For radioactive labelling: An aliquot of DNA was incubated with radioactive [γ - 32 P]dATP according to 2.7.5. Radioactive linear DNA was purified chromatographically via a Sephadex G-50 column and the intensity was measured on a Geiger-Müller counter. Labelled linear DNA was mixed with nonradioactive DNA at various r_b values of the corresponding Pt complex and incubated at 37°C in the dark for 24 hours. A denatured 1% agarose gel was kept overnight in denaturation buffer. Samples containing loading buffer and 0.03 M NaOH were loaded onto the gel in freshly prepared denaturation buffer. The gel was running over-night at 0.5 V/cm. The gel was dried under vacuum and a sensitive imaging plate was placed onto the gel. After 3 hours autoradiograph were read with a Fujifilm reader.

The autoradiogram shows interstrand cross-links with platinum (IEC/Pt) and single-strand DNA (IEC/DNA). The quantification of random distribution of Pt-based cross-links in the DNA was performed by Poisson equation of the IECs (Equation 2- 3) (Jones, Zhen et al. 1991),

Equation 2- 3 Poisson distribution of interstrand cross-links.

$$Pt/DNA = 2 \times 2464 \times r_b ;$$

$$IEC/DNA = -\ln(ss) ;$$

$$IEC/Pt = \frac{IEC/DNA}{Pt/DNA}$$

where 2464 – plasmid base pairs number; $\ln(ss)$ – negative \ln (fraction of DNA molecules free of IECs).

2.7.7 Inhibition of RNA synthesis

This work I performed in the Laboratory of Prof. Viktor Brabec, introduced by Dr. Nováková, B. Lišková. The whole experiment was performed according to the instructions of the Promega kit manual of Riboprobe® *in vitro* Transcription systems (Lemaire, Schwartz et al. 1991). Plasmid DNA pSP 73 KB (2455 bp) was cleaved by restriction enzymes, Nde I and Hpa I, and two fragments of specific size were obtained. After phenol deproteination followed by DNA precipitation with ethanol, the DNA was dissolved in 0.01 M NaClO₄. The linear DNA fragment (212 bp) was treated with the corresponding platinum complex ($r_b = 0.02$) for 24 hours at 37°C. After incubation $\frac{2}{3}$ of the sample was dialysed and the real concentration of Pt was

measured by FAAS analysed. The modified DNA ($\frac{1}{3}$) was placed into the reaction mixture of 1 x transcription buffer in the presence of all four NTPs (ATP, GTP, CTP, UTP) and the radioactive isotope [α - 32 P]dCTP at 37°C for 1 hour. In the case of nucleotide sequence analysis the reaction mixture was enriched with one of the 3'-dNTP terminators (3'-dATP, 3'-dGTP, 3'-dCTP, 3'-dUTP). Precipitation of the RNA transcript and the free nucleotides was carried out in 100% ethanol and 2.5 M ammonium acetate. The sediments were dissolved in water and precipitated again in 80% ethanol with 1 M ammonium acetate, washed with 100% ethanol and dried under vacuum for 10 minutes. The radioactivity of the aliquots was optimised with RNA-loading buffer for 250 Bq (1 Bq = 2.70×10^{-11} Ci = pulse pre seconds) on the Geiger-Müller counter. The denatured polyacrylamide (PAA) gel (PAA: 50% urea = 19:1; 0.3 mm thin) for RNA inhibition consisted of two parts. At first, the bottom gel was prepared from 8% acryl amide with 30 μ L of 25% APS + 50 μ L TEMED in 50 mL and polymerized ~6 hours before loading. Electrophoresis was performed in 1 x TBE buffer approximately for 90 minutes, 1 V/cm (length of electrophoresis glasses 40 cm). The bottom glass was removed and a sensitive imaging plate was placed onto the gel. After 3 hours a Fujifilm reader took autoradiographs and the plate was de-excited by Eraser.

2.7.8 Measurement of DNA-Pt content

2.7.8.1 Samples preparation for FAAS

This work I performed in the Laboratory of Prof. Viktor Brabec, introduced by Dr. Nováková. The amount of platinum in DNA samples was measured on a Zeeman Flame Atomic Absorbtion Spectrophotometer (FAAS). First, the platinum concentration was recalculated (Equation 2- 3) from known concentrations of DNA according to the sensitivity of the FAAS method, which is varying between 1×10^{-6} – 5×10^{-7} M of Pt. Samples were diluted in water and the experimental r_b value was calculated.

2.7.8.2 Samples preparation for ICP-OES

Pt contents were measured via Inductive Coupled Plasma Optical Emission Spectroscopy (ICPOES, BayCEER service). First, salmon sperm DNA (10 mg) was dissolved in 0.9 mL of TE buffer and 10 mM NaClO₄. The chalcone-Pt complex was

2. Material and Methods

dissolved in DMF to a final concentration of 100 μM . Negative controls contained just DMF, while 100 μM cisplatin (CDDP) served as a positive control. The DMF content per mL was 1%. After 48 h of incubation the samples were poured into the doubled volume of 100% ethanol, left standing overnight, and the resulting DNA precipitates were collected. They were washed with 70% ethanol, DMF and centrifuged (10 minutes, 8200 rpm). The pellets obtained were washed again with 70% ethanol, re-dissolved in 200 μL of TE buffer and 200 μL of DMF for 1 hour, and finally DNA was precipitated with 100% ethanol, washed and lyophilized. The DNA samples obtained were treated at 170 $^{\circ}\text{C}$ in a sealed vial with a mixture of 0.5 mL each of HNO_3 and HCl for 7 hours. After cooling to room temperature the resulting solutions were filled up with water up to a volume of 10 mL and submitted to ICP-OES.

2.8 Apoptotic signals

2.8.1 Colorimetric caspase assay

The caspase assay employs N-acetyl-Asp-Glu-Val-Asp-p-nitroaniline (Ac-DEVD-pNA) as a substrate for caspase-3 enzyme and the irreversible inhibitor Ac-DEVD-CHO. The HL 60 leukaemia cells were incubated with or without 1 μM of test compounds (dissolved in DMF). For each sample 6 million cells were used during a 24 hours incubation time, washed twice with PBS, centrifuged at 1200 rpm, and the pellet was stored at -20°C until used.

The cellular activity of caspases was studied in cell lysates, which were obtained by multiple freeze-thaw procedure in the presence of caspase buffer (Thornberry 1994). The assay was carried out in a total volume of 100 μL in a 96-well plate (Greiner bio-one). Crude extracts were diluted 10-fold with caspase buffer; caspase-inhibitor DEVD-CHO (Biomol) was added in 20 μM final concentration and incubated for 15 minutes at 37°C . The substrate for caspase 3 (Ac-DEVD-pNA) was supplied in a concentration 200 μM and absorbance was measured at 405 nm using MWG-Biotech micro-plate reader. Measurements were performed every 15 minutes over 3 hours. The initial rate of hydrolysis was determined from observed progress curves with/without inhibitor. The cleavage of caspase-substrate was calculated only from the initial slope of the absorbance vs. time curves (the linear portion of the progress curves). Concentration of cleaved substrate and rate of released p-

nitroaniline [pmol/min/ μg of protein] was calculated basing on the extinction coefficient of pNA ($9920 \text{ M}^{-1} \cdot \text{cm}^{-1}$) with initial slope kinetic in minutes.

2.8.2 Intracellular concentration of Ca^{2+}

The cells were incubated with/without test compounds, harvested, and cell pellets were resuspended in 2 mL of Ca-buffer. Cell concentrations were established for each sample. A centrifugation step (800 rpm) of the samples followed for 5 minutes, before the cell pellets were resuspended in fresh Ca-buffer. The samples were adapted to a density of 1.3×10^6 cells/mL. After resuspending the pellets in the individual volumes of Ca^{2+} -buffer, 0.75 mL of the sample was mixed with 0.25 mL of Ca^{2+} -suspension in a 1.5 mL Eppendorf vial followed by incubation in the dark for 30 minutes. A centrifugation (800 rpm, 5 minutes) as well as a washing step with Ca^{2+} -buffer followed. The resulting pellets were resuspended in 0.5 mL of fresh Ca^{2+} -buffer and kept in the dark for another 15 minutes.

The fluorescence of the samples was measured in a 3 mL glass cuvette (2 mL Ca^{2+} -buffer, 0.5 mL sample) at the emission wavelength ($E_m = 510 \text{ nm}$) during a time period of 10 minutes using a fluorescence spectrometer. The excitation wavelength was $E_x(1) = 340 \text{ nm}$ and $E_x(2) = 380 \text{ nm}$. About 3 minutes after starting of the measurement 10 μL of digitonin were added to the cuvette and later 50 μL of EGTA were pipetted into the sample. The fluorescence signals were visualized using VL WinLab Version 4.00.03.

2.9 Drug resistance

2.9.1 Activity of P-gp transporters in KBv1 cells - calcein assay

This assay was carried out with slight modifications according to a literature procedure (Kohno, Kikuchi et al. 1988). Briefly, KBv1/KBv1^{+vbl} cells were trypsinised on the 3rd or 4th day after passaging and washed with PBS at 25 °C. Cells ($1.3 \times 10^6/\text{mL}$) were resuspended in 0.75 mL of Ca-buffer and 0.25 mL of Cs-buffer was added. The samples were mixed with 50 μM of test substances, shortly vortexed and incubated for 15 minutes. Calcein-AM was added to achieve a concentration of 1 μM . After incubation (10 minutes, 37 °C, 5% CO_2), and centrifugation (800 rpm, 5 minutes, 4 °C) a cell pellet was obtained which was rinsed once with ice-cold PBS and re-suspended in 0.5 mL of Ca-buffer. The fluorescence of calcein ($\lambda_{E_x} = 485 \text{ nm}$, $\lambda_{E_m} = 535 \text{ nm}$) was measured in a black 96-well microplate on a TECAN Infinite

2. Material and Methods

F200 plate reader. Data were analysed and calculated relative to a positive control (verapamil).

2.9.2 Activity of BCRP transporters in MCF-7 cells - mitoxantrone assay

The assay was carried out according to literature procedures (Kuhnle, Egger et al. 2009). MCF-7^{Top} cells were incubated with 20 μ M mitoxantrone in 70% ethanol and vortexed. 10 μ M of the test compounds dissolved in DMF were added to allow maximal mitoxantrone uptake into the cells over a period of 30 minutes at 37 °C. After centrifugation (800 rpm, 5 minutes, 4 °C) the cells were washed twice with PBS, pipetted into a black microplate together with the positive control fumitremorgin C (FTC) and the negative control (only DMF). The plates were immediately placed in a TECAN fluorescence plate reader and the mitoxantrone fluorescence was measured at 620 nm excitation and 670 nm emission wavelengths. Three wells of each plate contained the internal standard FTC (10 μ M). Its cellular fluorescence was taken and set to 100% BCRP inhibition.

2.9.3 Repair DNA synthesis by human cell extracts

This work I performed in the Laboratory of Prof. Viktor Brabec, introduced by Prof. Dr. Kašpárková, Muchová T, Suchánková T. *Preparation of cell free extract CFE:* Cells were seeded into the flasks and were grown as monolayer. Trypsinated cells were washed with ice-cold PBS; the pellet was carefully re-suspended in 1 mL of lysis buffer I and was kept on ice for 10 minutes. After centrifugation (800 rpm 4°C 10 minutes) the pellet was carefully re-suspended by lysis buffer II and directly centrifuged as previously described. Into the pellet 0.5 mL of nuclear extraction buffer III was added and the sample was slowly rotated for 30 minutes at 4°C. After centrifugation (15 minutes, 12 000 rpm, 4°C) the supernatant was put into a new Eppendorf vial, which was directly frozen at -80°C.

The measurement of DNA repair by CFE was performed according to literature procedures (Henderson 1999). Repair DNA synthesis by cell-free extracts CFE was assayed using pUC19 plasmid. Each reaction of 50 μ L contained 600 ng of nonmodified pBR322 and 600 ng of nonmodified or platinated pUC19, 2 mM ATP, 30 mM KCl, 0.05 mg mL⁻¹ creatine phosphokinase (rabbit muscle), 20 mM each of dGTP, dATP, and dTTP, 8 mM dCTP, 74 kBq of [α -³²P]dCTP in a buffer composed of 40 mM HEPES-KOH, pH 7.5, 5 mM MgCl₂, 0.5 mM dithiothreitol, 22 mM

creatine phosphate, 1.4 mg of bovine serum albumin/mL, and 20 mg of CFE from the HeLa S3 or melanoma 518A2 cells. Reactions were incubated for 3 h at 30°C and terminated by adding Na₂H₂EDTA to a final concentration of 20 mM, SDS to 0.6%, and proteinase K to 250 mg mL⁻¹. After incubation for 20 minutes, the products were extracted with one volume of 1:1 phenol/chloroform. The DNA was precipitated from the aqueous layer by the addition of 0.1 volume of 3 M sodium acetate and 2.5 volumes of ethanol. After 30 minutes of incubation at -20 °C and centrifugation at 12 000 g for 30 minutes at 4 °C, the pellet was washed with 0.2 mL of 80% ethanol and dried in a vacuum centrifuge. DNA was linearized before electrophoresis on a 1% agarose gel. After staining with ethidium bromide, the agarose gel was dried under vacuum and an autoradiograph was prepared (Fujifilm reader). The autoradiograph was analysed using the AIDA program. The experiments were carried out in quadruplicate.

2.9.4 Reaction of Pt-complex with glutathione

The assay was performed according to (Ishikawa and Ali-Osman, 1993). Briefly, glutathione (GSH; 3.33 mM) was incubated with 1.67 mM cisplatin (or complexes **1**, **2**, **3**) in 1 mL of PBS at 37 °C. At different time points (48 hours period), 20 μL aliquots of the reaction mixture were taken, diluted with 980 μL of PBS, and the absorption spectra of the resulting solutions were measured by (Zoldakova and Schreder 2009) scanning spectrophotometry (Shimadzu UV-160 spectrophotometer).

Effects of chalcone (1)

Chalcones are 1,3-diaryl-2-propen-1-ones which build the core of many biologically active compounds (Biersack, 2009; Zoldakova, 2010). The methoxysubstituted chalcone (1) (Figure 3- 3) has shown high antitumor activity against leukaemia cells due to efficient tubulin polymerisation inhibition (Ducki et al., 1998). Because of its high activity and easy preparation chalcone (1) was chosen for testing and for further modifications leading to various platinum(II) and ruthenium(II) conjugates aiming at more potent drug candidates with multiple and synergistic modes of action.

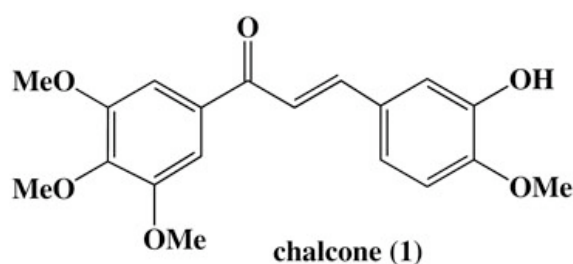


Figure 3- 1 Structure of the tubulin binding chalcone (1).

3.1 Inhibition of cell growth - MTT assay

The MTT assay is widely used as a rapid and sensitive method for the screening of the cytotoxic activity of anticancer drugs. It bases on the tetrazolium salt (3-[4,5-dimethylthiazol-2-yl]-2,5-diphenyltetrazolium bromide), which is turned into a formazane dye in the mitochondria of living cells. The formation of this formazane dye can be quantified colorimetrically. Hence, this assay was used to characterize chalcone cytotoxicity on different cell lines.

3.1.1 Neural cells

Chalcone (1) targets tubulin and microtubules (Hadfield et al., 2003). In addition, chalcone derivatives isolated from the stem bark extract of a Brazilian medicinal plant (*Myracrodruon urundeuva*) displayed neuroprotective properties (Nobre-Junior et al., 2009). Tubulin-rich cells of neural origin (astroglia, U87, neurons, NE-4C, C6) were obtained and assayed in the laboratory of Dr. Emília Madarasz (Neural Cell Biology Institute in Budapest, Hungary). Relative cytotoxicities of chalcone (1) against the neural cells as well as for WEHI 164 mouse fibrosarcoma are listed in Table 3- 1.

The murine astroglia cells remained resistant to compound 1 during the whole

3. Effects of chalcone (**1**)

48 h incubation period (Table 3- 1). The human U87 glioma cells responded well upon prolonged exposure. The primary neurons were likewise sensitive to a prolonged treatment with **1**. Surprisingly, the sensitivity of C6 rat glioma cells with IC_{50} (48 h) ~ 150 nM for chalcone treatment could be promising for further pharmacological investigations. NE-4C cells, derived from the fore- and midbrain vesicles of p53-deficient 9-day-old mouse embryos (Schlett and Madarasz, 1997), were also strongly sensitive towards **1** after exposure for 48 h. The tested WEHI 164 fibrosarcoma cells were less sensitive than NE-4C or glial C6 cell towards chalcone (**1**) ($IC_{50} > 10 \mu M$).

Table 3- 1: Inhibitory concentrations (IC_{50} in μM) of chalcones (1**) in various neural (astroglia, neurons, NE-4C, U87, C6) and non-neural cells (WEHI 164).**

Cell line	Astroglia	U87	Neurons	NE-4C	C6	WEHI 164
24 h (1)	55 \pm 5	45 \pm 5	38 \pm 6	2.8 \pm 0.6	0.5 \pm 0.08	11 \pm 1
48 h (1)	33 \pm 3	0.6 \pm 0.3	1.3 \pm 0.1	0.024 \pm 0.001	0.15 \pm 0.02	15 \pm 3

The *in vitro* cytotoxicities of chalcone (**1**) vary within the series of tested cell lines. It was shown that activation of p53 leads to apoptosis by affecting the cell cycle in the G1/S phase (Eliyahu et al., 1984; Finlay et al., 1989). The tumor suppressor protein p53 is involved in the prevention of cancer development. Obtained cytotoxicity results are indicating p53-independent mechanism of chalcone (**1**) due to rapid activity in NE-4C cells (after 48h $IC_{50} \sim 24$ nM). The specificity of complex **1** to glioblastoma (U87 and C6) cells differed dramatically when compared with neural astroglia cells (factor of ~ 100). How can we rationalize this observation?

The PI3K/Akt pathway plays a significant role for endocytotic drug uptake (see chapter 3.2.2). Remarkably, the PI3K/Akt pathway is highly up-regulated in gliomas due to deletion or mutation of tumor suppressor lipid phosphatase (PTEN). PTEN activation is associated with tumor malignancy (Puli et al., 2010). In addition, recent studies of glioma cells (including U87) have shown that the activation of the Akt-pathway induces premature senescence (Lee et al., 2010). It is possible that a correlation exists between up-regulation of PI3K/Akt pathway and higher cytotoxicity in gliomas.

3.1.2 Cancer cells expressing ABC-transporters

ABC-transporters pump drugs out of cancer cells and are responsible for chemoresistance (de Bruin et al., 1999; Rabik and Dolan, 2007; Robey et al., 2007). Their interference with chalcone (**1**) was investigated by using various non-neural cancer cells: MCF-7 breast, KBv1 cervix and HT-29 colon carcinomas. Each of these cell lines expresses a specific member of the ABC-transporters family. The protein expression can be enhanced in the presence of a suitable inducer or substrate (*c.f.* *Materials and Methods*). Hence, the cells were grown in the presence of specific substrates of their transporters (Table 3- 2).

Table 3- 2: Inhibitory concentrations (^aIC₅₀ in μ M) of chalcone (1**) in various ABC-transporter expressing cells.**

Cell line	MCF-7	MCF-7 ^{+Top}	KBv1	KBv1 ^{+Vbl}	HT-29	HT-29 ^{+Colc}
24 h (1)	10.7 \pm 1.3	12.5 \pm 3.1	1.6 \pm 0.1	2.0 \pm 0.3	43 \pm 3	37 \pm 6
48 h (1)	13.4 \pm 1.1	1.6 \pm 0.1	0.7 \pm 0.05	0.2 \pm 0.04	37 \pm 1	24 \pm 6

^aValues are derived from concentration-response curves obtained by measuring the percentual absorbance of vital cells relative to untreated controls (100%) after 24 and 48 h exposure of selected cells to test compounds in the MTT assay. Values represent means of at least three independent experiments \pm standard deviation.

By long-term exposure to topotecan resistant MCF-7^{+Top} cells were obtained which overexpress exclusively BCRP (breast cancer resistance protein). Chalcone (**1**) revealed cytotoxic activity in these MCF-7^{+Top} cells [IC₅₀ (24 h/48 h) \sim 12 / 1 μ M]. It showed the same IC₅₀ value in +wild type MCF-7 cells after 24 h, which remained constant for up to 48 hours. Resistant KBv1^{+Vbl} cells overexpressing P-gp were obtained by treating the cells with vinblastine. Chalcone (**1**) was highly and comparably efficacious against both cell lines with a slight edge for the vinblastine-treated cells.

HT-29 cells feature a high amount of multi-resistance protein 3 (MRP3) and a low amount of MRP1. Treatment of HT-29 cells with colchicine shift this ratio by overexpressing MRP1 and cutting back on MRP3 (Kok et al., 2000). Although chalcone (**1**) was little active in HT-29 cells, it showed a little bit higher activity in the HT29^{+Colc} cells. The net effect was positive and the efflux of chalcone (**1**) was reduced in HT29^{+Colc} cells.

3. Effects of chalcone (**1**)

3.1.3 518A2 melanoma and HL60 leukemia cells

Human 518A2 melanoma and suspension HL60 cells served, as reference cells since they do not express any ABC-transporter. The cytotoxicity of **1** in 518A2 cells reached IC_{50} values of $11.5 \pm 0.6 \mu\text{M}$ after 24 hours of incubation, which increased almost 12-fold ($IC_{50}=1.0 \pm 0.4 \mu\text{M}$) after 48 hours. A longer exposure led again to a decrease of the IC_{50} values ($32 \pm 7.5 \text{ nM}$ after 96 hours) (Schobert et al., 2009).

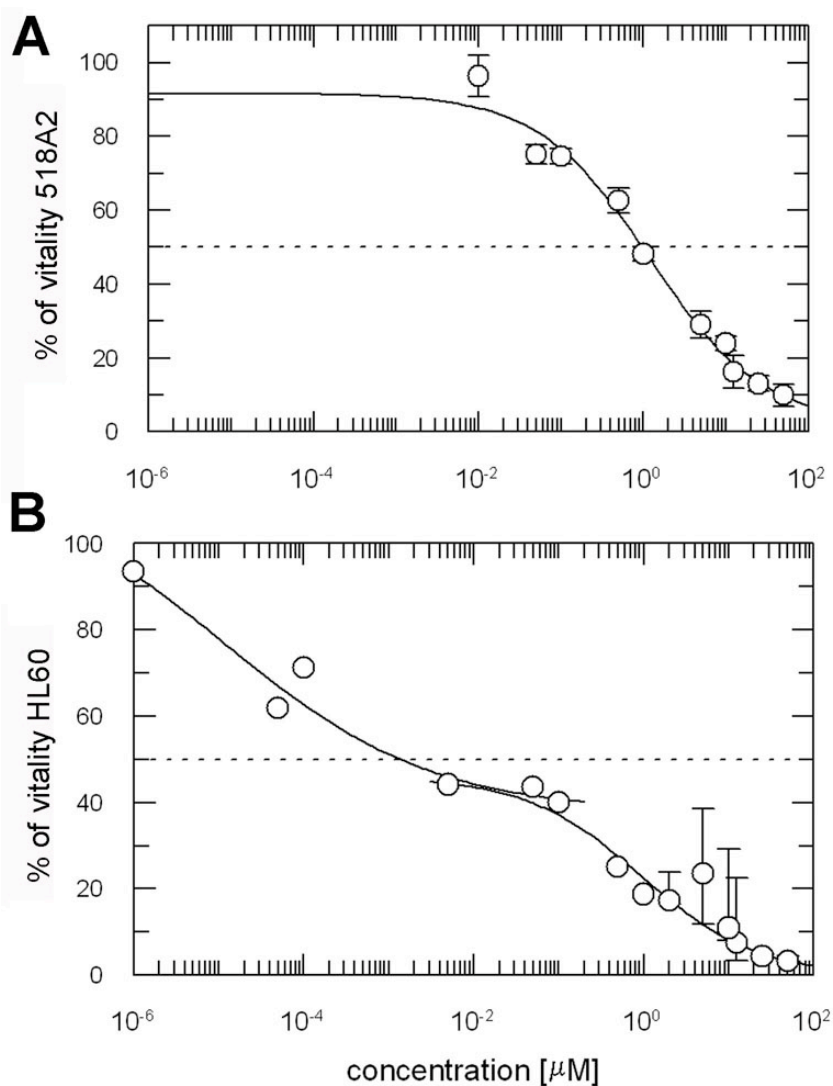


Figure 3- 2 Cytotoxicity of chalcone (**1**) on (A) 518A2 and (B) HL60 cells after 48 hours treatment. The solid lines are calculated IC_{50} curve-fits from equation 2-2 analysed by GraFit program.

The activity of **1** against HL60 leukemia cells was 1000-fold higher in comparison with the 518A2 melanoma cells (IC_{50} 24 h/48 h = $1.7 \pm 0.4/ 0.17 \pm 0.03 \text{ nM}$). The dose-response curves for the 518A2 and HL60 cells (Figure 3- 2) show an unusual biphasic profile which originates from its tubulin binding properties and, at high concentration, from an additional cytotoxic mode of action (see *chapter 4.1.3.*).

3.2 Cellular uptake of chalcone (1)

Chalcone (1) is known for its tubulin binding activity. Hence, it should enter the cell by passing the membrane and trigger an action inside of the cell. In order to ascertain how 1 enters the cells, several inhibition-based studies were performed.

3.2.1 Inhibition of endocytosis by temperature change

It is well known that the process of endocytosis is virtually halted at temperatures below 16 °C (Punnonen et al., 1998; Stirling et al., 2009). In this work the conditions were optimized for 518A2 melanoma cells at 4 °C and for the drug concentration close to IC₅₀. Generally, the IC₅₀ drug concentration approximates an inflection point of the dose-response curve. From the mathematical point of view, the greatest sensitivity and response toward changes is achieved at the inflection point. Moreover, for the small changes a linear dependence might be assumed.

After 3.5h incubation with 100 μM chalcone (1) ~50% of the cells were alive/dead. Almost twice as many 518A2 melanoma cells survived exposure to 100 μM of 1 at 4°C when compared to 37°C, which is an indication of this chalcone being taken up mainly *via* endocytosis (Figure 3- 3).

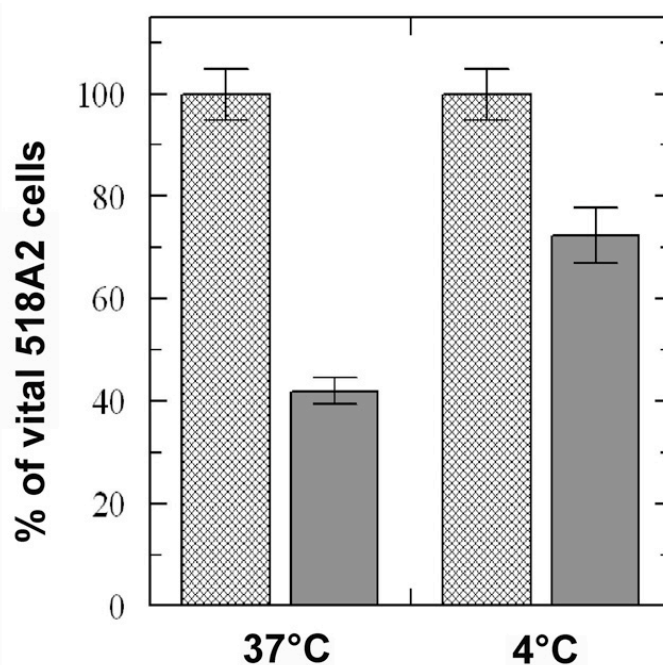


Figure 3- 3 Vitality of 518A2 cells after 3.5 h exposure to chalcone (1) (100 μM; grey bars). Vital cells were determined by MTT assay at 37 °C and 4 °C. Vital cells of untreated controls (hatched bars) set to 100%.

3.2.2 Inhibition of the uptake of chalcone (1) with specific inhibitors

Based on previous results, the detailed mode of uptake of chalcone (1) was studied. Specific inhibitors were used to inhibit pertinent pathways of drug entry

3. Effects of chalcone (**1**)

under the same conditions as described in chapter 3.2.1. Kapp et al. carried out similar studies by blocking individual transporters with specific inhibitors (Kapp et al., 2006).

Some endocytotic processes are dependent on a sodium gradient, which can be slowed down by ouabaine, an inhibitor of the Na^+/K^+ pump (Ivanov et al., 2004). Macropinocytosis, a special form of endocytosis, depends on a Na^+/H^+ exchanger that can be blocked by amiloride (Kapp et al., 2006; Meier et al., 2002). The enzyme phosphatidylinositol 3-kinase (PI3-kinase) plays a central role in the down-stream signalling cascade associated with macropinocytosis by F-actin microfilament rearrangement and can be inhibited by the fungal metabolite wortmannin (Zhang et al., 2003). Clathrine-mediated endocytosis can be blocked by chlorpromazine (Nawa et al., 2003). Alternative ways for the entry of positively charged complexes into cells involve copper transport receptor 1 proteins (Ctr1) and organic cation transporters (OCT- 1/2). The OCT conveys positively charged substances and may be inhibited by cimetidine (inhibitor) or tetraethylammonium chloride (TEA; competitor).

After optimisation of the inhibitor concentration, the influence of all these inhibitors on the uptake of chalcone (**1**) into 518A2 melanoma cells was examined as these cells lack all sorts of influx pumps. To this end, the cells were pre-incubated with non-toxic concentrations of the respective inhibitors for 15 min before chalcone (**1**) was added and its cytotoxicity was measured by the pertinent MTT assay. Figure 3- 4a illustrates the effects of the individual inhibitors on the cytotoxicity of chalcone (**1**) (grey bars) against 518A2 cells. An increase in cell vitality indicates interference with the uptake of **1** (Figure 3- 4b).

Treatment of 518A2 cells with $100 \mu\text{M}$ chalcone (**1**) for 3.5 h in the absence of any inhibitor left 40% of the cells alive. Pre-incubation with $5 \mu\text{M}$ ouabaine left $67 \pm 5\%$ of the cells alive. This means that ca. 40% of chalcone (**1**) were accumulated by the cells *via* Na^+/K^+ -dependent endocytosis. Addition of $10 \mu\text{M}$ amiloride led to $55 \pm 2\%$ of surviving cells. This corresponds to an uptake of ca. 24% *via* Na^+/H^+ pump driven macropinocytosis. Addition of $14 \mu\text{M}$ chlorpromazine resulted in ca. 50% of vital cells, which speaks for 18% uptake through clathrine-mediated endocytosis. In the presence of 10 nM wortmannin the percentage of vital cells decreased to $48 \pm 3 \%$, indicating a contribution of 13% from PI3-kinase associated macropinocytosis. Interestingly, the inhibitory effect of wortmannin was time-dependent and most pronounced at the beginning (1-2 hours – data not shown) of the incubation with **1**.

Inhibition of OCT-1/2 and Ctr1 had little influence (2-3%) on the cytotoxicity of **1**.

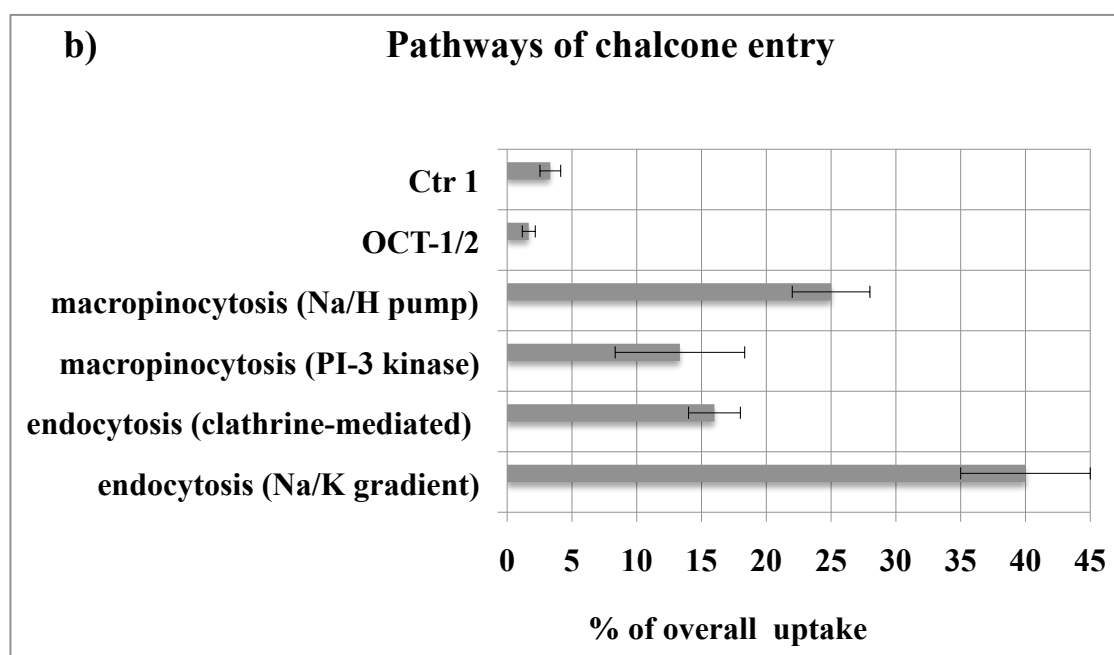
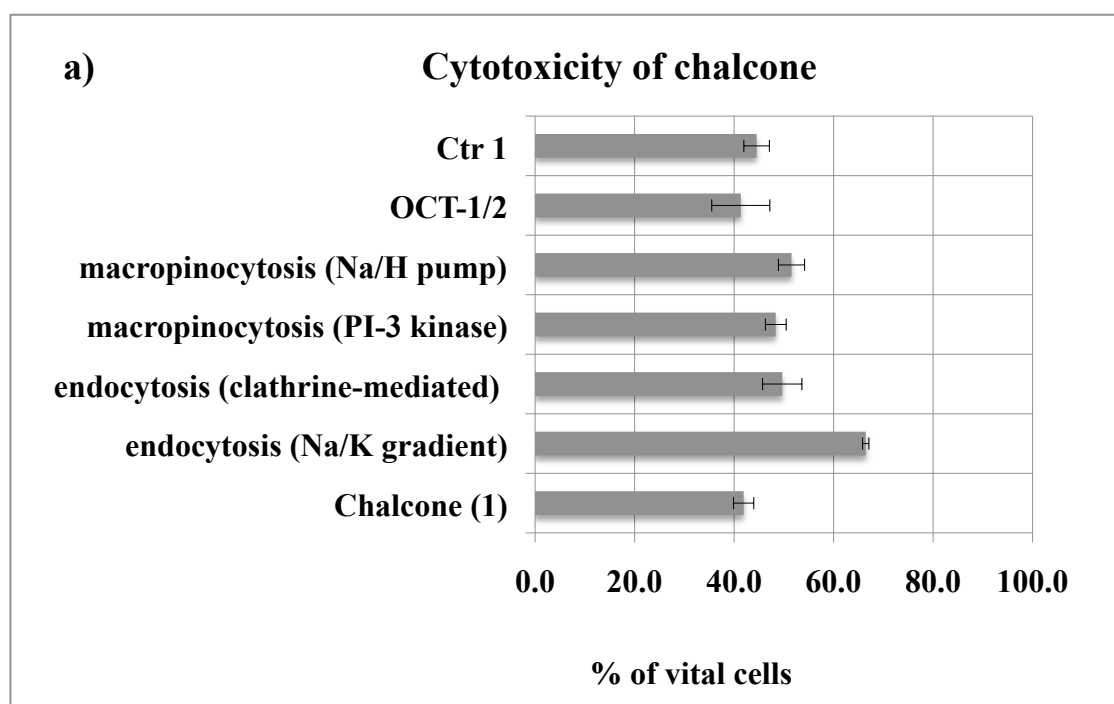


Figure 3- 4a) Effects of the individual inhibitors on the cytotoxicity of chalcone (**1**). b) Contribution of various pathways to the accumulation of chalcone (**1**) (grey bars) by 518A2 melanoma cells as calculated from the attenuation of their cytotoxicity (from a) upon addition of specific inhibitors.

All these inhibitors interfere with endocytotic processes by inhibiting different types of transporters. A pronounced effect of the PI3-K inhibitor after short-term treatment may indicate a switch between various uptake pathways. 518A2 cells are mTOR positive and PI3-K/Akt-signalling regulates mTOR activity (Beuvink et al., 2005; Biersack et al., 2010) whose expression may be affected by chalcone (**1**). Hence, any inhibition of PI3-kinase might postpone the cytotoxic effect of **1**. Indeed,

3. Effects of chalcone (1)

addition of chalcone (1) led to phosphorylation and activation of the Akt-protein as shown by Western blot analysis (Antje Grotemeier, personal communication).

3.3 Cellular and sub-cellular observations

3.3.1 Inhibition of drug uptake monitored *via* time-lapse recording

To verify the results from the uptake studies employing specific inhibitors, time-lapse micrographs of 518A2 cells pre-treated with 10 μ M amiloride (an inhibitor of the Na⁺/K⁺ pump and related endocytosis) were taken. First, cells were treated with chalcone (1) alone. After a few minutes, cell motility and detachment increased (Figure 3- 5). After pre-treated with 10 μ M amiloride, cells detachments and enhanced cell motility is postponed. These results are in line with aforementioned data (in chapter 3.2.2), where overall % uptake *via* Na⁺/H⁺ pump depending endocytosis (which is inhibited by amiloride) was ~25%.

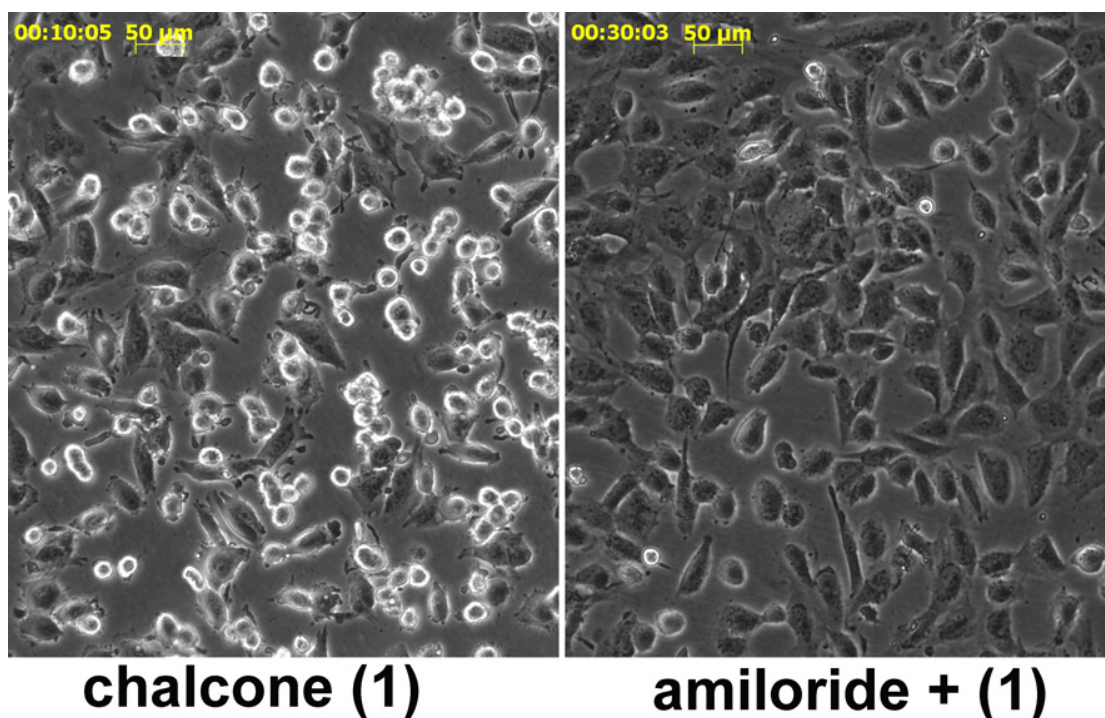


Figure 3- 5 Inhibition of chalcone uptake. Time-lapse recording micrographs of 518A2 melanoma cells incubated with 10 μ M chalcone (left) and pre-treated with 10 μ M amiloride (right), an inhibitor of endocytosis (micropinocytosis).

3.3.2 Altered cell shapes in cells treated with chalcone (1)

3.3.2.1 Altered cell shape in neural cells

Neurons are particularly rich in tubulin and so are well suited to test agents affecting microtubule organisation. Their regular growth requires microtubules being

transported from the cell body all the way down into the axon (Hasaka et al., 2004). The effect of chalcone (**1**) on the structure, development and movement of a network of rat neurons was now monitored by time-lapse microscopy (Hegedus et al., 2000).

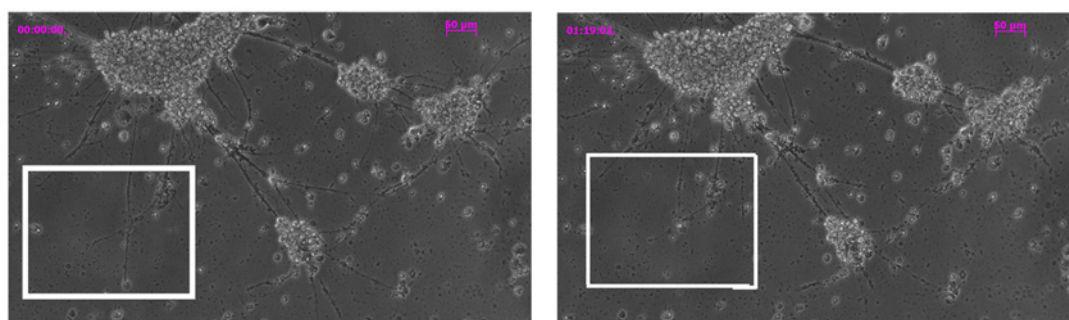


Figure 3- 6 Neuron treated with chalcone (1**) and its retraction process of dendrites and axon back to soma. The left picture shows neuron taken in the time of 0 minutes. The square is zoomed in the next Figure 3- 7. The right picture shows a neuron taken after long time exposure (1 hour 39 minutes) and the retraction processes are finished with dendrites debris.**

Neurons treated with 10 μM of the test compounds showed a retraction (Figure 3- 6) of their processes back to the soma within 20 – 30 minutes Figure 3- 7.

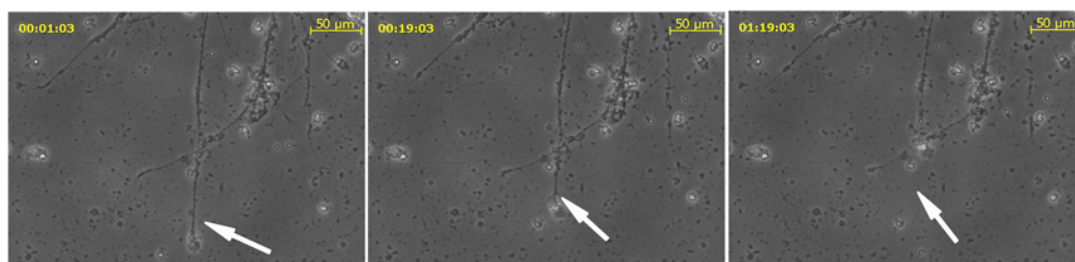


Figure 3- 7 Blow up of the white window shown in the Figure 3- 6 – time course of the axon retraction after addition of chalcone (1**).**

The anticancer agent combretastatin A-4 binds to the colchicine-binding site of β -tubulin and interferes with the polymerization of tubulin.

Chalcone (**1**) is a surrogate of combretastatine A-4 and its inhibition of tubulin polymerization was proved (Schobert et al., 2009). The neurons derived from mice brains showed similar behaviour (Figure 3- 8a, b) as isolated rat neurons. Neurons got closer to each other; their bodies were swelling and aggregating.

Most of the neural network lost its integrity and processes were disconnected from the cells bodies of adjacent neurons.

Altered neuron shapes after treatment with chalcone (**1**) may depend on the inhibition of tubulin polymerization and may indicate possible microtubule disruption in the cells.

3. Effects of chalcone (1)

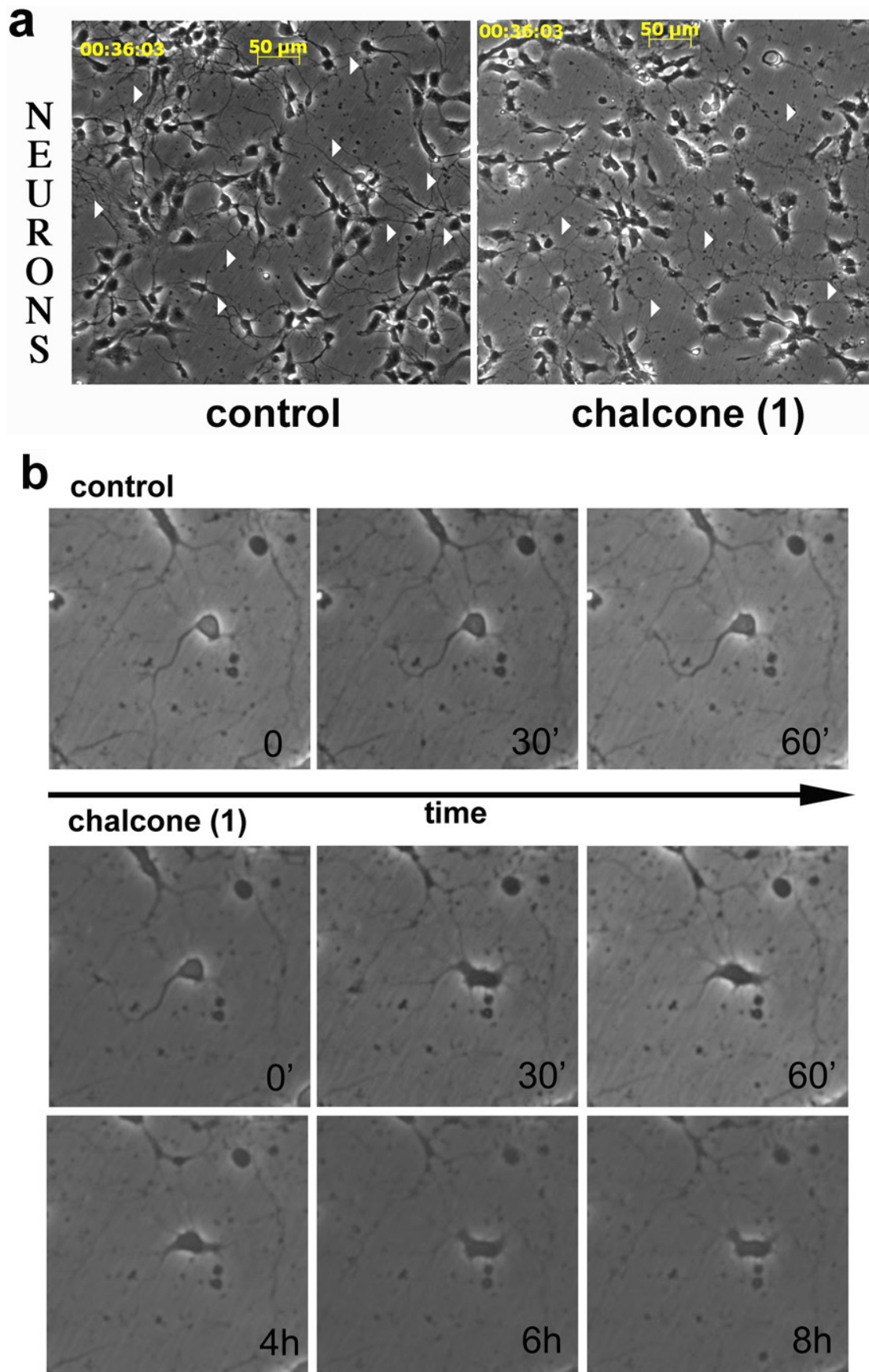


Figure 3- 8 a) *left*: Untreated mice neurons with prolonged axons (arrowheads); *right*: Retraction of neural axons back to soma or decay (arrowheads) upon treatment with 10 μ M of chalcone (1). Triangles are pointing at the missing neural connection. b) Zoomed neuron.

These dramatic morphological changes were observed at low drug concentration. How it is possible that the IC_{50} value of **1** in neural cells is relatively high after 24 hours ($\sim 38 \mu M$)? Cytotoxicities, as obtained from MTT-test, depend on the functional mitochondria. Thus, a trypan blue staining experiment was performed after 24 hours to qualitatively establish amount of dead cells. It proved that most of the neurons remained alive despite of the pronounced morphological changes (Figure 3- 9).

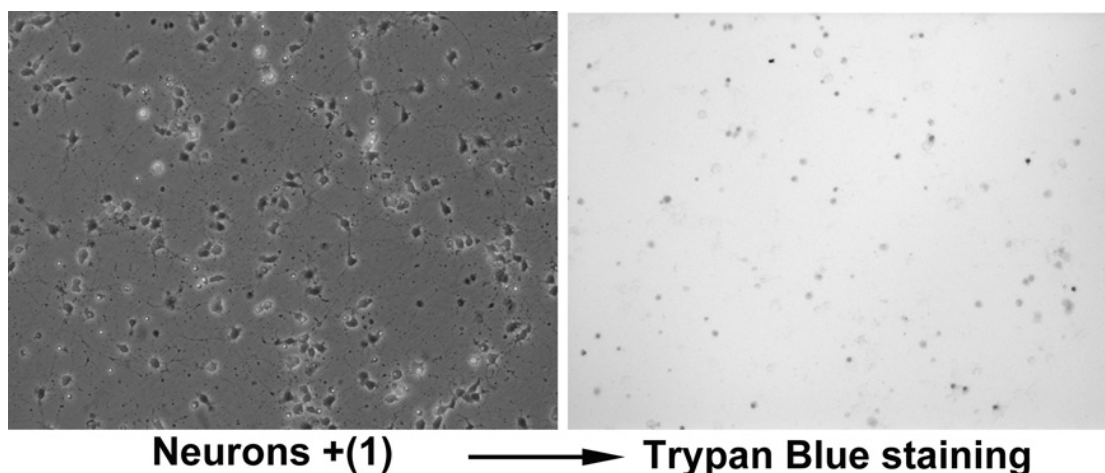


Figure 3- 9 Neurons after 24h incubation with chalcone (**1**) after Trypan Blues staining. Neurons showing blue somas are dead (right).

Similar experiments were performed with p53-deficient K11 stem cells derived from NE-4C stem cells (Madarasz, personal communication). The stem cells were treated with retinoic acid to promote differentiation to neurons (Figure 3- 10), and then they were treated with chalcone (**1**).

Control K11 cells have well defined neural networks; some cells were even still in the process of differentiation (Figure 3- 11).

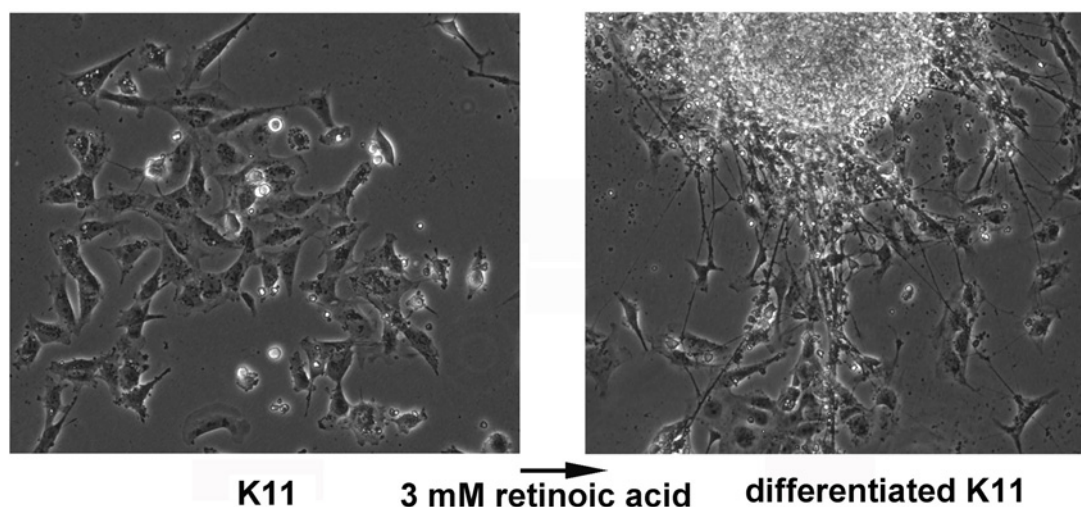


Figure 3- 10 Differentiation of K11 cells to neurons in the presence of 3 mM retinoic acid. The left figure shows undifferentiated cells. After treatment with 3 mM retinoic acid the K11 cells formed neurons (on the right).

3. Effects of chalcone (1)

The K11 cells treated with chalcone (1) ($1 \mu\text{M}$) lost most of their neural connections after 24 hours and the K11 (undifferentiated) cells were rounded or showed irregular cell-shape in contrary to the control cells.

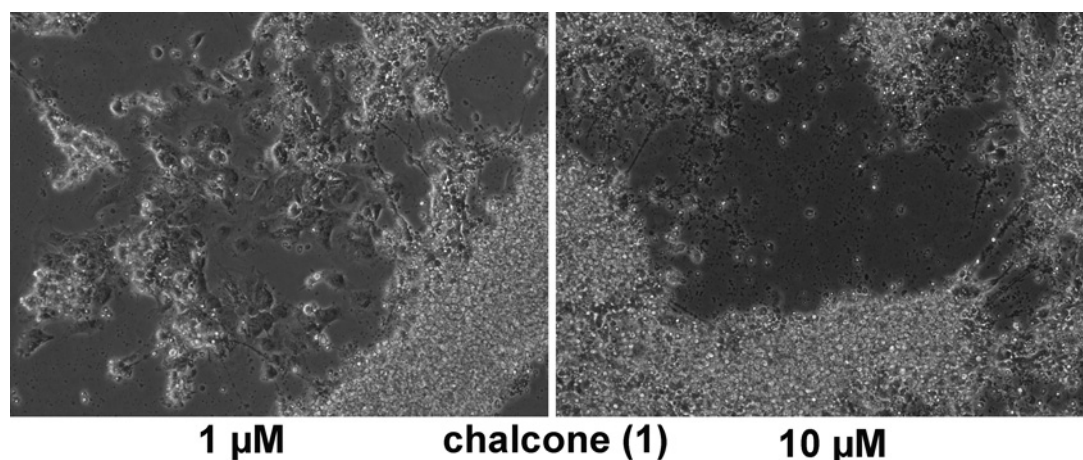


Figure 3- 11 K11 cells treated with different concentration of chalcone (1) after 24 hours.

An increased concentration chalcone (1) ($10 \mu\text{M}$) caused a complete depletion of neuronal network in K11 cells. Cell-debris remained visible as black dots (Figure 3- 11). Apparently, neural K11 cells are very sensitive towards chalcone (1), which is in line with the observed cytotoxicity of chalcone (1) in the parent NE-4C cells (24h/48h incubation, $\text{IC}_{50} = 2.8 \pm 0.6 / 0.024 \pm 0.001 \mu\text{M}$).

3.3.2.2 Altered cell shape in cancer cells

Changes of the 518A2 melanoma (adherent cells) and leukaemia HL60 (suspension cells) cells were investigated *via* the time-laps recording method. These cells were chosen because both cell lines show different principle of proliferation and living. The cytotoxic impact of chalcone (1) on the HL60 cells is very high (IC_{50} 24/48h = $1.7 / 0.17 \mu\text{M}$ in chapter 3.1.3). The HL60 cells changed their cell shape from the elliptic to irregular shape immediately after treatment with 1 (Figure 3- 12).

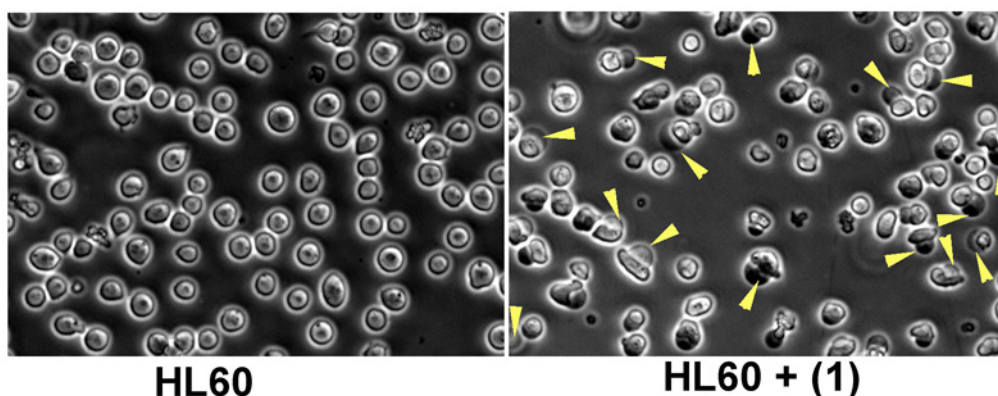


Figure 3- 12 Altered cells shape of suspension cells treated with chalcone (1). Shape of the control cells (left) was for many cells rounded with similar cell size. After incubation with $10 \mu\text{M}$ chalcone (1) the shape of HL60 became irregular and with variable cells size. Many cells were seen with vesicle “ghost” shown by yellow arrowheads.

Many cells swallowed and dead cells regurgitated their content in the form of “ghost” vesicles. These effects were irreversible; the cells did not recover with time and the amount of cell-debris increased.

An analogous experiment was performed with adherently growing 518A2 melanoma cells, which formed a tightly attached monolayer on the surface of the mini Petri dishes. Overall, dynamics and motility of untreated cells were slow as they underwent merely negligible morphological changes. Only a few cells detached from the monolayer within the first two hours. In contrast, exposure of 518A2 cells to chalcone (1) led to an immediate rounding and an enhancement of motility and cell shrinking dynamics (Figure 3- 13).

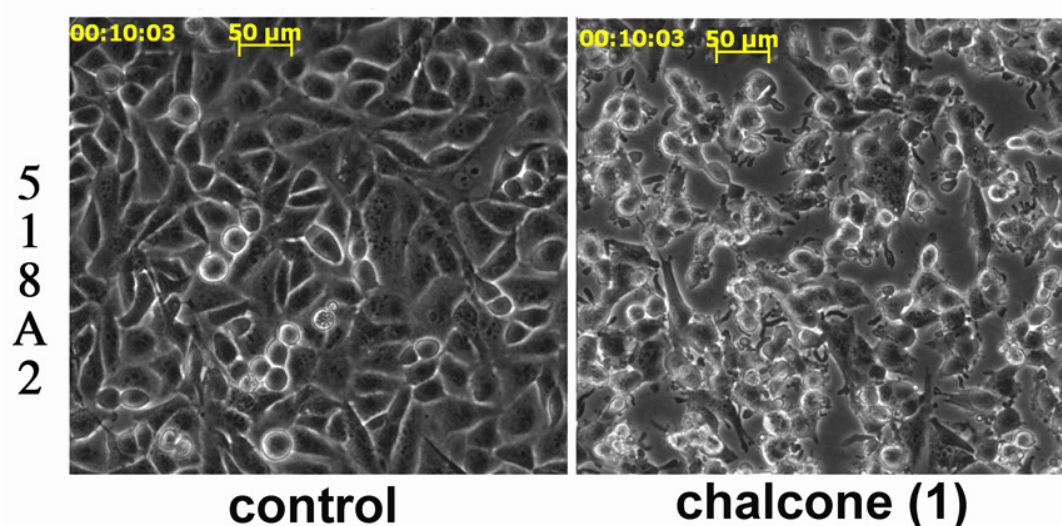


Figure 3- 13 Altered cell shape of 518A2 with chalcone (1). Dynamics and motility of untreated cells (left) vs. 518A2 cells treated with chalcone (1) (right).

The cells readily dissociated from the monolayer and their form turned from flat to spherical. This behaviour is in line with the generally accepted mechanisms of tubulin binding agents (TBAs) (Lippert, 2007) involving activation of RhoA/RhoA kinase, an intracellular coordinator of cytoskeletal rearrangement of microtubules and actin. However, in the case of chalcone (1), the 518A2 cells were able to repair the shrinkage effects and most of them spread again after three hours (Figure 3- 14). Thus, several aspects of chalcone (1) mechanism remained unresolved. Structural cell reorganization based on actin filaments and microtubule rearrangement is well known and important in many cell processes e.g. cell cycle. Hence, further experiments were necessary to clarify the mechanism of action of chalcone (1) during apoptosis.

3. Effects of chalcone (**1**)

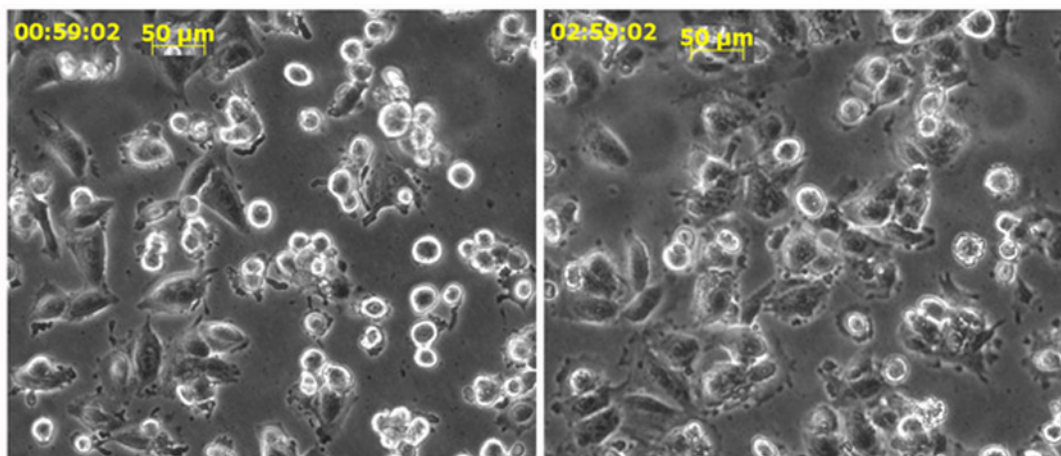


Figure 3- 14 Re-attachment of recovered 518A2 cells after treatment with chalcone (**1**), after 1h (left) and 3h (right).

3.3.3 Actin re-distribution induced by chalcone (**1**)

3.3.3.1 Actin distribution in astrocytes

An immunocytochemical analysis of the morphological changes of the actin filaments of astrocytes initiated by the chalcone (**1**) was carried out. Antibodies against astrocyte-specific GFAP intermediate filaments (glialfibrillary acidic protein) were employed to visualize the astroglial cells and phalloidin labelling was used to identify actin filaments. The micrographs showed that both types of filaments, actin (in green) and GFAP (in red), were disintegrated upon treatment with chalcone (**1**), mainly the actin filaments near the cell membrane. The GFAP filaments shrank only in the vicinity of the cell nuclei, which remained unaffected. Figure 3- 15 shows typical effects of chalcone (**1**) on astrocytes after 72 hours. These findings are in line with the observed weak cytotoxic activity of **1** in astrocytes ($IC_{50} \sim 50 \mu M$).

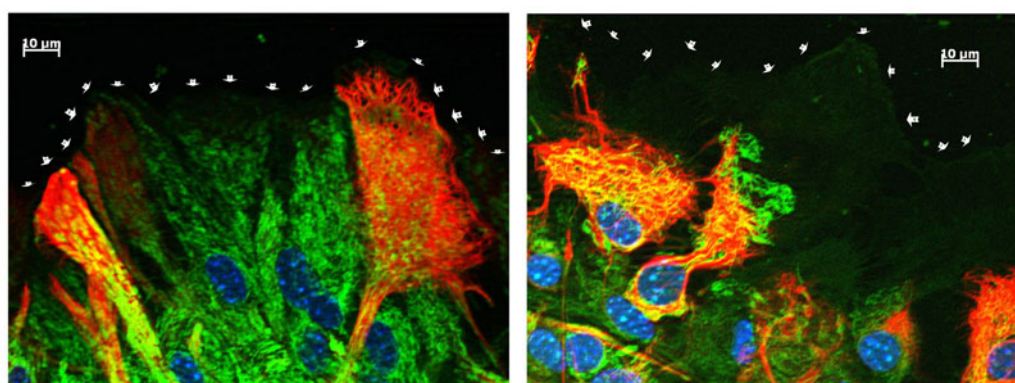


Figure 3- 15 Immunostaining of astroglia cells untreated (left) and treated with $10 \mu M$ chalcone (**1**) for 72 h (right). *Blue*: nuclei stained with DAPI (4',6-diamidino-2-phenylindole); *green*: actin cytoskeleton stained with phalloidin; *red*: glial fibrillary acidic proteins (GFAP). White arrowheads indicate the edge of cell membranes. The pictures were taken with a fluorescence microscope (Zeiss Axiovert 200M) with a 63 x oil immersion objective and the scanning module at 1024 x 1024 pixel resolution.

Similar effects on the filament distribution in astrocytes were observed after treatment with chalcone (1) for just 24 hours (Figure 3- 16).

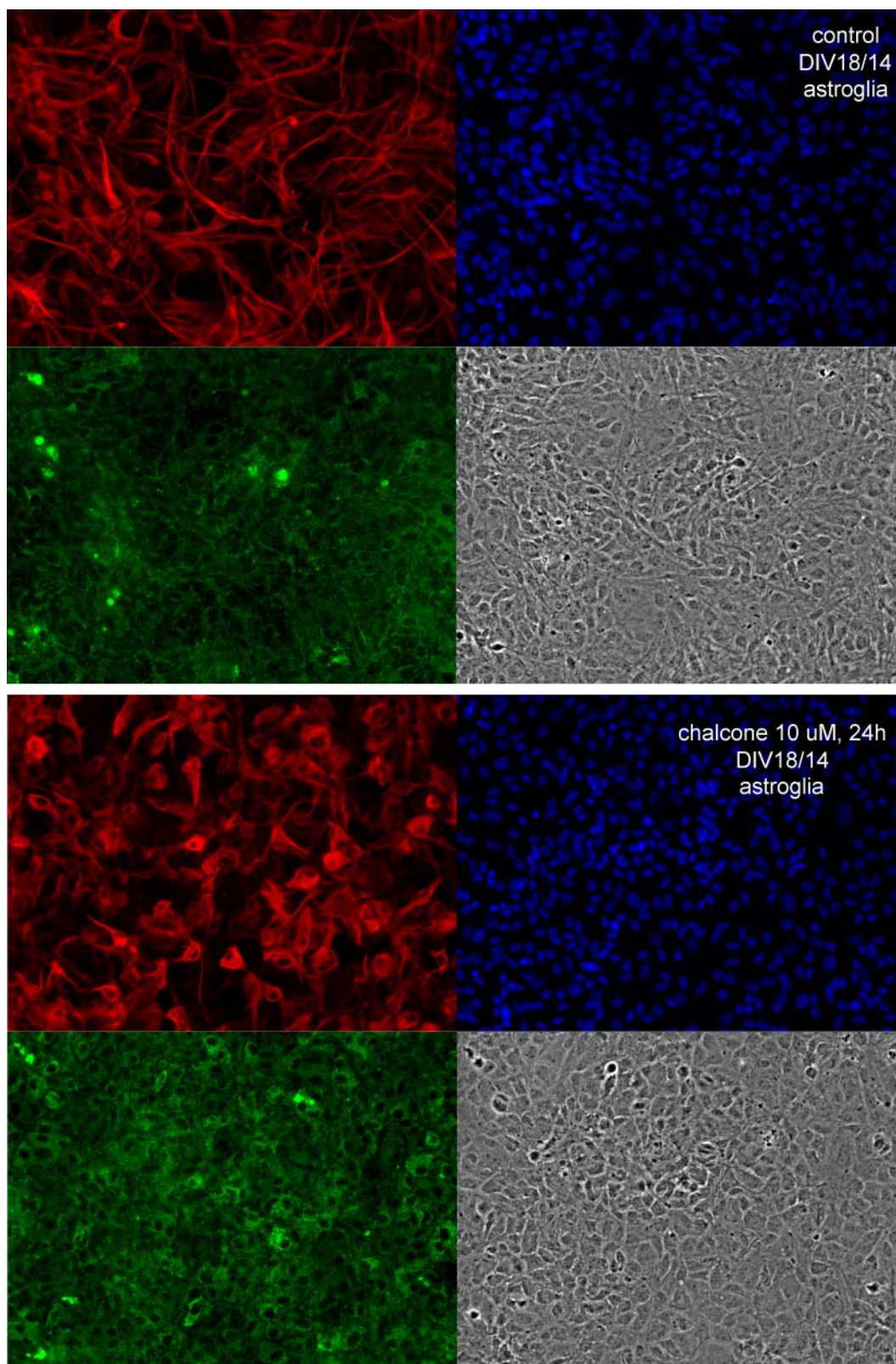


Figure 3- 16 Immunostaining of astroglia cells untreated (upper part) and treated with 10 μ M chalcone (1) after 24 hours. *Blue*: nuclei stained with DAPI (4',6-diamidino-2-phenylindole); *green*: actin cytoskeleton stained with phalloidin; *red*: glial fibrillary acidic proteins (GFAP). DIV means *days in vitro*.

3. Effects of chalcone (1)

The level of GFAP just started to diminish, the effect on mitochondrial function was minimal or none (MTT assays showed 100% vitality compared with control).

3.3.3.2 Actin distribution in 518A2 cells

Similarly, fluorescence micrographs of immunostained 518A2 cells revealed a significant breakdown of the actin network when treated with chalcone (1) (Figure 3-17).

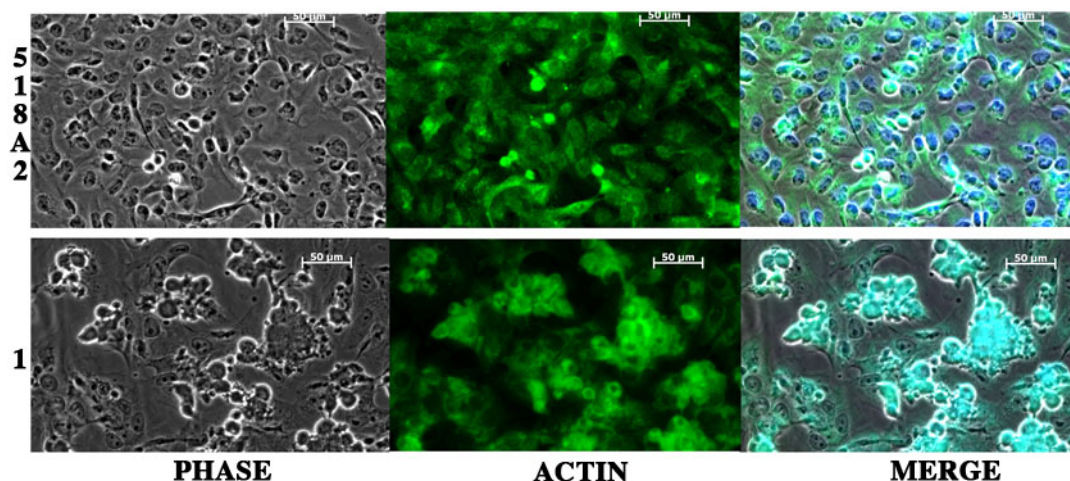


Figure 3- 17 Immunostaining for actin of untreated 518A2 cells (top row), and 518A2 cells after 24 h incubation with 10 μ M chalcone (1) (bottom row). Blue: nuclei stained with DAPI (4',6-diamidino-2-phenylindole); green: actin cytoskeleton stained with phalloidin.

The attached cells got closer and formed spherical structures after treatment with 1 for 24 hours. Facing the previous results (Figure 3- 14) we can conclude that those cells were unable to repair and cannot proliferate. The actin of 518A2 cells was mostly concentrated around the nucleus while further damages remained unclear. It is very likely that the damage of filaments induced by chalcone (1) is not the only signal leading to cell death.

3.3.4 Microscopic observations of 518A2 cells by Giemsa staining

In the previous chapter 3.3.3, the effect of chalcone (1) on filaments distribution was revealed. It was shown that the chalcone (1) is able to inhibit *in vitro* microtubule polymerization (Schobert et al., 2009), and the experiments with neural cells confirmed effect on the microtubule-based network system. While the nuclei of neural cells remained separate, the nuclei of 518A2 cells were located too close together. Therefore, internucleosomal DNA cleavage was monitored using Giemsa dye and examined under a light microscope.

First of all, the cytotoxic effect of the chalcone (**1**) ($11 \mu\text{M}$, i.e. IC_{50} concentration) on the proliferation as well as on the attachment of the adherent cells was analyzed upon exposure for 24 hours. The X-cross method was performed as it is described in the material and methods part. The cell behaviour was the same as it was observed in the previous experiments. Control cells were wide and spreads with a typical shape, the nuclei were well defined by a nuclear envelope with condensed chromatin visible as dark-blue dots. The number of cells decreased more rapidly after treatment with **1** than in the control sample. 518A2 cells got close to each other and formed branches with visible nuclear envelope. In this case, late apoptotic or dead cells were likewise visible as spread cells with purple cytoplasm. The cells did not grow over the X-cross scratching line that was performed before treatment. On the other hand, the control cells grew over the X-cross (Figure 3- 18).

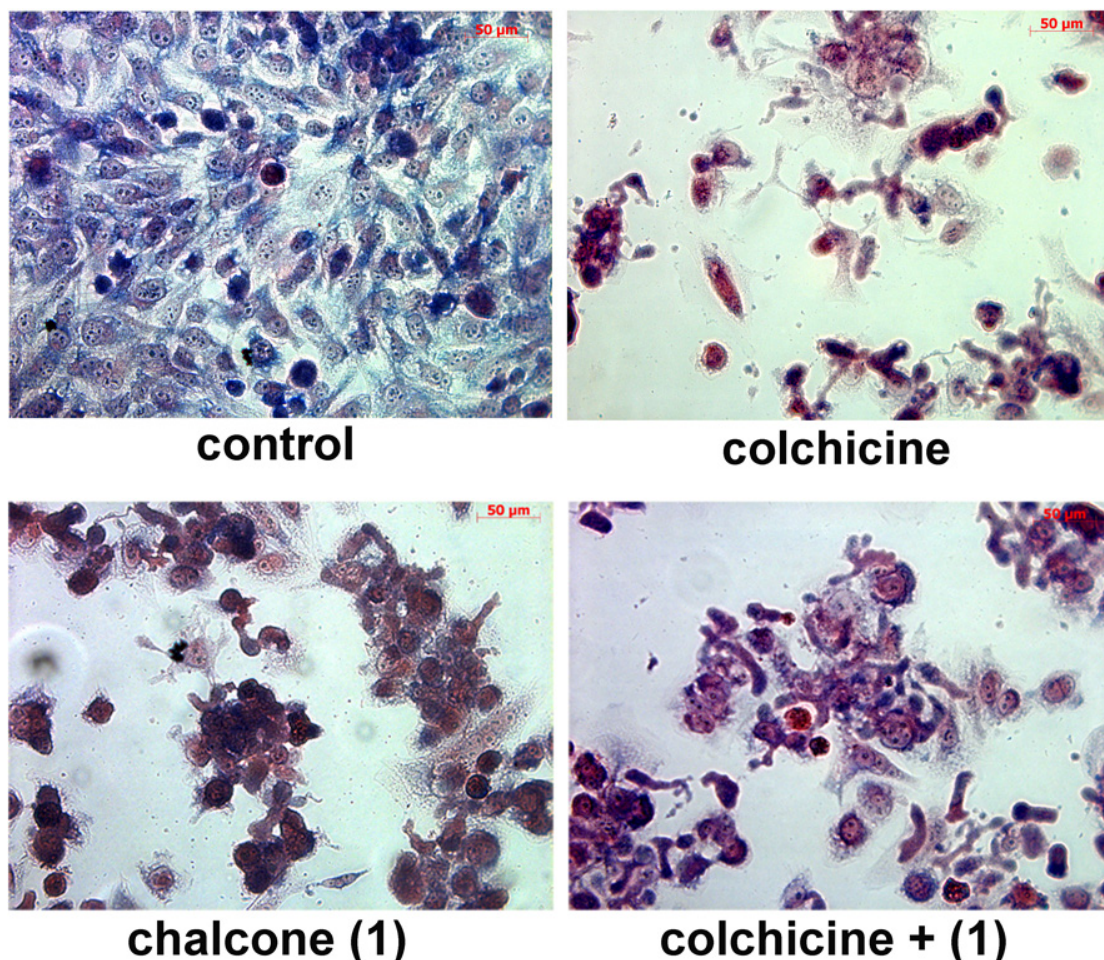


Figure 3- 18 Samples of 518A2 cells treated with test compounds were stained with Giemsa dye after 24 hours of incubation. Untreated control cells served as a reference. Colchicine 62.5 nM , chalcone (**1**) - $11 \mu\text{M}$, mixture: 31.3 nM of colchicine + $5.5 \mu\text{M}$ of chalcone (**1**).

Since chalcone (**1**) is an analogue of the anticancer agent combretastatin A-4, which binds to the colchicine-binding site of α -tubulin and interferes with the

3. Effects of chalcone (**1**)

polymerization of tubulin (Kanthou and Tozer, 2002), the effect of colchicine at its IC_{50} concentration (62 nM) was studied on 518A2 cells as well. The cell number after colchicine treatment decreased rapidly. The cells formed only a few brunch-like structures and they were slightly pink-purple, some were spread, some were still rounded. Surprisingly, no nuclei envelope was observed. This cell behaviour is different from that after treatment with chalcone (**1**). The combination of both drugs (31.3 nM of colchicine + 5.5 μ M of **1**) gave a mixture of the individually described phenotypes (Figure 3- 18). The cell number decreased but not as rapidly as after colchicine or **1** treatment. The cells came closer to each other, however, not as close as in the treatment with **1** alone. The nucleus envelope was hardly detectable in most cases. Colchicine differs structurally from chalcone (**1**). Hence, varying tubulin-binding mechanisms, cellular uptake mechanisms, and non-tubulin targets might play a role for the observed differences between chalcone (**1**) and colchicine in cancer cells.

3.3.5 Transmission electron microscopy

During apoptosis, the mitochondrial network is fragmenting which results into smaller and more numerous mitochondria (Mancini et al., 1997). The large mitochondrial network consists of externally extended and interconnected mitochondrial filaments and acts as an electrically united system (Westermann, 2008). The mitochondrial population mostly consists of short and long tubules, which migrate along the microtubule tracks (Chan, 2006). Any disruption of the microtubules/actin skeleton, e.g., by treatment with chalcone (**1**), might severely affect the mitochondrial trafficking and may cause mitochondrial disorganization.

In order to visualize effects of chalcone (**1**) on mitochondria, additional experiments with 518A2 cells were performed. The cells were treated with 0.1 mM chalcone (**1**) for 15 minutes, kept in fresh medium for ca. 1 hour, and finally monitored using transmission electron microscopy (TEM). Mitochondria of cells treated with the chalcone (**1**) were highly condensed and mainly localized at the apical side of the cells. While untreated control cells appeared prolate and undifferentiated having filopodia on the rim (Figure 3- 19a), cells incubated with chalcone (**1**) adopted a rounded shape (Figure 3- 19b, c). A similar morphological change has been reported for H460 non-small cell lung cancer cells treated with combretastatin A-4 (CA-4) (Vitale et al., 2007). In addition, the chalcone-treated 518A2 cells showed blebs on

their surface. In comparison with untreated cells, the large mitochondrial population of treated cells was localized close to membrane and nucleus having disorganized or condensed cristae (Figure 3- 19c).

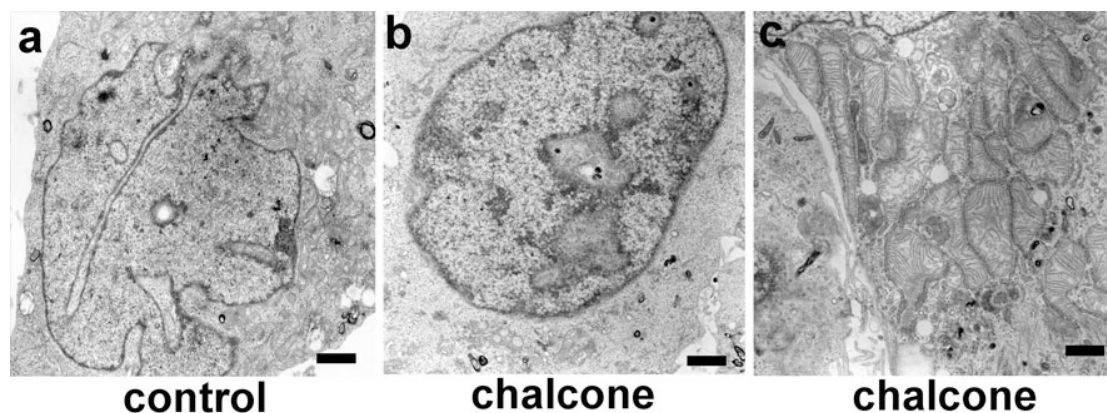


Figure 3- 19 Transmission electron micrographs of 518A2 cells illustrating the differentiation process induced by *in vitro* exposure to chalcone (**1**) (a) Untreated, undifferentiated control cell, black bar = 1.1 μm ; (b/c) cell exposed to chalcone (**1**) (100 μM) for 15 min, black bar = 1.7/1.1 μm . Performed according to section 2.5.5.

They frequently displayed dislocated inner membranes (Figure 3- 20e). Only a small percentage of the untreated control cells were found in G2/M phase with visible centrioles. The maintenance of the microtubule integrity plays a pivotal role in stabilization of the pericentriolar matrix. This is consistent with the notion that the microtubule depolymerising effect of chalcone (**1**) leads to a mitotic catastrophe and thus to an arrest in G2/M phase. A similar mitotic failure has been reported for H460 NSCLC cells treated with CA-4 (Vitale et al., 2007). At higher resolution, treated cells also revealed stress fibers (Figure 3- 20h). Multivesicular bodies (Figure 3- 20g) or autophages with double membranes were visible in most of the analyzed cells (Figure 3- 20f). Control cells and treated cells also differed concerning the state of their mitochondria, centrioles and Golgi apparatus (GA). The GA was frequently located next to the centrosomes or nuclei envelopes and showed no fragmentation after chalcone (**1**) treatment (Figure 3- 20f). After treatment with **1**, many cells showed visible centrioles (Figure 3- 20b). The occurrence of centrioles as a result of aberrant chromosome segregation could be due to DNA damage (possibly in tandem with defective checkpoints) or to a destabilization of the spindle apparatus (Castedo et al., 2004; Vitale et al., 2007)

3. Effects of chalcone (1)

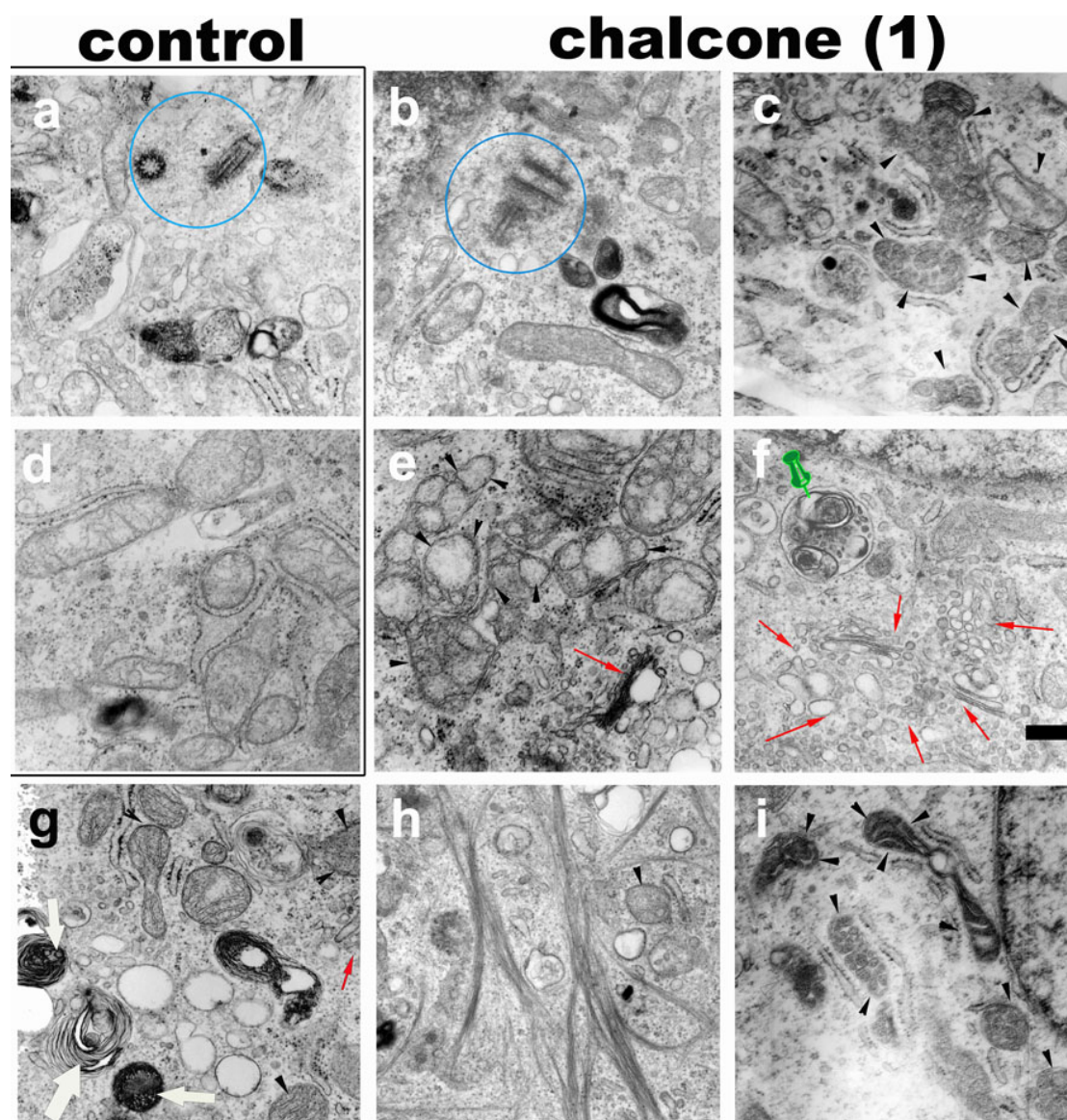


Figure 3- 20 TEM images of organelles in 518A2 cells. a, d: untreated cells with image a showing the cross and longitude section through the centrioles and image d showing mitochondria with cristae invaginations surrounded by endoplasmic reticulum. b, c, e, f, g, h, i: cells treated with chalcone (1). Images c, e, g, i show mitochondria at various stages of inner-membrane destruction and/or highly condensed contents (black arrowheads). Some mitochondria formed multi-lamellar bodies in image g (white thick-arrows). The formation of multivesicular bodies is shown in image f (green push-pin). For comparison, centrioles in control (a) and chalcone (b) are shown in blue rings. The frequently visible Golgi apparatus was pointed with red arrows. Stress fibers are visible in image h. Image f: black bar = 0.4 μm (valid for each image). Performed according to section 2.5.5.

3.4 DNA degradation of chalcone (1) during apoptosis

3.4.1 Cell cycle analysis

Chalcone was found to arrest cells of the human T24 and HT-1376 bladder cancers in the G2/M phase (Shen et al., 2007). According to the previous results 3.3.5, speculation could be made about the apoptotic mechanism. An effect similar to the one observed in human T24 and bladder cancers could be expected for chalcone (1), too. Effects on the cell cycle progression of melanoma 518A2 cells treated with

chalcone (**1**) was analysed by FACS (Figure 3- 21) after DNA staining with propidium iodide (PI).

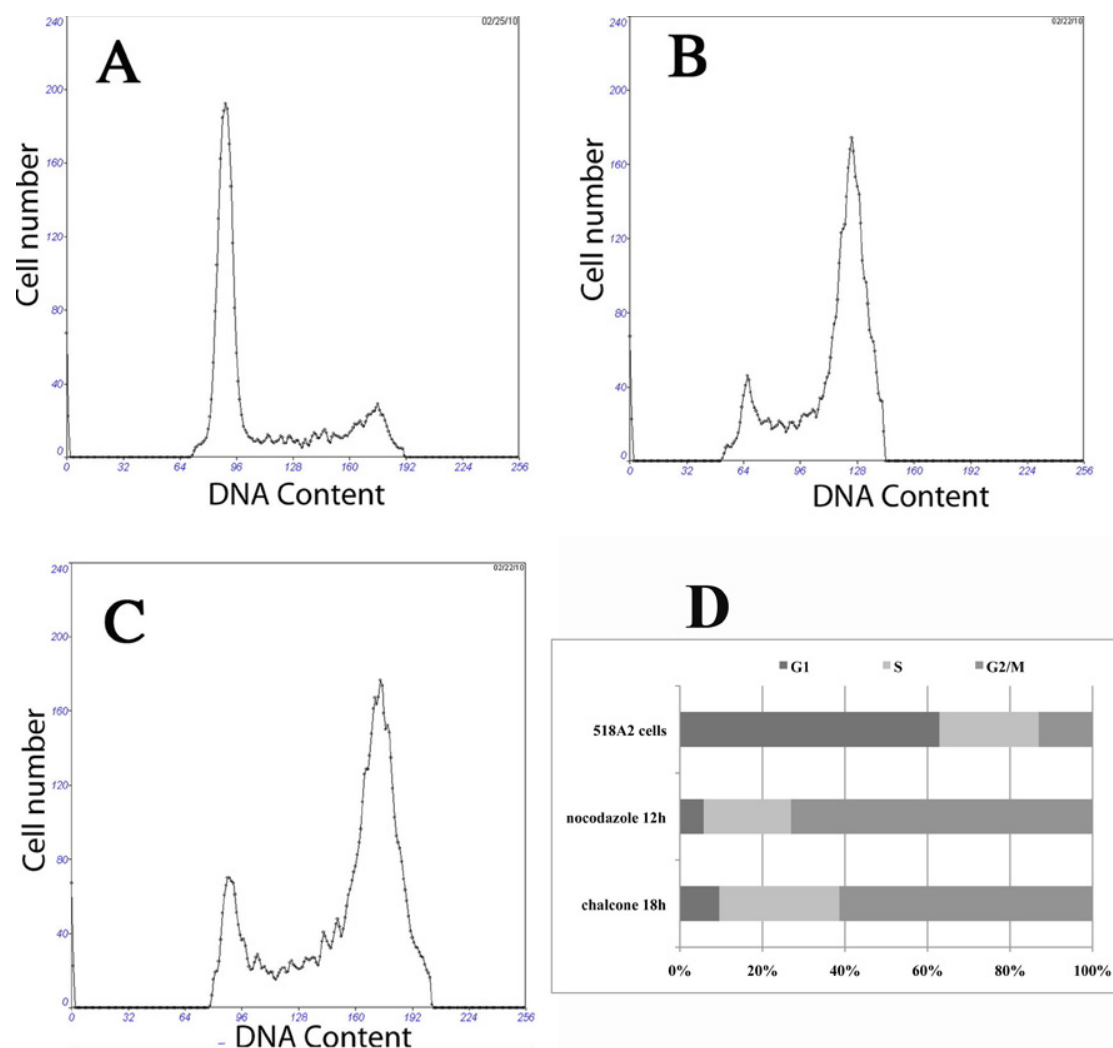


Figure 3- 21 (A) Flow cytometric analysis of 518A2 melanoma cells stained with propidium iodide. Cells were treated with 250 $\mu\text{g}/\text{mL}$ nocodazole (B) or with 10 μM chalcone (**1**) (C). Panel (D) summarises the results: G1 phase (dark grey), S phase (light grey) and G2/M phase (medium grey). The FACS measurements and analysis were performed with special assistance of Andreas Brown.

About 63% of untreated 518A2 cells were in G1 phase after 18 h, 24% in S phase and 13% in G2/M phase. 518A2 cells treated with 250 $\mu\text{g}/\text{L}$ nocodazole, a synthetic analogue of taxol, were mainly in sub-G1 phase after 18 h, a shorter 12 h exposure led to 76% of the cells being in G2/M phase. The presence of 10 μM of chalcone (**1**) revealed a similar effect arresting 61% in G2/M phase after 18 h incubation. Thus, further studies were performed regarding DNA degradation and chalcone-DNA interactions.

3. Effects of chalcone (**1**)

3.4.2 DNA fragmentation from isolated cells

The defined fragmentation of DNA *via* activated endogenous nucleases is characteristic of apoptosis (Arends et al., 1990; Bortner et al., 1995; Hughes and Cidlowski, 2000). During apoptosis, activation of certain endonucleases initiates DNA cleavage and the chromatin is degraded into two distinct fragments: nucleosomal fragments (multiples of 180-200 bp) and large fragments (30- to 50-kb). Since previous results showed high sensitivity of HL60 cells towards **1** ($IC_{50}=1.7/0.17 \mu M$), these leukaemia cells were exposed to **1** for 24 hours. The DNA of the treated cells was isolated and analyzed by agarose gel electrophoresis.

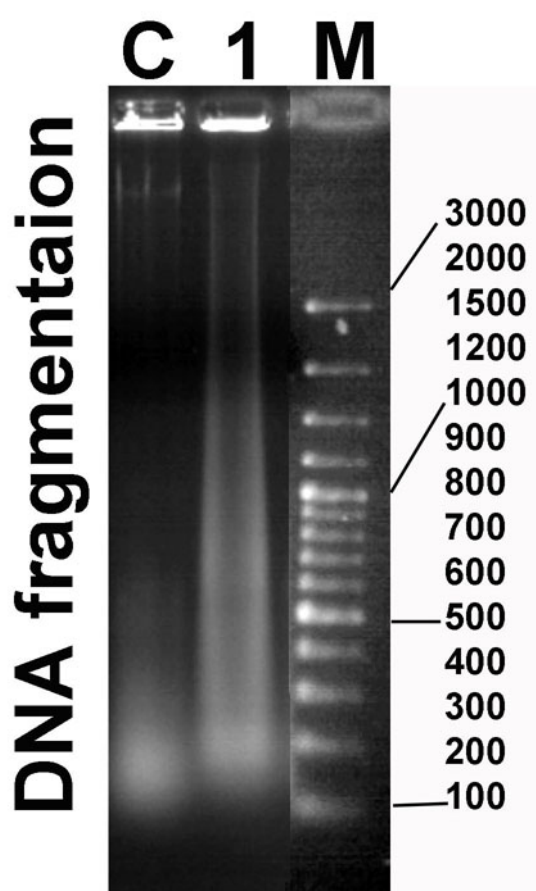


Figure 3- 22 Degraded DNA isolated from HL60 cells after treatment with chalcone (**1**). The DNA samples were applied to 1.5% agarose gel in lane C: sample of salmon sperm DNA for comparison, lane: **1** is DNA extract from cells treated with 0.25 mM chalcone; lane M: marker from 100-3000 bp.

Intact chromosomal DNA (lane C) and DNA from cells treated with **1** (lane 1) did not move in the agarose gel and remained in the loading well (Figure 3- 22). Only a ~100 bp band of DNA was visible in the control. After treatment with **1** lane 1 shows a strong band at 200 bp together with a lot of undefined bigger fragments which the control lane C does not show. Since proteinase K was added to the lysis buffer, no

active endogenous or exogenous deoxyribonuclease (DNase) should be present in the sample, which could have cleaved the chromosomal DNA after its isolation.

3.5 Characterization of DNA-chalcone interactions

Several DNA binding molecules act *via* intercalation (Neidle, 1979; Waring, 2006). For instance, the chalcone analogue AMC [AMC, 1-(4'-aminophenyl)-3-(4-N,N-dimethylphenyl)-2-propen-1-one] gave evidence for DNA intercalation (Shah et al., 2008). However, chalcones (1,3-diphenyl-2-propen-1-ones) are generally not known for their DNA-intercalating or DNA-binding behaviors, yet, some pivotal experiments were performed to study potential interactions of chalcone (**1**) with DNA.

3.5.1 Electrophoretic mobility shift assay of plasmid DNA

A large number of agents bind to duplex DNA in a covalent or non-covalent manner. The electrophoretic mobility shift assay (EMSA) is an important technique for the study of putative interactions between a drug candidate and DNA

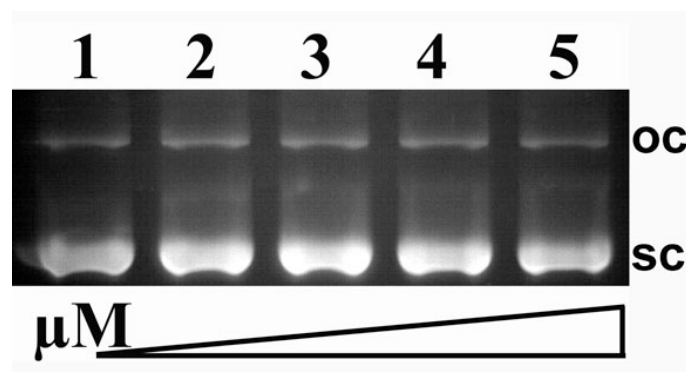


Figure 3- 23 Interaction of pBR322 plasmid DNA with increasing concentrations of chalcone (**1**). Top: open circular form (oc). Bottom - supercoiled form (sc). Concentrations of chalcone (**1**) increase from left to right: lane 1-2-3-4-5 \approx 0-5-20-40-60 μ M. Samples were applied on a 1% agarose gel for 3 h, 65-85 V in TAE buffer.

Hence, gel electrophoresis was carried out in order to investigate the conformational changes and damages caused to non-genomic pBR322 plasmid DNA due to the covalent binding with chalcone (**1**). The supercoiled form (sc) shows higher mobility and runs faster than the one-nicked open circular form (oc). Apparently, chalcone (**1**) did not cause any visible changes in the applied pBR322 plasmid DNA (Figure 3- 23).

3.5.2 Secondary structure study of DNA-chalcone (**1**) interactions

Circular dichroism (CD) is a useful means for the study of DNA interactions of molecules in solution (Alison Rodger and Nordén, 1997) in order to obtain more

3. Effects of chalcone (**1**)

information about the global changes in DNA conformation (Vrana et al., 1986) (Brabec et al., 1990).

First of all, the conformation of tested calf thymus (ct) DNA was compared with profiles (Ivanov et al., 1973) A-, B- and Z-DNA CD spectra (Figure 3- 24).

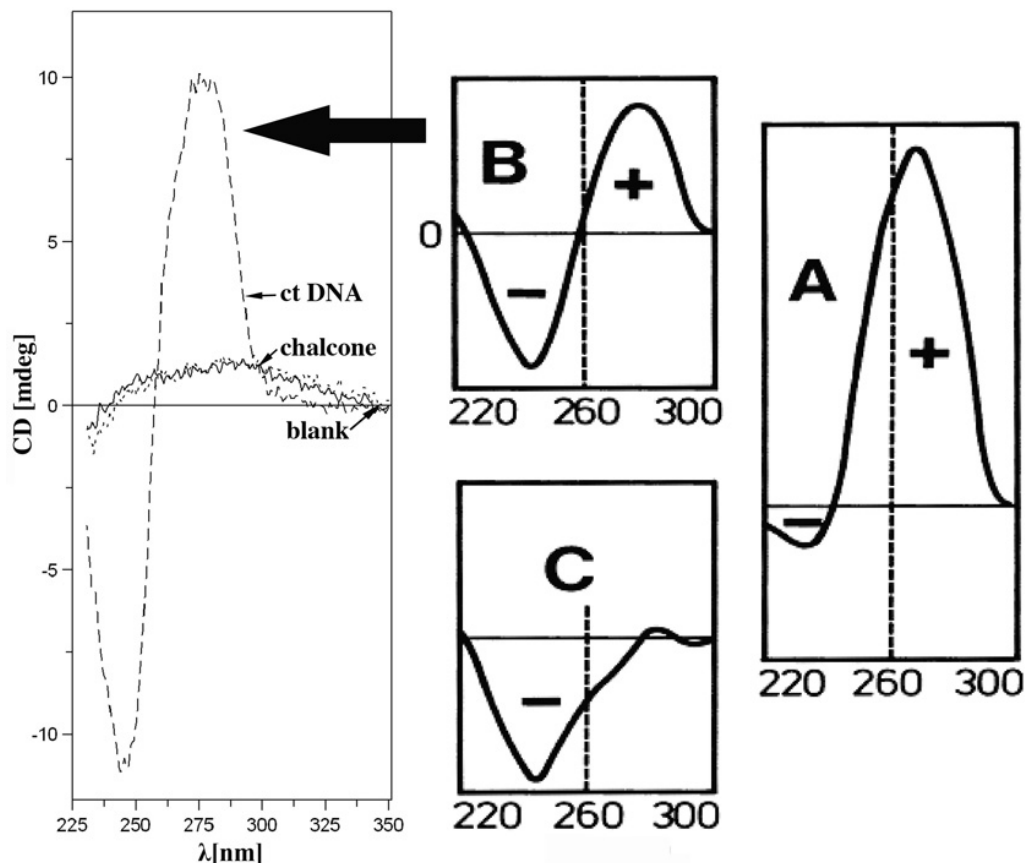


Figure 3- 24 Comparison of CD spectra of different DNA forms with calf thymus (ct) DNA (10^{-4} M dissolved in 0.01M NaClO_4). CD signals of chalcone (**1**) and blank (0.01M NaClO_4) are included. Spectra of A-, B-, C (Z)-DNA's (Ivanov et al., 1973).

The CD spectrum of ct DNA was very similar to B-DNA conformation crossing the zero line at about 260 nm. For canonical B-DNA conformation, the maximal ellipticity is reached at 275 nm and the minimum at 245 nm. Chalcone (**1**) showed no significant CD band within the investigated wavelength range.

In the next step ctDNA was incubated with **1** at various r_1 values for 24 hours. The blank spectrum was subtracted from the measured CD spectra and the obtained CD signal was re-calculated considering the molar DNA concentration (10^{-4} M) (Figure 3- 24). The intensity of the positive CD band at 275 nm is increased as a consequence of DNA-chalcone interaction. Similarly, the negative CD band at 245 nm decreased (Figure 3- 25A). To avoid unspecific interaction and to remove unbound or free chalcone (**1**), 12 hours lasting dialysis against 0.01 M NaClO_4 was performed. The concentration of ctDNA was determined and the molar ellipticity ($\Delta\epsilon$)

spectra were compared with non-dialysed sample. No significant changes were observed in the positive CD band. However, the decrease in the negative band was more pronounced for the dialysed sample.

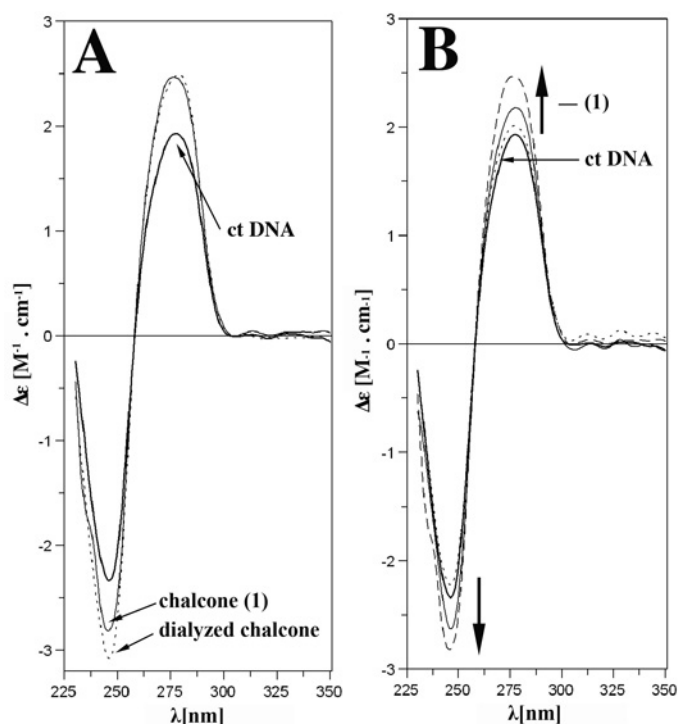


Figure 3- 25 Molar ellipticity spectra of ct-DNA and effect of chalcone (1). CD spectra, in units of millidegrees were converted to $\Delta\epsilon$ using the concentration of the DNA. A) Effect of $r_b = 0.4$ chalcone (1) on ct DNA and spectrum of the dialysed sample (dotted line) were compared with untreated ct DNA. B) Effect of dialysed 1 samples with increasing r_b : 0.08 (dotted line), 0.16 (full line) and 0.4 (dashed line). As a reference untreated ctDNA was used.

In Figure 3- 25B, the effect of dialysed chalcone-DNA samples with increasing r_b initiate ratio ($r_b = 0.08, 0.16, 0.4$) was compared with non-modified ctDNA. The intensity of the positive CD band increased and of the negative CD band decreased with increasing concentrations of **1**. Hence, a dose-dependent interaction between chalcone (**1**) and DNA occurs.

3.5.3 Melting temperatures of DNA-chalcone (1) adducts

Thermal denaturation of DNA provides basic information on thermodynamic stability. In this experiment the temperature is increased constantly. Heating of the sample results in denaturation of DNA, the initially double-stranded DNA is disconnected and both strands are separated. The midpoint of the transition is called melting point (T_m). DNA-bound compounds are able to (de-)stabilize DNA and thus (decrease) increase the T_m value.

3. Effects of chalcone (1)

Although no electromobility shift with plasmid DNA was observed, previous CD spectra showed DNA changes in the presence of **1**. Therefore, melting curves were measured in order to clarify the DNA interaction of chalcone (**1**). Dialysed CD samples were used for this experiment. The denaturing temperature of unmodified ctDNA was $65 \pm 1^\circ\text{C}$. Addition of chalcone (**1**) at the highest r_b value decreased the T_m value negligibly to $64.2 \pm 0.9^\circ\text{C}$ (data not shown). This result led to the conclusion that the interaction between chalcone (**1**) and ctDNA is very weak.

3.6 Activation of caspases after chalcone (1) treatment

Caspases are proteases, which are involved in apoptosis. They exist as inactive zymogens which are activated via proteolysis when cells undergo apoptosis (Thornberry et al., 1997). After treatment with chalcone (**1**), HL60 cells were monitored up to 24 hours. Figure 3- 26 shows the initial rate of cleavage of the substrate, DEVD-pNA, for caspase-3.

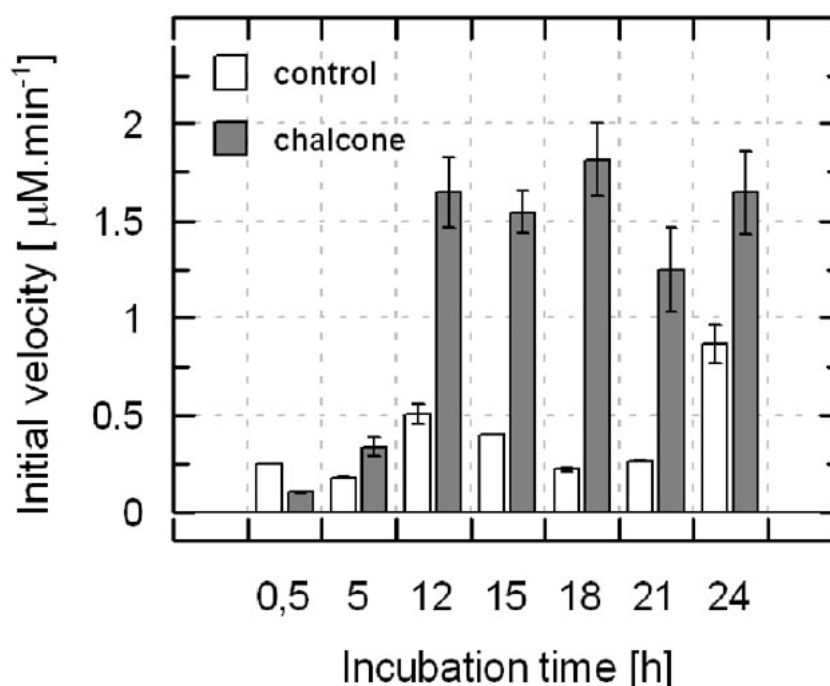


Figure 3- 26 Monitoring of caspase-3 activity in cell lysates of control HL60 cells and after chalcone (**1**) treatment. The caspase-3 inhibitor DEVD-CHO ($20\mu\text{M}$) was pre-incubated for 15 minutes at 37°C . The cleavage of caspase-3 (Ac-DEVD-pNA) ($200\mu\text{M}$) substrate was measured at 405 nm. The initial velocity of hydrolysis was determined from the linear portion of the progress curve. It measures the total amount of active enzyme presented in the cell lysate.

In the case of chalcone (**1**) the activity of caspase-3 is dramatically increased after 12 hours of incubation and reaches a constant value (initial velocity = $1.65\mu\text{M}\cdot\text{min}^{-1}$). The HL60 control cells exhibited a 6-7-fold lower cleavage activity.

3.7 Interference with ABC transporters

The role of efflux transporters in the detoxification of cancer cells represents one of the main topics of pharmaceutical studies. The interaction of chalcone (**1**) with drug transport proteins like ABCB1 (P-gp) (Hyde et al., 1990; Simstein et al., 2003; Smith et al., 2001) or BCRP (Borst et al., 1997) was investigated in a substrate- or inhibitor-like fashion.

3.7.1 Chalcone (**1**) efflux *via* P-glycoproteins

Calcein-AM is taken up and pumped out via diffusion because of the membrane permeability given by the hydrophobic AM-linker. However, inside the cell the AM-fragment can be cleaved by esterases producing highly fluorescent calcein which is, however, not membrane permeable anymore. Then, P-gp proteins exclusively perform the efflux of calcein. Thus, an inhibition of P-gp proteins leads to accumulation of the calcein in the cell whose fluorescence can be measured.

P-gp overexpressing KBv1^{+Vbl} cervix carcinoma cells (Schwab et al., 2003) and their wild type parent cells were treated with chalcone (**1**) in the presence of calcein-AM (Figure 3- 27).

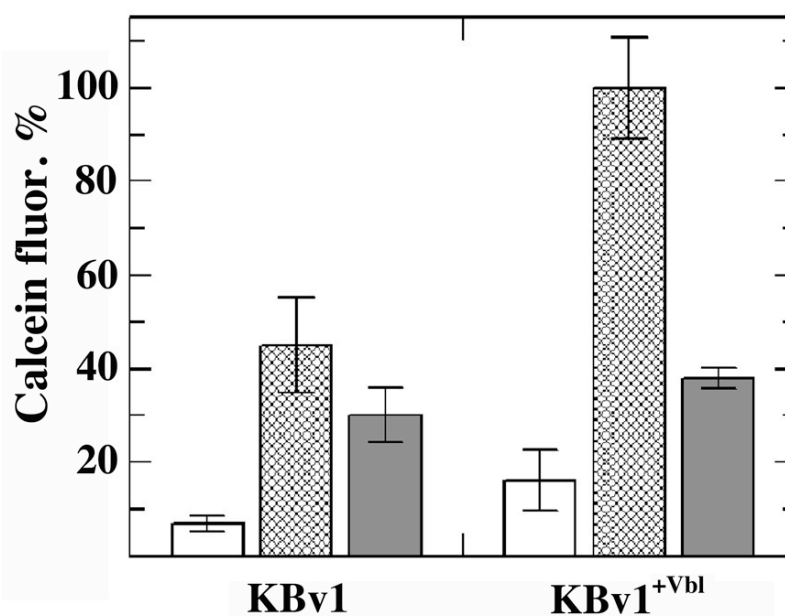


Figure 3- 27 Calcein-AM assay: % inhibition of P-gp drug transporters in KBv1 and KBv1^{+Vbl} cells by 50 μ M of chalcone (**1**) (grey bars) relative to the inhibition by verapamil (hatched bars) after 15 min exposure. White bars: negative control.

As a positive control, the fluorescence intensity of KBv1^{+Vbl} cells treated with 50 μ M of the clinically established chemosensitiser verapamil (Schwab et al., 2003; Sharom, 1997) was set to 100 %. Surprisingly, wild-type KBv1 cells under the same

3. Effects of chalcone (1)

conditions reached only ~45% of the calcein fluorescence of the resistant KBv1^{+Vbl} cells. Possibly, they obtained additional ways to eliminate calcein-AM or calcein, a phenomenon which is not without precedence (Marchan et al., 2008; Oku et al., 1995). Calcein fluorescence in KBv1 cells was also relatively low in the absence of verapamil. Treatment with chalcone (1) virtually led to the same fluorescence intensities in both resistant and wild type cells.

3.7.2 Chalcone (1) efflux via BCRP proteins

MCF-7 breast carcinoma cells produce BCRP drug transporters and after treatment with topotecan (550 nM over 40 generations) the concentration of the BCRP protein was increased (MCF-7^{+Top} cells). The mitoxantrone assay is based on the active export of the fluorescent dye mitoxantrone via BCRP transporters. The effects of chalcone (1) on the fluorescence of intracellular mitoxantrone in MCF-7 and MCF-7^{+Top} cells relative to that of the specific BCRP inhibitor fumitremorgine C (Oku et al., 1995) and to a negative control of cells treated only with mitoxantrone are shown (Figure 3- 28).

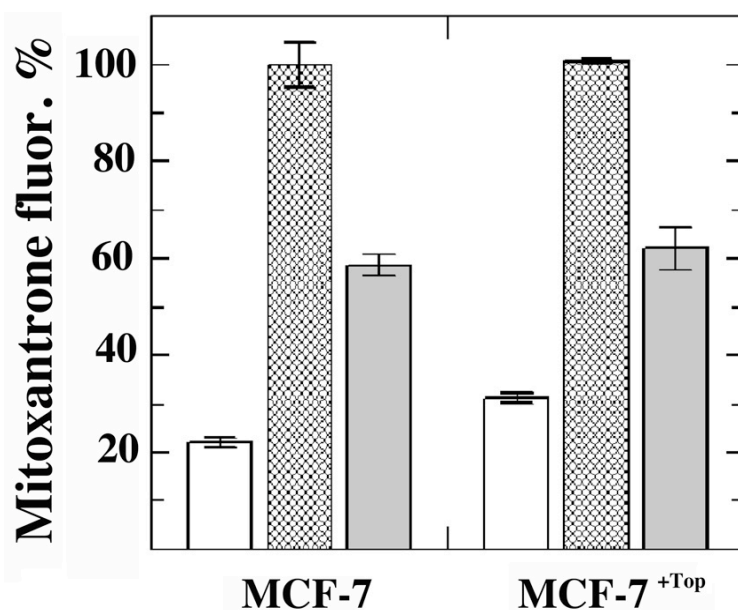


Figure 3- 28 Mitoxantrone assay: % inhibition of BCRP drug transporters in MCF-7 and MCF-7^{+Top} cells by 10 μ M of chalcone (1) (grey bars) relative to fumitremorgine C (hatched bars) after 30 min exposure. White bars: self-fluorescence of cells treated with mitoxantrone alone (negative control).

Chalcone (1) led to doubled mitoxantrone fluorescence in either cell line relative to the negative control, thus, they are likely competitive substrates for the BCRP proteins.

3.8 Conclusion

Chalcone (**1**) is preferentially accumulated by endocytosis. It vigorously depolymerised microtubules and actin filaments in neural and cancer cells and proved to be effective in damaging mitochondria and in arresting cancer cells in the G2/M phase. These observations are consistent with the notion that the microtubule depolymerising effect of chalcone (**1**) leads to mitotic catastrophe and thus to an arrest in the G2/M phase. A similar mitotic failure has been reported for H460 NSCLC cells treated with CA4 (Vitale et al., 2007).

Morphologically, **1** led to a rounding and detachment of 518A cells and an enhancement of their motility and cell shrinking dynamic. This behaviour is in line with the generally accepted mechanisms of tubulin binding agents (TBAs) (Lippert, 2007) involving activation of RhoA/RhoA kinase, an intracellular coordinator of cytoskeletal rearrangement of microtubules and actin. In my experiment with **1**, 518A2 cells were able to repair the shrinkage effects and most of them spread again after three hours. The results from the transmission electron microscopy experiments with 518A2 cells treated with the chalcone (**1**) are likewise in accordance with its effects on the cell cycle. The maintenance of the microtubule integrity plays a pivotal role in stabilizing the pericentriolar matrix. The occurrence of centrioles as a result of aberrant chromosome segregation could be due to DNA damage (possibly in tandem with defective checkpoints) or to a destabilization of the spindle apparatus (Castedo et al., 2004; Vitale et al., 2007). However, the DNA binding activity of **1** is rather minimal.

Effects of chalcone-Pt (2)

Initially, the chalcone dichloridoplatinum(II) (6-aminomethylnicotinate) complex **2** (chalcone-Pt) was chosen as an example of a chalcone Pt-conjugate (Biersack, 2009; Schobert et al., 2009). The extraordinary 6-aminomethylnicotinate ligand system was chosen due to previous anticancer investigations on terpene Pt(II) conjugates, where this ligand system proved to be much more active against 518A2 melanoma cells than saturated ligand systems (Bernhardt et al., 2008).

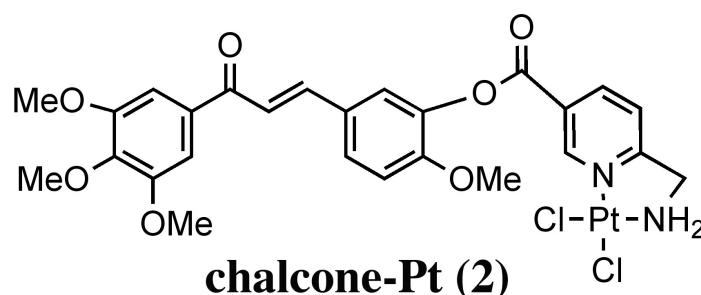


Figure 4- 1 Structure of the chalcone-Pt conjugate 2.

4.1 Inhibition of cell growth - MTT assay

4.1.1 Neural cells

The relative cytotoxicities of conjugate **2** against tubulin-rich cells of neural origin were analysed (Table 4- 1). Normal mouse astroglia did not reveal pronounced sensitivity towards the compound during the whole 48 h incubation period, while human U87 glioma cells were initially refractory to **2**, yet, they responded well upon prolonged exposure. The primary neurons were sensitive to a prolonged treatment, too. Strongly cytotoxic effects of **2** were observed against C6 rat glioma cells with IC_{50} (48 h) values of ~170 nM and likewise against NE-4C stem cells derived from the fore- and midbrain vesicles of p53-deficient 9-day-old mouse embryos (Schlett and Madarasz, 1997) after exposure for 48 h.

Table 4- 1: Inhibitory concentrations IC_{50} (μ M) of chalcone-Pt (**2**) in various neural and non-neural WEHI 164 cells (MTT-assay) after incubation for 24 and 48 hours.

Cell line	Astroglia	U87	Neurons	NE-4C	C6	WEHI 164
24 h (2)	100	-	60 ± 8	2.4 ± 0.7	0.38 ± 0.02	9 ± 1
48 h (2)	100 ± 4	0.14 ± 0.08	1.5 ± 0.3	0.04 ± 0.02	0.17 ± 0.02	24 ± 4

- IC_{50} was not reached

The WEHI 164 fibrosarcoma cells, which were included for comparison purposes, remained resistant to the chalcone platinum complex **2**.

4.1.2 Tumor cells expressing ABC-transporters

ABC-transporters pump drugs out of cancer cells and are responsible for chemoresistance. Their interference with **2** was investigated by using various human cancer cells expressing these transporters, such as MCF-7 breast, KBv1 cervix and HT-29 colon carcinomas (Table 4- 2). These cells had been grown in the presence of specific substrates of their transporters to stimulate their overexpression. By long-term exposure to topotecan resistant MCF-7^{+Top} cells over-expressing exclusively BCRP (breast cancer resistance protein) were obtained. Chalcone-Pt (**2**) exhibited a distinctly lower activity in both MCF-7 cell lines. Resistant KBv1^{+Vbl} cells over-expressing P-gp were obtained by treating the wild type cells with vinblastine. Complex **2** was highly efficacious against both KBv1 cell lines with a slight edge for the resistant KBv1^{+Vbl}. HT-29 cells feature a high amount of multi-resistance protein 3 (MRP3) and a low amount of MRP1. When treated with colchicine, HT-29 cells shift this ratio by overexpressing MRP1 and cutting back on MRP3 (Cummings et al., 2004; Kok et al., 2000). Chalcone-Pt (**2**) was little active in HT-29 cells but performed a little bit better in the HT29^{+Colc} cells. A similar trend was observed for cisplatin (*chapter 5.3.1*). According to literature (Kok et al., 2000) colchicine-induced overexpression of MRP1 is accompanied by changes in sphingolipid composition. It has to be mentioned that the sphingolipid metabolism is performed in Golgi apparatus (*cf. chapter 4.3.5*)

Table 4- 2: Inhibitory concentrations IC₅₀^a (μM) of chalcone-Pt (2**) for various ABC-transporter expressing cells (MTT-assay).**

Cell line	MCF-7	MCF-7 ^{+Top}	KBv1	KBv1 ^{+Vbl}	HT-29	HT-29 ^{+Colc}
24 h (2)	40 ± 2	34.6 ± 3.6	0.8 ± 0.09	1.2 ± 0.3	76 ± 4	47 ± 1
48 h (2)	28 ± 4	18 ± 1.2	0.5 ± 0.03	0.12 ± 0.02	38 ± 6	24 ± 0.7

^aValues are derived from concentration-response curves obtained by measuring the percentual absorbance of vital cells relative to untreated controls (100%) after 24 and 48 h exposure of selected cells to test compounds in the MTT assay. Values represent means of at least three independent experiments ± standard deviation.

4.1.3 Cancer cells

HL60 leukaemia cells and 518A2 human melanoma cells served as control cells, which do not overexpress any ABC-transporter. They were likewise chosen for

4. Effects of chalcone-Pt (2)

cytotoxicity tests for chalcone-Pt (2) via MTT assay. The cytotoxic activities, represented as IC₅₀ (μM) values, were evaluated from a plot of percent cytotoxicity against the sample concentrations. Figure 4- 2 shows the cytotoxicity profiles of against 2 against HL60 and 518A2 cells. A biphasic activity of was observed for 2 very similar to the profile of the previously tested chalcone (1) (chapter 3.3.3).

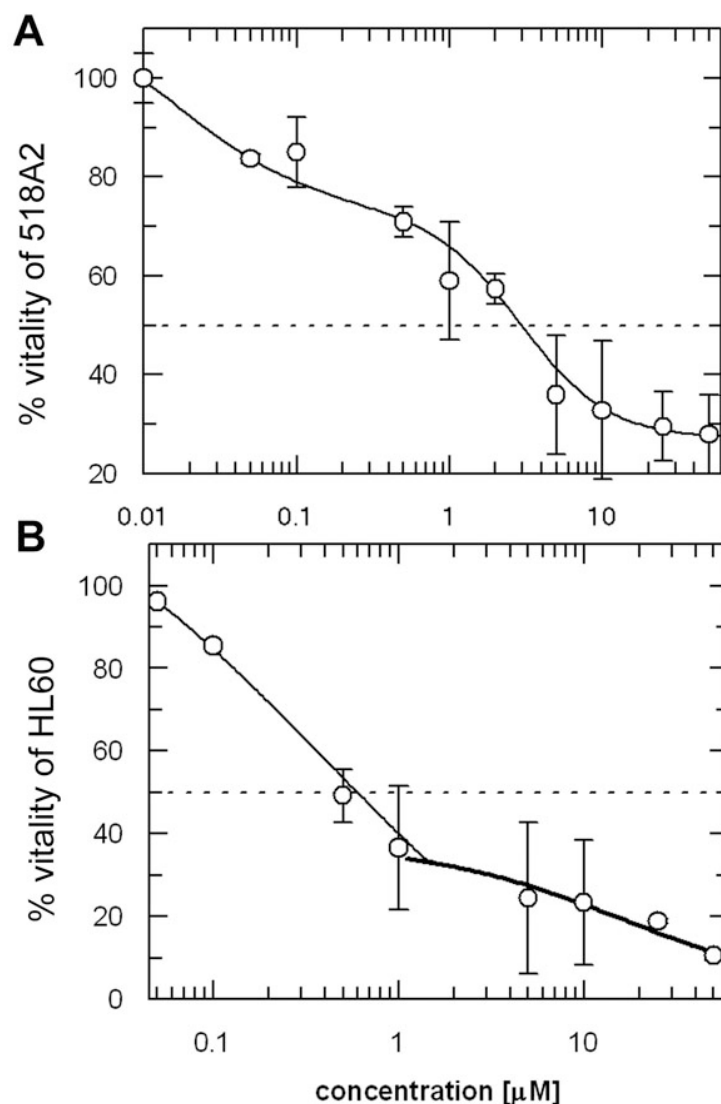


Figure 4- 2 Dose response curves (MTT assay) of chalcone-Pt (2) in 518A2 (A) and HL60 cells (B).

Their vitality rapidly decreased after treatment with 2 (IC₅₀'s in Table 4- 3). Similar results were reported for parent chalcone (1) revealing high (nM) activity against K562 leukemia cells (Ducki et al., 1998; Schobert et al., 2009).

Table 4- 3 Inhibitory concentrations IC₅₀^a (μM) of chalcone-Pt (2) in HL60 leukaemia and 518A2 melanoma cells (MTT-assay).

Compound/ Cell line	2 (24 h)	2 (48 h)
HL60	0.57 ± 0.15	0.26 ± 0.01
518A2	21 ± 0.7	3.4 ± 0.9

The adherently growing 518A2 cells responded better after longer exposure to complex **2** giving IC_{50} values of $\sim 3.4 \mu M$ (48 h) and $57.2 \pm 11 \text{ nM}$ (96 h) (Schobert et al., 2009). It was also shown that conjugate **2** exhibited excellent antiproliferative activities with similar magnitude and cell line specificity as shown for chalcone (**1**) (Schobert et al., 2009).

4.2 Cellular uptake of chalcone-Pt (**2**)

In order to ascertain whether the platinum complex **2** is crossing the cell membrane by endocytosis, a temperature-dependent experiment was performed. The experimental conditions for 518A2 melanoma cells were optimized for conjugate **2** and applied for all uptake experiments.

4.2.1 Inhibition of endocytosis by temperature change

Treatment of 518A2 cells with $200 \mu M$ chalcone-Pt (**2**) was carried out at two different temperatures, $37^\circ C$ and $4^\circ C$. Untreated cells served as a reference (Figure 4-3).

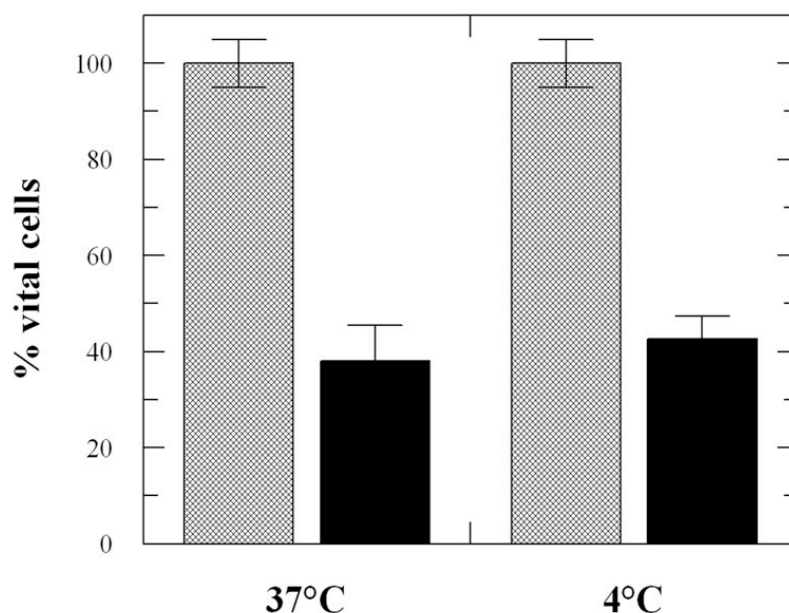


Figure 4- 3 Time dependent effect of 518A2 cells after 3.5 h exposure to chalcone (**2**) ($200 \mu M$; black bars). Vital cells were determined by MTT assay at $37^\circ C$ and $4^\circ C$. Vital cells of untreated controls (hatched bars) were set to 100%.

The cytotoxic effect of **2** on the melanoma cells was not postponed after their incubation at $4^\circ C$ and showed almost identical data with incubation at $37^\circ C$, which left ca 40% cells alive. This result opened another question: How does chalcone-Pt enter the cells?

4. Effects of chalcone-Pt (**2**)

4.2.2 Inhibition of drug uptake with specific inhibitors

A detailed analysis of chalcone-Pt (**2**) uptake was carried out. Specific inhibitors were used to inhibit several pathways of drug entry with the same concentrations and timing as described in chapter 4.2.1. Alternative ways for the entry of platinum complexes into cells involve copper transport receptor 1 proteins (Ctr1) and human organic cation transporters (OCT). Gust et al. studied their relevance by switching off individual transporters with specific inhibitors (Kapp et al., 2006). The OCT conveys positively charged substances and may be inhibited by cimetidine (inhibitor) or by tetraethylammonium chloride (TEA; competitor).

Based on the low temperature experiments, the role of endocytotic processes appears to be minor. Several endocytotic inhibitors were used to block different transporters and/or ion-porters. Endocytosis depends also on the Na^+/K^+ pump depending sodium gradient, which is inhibited by ouabaine (Ivanov et al., 2004). Macropinocytosis, a distinct form of endocytosis, depends on Na^+/H^+ exchange that can be blocked by amiloride (Kapp et al., 2006; Meier et al., 2002). The enzyme phosphatidylinositol 3-kinase plays a central role in the down-stream signalling cascade associated with macropinocytosis by F-actin microfilament re-arrangement, and can be inhibited by the fungal metabolite wortmannin (Zhang et al., 2003). Clathrine-mediated endocytosis can be blocked by chlorpromazine (Nawa et al., 2003).

The inhibitors doses were varied to find out the concentration range with negligible toxic effects on the cells within the given time range. After optimisation, their influence on the uptake of chalcone-Pt (**2**) into 518A2 melanoma cells was examined. First of all, the cells were pre-incubated with non-toxic concentrations of the respective inhibitors for 15 min before the chalcone-Pt (**2**) was added, and its cytotoxicity was measured by the common MTT assay. Figure 4- 4 illustrates the effects of the individual inhibitors on the cytotoxicity of complex **2** (black bars) against 518A2 cells and so indirectly also the share that the various transport pathways blocked by these inhibitors have in the uptake of **2**.

The previously described results were confirmed, i.e, treatment of the cells with 200 μM chalcone-Pt (**2**) in the absence of any inhibitors for 3.5 h left $40 \pm 5\%$ of the cells vital. Pre-incubation with 5 μM ouabaine (Na^+/K^+) attenuated the cytotoxicity of **2** by ca. 24% leaving $58 \pm 4\%$ of the cells alive.

Clathrine-dependent endocytosis contributed marginally (ca 14%) to the uptake of complex **2**. Uptake of **2** *via* Na⁺/H⁺ pump driven macropinocytosis seemed to play no role. Cell entry of complex **2** took place mainly *via* OCT (32%) as shown by an increase of viable cells to ca. 61% and *via* Ctr1 (20%) as the addition of 8 nM CuCl₂ increased the percentage of viable cells to ca. 55%.

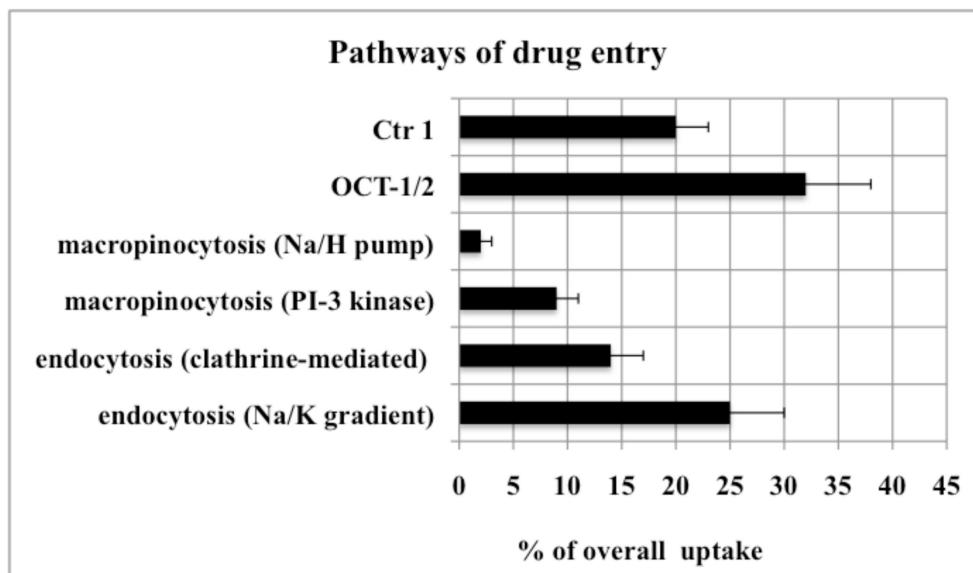


Figure 4- 4: Contribution of various pathways to the accumulation of complex **2** (black bars) by 518A2 melanoma cells as calculated from the attenuation of their cytotoxicity upon addition of specific inhibitors.

4.2.3 Western blot analysis of OCT1/2 in melanoma 518A2 cells

The copper transporters Ctr1 exist in all eukaryotic cells (Petris, 2004). It is known that cisplatin is transported *via* OCT1 (=SLC22A1 and OCT2 (=SLC22A2) transporters (Zhang et al., 2006). Koepsell et al. and others have assessed the organ/tissue distribution of the various types of Organic Cation and Carnitine transporters and have found evidence for their presence in pertinent cancer cell lines, too (Koepsell et al., 2007). An abundance of OCT's transporters in tumor cells was assumed (Schobert et al., 2009) but the expression of studied transporters in 518A2 cells was not confirmed, yet. Therefore, the presence of the solute carrier transporters family (SLC22A1-2) in tested melanoma 518A2 cells and cervix carcinoma KBv1^{+Vbl} cells has been identified by Western blot analysis. The blots showed the presence of several bands after staining with organic cation transporters-1. The band showing ~54 kDa size was indentified as organic cation transporter-1. Several isoforms of OCT-1 found in humans are known (UniProtKB). The primary antibody of OCT-1 recognized the N-terminus of the transporter. The N-termini of OCT-1 and OCT-2 transporters showed highly (~85%) conserved amino-acid sequences. Hence, staining

4. Effects of chalcone-Pt (**2**)

against the OCT-2 C-terminus was likewise carried out and it was possible to detect this protein in 518A2 cells, too.

It was shown for the first time that both melanoma 518A2 and KBv1^{+Vbl} cells readily express organic cation transporters (OCT-1 and OCT-2).

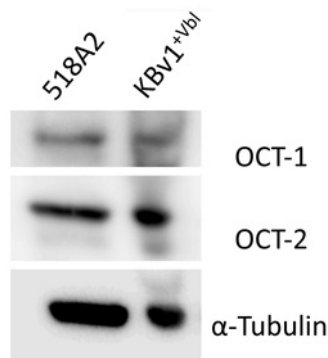


Figure 4- 5 Detection of organic cation transporters in 518A2 and KBv1^{+Vbl} cells by Western blot analysis; α -tubulin serves as a control. The shown experiment was performed by Andreas Brown.

4.2.4 Platinum contents of 518A2 cells treated with **2** (via ICP-MS)

To confirm the uptake results the platinum content of 518A2 cells optionally pre-incubated with individual inhibitors (5 μ M ouabain, 500 μ M cimetidine, 100 μ M TEA) was determined after treatment for 3.5 h with 200 μ M of complex **2**. The maximum amount of **2** taken up in the absence of the mentioned inhibitors was 4 μ g/L Pt *per* mg cells. The Pt-content of cells pre-incubated with 5 μ M of the Na⁺/K⁺-pump inhibitor ouabain was reduced to 1.3 μ g/L *per* mg cells corresponding to a decrease in uptake of **2** by 68% (Table 4- 4).

Table 4- 4 Pt-content by ICP-MS of 518A2 cells treated for 3.5 h with 200 μ M complex **2**.

Incubation of 518A2 cells	Amount of Pt [μ g/L]/mg cells	Decrease of uptake [%]
200 μ M chalcone-Pt (2)	4 \pm 1.1	0
5 μ M ouabain + 200 μ M (2)	1.3 \pm 0.1	68 \pm 6
500 μ M cimetidine + 200 μ M (2)	1.6 \pm 0.2	60 \pm 9
100 μ M TEA + 200 μ M (2)	0.8 \pm 0.2	79 \pm 21

Pre-incubation with the OCT inhibitor cimetidine diminished the Pt-uptake by ca. 60%. An even greater reduction (80%) of the Pt-content was found in cells pre-incubated with 100 μ M tetraethylammonium chloride (TEA), a competitive substrate for OCT. The effects of the various inhibitors on the uptake of complex **2** differ significantly when determined from the decrease of the platinum content *versus* the cytotoxicity assays.

The ICP-MS results advocate a 2–3.5 times greater inhibitory effect when compared to those from the MTT tests. While cytotoxicity is a complex phenomenon elicited by, yet not restricted to the effects of the intact drug administered, the platinum content is just the amount of platinum inside of and attached to the cells.

Taken together, these results represent strong evidence for the Na^+/K^+ -pump driven endocytosis and OCT's as the main mechanisms of accumulation of platinum complex **2** by 518A2 melanoma cells.

4.3 Cellular and sub-cellular observations

4.3.1 Inhibition of drug uptake monitored by time-lapse microscopy

To verify the results from the uptake studies employing specific inhibitors time-lapse micrographs were taken from 518A2 cells pre-treated with $10\ \mu\text{M}$ amiloride, an inhibitor of endocytosis. The cells treated with complex **2** showed the same effects of cell rounding and increased motility as without addition of amiloride (Figure 4- 6). This finding corroborates that the Pt-complex **2** relies on dedicated transporters (OCT's and Crt1).

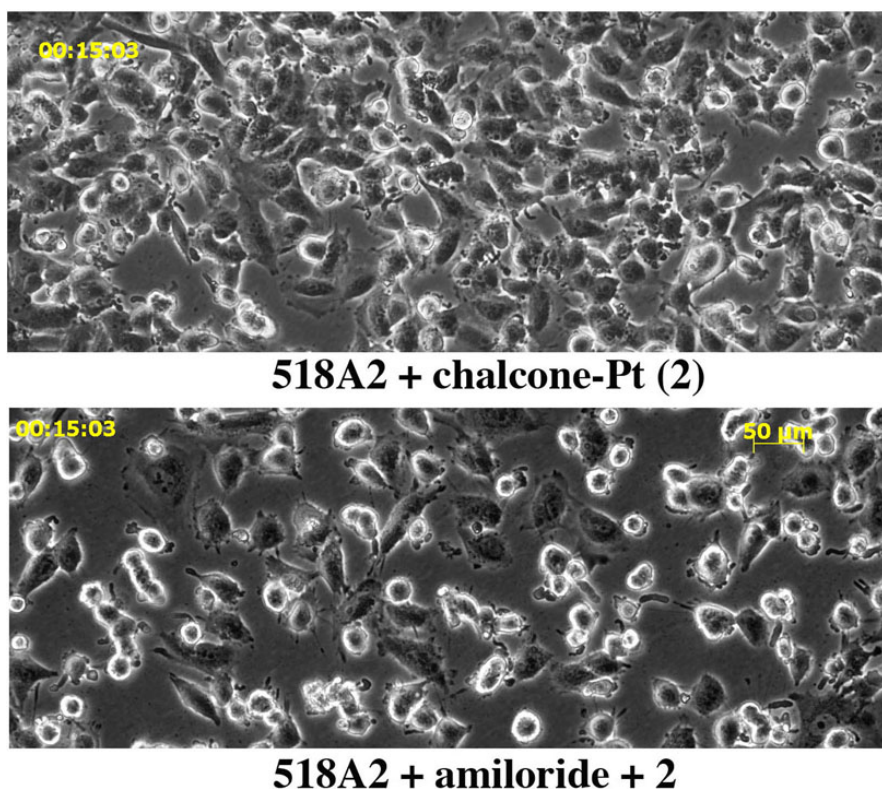


Figure 4- 6 Time-lapse recording micrographs of 518A2 melanoma cells pre-treated with $10\ \mu\text{M}$ amiloride (bottom), an inhibitor of endocytosis (macropinocytosis), and incubated with $10\ \mu\text{M}$ Pt-complex **2** (top).

4. Effects of chalcone-Pt (2)

4.3.2 Altered cell shapes of cells treated with chalcone-Pt (2)

4.3.2.1 Altered cell shapes in neural cells

Neurons are particularly rich in tubulin and so are well suited to test agents affecting microtubule organisation. Neurons treated with 10 μM **2** caused only an incomplete disruption of the networks (Figure 4- 7).

Some cells got closer to each other; their bodies were swelling and aggregating. Most of the somas coagulated and neural network processes were disconnected from the cell bodies of adjacent neurons.

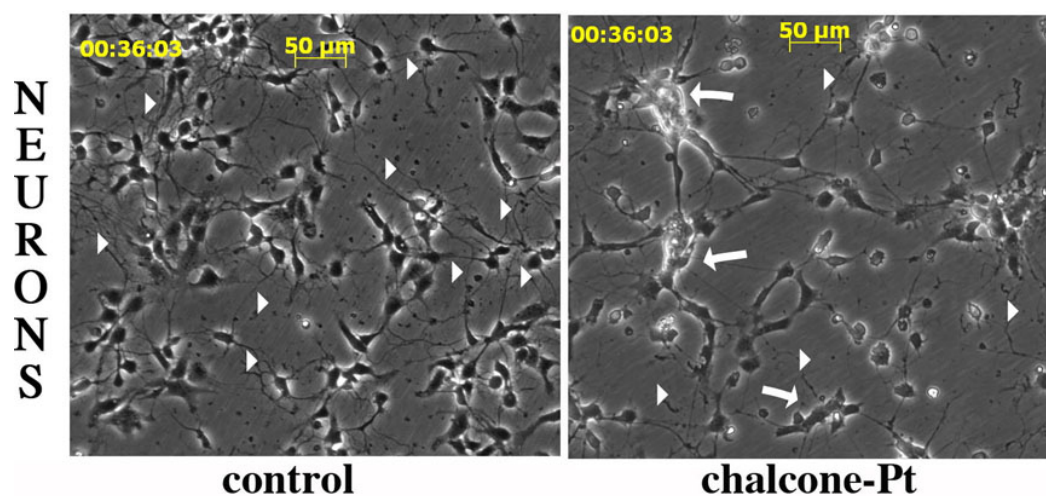


Figure 4- 7 Altered cell-shape of neurons treated with chalcone-Pt (2). Left: untreated neurons with prolonged axons (arrowheads); right: upon incubation with 10 μM **2** some axons (arrowheads) retracted and most somas coagulated (arrows).

4.3.2.2 Altered cell shapes in 518A2 cells

An analogous experiment was performed with 518A2 melanoma cells, which were initially attached as a monolayer to the surface of the mini Petri dish. Overall, dynamics and motility of untreated cells was slow as they underwent merely negligible morphological changes. Only a few cells detached from the monolayer within the first two hours. In contrast, exposure of 518A2 cells to chalcone-Pt (**2**) has led to a rounding and an enhancement of motility and cell shrinking dynamic already after 15 minutes (Figure 4- 8).

The cells readily dissociated from the monolayer and their form turned from flat to spherical. This behaviour is in line with the generally accepted mechanisms of tubulin binding agents (TBAs) (Lippert, 2007) involving activation of RhoA/RhoA kinase, an intracellular coordinator of cytoskeletal rearrangement of microtubules and actin. In the experiment with conjugate **2**, 518A2 cells were able to repair the shrinkage effects and most of them spread again after three hours.

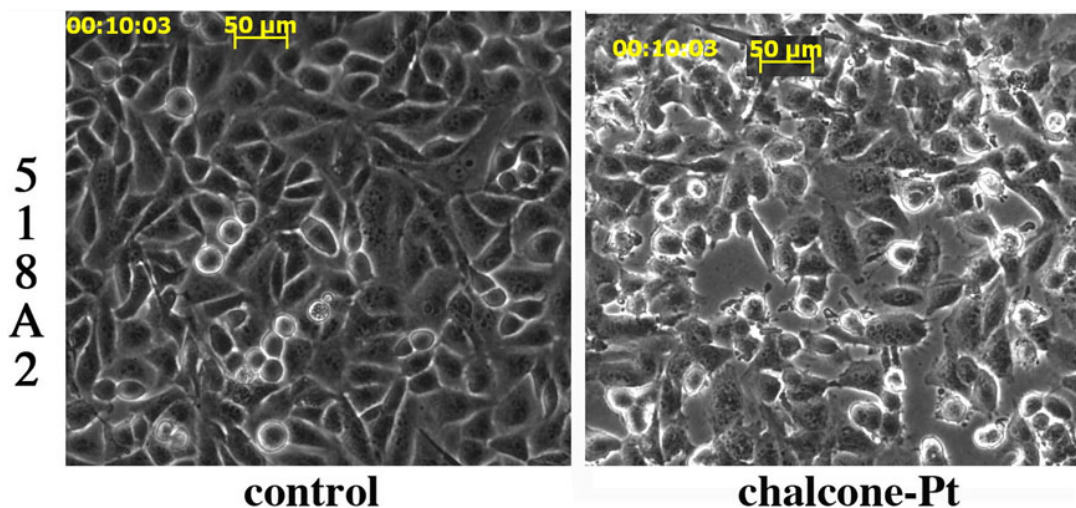


Figure 4- 8 Altered cell-shape of 518A2 cells treated with chalcone-Pt (2). Left: untreated 518A2 melanoma cells (control); right: effect upon treatment with 10 μ M of complex 2.

4.3.3 Actin distribution induced by chalcone-Pt (2)

4.3.3.1 Actin distribution in astrocytes

An immunocytochemical analysis of the morphological changes of the actin filaments of astrocytes initiated by conjugate **2** was carried out and compared with the behaviour of 518A2 melanoma cells.

Antibodies to astrocyte-specific GFAP intermediate filaments (glialfibrillary acidic protein) were employed to visualize the astroglial cells and phalloidin labelling was used to identify actin filaments. The micrographs showed that both types of filaments, actin (in green) and GFAP (in red), were disintegrated upon treatment with the test compound, most pronouncedly the actin filaments near the cell membrane. The GFAP filaments shrank only in the vicinity of the cell nuclei, which remained unaffected. Figure 4- 9 shows typical effects of chalcone-Pt (**2**) on astrocytes.

Their proliferating activities are clearly visible by spread GFAP and actin connections forwarded into the unoccupied place. The GFAP and actin filaments concentrated around the nuclei. The space in the vicinity of the cell membrane stayed empty.

4. Effects of chalcone-Pt (2)

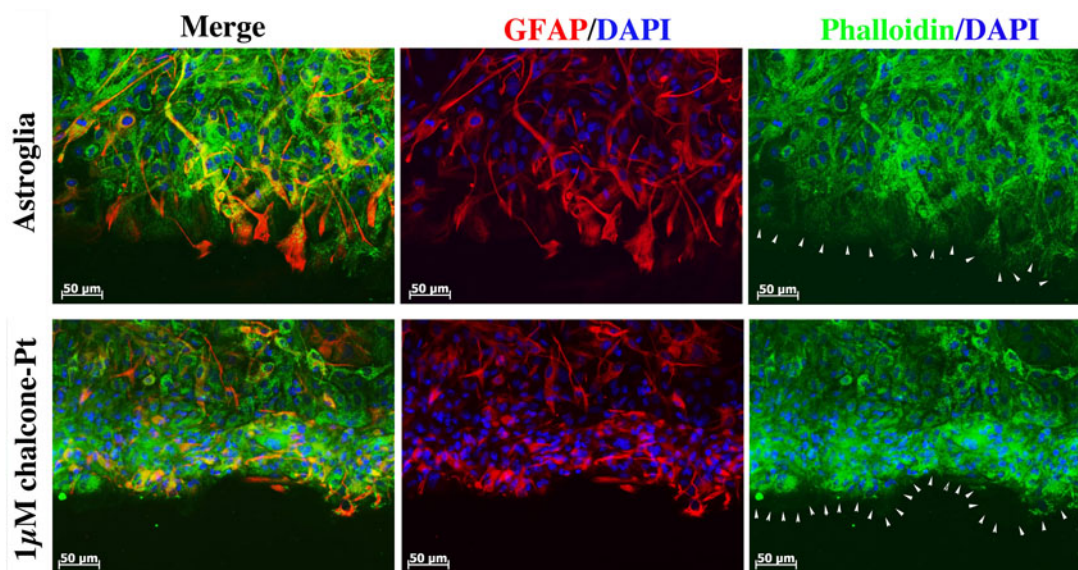


Figure 4- 9 Immunostaining of astroglia cells untreated and treated with 1 μ M chalcone-Pt (2) for 72 h (right). *Blue*: nuclei stained with DAPI (4',6-diamidino-2-phenylindole); *green*: actin cytoskeleton stained with phalloidin; *red*: glial fibrillary acidic proteins (GFAP). White arrowheads indicate the cell membrane.

4.3.3.2 Actin distribution in 518A2 cells

Fluorescence micrographs of immunostained 518A2 cells were performed. Similarly to the results obtained from the astrocytes, a significant breakdown of the actin network was evoked after treatment with chalcone-Pt (2) (Figure 4- 10).

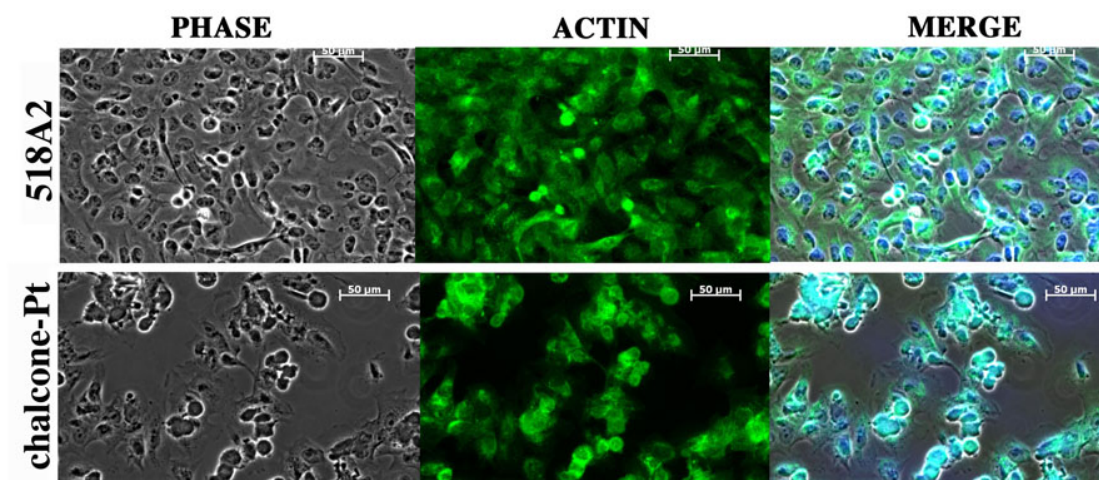


Figure 4- 10 Actin immunostaining of untreated 518A2 cells and cells treated with 10 μ M Pt-complex 2 for 24 hours (bottom row). *Blue*: nuclei stained with DAPI (4',6-diamidino-2-phenylindole); *green*: actin cytoskeleton stained with phalloidin; bar represents 50 μ m scale.

4.3.4 Microscopic observations of 518A2 cells by Giemsa staining

An effect of conjugate 2 on filament distribution was discovered in the previous chapter 4.3.3. It was shown recently that 2 is able to inhibit *in vitro* microtubule polymerization (Schobert et al., 2009), and the described neural experiments confirmed effects on its microtubule-based network system. In neural cells nuclei remained untouched but in 518A2 cells nuclei were close together.

Therefore, internucleosomal DNA cleavage was monitored with Giemsa staining and examined under a light microscope. Using a 10 μ L tip, the plate was scratched to form letter X (*cf.* material and methods part).

The cytotoxic effect of the 22 μ M chalcone-Pt (IC_{50} concentration) on the proliferation as well as on the attachment of the adherent cells was analyzed upon exposure for 24 hours Figure 4- 11. The altered cell shape was very similar to that already observed in the previous experiments. The control cells were wide and spread with typical 518A2 shapes, the nuclei were well defined by their nuclear envelope showing condensed chromatin as a dark blue–dots. The scratched X-cross disappeared during incubation for 24 hours. The number of chalcone-Pt (2) treated cells decreased. These 518A2 cells got close to each other and formed aggregates with visible nuclear envelopes. Some late apoptotic or dead cells were visible featuring spread cells with purple cytoplasm.

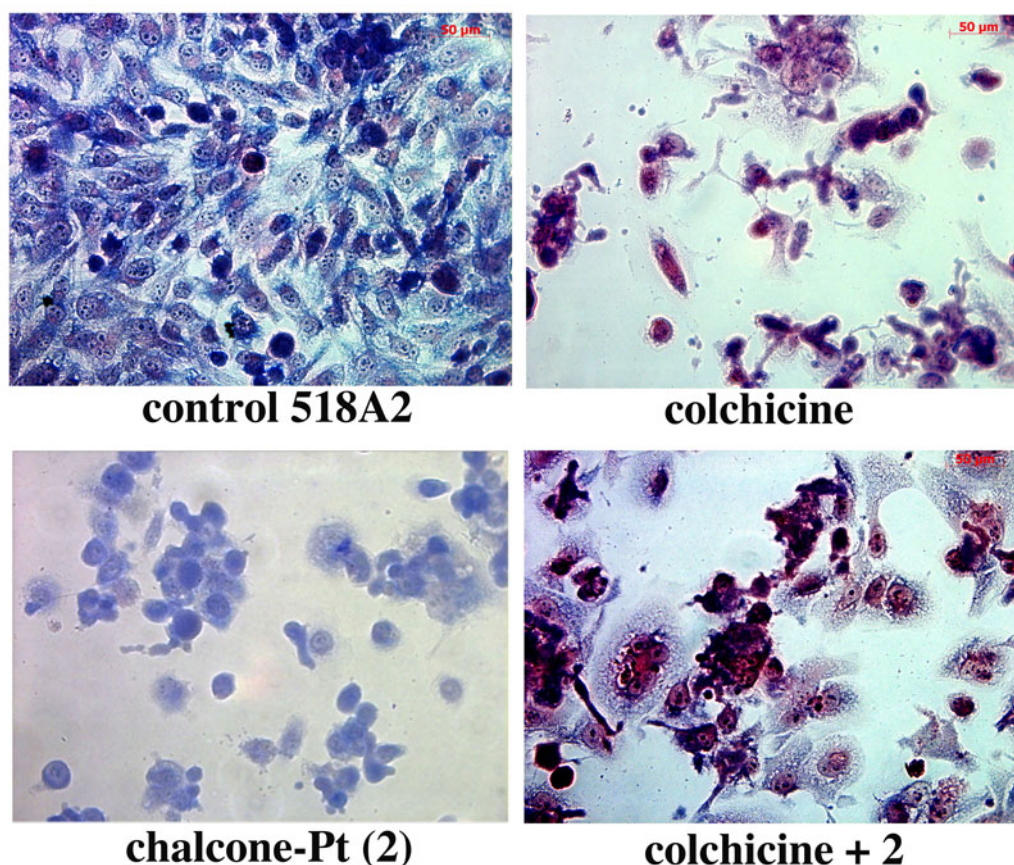


Figure 4- 11. Samples of 518A2 cells treated with test compounds were stained with Giemsa dye after 24 hours of incubation. Untreated control cell served as a reference. Applied concentrations: colchicine 62.5 nM, chalcone-Pt (2) 22 μ M, mixture: 31.3 nM of colchicine + 11 μ M of chalcone-Pt (2).

The effect of the known tubulin inhibitor colchicine on 518A2 cells has not been investigated, yet. Therefore, similar experiments were performed with colchicine (62 nM) on 518A2 cells. The cell number of colchicine treated cells rapidly decreased.

4. Effects of chalcone-Pt (2)

The cells occasionally formed aggregated structures. Surprisingly, no nuclei envelopes were observed and all cells were slightly pink-purple, some were spread, and some were still rounded. This cell behaviour is different from that observed for chalcone-Pt (2). The combination of both drugs in using halved IC₅₀ concentrations (31.3 nM of colchicine + 11 μM of the chalcone-Pt) led to a mixture of the individually described phenomena Figure 4- 11. The cell number decreased but not as rapidly as after single agent-treatments with colchicine or 2. The nucleus envelope was hardly detectable in most of the cells. Colchicine structurally differs from chalcone-Pt (2). It is possible that their effect on α-tubulin binding in *in vitro* tubulin polymerization experiments could be similar, however, in living cells additional mechanisms like the uptake can play a key-role. It is also possible that the chalcone fragment has a different binding mechanism and/or a higher affinity to different kinds of tubulin.

4.3.5 Transmission electron microscopy

Morphological and sub-cellular effects of conjugate 2 on 518A2 melanoma cells were studied by transmission electron microscopy (TEM). The cells were treated with 0.1 mM chalcone-Pt (2) for 15 minutes, kept under fresh medium ~1 hour and monitored using transmission electron microscopy (TEM). The mitochondria population is more condensed in drug-treated cells (in Figure 4- 12 visible as prolonged darker dots) in comparison to untreated cells. While untreated cells appeared prolate and undifferentiated showing filopodia for cell attachment on the rim, cells incubated with chalcone-Pt (2) adopted a rounded shape. A similar morphological change has been reported for H460 non-small cell lung cancer cells treated with combretastatin A-4 (CA-4) (Vitale et al., 2007). In addition, the treated 518A2 cells showed blebs emerging on their surface. Untreated cells appeared undifferentiated revealing filopodia residues for cell attachment around the cell edge (Figure 4- 12). Control cells and treated cells also differed concerning the state of their mitochondria, centrioles and Golgi apparatus (GA). Upon treatment with 100 μM 2 for 15 min a rounded cell shape and blebs emerging on the surface was observed.

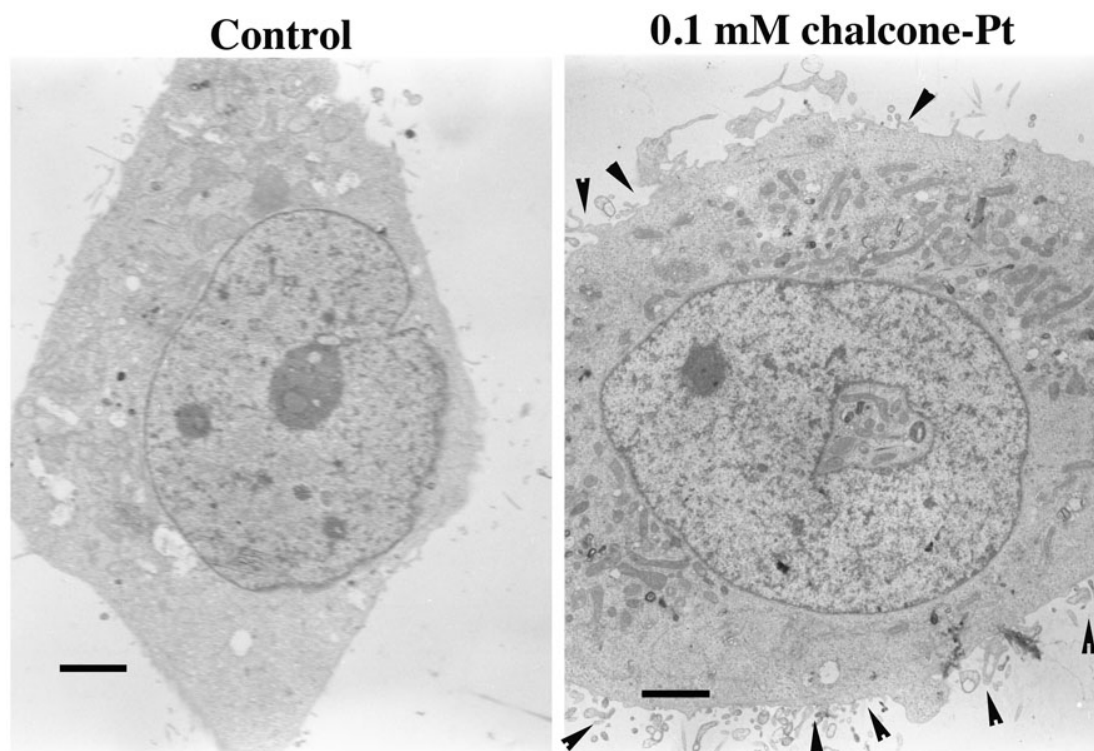


Figure 4- 12 Transmission electron micrographs of 518A2 cells illustrating the differentiation process induced by *in vitro* exposure to chalcone-Pt (**2**). An untreated, undifferentiated control cell was compared with a cell exposed to 100 μM **2** for 15 min. The arrowheads point at the rounded cell shape and blebs emerging on their surface. Black bar = 2.5 μm . Performed according to section 2.5.5.

Mitochondrial populations usually consist of short and long tubules, which constantly migrate along microtubule tracks (Chan, 2006). Any disruption of the microtubules/actin skeleton, e.g., by treatment with chalcone-Pt (**2**), should severely affect the mitochondrial trafficking and cause mitochondrial disorganization. Mitochondria of cells treated with chalcone-Pt (**2**) were highly condensed and localized mainly at the apical side of the cells. They frequently displayed dislocated inner membranes (Figure 4- 13c, e, f). Only a small percentage of the untreated control cells were found in the G2/M phase having visible centrioles. After treatment with **2**, many cells had visible pro-centrioles (Figure 4- 13b), which is an indication for an arrest in the G2/M phase. This observation is in line with results from the cell cycle analysis described above. Stress fibers (Figure 4- 13h) were observed less frequently than in cells treated with **2**. Multivesicular bodies and autophages appeared very often (Figure 4- 13f, h, i), their double membranes were visible in most of the analyzed cells. Maintenance of the microtubule integrity plays a pivotal role for the stabilization of the pericentriolar matrix. The tubulin depolymerising effect of **2** leads to mitotic catastrophe and thus to an arrest in G2/M phase. These observations are consistent with similar mitotic failures of H460 NSCLC cells treated with CA-4

4. Effects of chalcone-Pt (2)

(Vitale et al., 2007). The occurrence of centrioles as a result of aberrant chromosome segregation could be due to DNA damage (possibly in tandem with defective checkpoints) or to a destabilization of the spindle apparatus (Castedo et al., 2004; Vitale et al., 2007).

In 518A2 cells the Golgi apparatus (GA) is frequently located in the vicinity of centrosomes or nuclei envelopes. However, a fragmentation of the GA was observed in 518A2 cells treated with complex 2 (in Figure 4- 13*b, c, f, i* as red arrows). The fragmentation of the GA is, however, an early event that occurs independently of major changes to the actin and tubulin cytoskeleton (Mukherjee et al., 2007). The GA undergoes irreversible fragmentation during apoptosis partially as a result of caspase-mediated cleavage of several Golgi-associated proteins (Mukherjee et al., 2007).

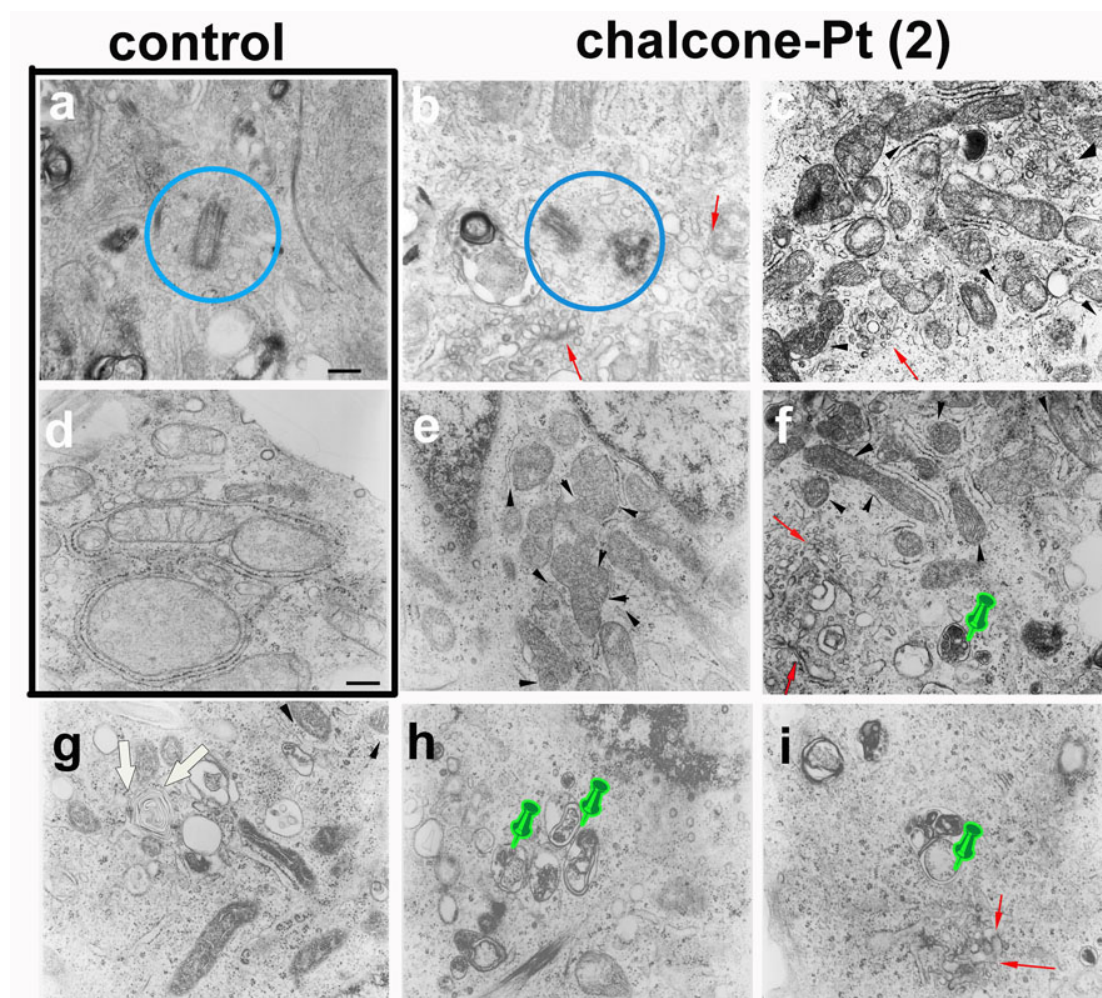


Figure 4- 13 TEM images of organelles in 518A2 cells *a, d*: untreated cells with image *a* showing the longitude section through the centrioles and image *d* shows mitochondria with cristae invaginations surrounded by endoplasmic reticulum. *b, c, e-i* cells treated with 2. Image *e* shows mitochondria at various stages of inner-membrane destruction, image *f* the formation of multivesicular bodies (arrowheads). Some mitochondria were highly condensed (*i, g* stars) and some formed multi-lamellar bodies (arrows). Stress fibers are visible in panel *h*. Black bar = 0.4 μm . Performed according to section 2.5.5.

4.4 Activation of caspase-3 after chalcone-Pt (2) treatment

Caspases involved in apoptosis exist as inactive zymogens that become activated proteolytically when cells are undergoing apoptosis (Thornberry et al., 1997). HL60 cells were monitored up to 24 h and the suspension cells were continuously treated with complex **2**. The initial rate of cleavage of the colorimetric substrate for caspase-3 was determined (Figure 4- 14).

In the case of chalcone (**1**) the activity of caspase-3 is dramatically increased after 12 hours of incubation and reaches a constant value of $1.65 \mu\text{M}$. On the other hand, in the presence of chalcone-Pt (**2**) an increase in activity of caspase-3 is observed after 15 hours. Control HL60 cell extracts had minimal cleavage activity ($\sim 0.25 \mu\text{M}$).

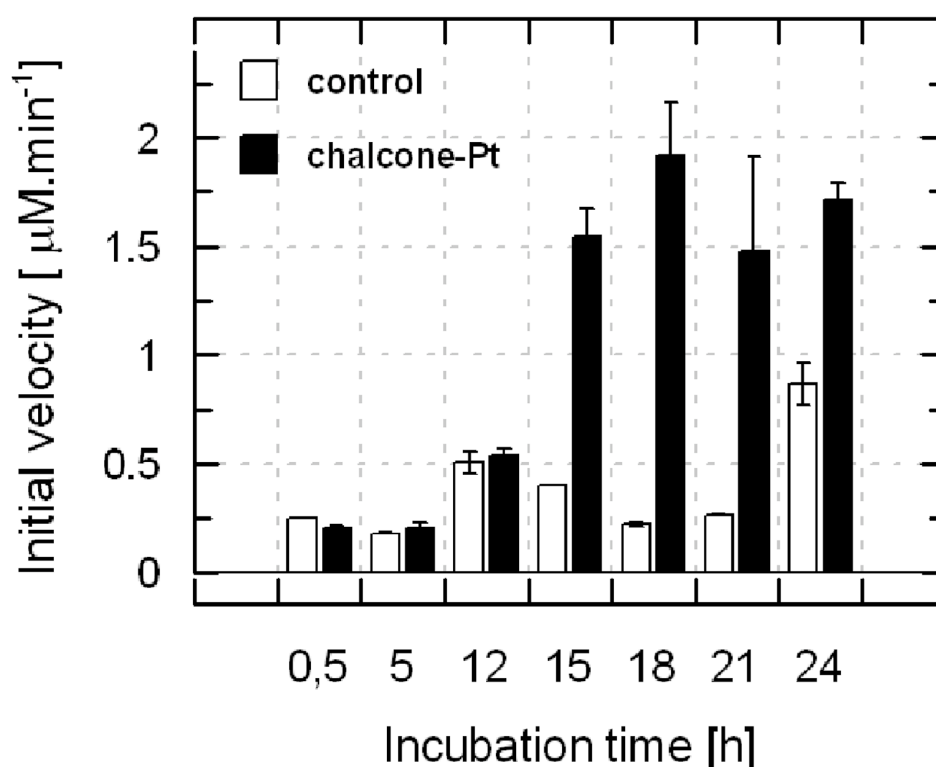


Figure 4- 14 Time dependent caspase-3 activity in HL60 cells after chalcone-Pt treatment ($1 \mu\text{M}$). The assay was carried out in a total volume of $100 \mu\text{L}$. Crude extract of 6 million cells was 10-fold diluted with caspase buffer. Substrate for caspase-3 (Ac-DEVD-pNA) was supplied in concentration $200 \mu\text{M}$ and absorbance at 405 nm was measured using micro-plate reader. To subtract unspecific protease activity, caspase-inhibitor DEVD-CHO was added in $20 \mu\text{M}$ final concentration and incubated for 15 minutes at $37 \text{ }^\circ\text{C}$.

4.5 The role of DNA degradation during apoptosis

4.5.1 Effects of conjugate **2** on chromosomal DNA

Fragmentation of chromosomal DNA and degradation of nuclear matrix is typical for apoptotic cells. Activation of endonucleases initiates DNA cleavage and chromatin is degraded into two distinct fragments: nucleosomal length fragments

4. Effects of chalcone-Pt (2)

(multiples of 180-200 bp) and large (30- to 50-kb) fragments. Level of DNA fragmentation has characteristic-banding pattern commonly known as an "apoptotic ladder" (Peitsch et al., 1993).

The cytotoxic activity of **2** against KBv1^{+vbl} cells was $\sim 1 \mu\text{M}$. Thus, 24 hours incubation was performed followed by DNA isolation and electrophoretic analysis (Figure 4- 15). Indeed, treatment with conjugate **2** caused apoptotic laddering and strong bands of ~ 200 bp.

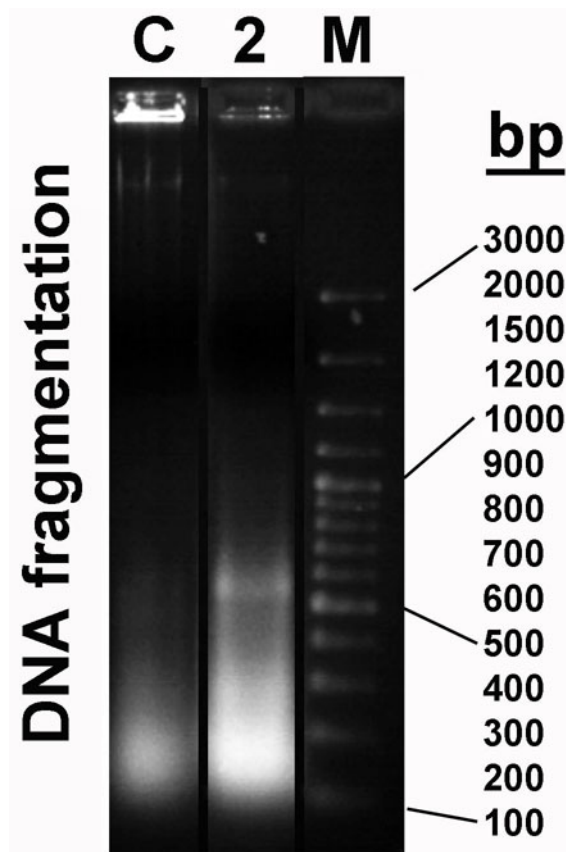


Figure 4- 15 DNA fragmentation in KBv1^{+vbl} cells after treatment with $1 \mu\text{M}$ chalcone-Pt (**2**). Control cells, lines 1 and 2. Cells treated with chalcone-Pt (**2**), line 3. Commercially available DNA ladder between 3kbp - 100bp was used, line 4. Electrophoresis was carried out on a 1.5% agarose gel for 4 h at 12V/cm.

4.5.2 Cell cycle analysis

Chalcone (**1**) was found to arrest cells of the human T24 and HT-1376 bladder cancers in the G2/M phase (Shen et al., 2007). We now assessed the cell cycle progression of melanoma 518A2 cells treated with chalcone-Pt (**2**) by FACS analysis after DNA staining with propidium iodide (PI) (Figure 4- 16).

The FACS analysis showed 63% of untreated 518A2 cells in G1 phase, 24% in S phase and 13% in G2/M phase after 18 h. 518A2 cells treated with $250 \mu\text{g/L}$ nocodazole, a synthetic analogue of taxol, were mainly in sub-G1 phase after 18 h, a shorter 12 h exposure led to 76% of the cells in G2/M phase. 518A2 cells treated with

10 μ M of Pt-complex **2** stopped in G2/M phase (59%) which is typical for chalcones, but the amount of cells in G1 phase increased as well (19%). 22% of the cells stayed in the S phase. For comparison, treatment with cisplatin led to 69% of 518A2 cells arrested in G1 phase.

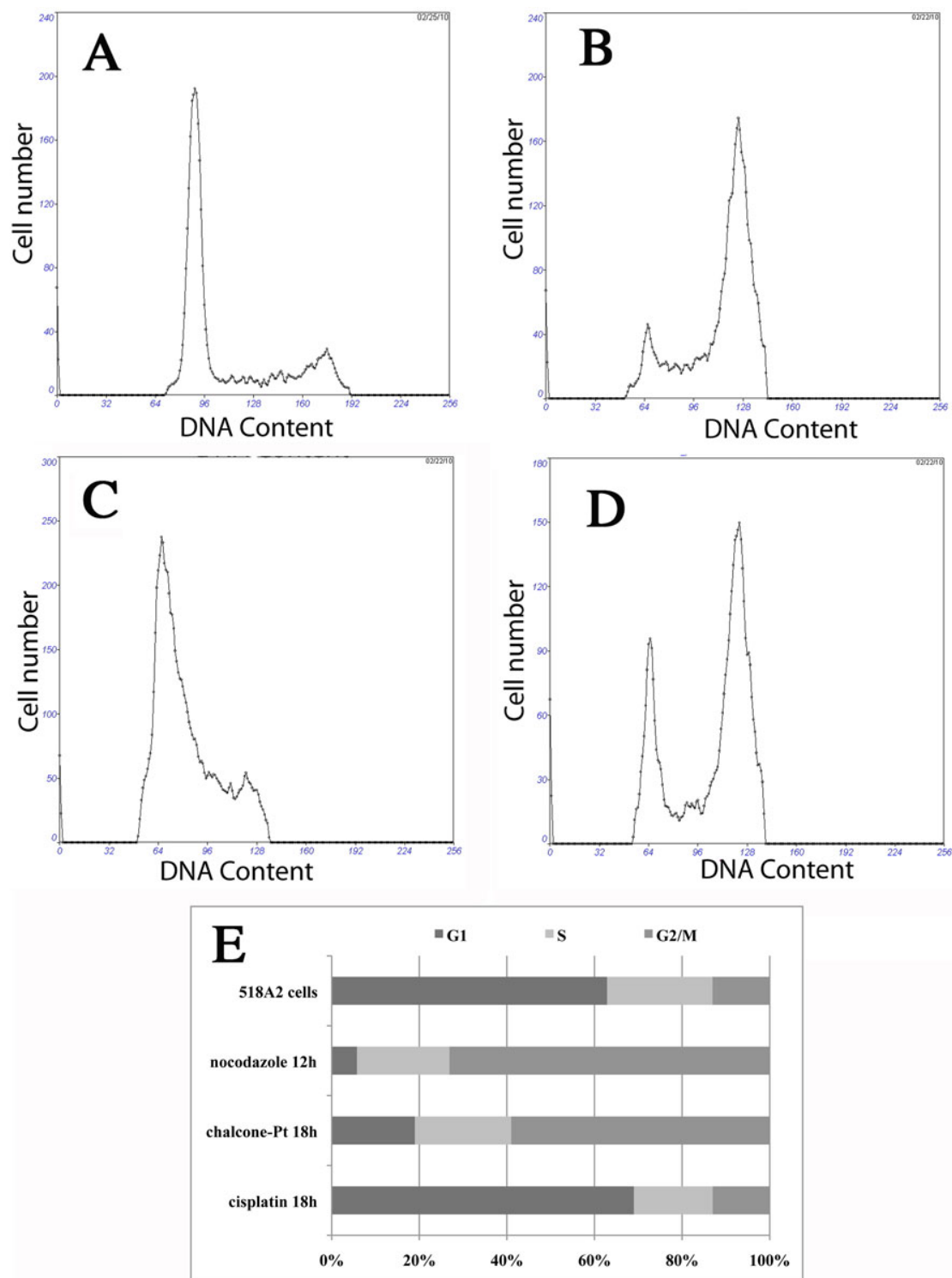


Figure 4- 16 Flow cytometry analysis of 518A2 melanoma cells stained with propidium iodide. The cells were treated with 250 μ g/mL nocodazole or with 10 μ M of **2** or cisplatin. The FACS measurements and analysis were performed with special assistance of Andreas Brown.

4. Effects of chalcone-Pt (**2**)

Probably, complex **2** has a dual impact on the cell cycle of 518A2 melanoma cells combining the effects of Pt-complexes and of combretastatin A-4 analogues. To dismiss a conceivable hydrolytic cleavage of **2** during incubation, 100 μM of dichlorido(6-aminomethylnicotinic acid)platinum(II), the assumed hydrolysis product of ester **2**, was tested but had no effect on the cell cycle at all. The DNA binding activity of **2** was found to be four times lower than that of the good DNA-binder cisplatin (Schobert et al., 2009). This could be a reason of the lower cells number arrested in G1 phase upon treatment with **2**.

4.6 DNA interaction with conjugate **2**

Up to date, chalcones (1,3-diphenyl-2-propen-1-one) are not known as intercalating or DNA-binding agents. Contrary to the chalcones, platinum based derivatives like cisplatin are well known DNA-binding agents (Lippert, 1999). The main objective of this study is the elucidation of DNA binding properties of Pt conjugates with chalcone (**1**). In order to pinpoint the role of platinum in the anticancer effect of conjugate **2**, its DNA binding behaviour was investigated in greater detail.

4.6.1 Electrophoretic mobility shift assay of plasmid DNA

Agarose gel electrophoresis was applied for the investigation of conformational changes and damages caused to non-genomic DNA (plasmid DNA). The supercoiled circular form (sc) of plasmid DNA possesses higher mobility than the one-nicked open circular form (oc).

Many reports provided evidence for platinum interaction with DNA (Brabec, 2002; Brabec and Balcarova, 1993; Brabec et al., 1990). The unwinding ability of **2** on plasmid DNA was investigated in absence or presence of 0.01 M NaClO_4 . In general, perchlorate allows hydrolysis of Pt complexes (Butour et al., 1990). Surprisingly, in the absence of perchlorate no changes were visible in the DNA mobility of pBR322 plasmid DNA after addition of chalcone-Pt (**2**) (Figure 4- 17A).

In the presence of perchlorate, increased concentrations of **2** incurred dose-dependent unwinding of negatively supercoiled pUC19 DNA (Figure 4- 17B). The amount of plasmid sc-form was reduced with increasing r_b value. The increasing drug concentration led to increased intensity of oc-form probably due to DNA-nicks.

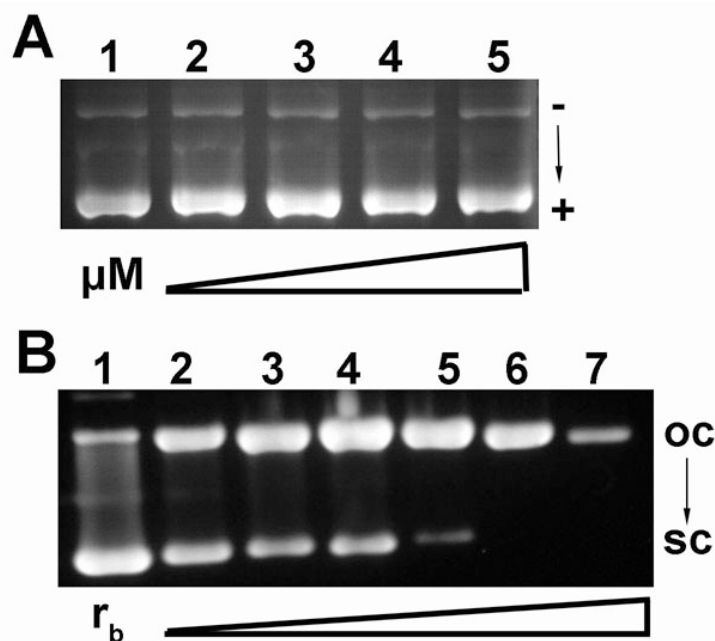


Figure 4- 17 Interaction of plasmid DNA with increasing concentrations of chalcone-Pt (**2**). Open circular form (oc - nicked plasmid). Supercoiled form (sc - closed negatively supercoiled plasmid). Electrophoretogram A) pBR322 DNA incubated with **2** (dissolved in DMF) for 24 hours in different concentrations (line 1-5 \approx 0-5-20-40-60 μ M) applied in 1% agarose gel for 3 h, 65-85 V in TAE buffer. B) Unwinding of supercoiled pUC19 plasmid DNA modified by **2** (resolved in NaClO₄) with r_b 1-7 \approx 0.003, 0.011, 0.019, 0.025, 0.032, 0.07.

4.6.2 Kinetic of DNA binding by chalcone-Pt (**2**)

The previous experiments confirmed the binding ability of chalcone-Pt (**2**) in plasmid DNA. For the next experiments the kinetic of binding and the maximum amount of Pt able to bind to DNA was investigated.

Initially, compound **2** caused platination of calf thymus DNA and r_b values were determined *via* FAAS (Figure 4- 18).

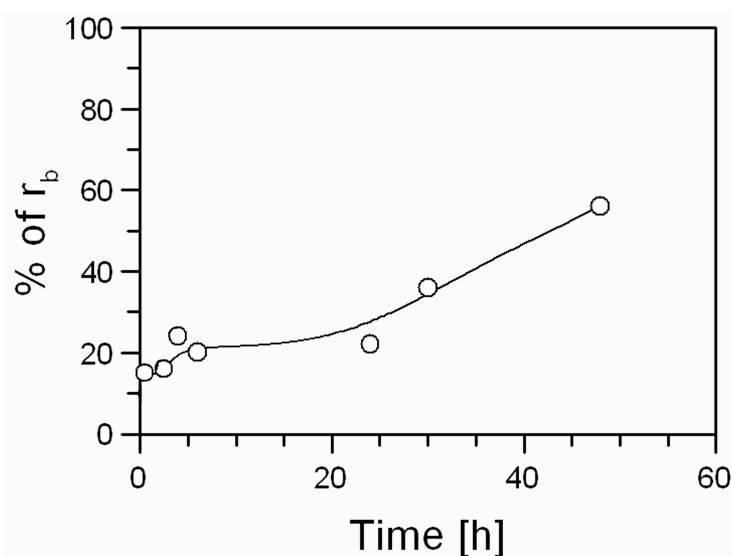


Figure 4- 18 Kinetic of chalcone-Pt binding into the calf thymus DNA in 0.01 M NaClO₄ (r_b-molar ratio of platinum bound to nucleotides).

4. Effects of chalcone-Pt (2)

The binding activity curve reached a maximum of 55% Pt (relative to r_b) after 48 h. A higher concentration of **2** caused (yellowish) precipitation of the whole DNA after 18 hours of incubation. Due to this limitation only a few experiments were performed.

4.6.3 DNA secondary structure changes

To gain further information on the structural changes induced by platinum complex **2**, circular dichroism (CD) spectra of modified DNA were recorded (Figure 4- 19). It has already been mentioned in chapter 3.5.2 that the CD spectrum of ct DNA is very similar to the spectrum of B-DNA (crossing the zero line at 260 nm). The spectrum of conjugate **2** alone showed no changes (Figure 4- 19-A). Conjugate **2** had no intrinsic CD signals so that any CD signal above 350 nm can be attributed to the interaction of complex **2** with DNA. Below 300 nm differences from the untreated DNA spectrum were visible due to DNA perturbation by complex **2**. The spectrum of complex **2** bound to ct DNA showed positive CD bands centered at 278 nm and a negative CD band at 245 nm (Figure 4- 19-B,C). The CD spectra of DNA modified by increasing concentration of **2** indicate that the binding results in conformational alterations in the double-helical DNA. Increased binding of **2** to ct DNA decreased positive CD and increased negative CD.

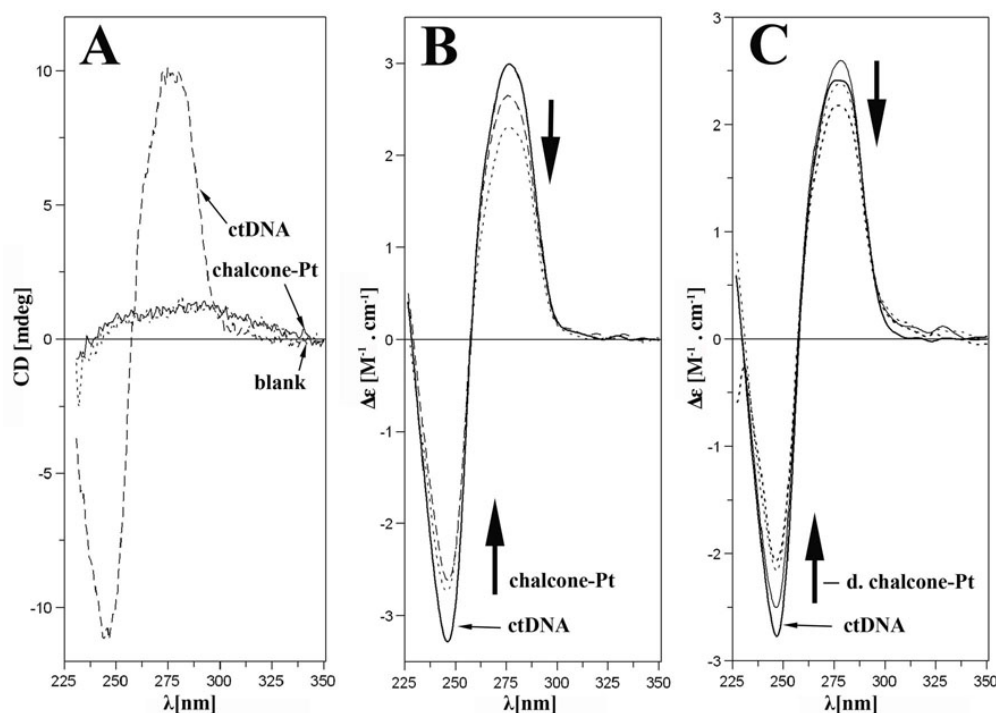


Figure 4- 19 Comparison of chalcone-Pt CD spectra with calf thymus (ct) DNA (10^{-4} M) dissolved in 0.01M NaClO₄. A) Profiles of chalcone-Pt (**2**) and blank (0.01M NaClO₄) were measured. Panels B and C show molar ellipticity spectra of ctDNA affected by chalcone-Pt (**2**). CD spectra were converted to $\Delta\epsilon$ using the concentration of DNA. B) Effect of $r_b = 0.009, 0.02$ of (**2**) on ctDNA and C) effect of dialysed (**2**) samples with increasing $r_b = 0.009, 0.02$. Complex-free ctDNA served as a reference.

4.6.4 Melting temperatures of DNA-chalcone-Pt (2) adducts

The melting points (T_m) of DNA modified by chalcone-Pt (2) were measured. Drug-modified DNA could be (de) stabilized and thus (decrease) increase its T_m . For these measurements the dialysed samples from the CD experiments were used. Denaturing temperature of unmodified ctDNA was $61 \pm 1^\circ\text{C}$. Addition of complex 2 decreased the T_m value up to $56 \pm 4^\circ\text{C}$ at $r_b = 0.02$. Higher concentrations could not be used because of precipitation.

Table 4- 5 Melting points (T_m) of dialysed DNA modified with complex 2 at various r_b values.

r_b	0	0.009	0.02	0.04	0.05
T_m [$^\circ\text{C}$]	61	57 (-3)	56 (-4)	61	59.2 (-2)

It can be concluded that the interaction between the Pt complex 2 and ctDNA had rather minor destabilising effects because of the slight decrease of the melting points.

4.7 Drug resistance

4.7.1 Interference with ABC transporters

The interaction of chalcone conjugate 2 with drug transport proteins like ABCB1 (P-gp) (Hyde et al., 1990; Simstein et al., 2003; Smith et al., 2001) or BCRP (Borst et al., 1997) in a substrate- or inhibitor-like fashion was investigated in this chapter.

4.7.1.1 Chalcone-Pt (2) efflux via P-glycoproteins

P-gp overexpressing KBv1^{+Vbl} cervix carcinoma cells (Schwab et al., 2003) and their wild type parent KBv1 cells were treated with chalcone-Pt (2) in the presence of calcein-AM (Figure 4- 20). The inhibition of P-gp leads to cleavage of calcein-AM taken up by the cells resulting into the formation of fluorescent calcein. As a positive control, the fluorescence intensity of KBv1^{+Vbl} cells treated with $50\ \mu\text{M}$ of the clinically established chemosensitiser verapamil (Schwab et al., 2003; Sharom, 1997) was set to 100 %. Surprisingly, wild-type KBv1 cells reached under the same conditions only ~45% of the calcein fluorescence of the resistant KBv1^{+Vbl} cells. Possibly, they have other ways to eliminate calcein-AM or calcein, which is not without precedence (Marchan et al., 2008; Oku et al., 1995). Calcein fluorescence in KBv1 cells was also relatively low in the absence of verapamil. Treatment with Pt-

4. Effects of chalcone-Pt (2)

complex **2** was more effective in the KBv1^{+Vbl} cells, in both cell lines conjugate **2** showed half of the activity of verapamil.

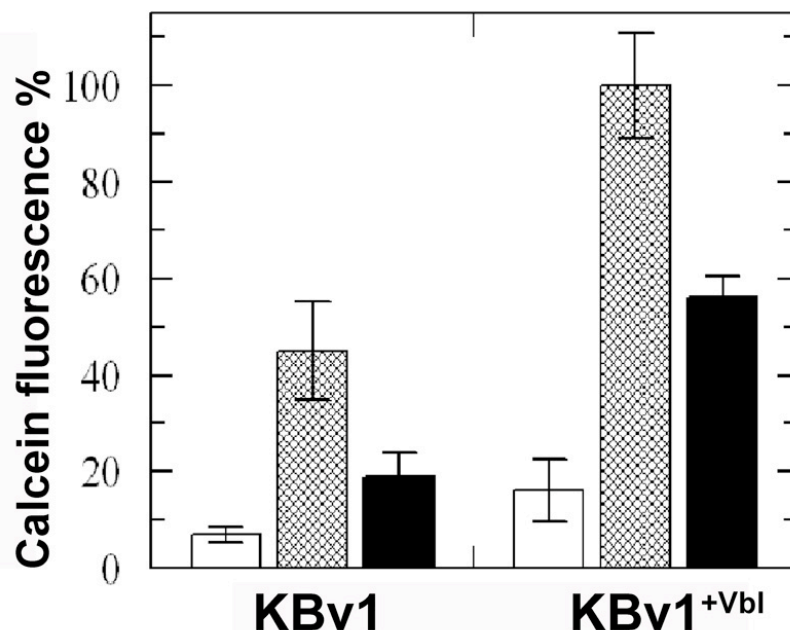


Figure 4- 20 Calcein-AM % inhibition of P-gp drug transporters in KBv1 and KBv1^{+Vbl} cells by chalcone-Pt (2) (50 μM, black bars) relative to the inhibition of KBv1^{+Vbl} cells by verapamil (50 μM, hatched bar) after 15 min exposure. White bars: negative control.

4.7.1.2 Chalcone-Pt (2) efflux via BCRP proteins

MCF-7 breast carcinoma cells express BCRP drug transporters. When treated with topotecan (550 nM over 40 generations) MCF-7 cells start to over-express these proteins (MCF-7^{+Top} cells). The mitoxantrone assay is based on the active export of the fluorescent dye mitoxantrone through BCRP, which enters the cells *via* diffusion. The effects of **2** on the fluorescence of intracellular mitoxantrone in MCF-7 and MCF-7^{+Top} cells relative to that of the specific BCRP inhibitor fumitremorgine C (Oku et al., 1995) and to a negative control of cells treated only with mitoxantrone are shown in Figure 4- 21. Both compounds gave rise to a doubling of the mitoxantrone fluorescence in either cell line relative to the negative control and so are likely to be competitive substrates for the BCRP proteins.

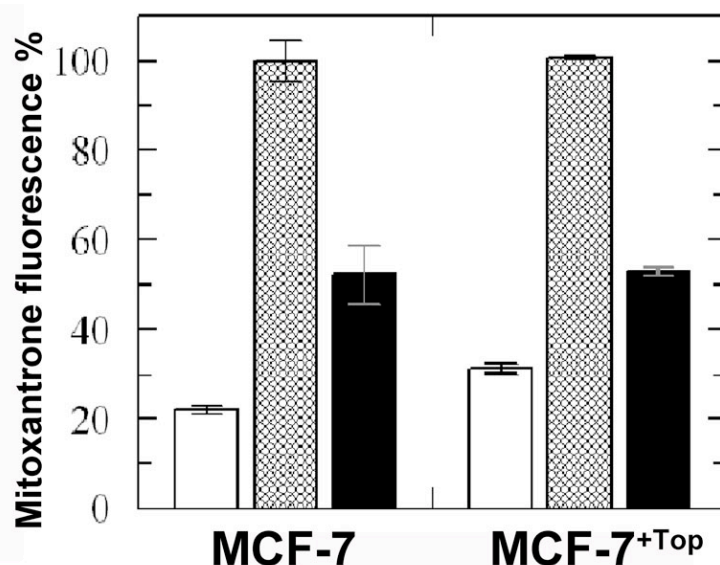


Figure 4- 21 Mitoxantrone % inhibition of BCRP drug transporters in MCF-7 and MCF-7^{+Top} cells by 10 μ M each of chalcone Pt (black bar) relative to fumitremorgine C (hatched bar) after 30 min exposure. White bar: fluorescence of cells after addition of mitoxantrone (negative control).

4.7.2 Interaction of chalcone-Pt (**2**) with glutathione

Glutathione (GSH) plays a key role in the metabolism and mechanism of anticancer action of platinum drugs (Townsend and Tew, 2003). DNA damaging agents such as cisplatin get frequently deactivated by the high concentrations of glutathione and glutathione-*S*-transferase, which are present in resistant tumor cells (McIlwain et al., 2006; Pompella et al., 2007; Tsuchida and Sato, 1992).

Depletion of GSH levels usually leads to an enhanced cytotoxicity of cisplatin (Fuertes et al., 2003), and maybe of the complexes **2** as well. Two possible binding sites for GSH exist in complex **2**: the metal center (280 nm) and the β -carbon atom of the propenone linker (~360 nm), both are shown in Figure 4- 22A. In order to identify the site at which S-nucleophiles prefers to attack, reaction of **2** was monitored with an excess of GSH at 37°C over two days. The reaction of GSH with compound **2** and dichlorido(6-aminomethylnicotinic acid)Pt(II) (= **nic-Pt**), the putative hydrolysis product of **2**, (Schobert and Biersack, 2005) was monitored by measuring the absorbance at 280 nm (Ishikawa and Ali-Osman, 1993). The absorption band at this wavelength is indicative of the covalent binding interaction of platinum complexes with the thiolate group of GSH. The progress of the reactions was slow and they were finished only after 24 hours (Figure 4- 22B).

4. Effects of chalcone-Pt (2)

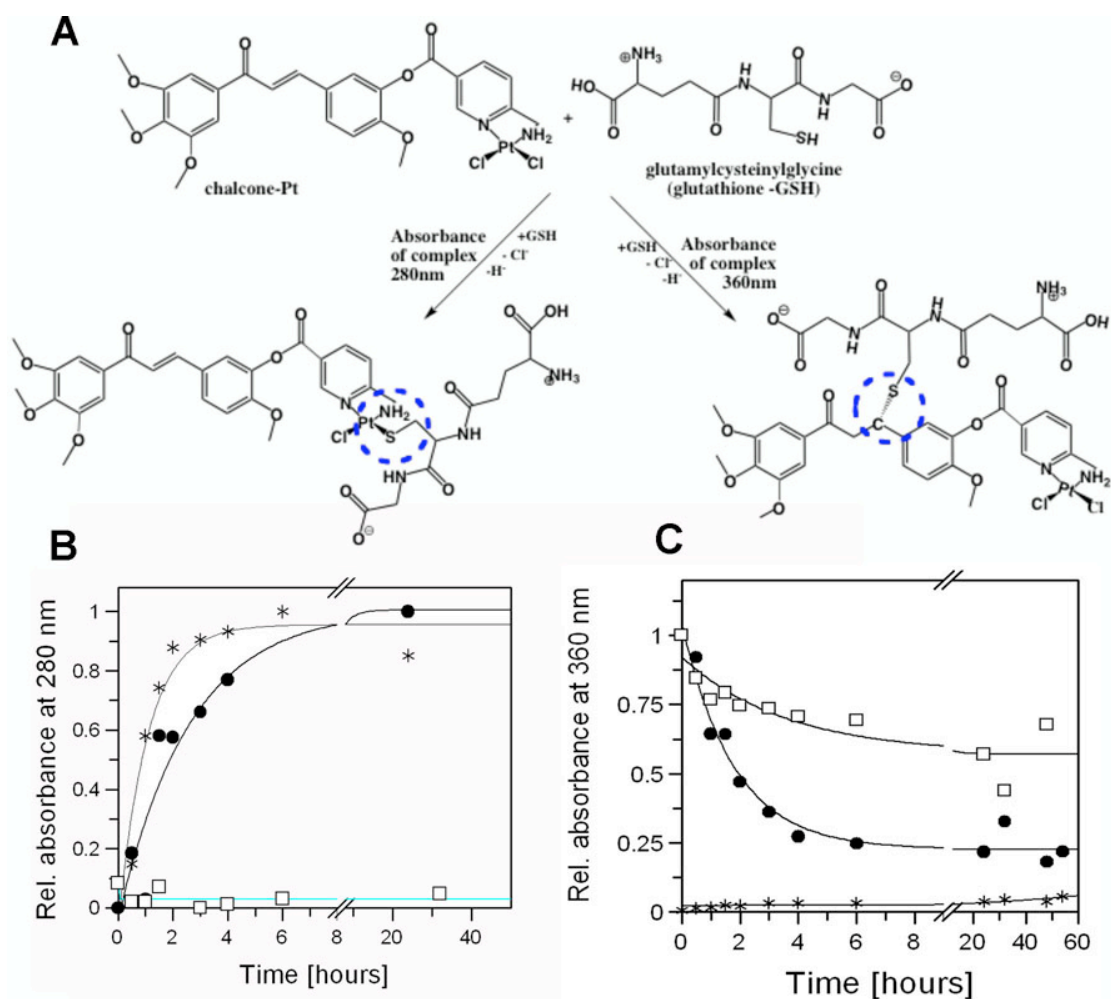


Figure 4- 22 (A) Scheme of the reaction between GSH and chalcone-Pt. Time-dependent relative absorbance at 280 (shown in (B) and 360 nm (C) of the reaction of two equiv. GSH (3.33 mM) with chalcone (1) (squares), 2 (black dots), and nic-Pt (asterisks) in 1 mL of PBS (pH 7.4) at 37°C. Curves obtained from mono-exponential fitting; apparent rate constants at 280 nm (B) were 0.38 and 0.94 h⁻¹ for 2 and nic-Pt, respectively. At the same time, reactions observed at 360 nm (C) showed rate constants 0.56, 0.28 and -0.015 h⁻¹ for chalcone (1), 2 and nic-Pt.

The reaction between GSH and **nic-Pt** was the fastest one. Although complex 2 showed a high affinity to GSH, its cytotoxicity in GSH-rich HCT-116 cells was comparable to that observed in 518A2 cells ($1 \pm 0.1 \mu\text{M}$). Absorbance decrease was

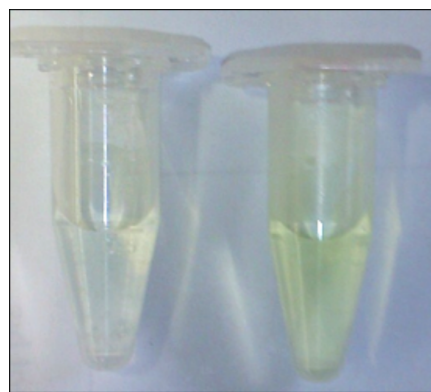


Figure 4- 23 The yellowish solution turned colourless after reaction of 2 with GSH.

detected at 360 nm with time (Figure 4- 22C). The π -electron flow was distorted in chalcone and, consequently, absorbance was affected. The reaction changed from a yellowish solution to a colourless one (Figure 4- 23, (Zoldakova and Schreder, 2009)).

4.8 Conclusion

The uptake of the Pt conjugate **2** into 518A2 melanoma cells occurs mainly *via* the organic cation and copper related transporters. Insofar, complex **2** resembles oxaliplatin, which was shown to be an excellent substrate for the human organic cation transporters OCT-1 and OCT-2. (Zhang et al., 2006)

The platinum complex **2** was highly efficacious against cells overexpressing P-gp transporters. The results obtained from calcein-AM assays showed that complex **2** inhibits the efflux functionality of P-gp by acting as a genuine inhibitor or a modulator. As a consequence, complex **2** was more efficacious in multi-drug resistant cancer cells featuring this particular ABC-transporter, e.g., KBv1^{+Vbl}. Complex **2** showed a high affinity towards GSH, however, its cytotoxicity in GSH-rich HCT-116 cells ($1 \pm 0.1 \mu\text{M}$) was comparable to that observed in 518A2 cells ($\text{IC}_{50} \sim 3.4 \mu\text{M}$). Chalcone-Pt (**2**) was little active in HT-29 cells but distinctly more so in HT29^{+Colc} cells. Colchicine-induced overexpression of MRP1 is accompanied by a changed sphingolipid composition (Kok et al., 2000). Sphingolipid metabolism is performed in the Golgi apparatus. Vigorous fragmentation of Golgi apparatus after treatment with **2** was observed *via* transmission electron microscopy. It could be an indication that the sphingolipid pathway plays a crucial role in the metabolism of complex **2**.

Chalcone-Pt (**2**) was shown to depolymerise microtubules and actin filaments in neural and cancer cells. It proved effective in damaging mitochondria. In 518A2 melanoma cells the good tubulin binder colchicine led to different morphological changes compared with compound **2**. These results also support the assumption of different molecular mechanisms of action for **2** being based not only on tubulin-disruption.

The DNA binding abilities of conjugate **2** were confirmed by changes in the secondary structure of ctDNA and unwinding of supercoiled plasmid DNA. Cell cycle analyses on complex **2** led to arrested cancer cells in G2/M phase. Additionally, it led to a slight accumulation of cells in the G1 phase, probably as a reminiscent of the effect of cisplatin. Hence, chalcone-Pt (**2**) has a dual impact on the cell cycle of 518A2 melanoma cells by combining the effects of active Pt-complexes and of chalcones or combretastatin A-4 analogues in general.

Effects of chalcone-DAP-Pt (3)

The platinum conjugate chalcone-DAP-Pt (**3**) is a chimera of the combretastatin A-4 analogous *m*-hydroxychalcone (**1**) and a dichloride (diaminopropionate)Pt(II) fragment featuring a close analogue of conjugate **2** possessing a saturated 2,3-diaminopropionate *N,N*-ligand (Biersack, 2009; Zoldakova, 2010).

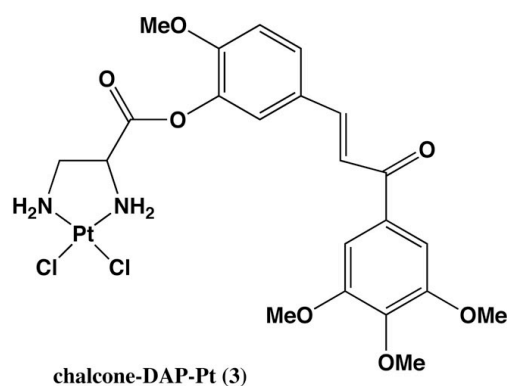


Figure 5- 1 Structure of chalcone-DAP-Pt (**3**).

5.1 Inhibition of cell growth - MTT assay

5.1.1 Tumor cells expressing ABC-transporters

ABC-transporters pump drugs out of cancer cells and are responsible for chemoresistance. Their interference with chalcone-DAP-Pt (**3**) was investigated by using various cancer cells rich in these transporters such as KBv1 cervix and HT-29 colon carcinomas. These cells had been grown in the presence of specific substrates of their transporters to stimulate their overexpression (Table 5- 1). A comparison with cisplatin was performed for all tested cell lines.

Table 5- 1: Inhibitory concentrations (³IC₅₀ in μ M) of compound (**3**) and cisplatin (CDDP) in various ABC-transporter expressing cells.

Cell line	MCF-7 ^{+Top}	KBv1	KBv1 ^{+Vbl}	HT-29	HT-29 ^{+Colc}
24 h (3)	*	1.5 \pm 0.5	0.4 \pm 0.1	48 \pm 2	>77
48 h (3)	*	0.1 \pm 0.08	0.1 \pm 0.05	36 \pm 4	30 \pm 3
24 h (CDDP)	20 \pm 3.2	*	17 \pm 3	66 \pm 3.1	44 \pm 1.3
48 h (CDDP)	9 \pm 1.4	*	10 \pm 2.5	39 \pm 3.8	23 \pm 4.1

^aValues are derived from concentration-response curves obtained by measuring the percentual absorbance of vital cells relative to untreated controls (100%) after 24 and 48 h exposure of selected cells to test compounds in the MTT assay. Values represent means of at least three independent experiments \pm standard deviation.

*Not tested

Resistant KBv1^{+Vbl} cells overexpressing P-gp proteins were obtained by treatment with vinblastine. Conjugate **3** was highly efficacious against KBv1 cells even after long time exposure, in both cell lines similar IC₅₀ values (~100 nM) were reached. Cisplatin is a known substrate of P-gp proteins (Hori et al., 1993; Komatsu et al., 2000) and its cytotoxicity against KBv1^{+Vbl} was 100-times lower compared with conjugate **3**.

HT-29 cells feature a high amount of multi-resistance protein 3 (MRP3) and a low amount of MRP1. Chalcone-DAP-Pt (**3**) was only little active in both HT-29/HT-29^{+Colc} cell lines. MRP1 and BCRP (breast cancer resistance protein) cause cisplatin resistance, which was confirmed from these results (Rabik and Dolan, 2007).

5.1.2 Cancer cells

The antiproliferative activity of chalcone-DAP-Pt (**3**) was evaluated in MTT-assays against HL-60 leukaemia, 518A2 melanoma, and HCT-116 colon carcinoma cells (Figure 5- 2, Table 5- 2). All of the mentioned cancer cell lines complex **3** showed the highest activity against HL-60 leukemia cells. The high effect of **3** in the leukaemia cells is not surprisingly amplified since leukaemia cells are quite sensitive to both combretastatin A-4 derivatives and DNA-binding compounds (Ducki et al., 1998) (Ochoa, 1969).

Table 5- 2 Inhibitory concentrations ^a IC₅₀ (μM) of compound 3 and cisplatin (CDDP) when applied to 518A2 melanoma, HL-60 leukaemia, and HCT-116 colon carcinoma cells.

Cell line	24 h (3)	48 h (3)	24 h (CDDP)	48 h (CDDP)
HL60	0.013 ± 0.009	0.001 ± 0.0006	2.5 ± 1	0.5 ± 0.3
518A2	5 ± 1.7	0.373 ± 0.004	21 ± 5.3	9 ± 2.3
HCT-116		0.79 ± 0.05	-	17 ± 0.2

The finding that complex **3** is superior in efficacy against the melanoma cells is at variance with test results recently obtained for a series of terpene-Pt-complex conjugates which inhibited the growth of 518A2 melanoma cells most when bearing a 6-aminomethylnicotinate rather than a diaminopropionate ligand (Bernhardt et al., 2008; Schobert et al., 2007). The relatively low IC₅₀ values of the platinum complex **3** in the glutathione-rich HCT-116 colon carcinoma cells (Arnould et al., 2003) are a

5. Effects of chalcone-DAP-Pt (3)

hint at the general robustness of chalcone Pt-complex conjugates against the glutathione-based detoxification / deactivation mechanism of resistant cancer cells.

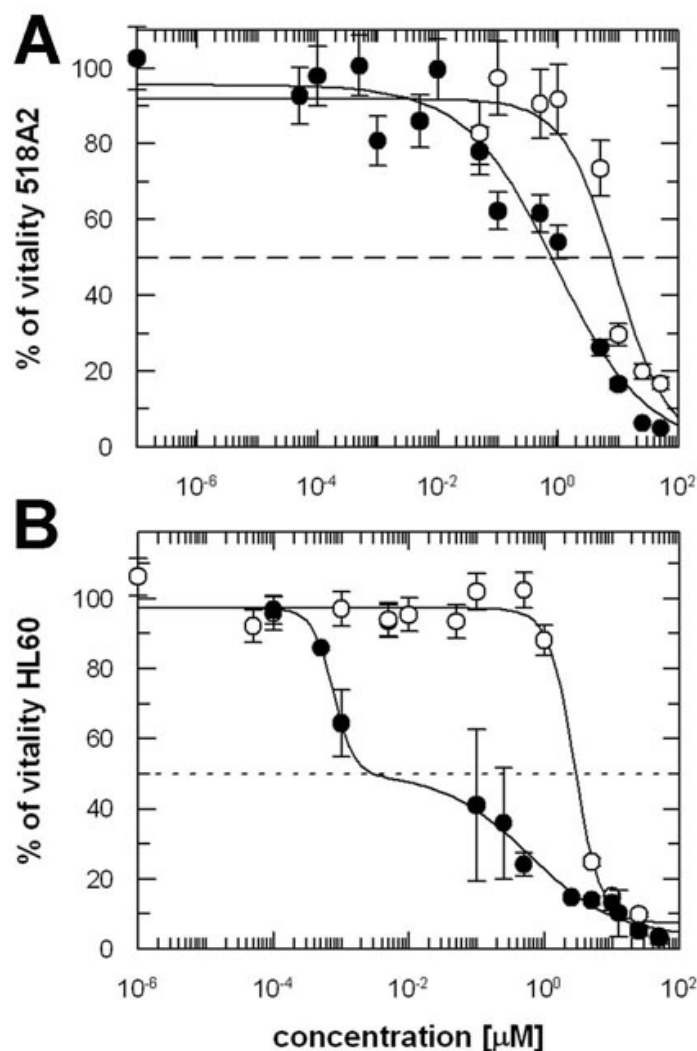


Figure 5- 2 Cytotoxicity of chalcone-DAP-Pt (3) after treatment for 48 hours with different concentrations in (A) 518A2 and (B) HL60 cells. Solid lines are curve-fits of compound 3 (black points) and cisplatin (white points) and were fitted by GraFit program according to equation 2-2.

5.2 Microscopic observations of 518A2 cells by Giemsa staining

Internucleosomal DNA cleavage of chalcone-DAP-Pt (3) was monitored with a light microscope after staining with Giemsa dye. Treatment with the IC_{50} concentration of 3 for 24 h showed an effect on proliferation as well as on the degree of attachment of the adherent cells. The untreated control cells appeared typically shaped and regularly spread showing well defined nuclei and condensed chromatin visible as dark blue dots (Figure 5- 3).

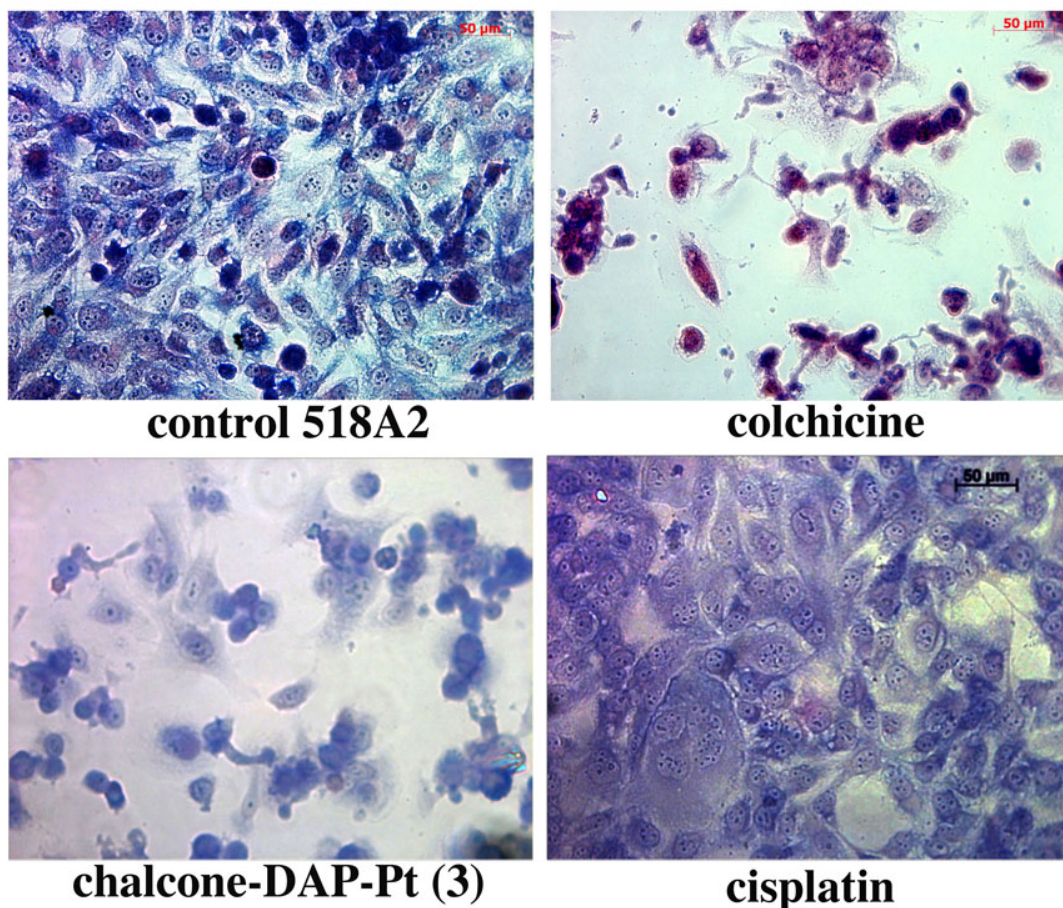


Figure 5- 3 Light microscopic images of 518A2 cells treated with IC_{50} concentrations of test and reference compounds for 24 hours, fixed and stained with Giemsa dye.

Treatment of 518A2 cells with **3** led to reduced cell numbers. The cells were packed more densely in insular aggregates and some of them formed connective invaginations. Treatment with complex **3** gave rise to cells with a blue colored cytoplasm due to DNA platination and a rounded morphology typical of exposure to chalcone (**1**). Very late apoptotic or dead cells were sprawled out with a purple or even missing cytoplasm. In contrast, 518A2 cells treated with cisplatin appeared swelled in comparison with control cells but remained equally distributed. Exposure to colchicine (62 nM), the archetypal inhibitor of tubulin polymerization, rapidly reduced the number of 518A2 cells which no longer displayed nuclei envelopes, took on a pink-purple hue, and were either sprawled out or rounded. Thus, the good tubulin binders colchicine and chalcone-DAP-Pt (**3**) led to different morphological changes in 518A2 cells which might be an indication of quite different molecular mechanisms.

5.3 DNA degradation of chalcone-DAP-Pt (3) during apoptosis

Previous results showed an extremely high sensitivity of KBv1 cells towards complex **3** ($IC_{50}=1.5/0.1 \mu M$). Fragmentation of DNA through activated endogenous nucleases is a final commitment step characteristic for apoptosis (Arends et al., 1990; Bortner et al., 1995; Hughes and Cidlowski, 2000). Activation of endonucleases initiates DNA cleavage creating nucleosomal length fragments (multiples of 180-200 bp) and large (30- to 50-kb) fragments.

The cervix carcinoma (KBv1) cells were exposed to $1.5 \mu M$ of **3** for 24 hours. The DNA of the treated cells was isolated and analyzed by agarose gel electrophoresis (Figure 5- 4).

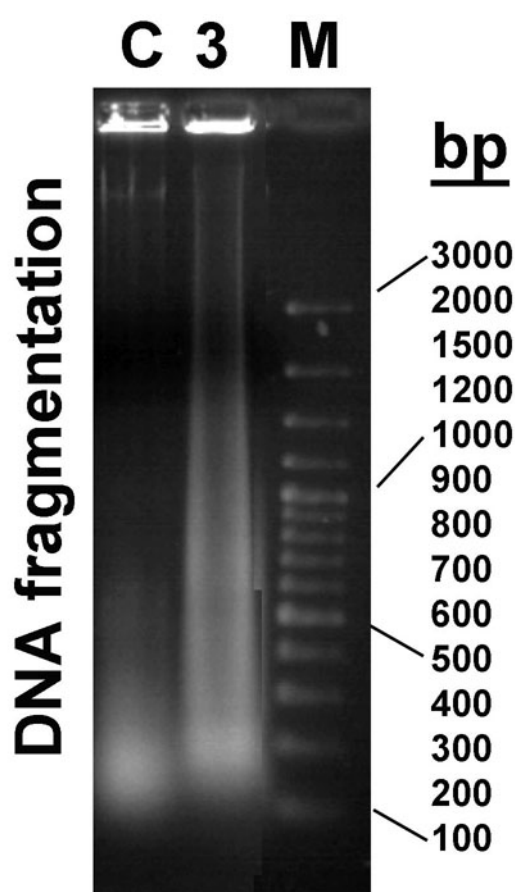


Figure 5- 4 Chalcone-DAP-Pt (3) induced DNA degradation in KBv1 cells. The DNA samples were applied to 1.5% agarose gel. Lane C: control – untreated cells; lane 3 is the DNA extract from cells treated with $1.5 \mu M$ chalcone-DAP-Pt (3); lane M: 100 – 3000 bp DNA ladder for comparison.

A huge amount of DNA remains in the loading well featuring intact chromosomal DNA (lane C). DNA of isolated cells treated with **3** (lane 3) likewise contained intact chromosomal DNA in well of electrophoresis gel. A DNA fragmentation comparable to the control DNA ladder could be detected in the lane containing DNA from the treated cells together with a large amount of ~ 200 bp fragments.

5.4 Characterization of DNA-chalcone-DAP-Pt (**3**) interactions

Several DNA binding molecules interact *via* intercalation (Neidle, 1979; Waring, 2006). DNA intercalation was observed for the chalcone analogue AMC [AMC, 1-(4'-aminophenyl)-3-(4-N,N-dimethylphenyl)-2-propen-1-one] (Shah et al., 2008). Chalcone (**1**) is not known as intercalating or DNA-binding agent, yet, the Pt(II) fragment of conjugate **3** might be able to coordinate nucleobases of the DNA quite efficiently.

5.4.1 Electrophoretic mobility shift assay of plasmid DNA

Gel electrophoresis was used to investigate the conformational change and damage caused to non-genomic DNA (pUC19 plasmid DNA) by covalent binding with chalcone-DAP-Pt (**3**). The supercoiled circular form (sc) possesses higher mobility and runs faster than the one-nicked open circular form (oc).

In order to quantify the unwinding capacity of complex **3**, its effect on pUC19 plasmid DNA was investigated. The plasmid was incubated with **3** for 24 h at 37 °C at various r_b values. The native agarose gel resulting from DNA modifications by cisplatin and **3** is shown in Figure 5- 5.

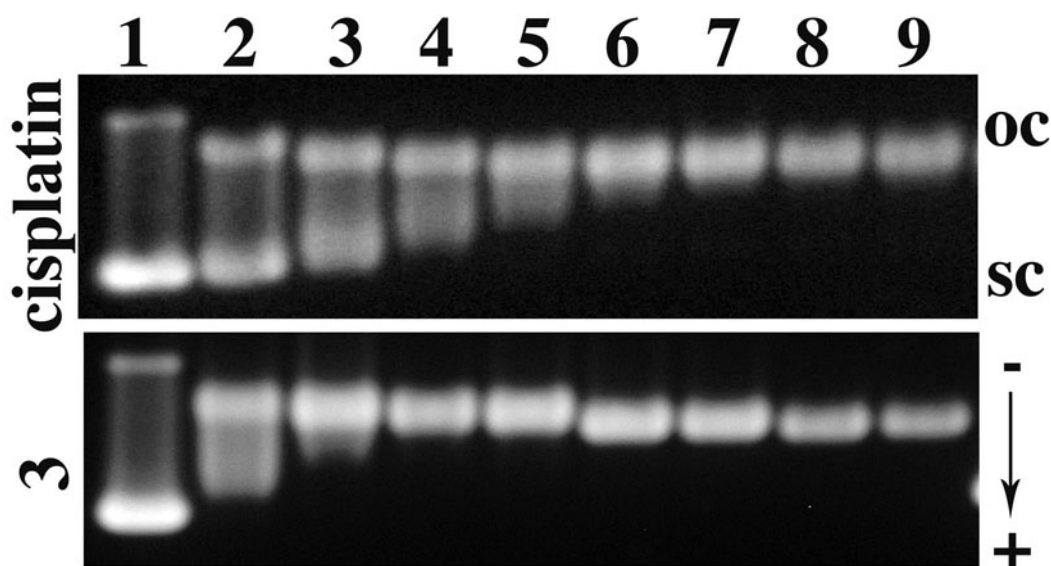


Figure 5- 5 Unwinding of supercoiled pUC19 plasmid DNA modified by cisplatin (2–9): $r_b = 0.02, 0.03, 0.04, 0.05, 0.06, 0.07, 0.08, 0.09$; by **3**: $r_b = 0.022, 0.032, 0.044, 0.048, 0.108, 0.096, 0.150, 0.152$ (lanes 2–9). Lane (1): control, untreated DNA; oc = nicked plasmid; sc = closed negatively supercoiled plasmid.

A slower migration is the result of DNA unwinding since this reduces the supercoiling degree. The mean unwinding angle Φ can be calculated according to Equation 5 - 1,

5. Effects of chalcone-DAP-Pt (3)

Equation 5 - 1 Calculation of unwinding angle
$$\Phi = -\frac{18\sigma}{r_b(c)}$$

where σ is the superhelical density and $r_b(c)$ is the r_b value at which the supercoiled and nicked forms co-migrate (Brabec et al., 2007). Under the applied experimental conditions σ was calculated (Equation 5 - 1) to be -0.058 . For the positive control, cisplatin was used taking its unwinding angle $\Phi = 13^\circ$ at $r_b(0.08)$ (Keck MV and SJ, 1992). Figure 5- 5 shows that complex **3** caused a significant DNA unwinding ($\Phi = 21$ - 23°).

The co-migration point $r_b(c)$ of DNA treated with complex **3** was reached at $r_b = 0.046 \pm 0.002$. The notably high level of DNA unwinding induced by **3** is even higher than that induced by adducts of cisplatin.

5.4.2 Kinetic of chalcone-DAP-Pt (3) DNA binding

In order to pinpoint the role of the platinum fragment for the anticancer effect of conjugate **3** in comparison with cisplatin, the DNA binding behavior of **3** was investigated in detail. Initially, the metallation of calf thymus DNA by compound **3** (75%, Figure 5- 6) was determined *via* FAAS.

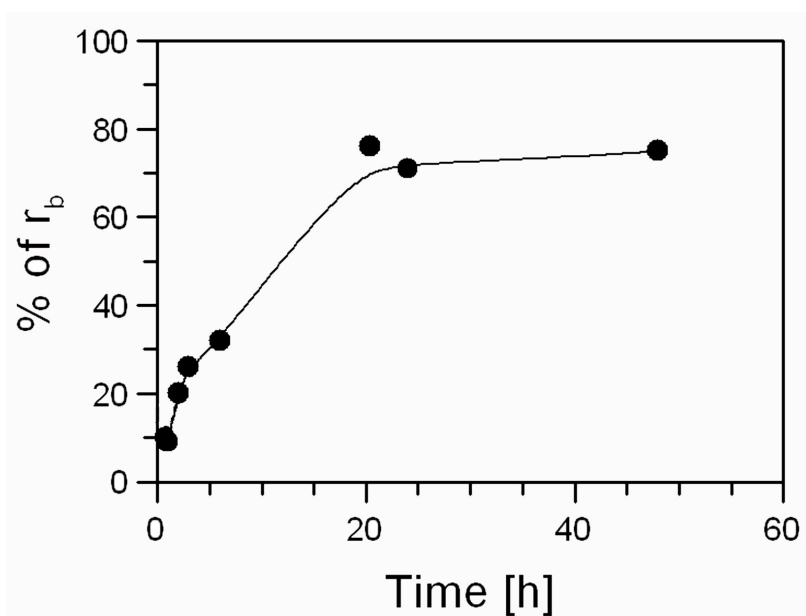


Figure 5- 6 Kinetic of chalcone-DAP-Pt binding to ctDNA in 0.01 M NaClO₄.

5.4.3 Changes of the DNA secondary structure

ctDNA was incubated with complex **3** at various r_b values for 24 hours. Measured CD spectra were processed with respect to the blank and ctDNA molar concentration (10^{-4} M) (Figure 5- 7). The spectra showed that the intensity of the

positive CD band at 275 nm is increased as a consequence of Pt binding. Similarly, a decrease in negative CD band at 245 nm was observed (Figure 5- 7A). To avoid unspecific interaction unbound **3** was removed by dialysis against 0.01 M NaClO₄. The concentration of ctDNA was determined and molar ellipticity ($\Delta\epsilon$) spectra were compared with those of un-dialysed samples (Figure 5- 7B). A slight decrease was observed in both positive and negative CD bands. The decrease was more pronounced in the dialysed samples. The effects of dialysed samples (Figure 5- 7C) with increasing amount of bound **3** ($r_i = 0.007, 0.015, 0.03$) were compared with non-modified ctDNA.

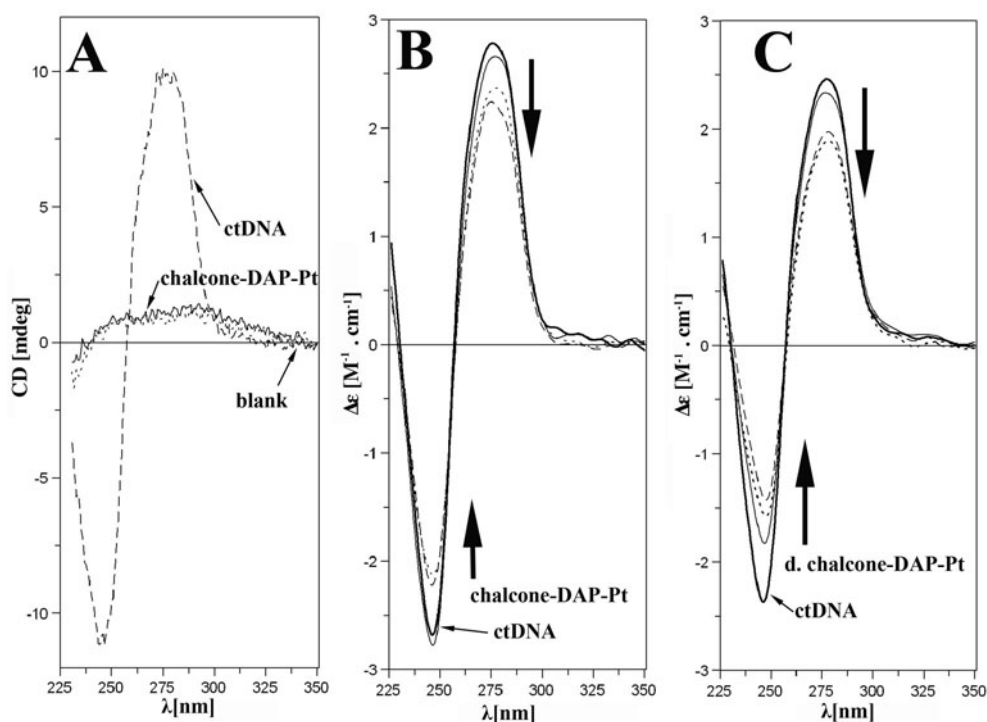


Figure 5- 7 A) CD spectra of pure ctDNA (10^{-4} M), chalcone-DAP-Pt (**3**) and of the blank medium (0.01M NaClO₄) in millidegrees. B, C: Molar ellipticity spectra of ctDNA affected by chalcone-DAP-Pt (**3**) in millidegrees were converted to $\Delta\epsilon$ using the concentration of the DNA. B) Effect of $r_i = 0.009, 0.02$ (**3**) on ctDNA. C) Effect of dialysed samples with increasing r_i : 0.007, 0.015, 0.03. As a reference chalcone-free ctDNA was used.

5.4.4 Melting temperatures of DNA modified with complex (**3**)

High temperature leads to the separation of the two DNA strands (DNA melting), which is accompanied by a hyperchromic shift. Thus, a melting point (the temperature at which half of the DNA is molten, T_m) can be assessed. Metal compounds bound to DNA influence the thermal stability of DNA. Metal binding can lead either to stabilization (higher T_m) or destabilization (lower T_m) of the double strand structure. Stabilizing factors include interstrand cross-linking and the effect of

5. Effects of chalcone-DAP-Pt (**3**)

the positive charges. On the other hand, local distortions destabilize the double strand and lead to lower T_m .

Melting curves were recorded to characterize the DNA interaction of complex **3**. Dialyzed samples were used in these experiments. The spectra were recorded at high ionic strength (0.1M NaClO₄) to reduce the stabilizing effect of the positive charge. Under these conditions the melting temperature of unmodified ctDNA was $84 \pm 1^\circ\text{C}$. Chalcone-DAP-Pt (**3**) applied at the highest r_b value decreased T_m to $78.2 \pm 0.9^\circ\text{C}$. Hence, modification by **3** results in thermal destabilization of the double strand DNA structure.

Table 5- 3 Melting temperatures (T_m) of DNA modified by **3 at various r_b values in 0.1 M NaClO₄, 0.5°C per minute at 260 nm.**

0.1M NaClO ₄	
r_b	T_m [°C]
0	84.01
0.015	80.12
0.03	79.16
0.05	78.20

5.4.5 Mono- or bi-functional character of DNA-(**3**) adducts

Anticancer active Pt(II) complexes bind to DNA in a bi-functional way (Brabec, 2002; Bursova et al., 2005). Their antitumor efficiency is based on their ability to form bi-functional adducts (intra- or interstrand cross-links). Among the alterations of secondary structure such as local unwinding, bending, interstrand cross-linking or local denaturation, the role of DNA unwinding is recognized to be potentially important in regulating replication and transcription functions through specific DNA-protein interactions. The elucidation of the binding character for chalcone-DAP-Pt is warranted. Therefore, suitable experiments on the role of Pt(II)complex **3** for the formation of DNA adducts were carried out.

An oligodeoxyribonucleotide duplex (21-bp) containing the single, site-specific bifunctional adduct at G-residues of the central sequences 5'GGT/CCA was prepared and the formation of mono- and/or bifunctional adducts of **3** was identified by FPLC (Figure 5- 8). Completion of the reaction was determined from the elution patterns of the ion-exchange FPLC analysis of the top strands of the 5'GGT-3' duplexes. The marked peaks relate to the platinated or unmodified products, respectively. The fractions corresponding to mono- and bifunctional adducts were purified by HPLC under the same conditions.

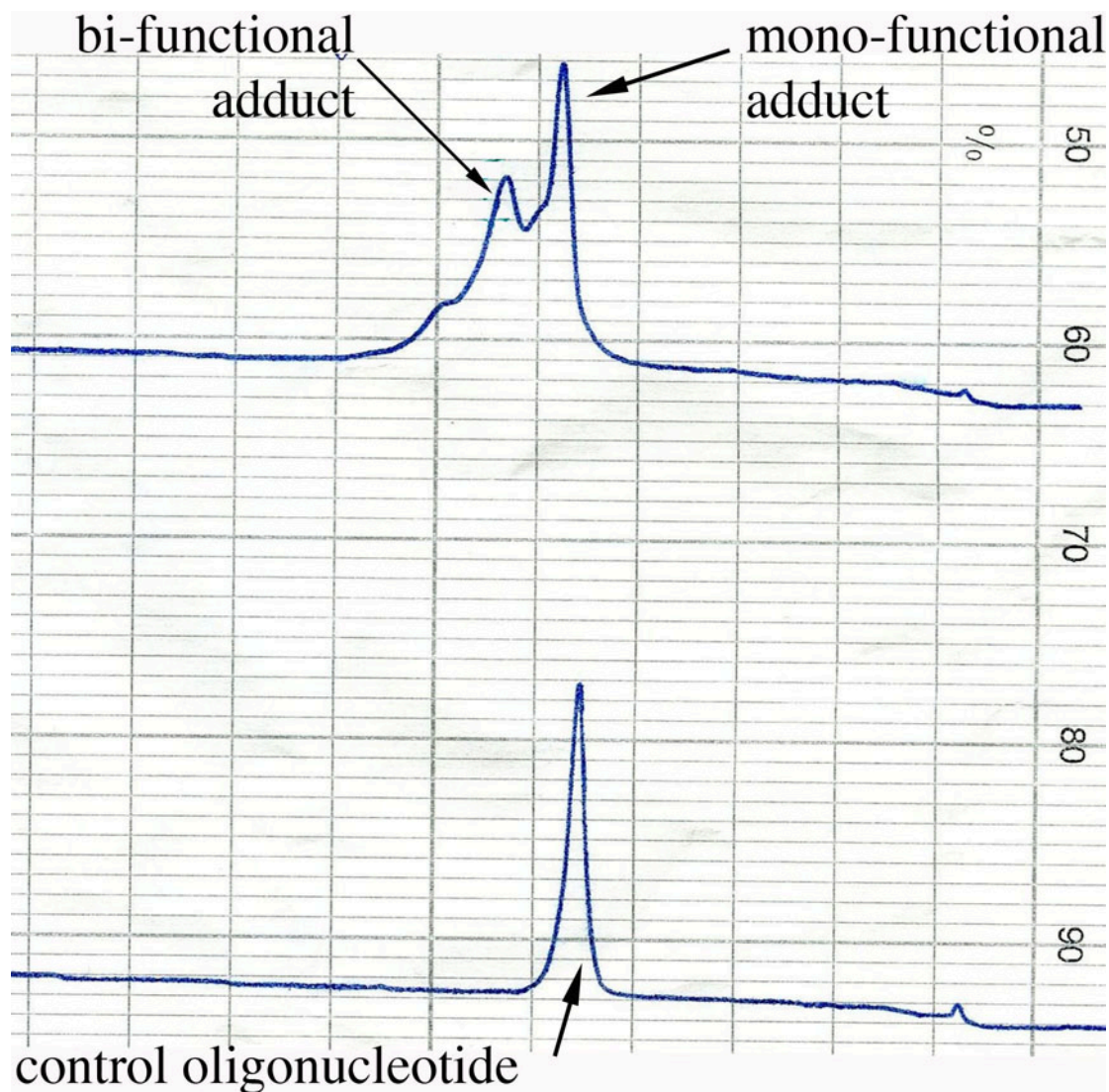


Figure 5- 8 The elution patterns of the ion-exchange FPLC analysis of the top strands GGT duplexes. The oligonucleotide was modified by chalcone-DAP-Pt. The peaks of bifunctional and monofunctional adducts are marked and were compared with the control peak (bottom profile).

The 5'-ends of oligonucleotides were labelled by radioactive $[\gamma\text{-}^{32}\text{P}]\text{ATP}$ using T4-polynucleotidekinase (T4-PNK) and purified by Sephadex G50. DNA-samples were analyzed on a 24% PAA gel under denaturing conditions (Figure 5- 9). The radioactive label was used to identify the band positions (*left*) in the agarose gel when 21-mer oligonucleotides were cut out from the gel (*right*). Radioactive gel samples for bi-functional (B), mono-functional (M) adducts and control (C) oligonucleotides were shaken over-night to transfer radioactive bands into the water phase. DNA samples were precipitated, centrifuged and dissolved in water. The DNA concentration (spectrophotometry) and Pt concentration (FAAS) was determined and the values confirmed that one Pt atom corresponds to one oligonucleotide top strand.

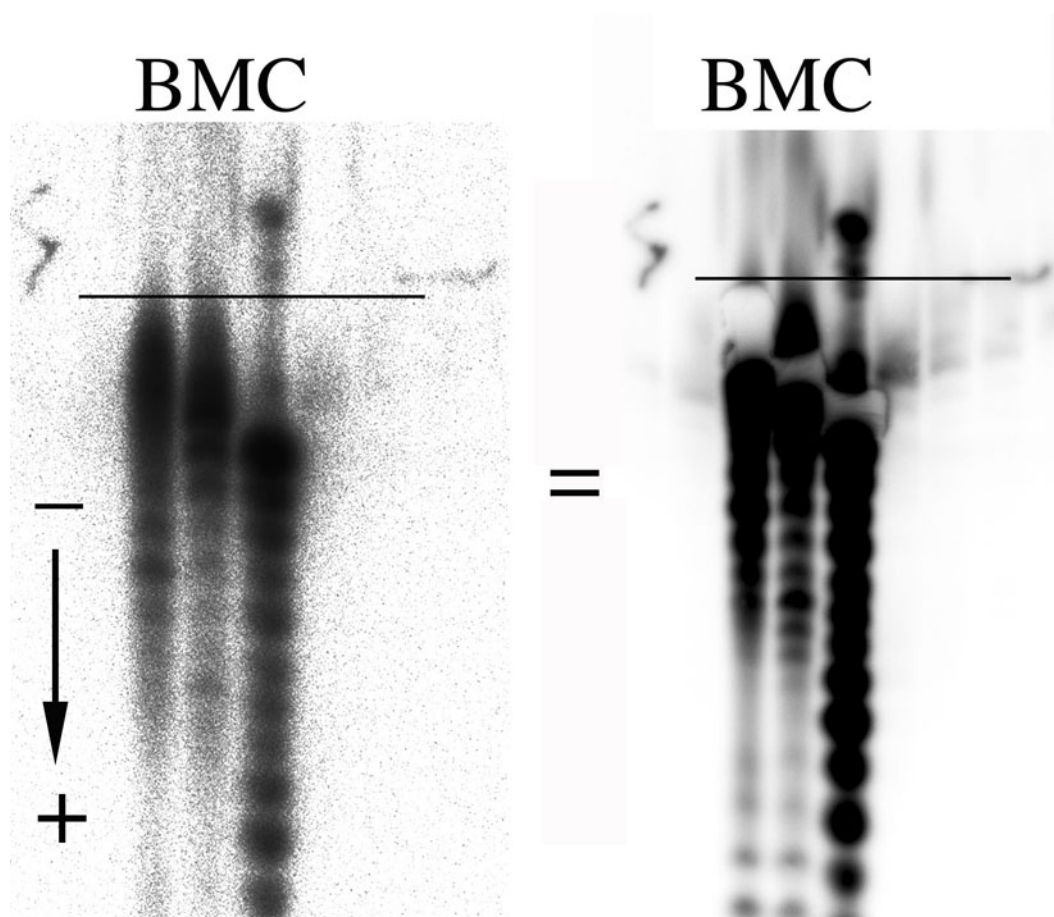


Figure 5- 9 (B) Bi-, (M) Mono- functional adducts of GGT-oligonucleotide and control oligonucleotide (C) in a denaturated 24% PAA gel. *Left*: the radioactive labels were used to identify the positions of band on the gel when 21-mer oligonucleotides were cut out from the gel (*right*).

DMS footprinting of DNA (Brabec and Leng, 1993; Leng and Brabec, 1994) is used to verify the platination site at the N7 position of both neighboring guanines, which is not accessible to DMS, induces cleavage. Thus, platinated and nonmodified top strands (5'-end-labeled with ^{32}P) were reacted with DMS. DMS methylates the N7 position of guanine residues in DNA, producing alkali-labile sites (Maxam and Gilbert, 1980). Following the methylation, the platinated samples were incubated with 0.2 M NaCN (2 hours, 55 °C) to remove the metal compound.

If guanine-N7 is coordinated to platinum, it cannot be methylated. The oligonucleotides were then treated with hot piperidine and analyzed by denaturing polyacrylamide gel electrophoresis. Two new bands appeared in the case of the nonmodified oligonucleotide. They correspond to fragments cleaved at the G sites. In the case of the monofunctional adduct, both bands are present, in a weaker fashion. This means that one portion of the oligonucleotides was cleaved at the G-1 site whereas the other portion was cleaved at the G-2 site. Both fractions cannot be separated under the applied conditions. In the case of the bifunctional adduct, no band

corresponding to cleaved oligonucleotides is present. This means that both guanine - N7 sites are bound to Pt and thus no methylation and cleavage can occur. These results together with the finding that one Pt atom corresponds to one oligonucleotide strand indicate that one chalcone-DAP-Pt molecule was successfully coordinated to neighbouring guanine residues forming a 1,2-d(GpG) intrastrand cross-link (Figure 5-10).

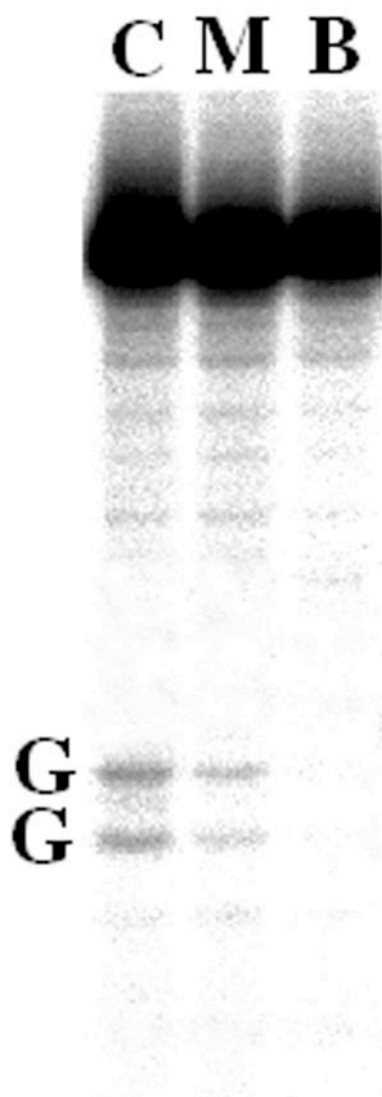


Figure 5- 10 Autoradiogram of the 24% PAA denaturing gel. The oligonucleotides were 5'-end-labeled and submitted to DMS footprinting. Lanes C – control, unmodified oligonucleotide. Lane M – monofunctional adduct of **3**. Lane B – bifunctional adduct of **3**.

5.4.6 Interstrand-crosslink ability of chalcone-DAP-Pt (**3**)

Cisplatin forms various types of interstrand and intrastrand cross-links (CLs) (Halamikova et al., 2007; Scovell and Collart, 1985). Cisplatin and platinum complex **3** were compared in terms of their capacity to form interstrand cross-links in a 213-bp DNA fragment, which was obtained by linearization of pSP73KB plasmid DNA with

5. Effects of chalcone-DAP-Pt (3)

EcoRI. The samples were analyzed for interstrand CLs *via* agarose gel electrophoresis under denaturing conditions as described in the experimental section. Upon electrophoresis, the non-cross-linked strands of 213-bp DNA labelled with ^{32}P at the 3'-end migrated as a 213-mer single strand, whereas the high molecular interstrand cross-linked strands migrated more slowly. The intensity of the more slowly migrating band increased with the growing number of CLs induced by **3** (Figure 5-11). The radioactivity of the individual bands in each lane was measured to determine the fractions of non-cross-linked *vs.* cross-linked DNA. The frequency of interstrand CLs was calculated using the Poisson distribution from the fraction of non-cross-linked DNA in combination with the r_b values and the fragment size. While the interstrand CL frequency induced by cisplatin was calculated to be ca. $6 \pm 0.5\%$, which is in agreement with previous results, (Brabec and Leng, 1993) the corresponding value for complex **3** was $58 \pm 2.3\%$, i.e., ten-fold higher compared with cisplatin.



Figure 5- 11 Electrophoretic autoradiograms of 3'-end ^{32}P -labeled 213-bp fragments of linear pSP73KB plasmid DNA (2455 bp) on denaturing 1% agarose gels after incubation (24 h) with cisplatin (lane 1) at $r_b = 0.001$, or with complex **3** (lanes 2–5) at $r_b = 0.00001, 0.00003, 0.0002, 0.001$. Lane C = control; ICL = interstrand cross-linked DNA; ss = single-strand DNA.

5.4.7 Inhibition of RNA synthesis

The preference of complex **3** towards distinct nucleotide sequences was investigated by a transcription-mapping assay.

Cleavage of pSP73KB DNA by *NdeI* and *HpaI* restriction endonucleases yields a 212-bp fragment (a substantial part of its nucleotide sequence is shown in Figure 5-12) that contains a T7 RNA polymerase promoter. *In vitro* RNA synthesis from this DNA template modified by complex **3** ($r_b = 0.02$ or 0.03) can be prematurely terminated at or in the proximity of the sites where the platinum complex is coordinated to DNA bases (Figure 5- 12A). DNA lesions originating from bis-dentate coordination of platinum fragments can efficiently terminate RNA synthesis at the position of the defect whereas monodentate coordination of Pt fragments such as $[\text{PtCl}(\text{dien})]^+$ (dien=diethylenetriamine) is insufficient for the termination of RNA synthesis. The major stop sites, mainly guanine and adenine residues, were proven to

be roughly identical for complex **3** and cisplatin (Figure 5- 12B). These results suggest that complex **3** preferentially binds DNA at GG and AG sites.

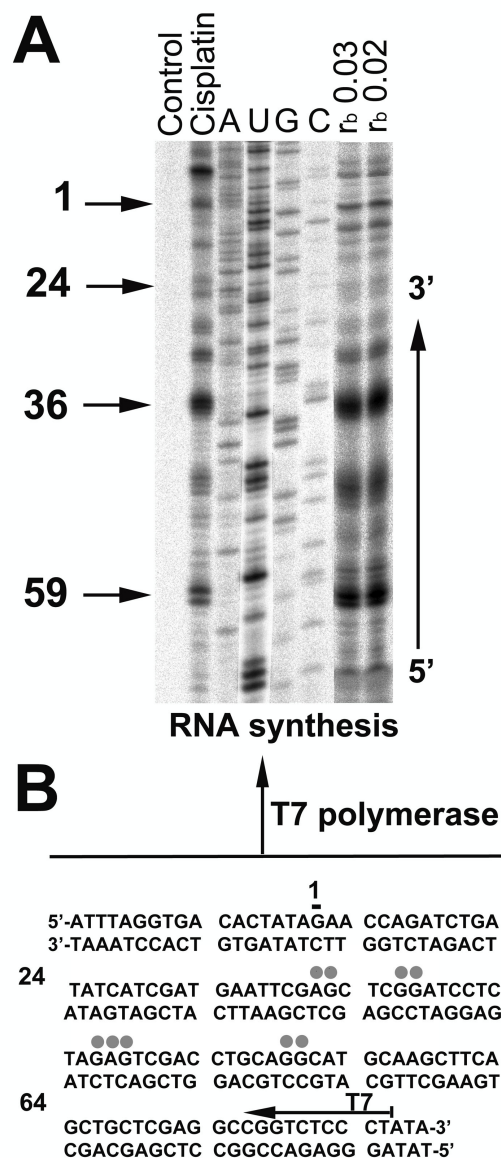


Figure 5- 12 Inhibition of RNA synthesis by T7 RNA polymerase on the NdeI/HpaI fragment of pSP73KB plasmid DNA containing adducts of complex **3** or cisplatin. A: Autoradiograph of 8% PAA/8M urea sequencing gel; lanes: control (non-platinated template); cisplatin at rb 0.01; A, U, G and C, chain-terminated marker RNAs; and complex **3** at rb 0.03 and 0.02 (determined by FAAS). Numbers correspond to the nucleotide sequence numbering of B. B: Schematic diagram of the NdeI/HpaI fragment sequence, arrow indicates the promoter for T7 RNA polymerase, grey dots indicate the sites corresponding to the stop signals in A, numbers correspond to the nucleotide numbering in the sequence map of the pSP73KB plasmid.

5.5 Chalcone-DAP-Pt (**3**) resistance

5.5.1 Interference with ABC transporter

The role of efflux proteins in the detoxification of cancer cells is being one the main interest of pharmaceutical studies. The interaction of chalcone-DAP-Pt (**3**) with drug transport proteins like ABCB1 (P-gp) (Hyde et al., 1990; Simstein et al., 2003;

5. Effects of chalcone-DAP-Pt (**3**)

Smith et al., 2001) or BCRP (Borst et al., 1997) was investigated in a substrate- or inhibitor-like fashion.

5.5.1.1 Chalcone-DAP-Pt efflux via P-glycoproteins

P-gp overexpressing KBv1^{+Vbl} cervix carcinoma cells (Schwab et al., 2003) alongside their wild type parent cells were treated with **3** in the presence of calcein-AM (Figure 5- 13).

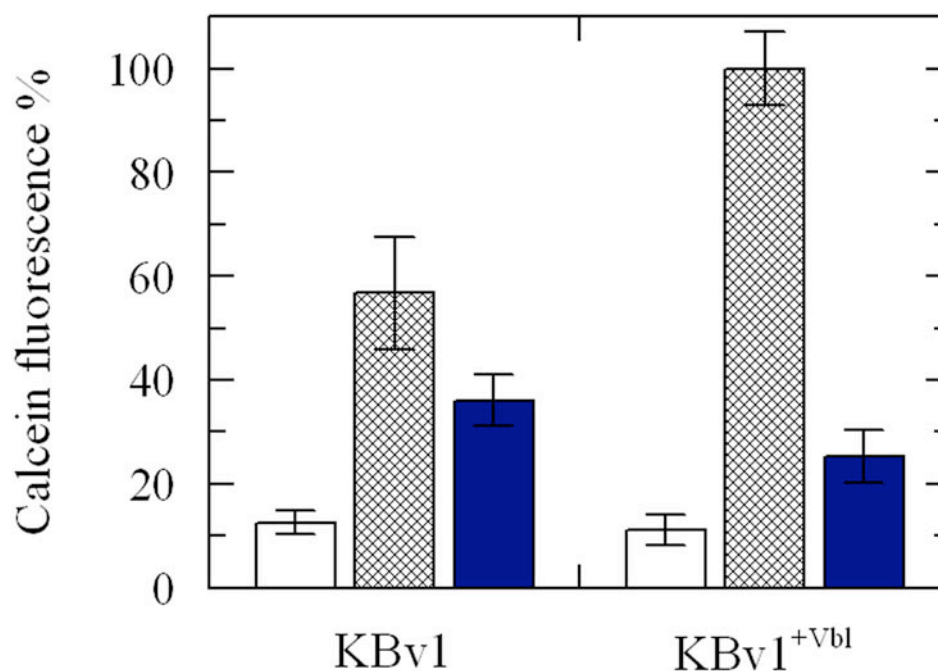


Figure 5- 13 Calcein-AM assay: Interference of chalcone-DAP-Pt (**3**) with P-gp. Inhibition (in %) of P-gp transporters in KBv1 and KBv1^{+Vbl} cells by 50 μ M of chalcone-DAP-Pt (**3**) (dark blue bars) relative to the inhibition of cells by verapamil (hatched bars) after 15 min exposure. White bars: negative control.

The inhibition of P-gp allows cleavage of intracellular calcein-AM forming fluorescent calcein. As a positive control, the fluorescence intensity of KBv1^{+Vbl} cells treated with 50 μ M of the clinically established chemosensitiser verapamil (Schwab et al., 2003; Sharom, 1997) was set to 100 %. Surprisingly, wild type KBv1 cells reached only ~55% of the calcein fluorescence of the resistant KBv1^{+Vbl} cells. Possibly, they have other ways to eliminate calcein-AM or calcein, which is not without precedence (Marchan et al., 2008; Oku et al., 1995).

Treatment with chalcone-DAP-Pt (**3**) led to almost the same absolute fluorescence intensity of calcein in both resistant and wild type cell lines. A similar effect was observed for chalcone (**1**) (Zoldakova, 2010).

5.5.2 DNA repair

DNA-damage caused by chemotherapeutics such as cisplatin can be removed by DNA repair mechanisms leading to tumor cell survival (Brabec, 2002). In order to determine how readily the DNA damage induced by platinum complex **3** is repaired we used an assay that quantifies the extent of DNA repair synthesis by tumor cell extracts (Figure 5- 14).

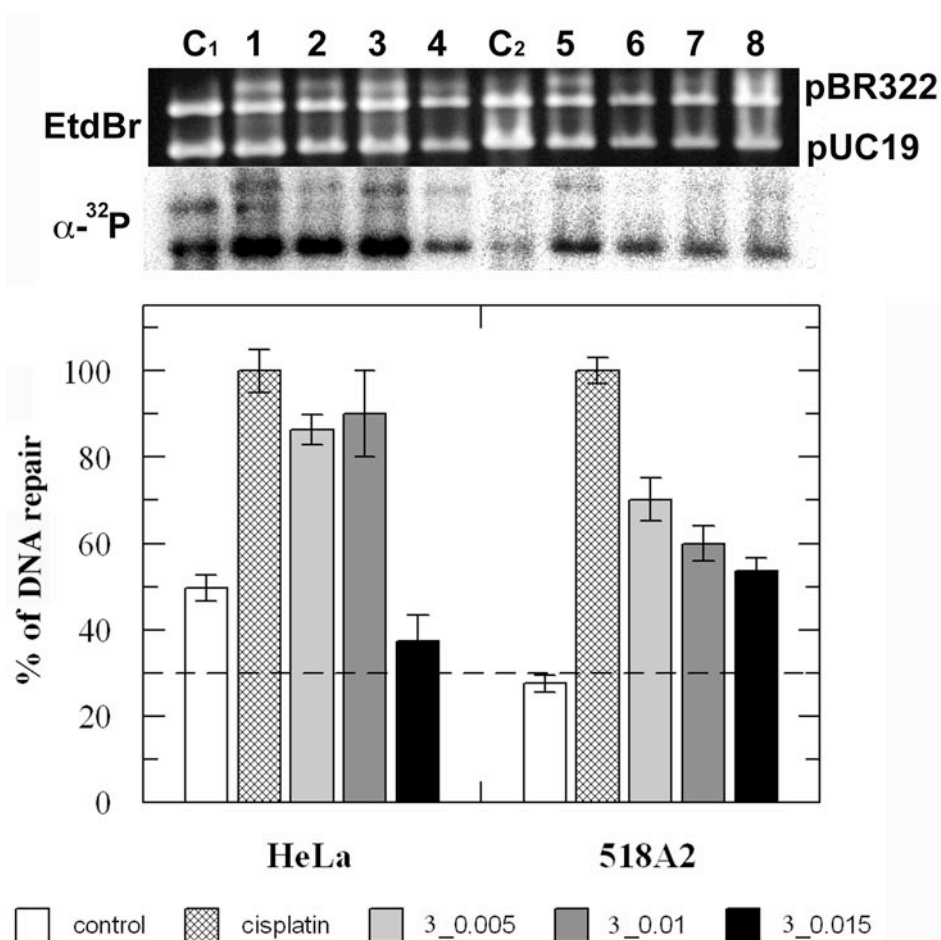


Figure 5- 14 DNA repair of pUC19 pre-treated with cisplatin or **3.** Top row: untreated pBR322 DNA (control). Repair efficiency is given by incorporated $[\alpha\text{-}^{32}\text{P}]$ dATP. Samples repaired by repair-proficient extracts of HeLa cells (lanes 1–4) and melanoma 518A2 cells (lanes 5–8). Cisplatin: r_b ≈ 0.01; 6: r_b ≈ 0.005, 0.01, 0.015.

The efficiency of cell-free extracts (CFE) of repair-proficient HeLa cells or 518A2 melanoma cells to repair defects in pUC19 plasmid (2686 bp) globally modified by **3** at r_b = 0.005–0.015 or cisplatin at r_b = 0.01 was ascertained by measuring the amount of incorporated radiolabeled nucleotide. Figure 5- 14 shows that DNA repair synthesis in the plasmid modified by **3** was considerably lower than that found for cisplatin. This effect was more pronounced in the CFE of melanoma 518A2 cells.

5.5.3 Reaction of chalcone-DAP-Pt (**3**) with glutathione

Glutathione (GSH) plays a key role in the metabolism and mechanism of anticancer action of platinum drugs (Townsend and Tew, 2003). Depletion of GSH levels usually leads to an enhanced cytotoxicity of cisplatin (Fuertes et al., 2003).

The reactions of GSH with complex **3** and cisplatin were monitored *via* the absorbance at 280 nm (Ishikawa and Ali-Osman, 1993). The absorption band at this wavelength is indicative of the binding interaction of platinum complexes with the thiolate group of GSH. The progress of the reactions was slow; the reactions were finished after 24 hours (Figure 5- 15). The reaction between GSH and **nic-Pt** was the fastest whereas **3** reacted slowly. The affinity of **3** to GSH was even lower than that of cisplatin, which bodes well for future tests against cisplatin-resistant tumors having high GSH levels. Complex **3** was shown as a poor GSH-binder compared to cisplatin. Moreover, its cytotoxicity was also higher ($IC_{50} \sim 0.7 \mu M$) in GSH-rich HCT-116 cells compared with cisplatin ($IC_{50} \sim 17 \mu M$).

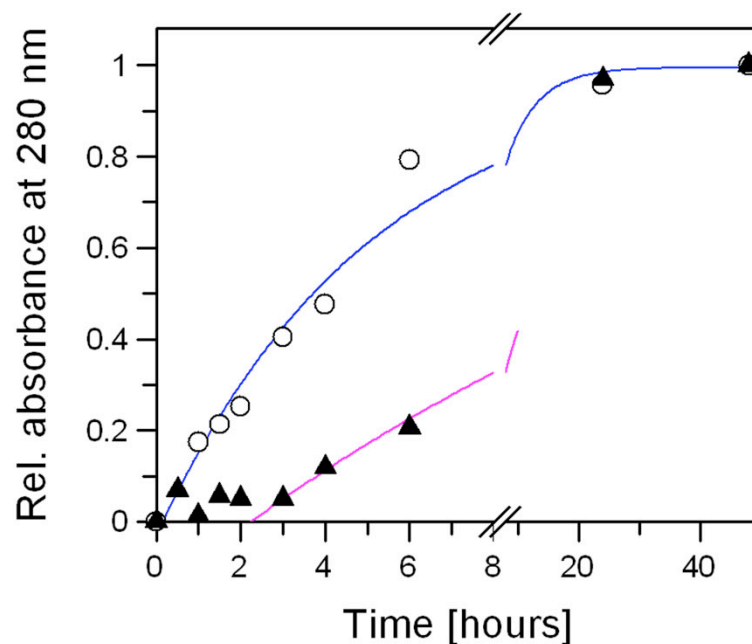


Figure 5- 15 Time-dependent monitoring (relative absorbance at 280 nm) of the reaction of two equiv. GSH (3.33 mM) with **3** (triangles) or cisplatin (circles) in 1 mL of PBS (pH 7.4) at 37°C. Curves were obtained from mono-exponential fitting. The apparent rate constants were 0.2 and 0.38 h⁻¹ for **3** and cisplatin, respectively.

5.6 Conclusion

The new chalconyl dichlorido(2,3-diaminopropionate)Pt(II) complex **3** differs significantly and advantageously from cisplatin. Its superior *in vitro* anticancer activity against melanoma 518A2, leukemia HL-60 and colon carcinoma HCT-116 cells, its capacity to platinate DNA to a larger extent inflicting much greater DNA unwinding and a greater amount of interstrand cross-links which are less amenable to DNA repair, and its robustness against deactivation by S-nucleophiles like glutathione make complex **3** a promising candidate for further anticancer tests. The decisive role of the diamino ligand leaves room for future fine-tuning and optimization.

Some similarities between **3** and its analogue chalcone-Pt (**2**) were observed concerning the morphological changes inflicted in 518A2 melanoma cells, which were quite different from those caused by cisplatin. Mode of action of complex **3** synergistically combines the traits of DNA-binding platinum drugs and tubulin-binding chalcones.

Effects of retinoic acid conjugate of illudin M (5)

This study is focused on the selective impact of a new retinoic acid conjugate (5) compared to parent illudin M (4, Figure 6- 1). Illudin M from *Omphalotus olearius* cultures was isolated according to literature procedures (Knauer et al., 2009; Schobert et al., 2008). Its ester with retinoic acid was synthesized *via* Yamaguchi esterification (Biersack, 2009).

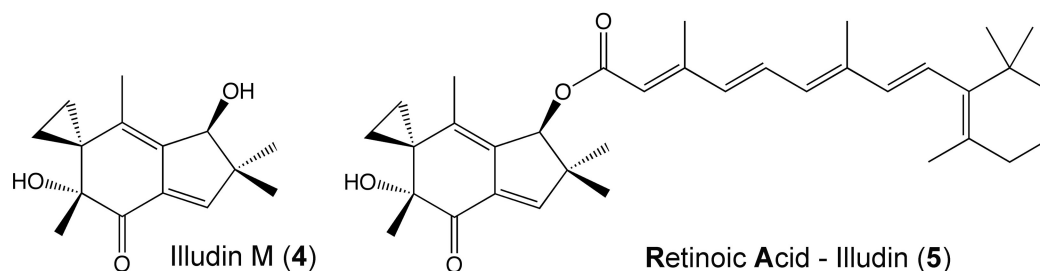


Figure 6- 1 Structure of illudin M (4) and of its retinoate (5).

6.1 Inhibition of cell growth - MTT assay

The anti-proliferative activity of compounds 4 and 5 was evaluated in a series of different (non-) malignant neuronal cells and multi-drug resistant tumor cells.

6.1.1 Neural derived cell lines

In the neural cells compound 4 exhibited activities in the range of $IC_{50} = 50$ nM (NE-4C neuroectodermal stem cells) to 400 nM (C6 rat glioma). Contrary, the retinoid conjugate 5 revealed excellent selectivity towards U87 human glioblastoma and NE-4C stem cells compared with mouse neuron and astrocytes and IC_{50} values still lying in the clinically relevant low one-digit micromolar range (2-3 μ M).

Table 6- 1 Inhibitory concentrations^a IC_{50} of compounds 4 and 5 in neural derived cells.

Cell line	neurons	astrocytes	NE-4C	C6	U87
24 h (4)	600 ± 120 nM	1.5 ± 0.4	400 ± 98 nM	1 ± 0.3	629 ± 44 nM
48 h (4)	190 ± 40 nM	200 ± 30 nM	50 ± 16 nM	400 ± 60 nM	130 ± 27 nM
24 h (5)	25.5 ± 1.1	45 ± 2.4	7 ± 3.2	40 ± 4.3	37.3 ± 3.2
48 h (5)	14 ± 2.2	33 ± 3.6	2 ± 1.2	12 ± 1.3	2.7 ± 0.7

Compound 5 is far less toxic to neurons than the parent compound illudin M. The toxicity of conjugate 5 against mouse neurons is 40-70 times lower compared with illudin M (4) and a similar effect is observed in astroglia cells (Figure 6- 2).

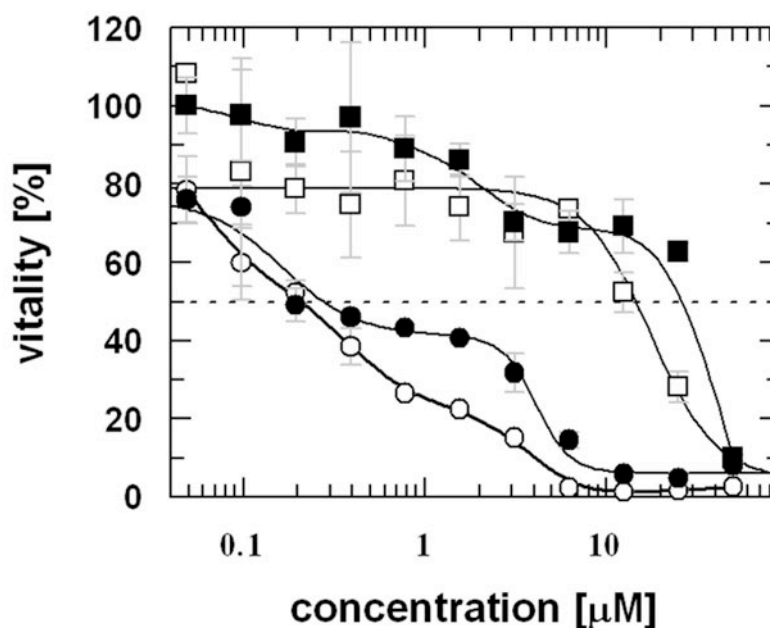


Figure 6- 2 Dose-response curves of neurons and astroglia cells after treatment with illudin M (**4**) and RA conjugate **5** for 48 h. Neurons: **4** (open circles), **5** (open squares). Astroglia: **4** (closed circles), **5** (closed squares).

Illudin M caused cytotoxicity at the nanomolar concentration in all tested neural cell lines, which is an indication of very low selectivity. The retinoic acid derivative **5** was less cytotoxic against neurons and astroglia cells even after long-time exposure. These results are in line with the fact that RA is an inhibitor of Jun N-Terminal Kinase (JNK) (Lee et al., 1999). Illudin derivatives such as irofulven are known to induce apoptosis by a mechanism mediated *via* activated JNK and ERK kinases (Wang et al., 2002). The putative inhibition of JNK-signaling in neurons treated with RA or derivative **5** could probably postpone eventual toxic effects of **4**.

6.1.2 Tumor cells expressing ABC-transporters

Illudin M also showed high activity in KBv1^{+vbl} cervix carcinoma cells expressing Pgp transporters, however, its activity was reduced about 5-fold in the other multi-drug resistant MCF-7^{+Top} breast cancer (BCRP) and HT-29 colon cancer (MRP-1, MRP-3) cells. Conjugate **5** showed less growth inhibiting activity than **4** lying in the low one-digit micromolar range (Table 6- 2). However, it showed a different activity profile and appeared to be especially active in the MDR cell line MCF-7^{+Top} reaching the activity of free illudin M in the two-digit nanomolar range.

This is a significant result as BCRP transporters are assumed to contribute to cancer stem cell resistance and inefficient trespassing of the blood brain barrier (Robey et al., 2007). In addition, this breast cancer cell line depends on estrogen signaling

6. Effects of the Illudin M (4) and its derivative RA-Illudin (5)

(Levenson and Jordan, 1997) which might explain the particularly high activity of the retinoid **5** in these cells since retinoids also interfere with estrogen receptor-based pathways (Hua et al., 2009).

Table 6- 2: Inhibitory concentrations (^aIC₅₀ in μM) of illudins (1,2) in various ABC-transporter expressing cells.

Cell line	MCF-7	MCF-7 ^{+Top}	KBv1	KBv1 ^{+Vbl}	HT-29
24 h (4)	1 ± 0.0059	0.35 ± 0.13	51 ± 7.5 nM	32 ± 4.6 nM	1.5 ± 0.6
48 h (4)	48 ± 4.9 nM	50 ± 10 nM	< 24.4 nM	16 ± 1.0 nM	60 ± 8 nM
24 h (5)	32.7 ± 1.3	2.5 ± 0.6	4.1 ± 0,16	1.6 ± 0.4	38 ± 4
48 h (5)	2.1 ± 0.20	80 ± 15 nM	2.3 ± 0.32	1.2 ± 0.13	4 ± 1.3

^aValues are derived from concentration-response curves obtained by measuring the percentual absorbance of vital cells relative to untreated controls (100%) after 24 and 48 h exposure of selected cells to test compounds in the MTT assay. Values represent means of at least three independent experiments ± standard deviation.

6.1.3 Cancer cells

HL-60 leukemia and 518A2 melanoma cells are examples for drug sensitive suspension and adherent tumor cells, respectively. Both cell lines were found to be extremely sensitive (nM) towards illudin M (**4**) already after 24 h of incubation. The cytotoxicity of **5** for both cell lines was randomly 100-times lower (Table 6- 3).

Table 6- 3 Inhibitory concentrations^a (IC₅₀ in μM) of compounds 4, 5 when applied to 518A2 melanoma and HL-60 leukaemia cells.

Cell line	24 h (4)	48 h (4)	24 h (5)	48 h (5)
HL-60	70 ± 21 nM	10 ± 5 nM	6.8 ± 2.8	4.5 ± 1.1
518A2	35 ± 11 nM	19 ± 8 nM	5.0 ± 0.26	4.0 ± 0.75

^aValues are derived from concentration-response curves obtained by measuring the percentual absorbance of vital cells relative to untreated controls (100%) after 24 and 48 h exposure of selected cells to test compounds in the MTT assay. Values represent means of at least three independent experiments ± standard deviation.

These results were in line with already published data for **4** (Kelner et al., 1987). All-trans retinoic acid (**RA**) is known to play a major role in regulating the growth and differentiation of a wide variety of normal and malignant cell types and can inhibit cell proliferation and induce differentiation and apoptosis at the cellular level (De Luca, 1991). The ability of retinoids to regulate cellular processes *in vivo* is unfortunately associated with a high incidence of undesirable side effects (Boehm et

al., 1995). For comparison, the apoptosis inducing activity of RA was above 50 μM in HL60 cells after 24 h (Simoni et al., 2001). The RA-Illudin showed an enhanced cytotoxic activity in HL60 cells ($\text{IC}_{50} \sim 7 \mu\text{M}$).

6.2 Cellular and sub-cellular observations

6.2.1 Altered cell-shape in neural cells

Elevated RA signaling triggers axon outgrowth and, consequently, nerve regeneration in the adult (Maden, 2007). All-trans retinoic acid (RA) and other active retinoids are generated from vitamin A (retinol), but key aspects of the signalling pathways required to produce active retinoids remain unclear (Gudas and Wagner, 2010). In order to induce neuron differentiation in K11 cells 3 mM RA was used according to the procedure described in the experimental section. Figure 6- 3 shows developed neural K11 cells together with some undifferentiated cells.

Microscopic changes of K11 cells were observed after exposure to illudin M **4** and **5**. The neural K11 network showed complete disruption of neural connections and its bodies after treatment with **4** (10 μM). Only a few undifferentiated K11 cells remained. A similar result has been observed after treatment with a smaller amount of **4** (1 μM). After fixation only cell debris remains and the neural network lost its integrity completely. Contrary, treatment with the retinoic acid ester **5** showed benefits of neural development at both concentrations (Figure 6- 3).

In order to evaluate the selectivity of illudins **4** and **5** towards U87 glioma cells we investigated a co-culture of neural cells with U87 cells and treated this culture with compounds **4** or **5**.

The isolated murine neurons were grown on IBIDI dishes and after 5 days a sample of glioma U87 cells (~25 000 cells) was added into the neural culture. After 12 hours, illudins **4** and **5** (1 μM) were added and the response of the different cells was monitored (15 – 96 hours).

6. Effects of the Illudin M (4) and its derivative RA-Illudin (5)

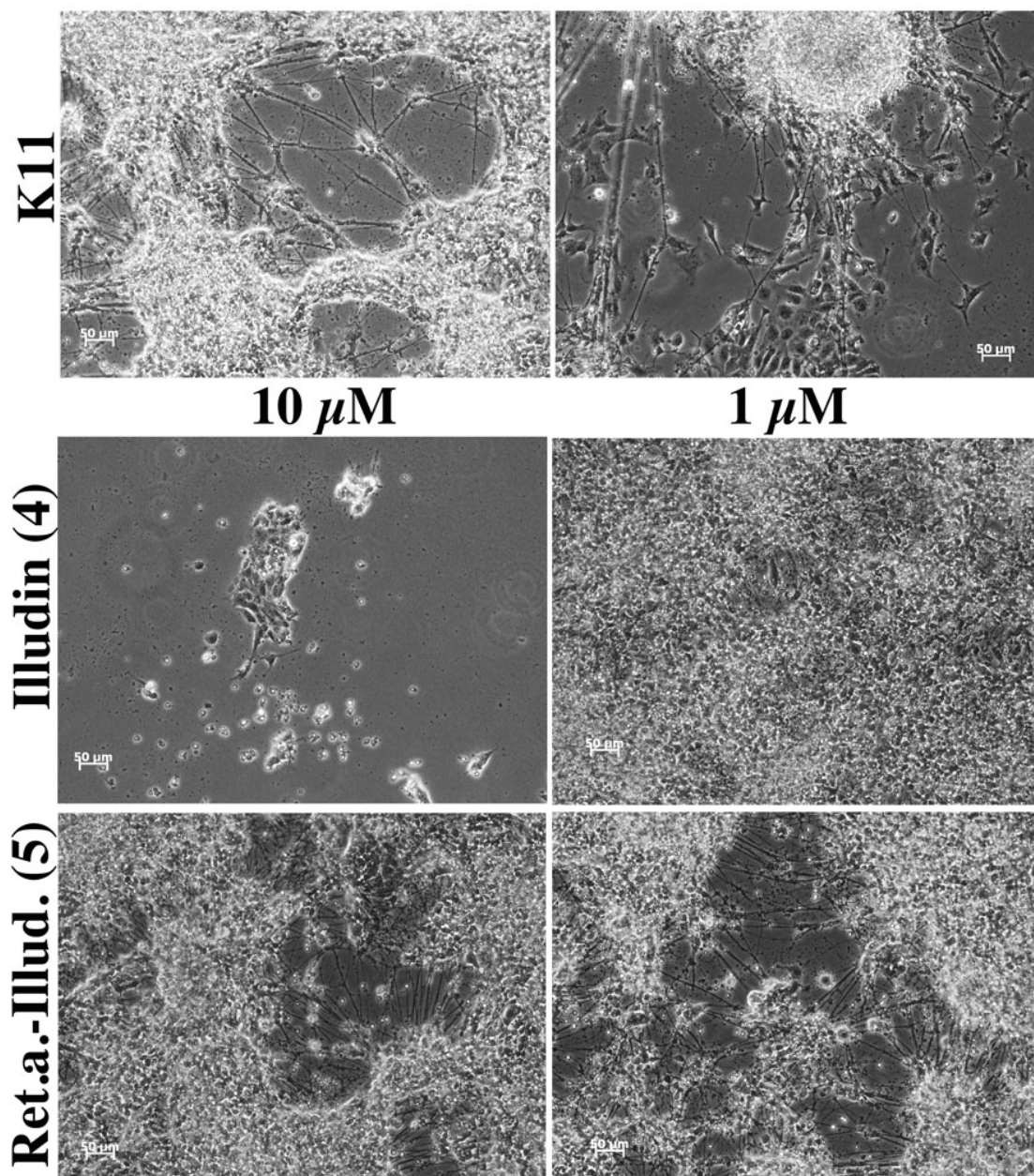


Figure 6- 3 Top figures show microscopic observations of K11 cells treated with 3 mM retinoic acid. Middle and bottom figures show K11 cells treated with illudin M (4) and RA-illudin (5) for 24 hours.

In the control samples the number of proliferating U87 cells increased with time and overgrew the diminishing number of differentiating neurons. The neuronal bunches are marked by arrowheads (Figure 6- 4). The neurons and U87 cells incubated with illudin M (4) showed cellular fragmentation already after 15 h, after 48 h only cell debris was visible. Incubation of the co-culture with RA conjugate 5 revealed a higher neuronal differentiation degree after 15 h compared with the control cells. After treatment for 48 h neurons were still present in the culture, yet, the number of U87 cells was reduced distinctly compared with the control sample and with the situation after 15 h. This shows vividly the selective antitumor activity of compound 5.

15 hours Neurons vs. U87 48 hours

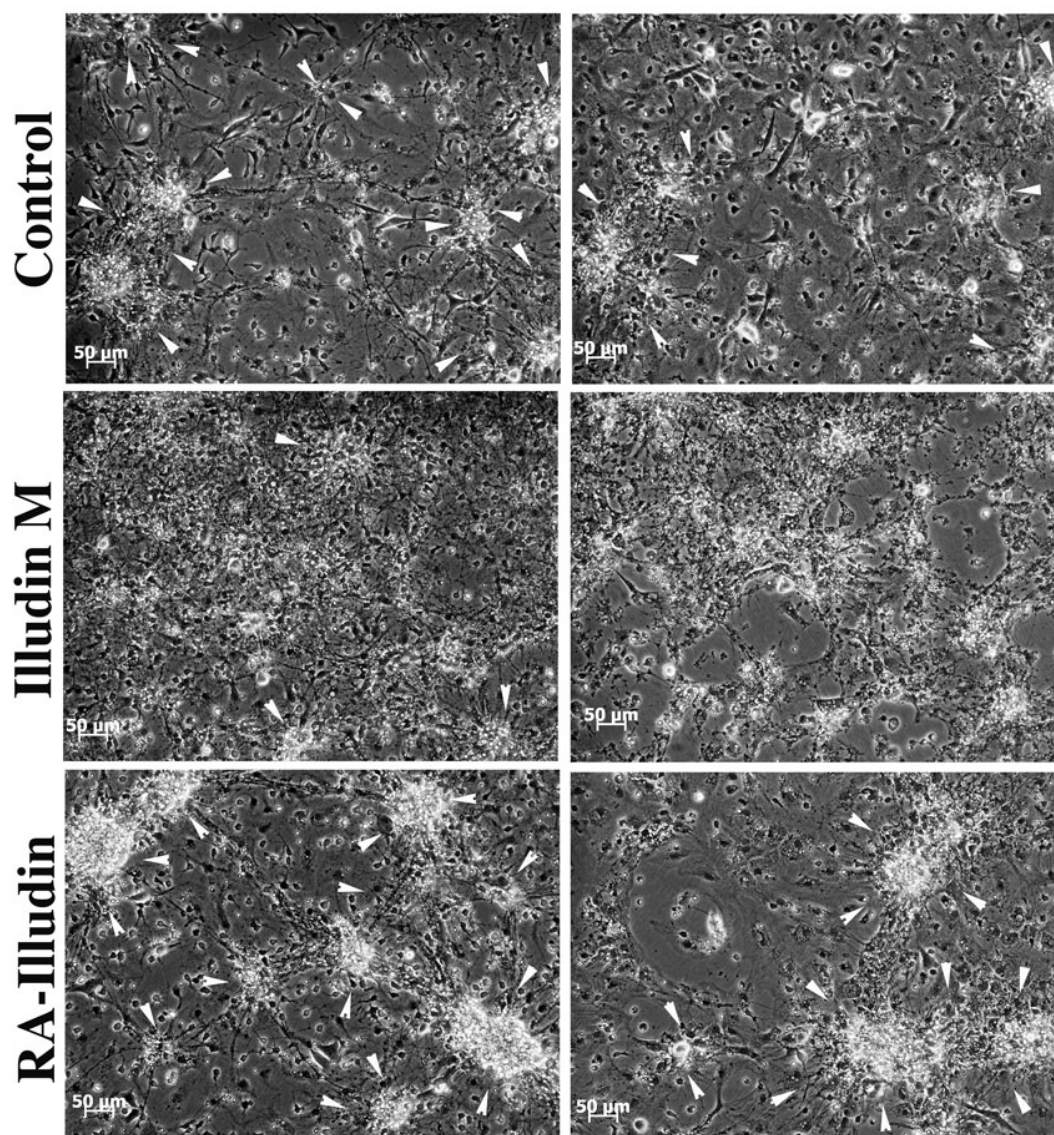


Figure 6-4 Co-cultivation of neural cells with U87 glioma cells in the absence or presence of 1 μ M of illudin M (4) or RA-illudin (5).

6.2.2 Altered cell-shape in cancer cells

The effects of illudins **4** and **5** on the structure, development and mobility of cancer cells were monitored. A monolayer of tightly attached KBv1^{+Vbl} cells was observed initially. The untreated control cells were spread and underwent merely negligible morphological changes. Only a few cells were rounded which were probably dividing. In contrast, exposure of KBv1^{+Vbl} cells to illudin M **4** led to a decreased cell number after 24 hours and to an enhancement of motility and cell shrinking (Figure 6- 5). A very similar behaviour of KBv1^{+Vbl} cells was observed upon incubation with complex **5**.

6. Effects of the Illudin M (4) and its derivative RA-Illudin (5)

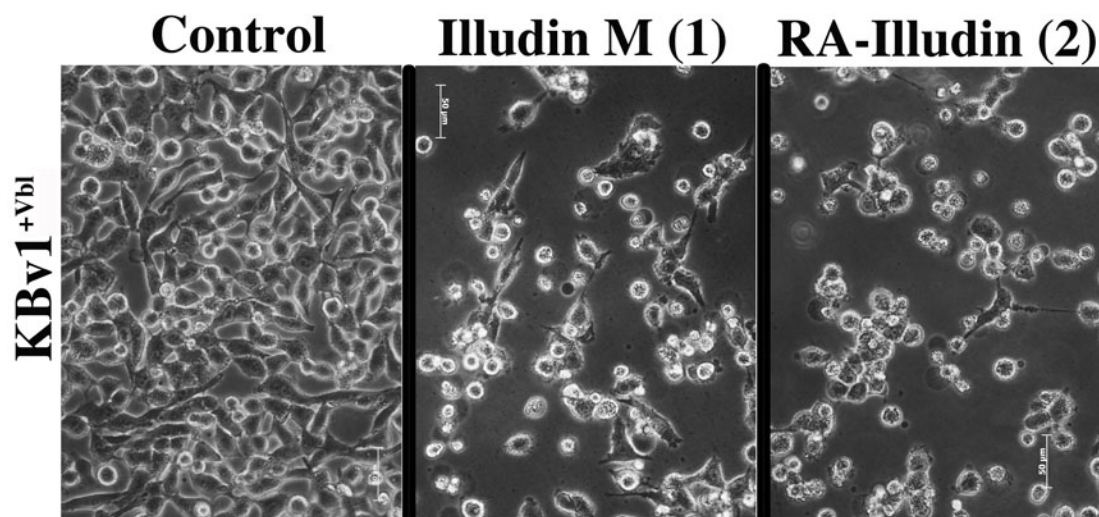


Figure 6- 5 Untreated KBv1^{+Vbl} cervix carcinoma cells (control); *middle*: rounded, partially detached cells with increased motility after 24 hours of incubation with 50 nM of 4; *right*: similar effects upon treatment with 2 μ M of complex 5. The cells were not fixed.

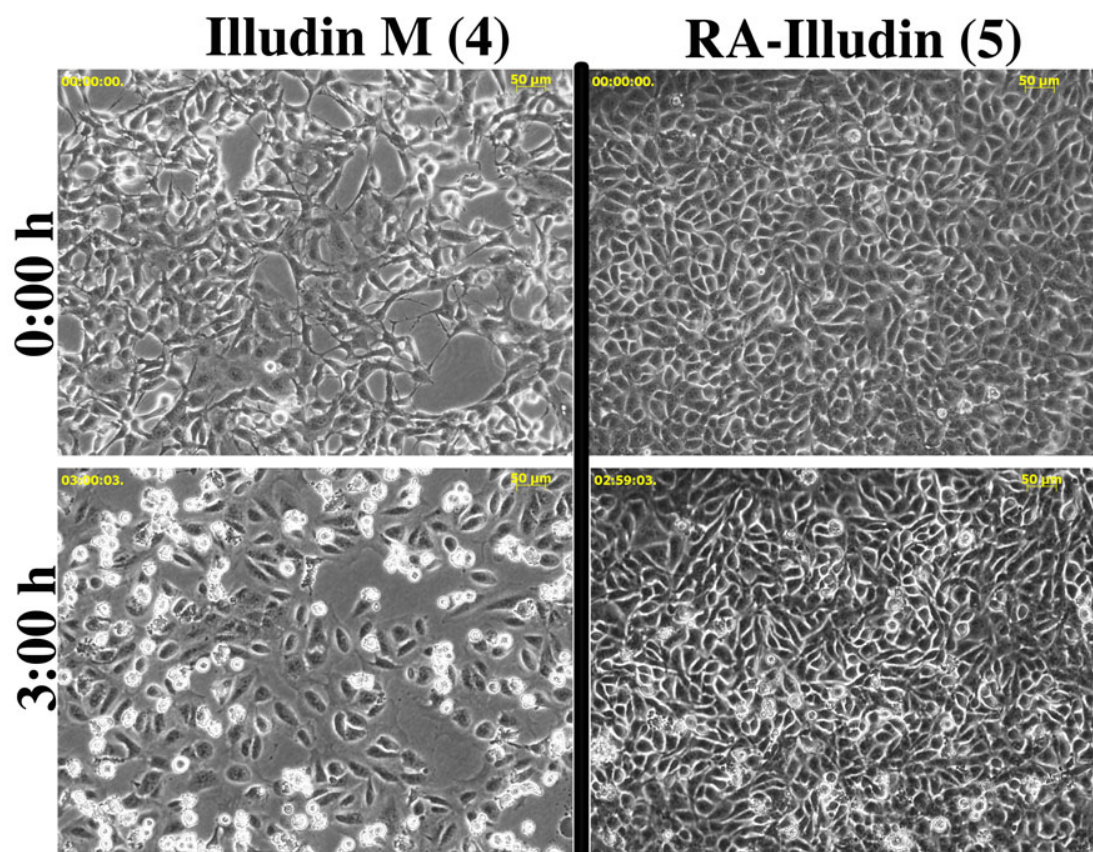


Figure 6- 6 Time lapse microscopic observation of 518A2 cells with time after treatment (10 μ M) with illudin M (4) and its retinoate derivative (5).

Time-lapse recording of the relatively less sensitive 518A2 cells also revealed this cell-rounding phenomenon (Figure 6- 6). After treatment with 4 cells slowly detached and shrank. A slower effect was observed after treatment with 5, the cells readily dissociated from the monolayer and changed their form from flat to spherical.

6.2.3 Microscopic observations of 518A2 cells by Giemsa staining

Effects of Illudin M (**4**) and its retinoate derivative **5** were monitored for internucleosomal DNA cleavage after staining with Giemsa dye (Figure 6- 7). The test compounds were applied at a concentration of 10 μ M for 12 h or 24 h and the effect on the proliferation as well as on the attachment of the adherent cells was analyzed. The total number of 518A2 melanoma cells increases in the untreated negative control due to normal cell proliferation. They showed typical cell-shape, were regularly spread. The nuclei revealed condensed chromatin visible as dark blue dots and they were well defined by their nuclear envelopes. Cells treated with **4** led to a reduced cell number after 12 hours and 24 hours. Completely destroyed (lysed) cells could be identified, which are characteristic of necrosis. In the Giemsa assay the applied concentration of **4** was \sim 200 times higher than its IC₅₀ value. Thus, the strong cytotoxic effect was expected to appear earlier (3 hours data shown in (Zoldakova and Münzner, 2009Advisor: Zoldakova Miroslava)).

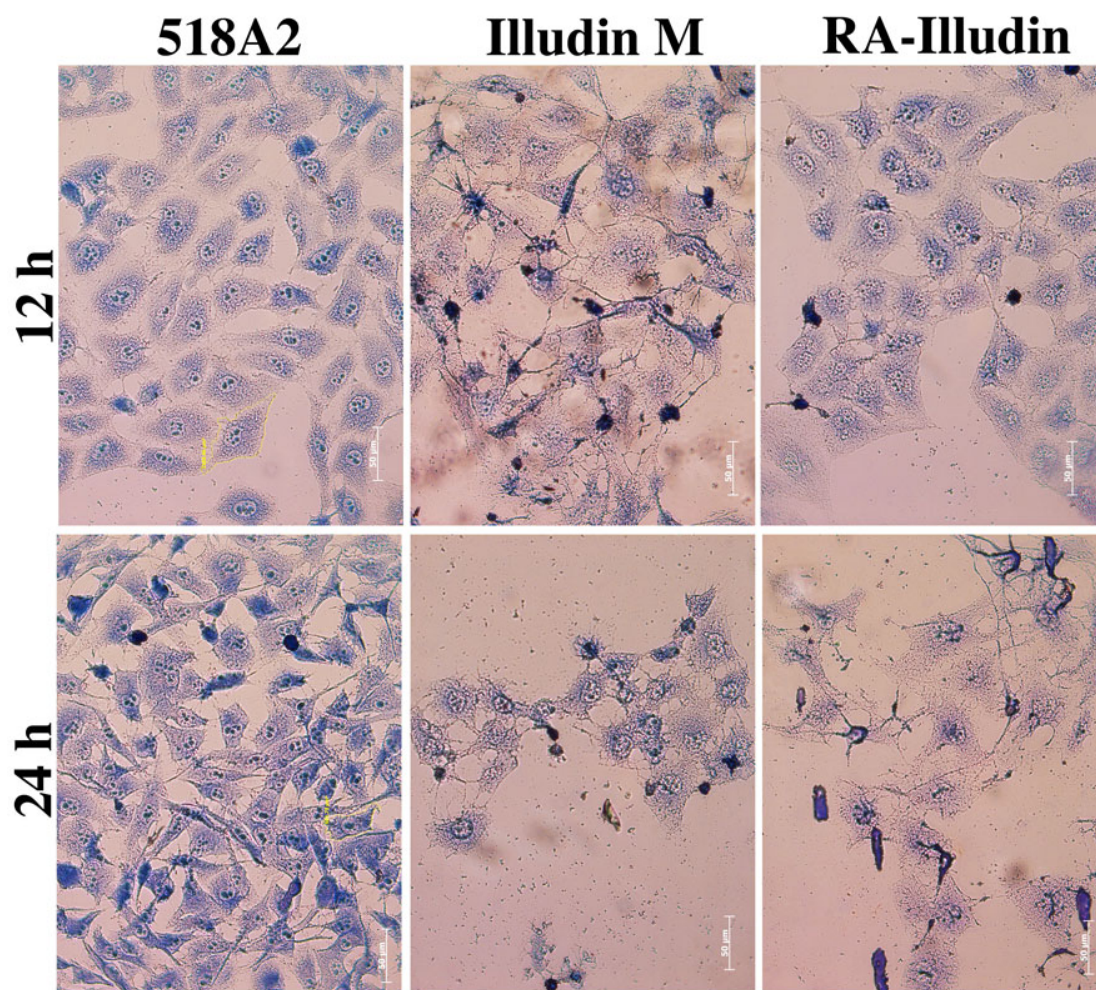


Figure 6- 7 518A2 cells were treated with illudins **4** and **5** (10 μ M) and visualized by Giemsa stain.

6. Effects of the Illudin M (4) and its derivative RA-Illudin (5)

Treatment with retinoate **5** resulted in reduced cell numbers compared with the untreated negative control and promoted the detachment of the cells from the glass slides (24h). After 12 hours still some cells were alive probably due to a more controlled cytotoxicity of **5**. Very late apoptotic or dead cells were sprawled out showing purple or totally missing cytoplasm.

6.2.4 Immunostaining of β -tubulin in treated neurons

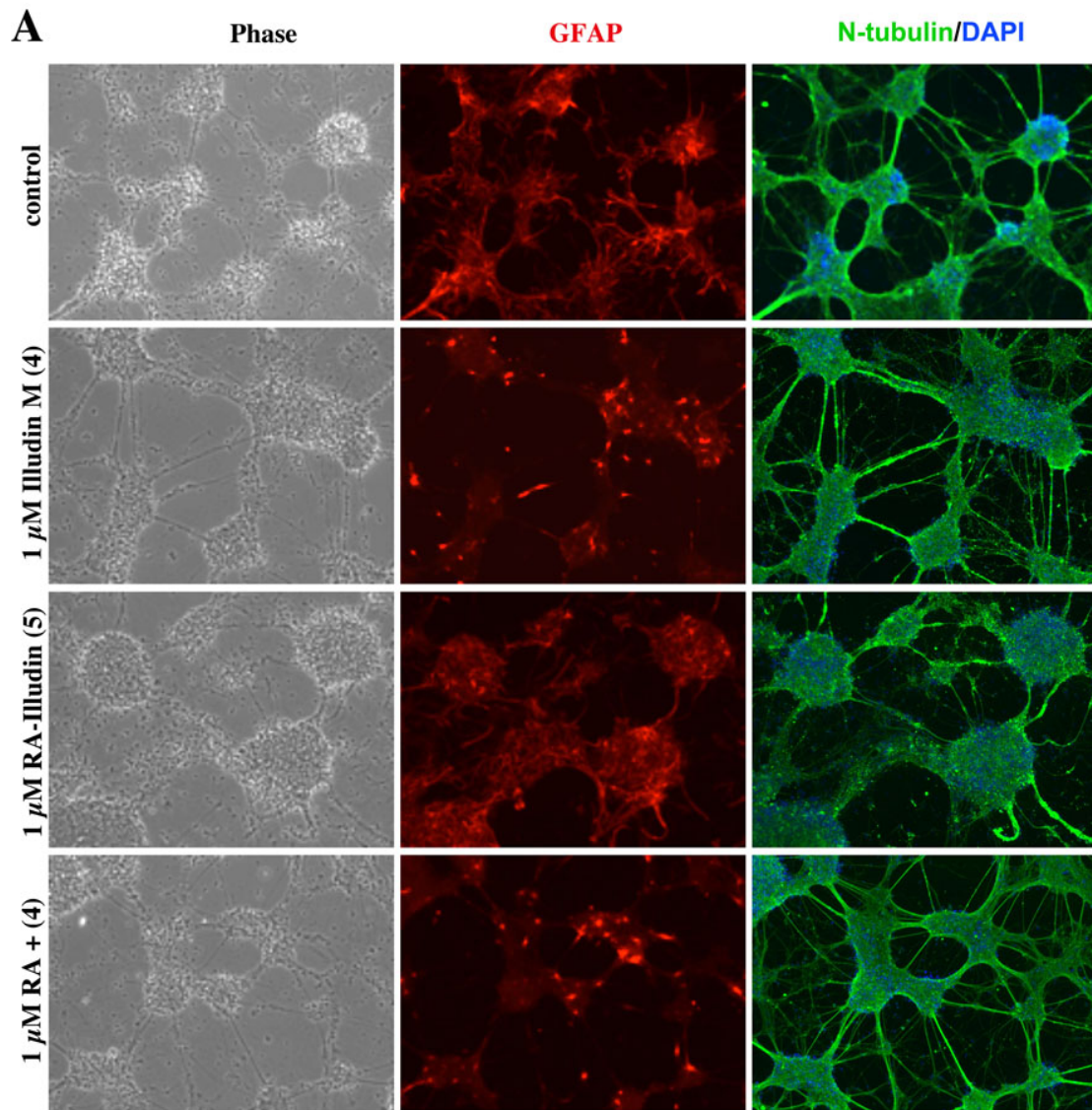
Retinoic acid (RA) is involved in the induction of neural differentiation, motor axon outgrowth and neural patterning (Maden, 2007; Schlett and Madarasz, 1997). Elevated RA signalling in the adult triggers axon outgrowth and nerve regeneration (Maden, 2007). After immunocytochemical staining detailed analyses of the morphological changes initiated by the illudins **4** and **5** after 48 hours were carried out using primary neurons and astrocytes (Figure 6- 8A, Figure 6- 9).

Antibodies to astrocyte-specific GFAP intermediate filaments (glial fibrillary acidic protein) were employed to visualize the astroglial cells. Anti-mouse neuron specific β III-tubulin labelling was used to identify tubulin filaments. The micrographs showed that both types of filaments, β -tubulin (in green) and GFAP (in red), were dismissed upon treatment with illudin M **4** (Figure 6- 8A, Figure 6- 9).

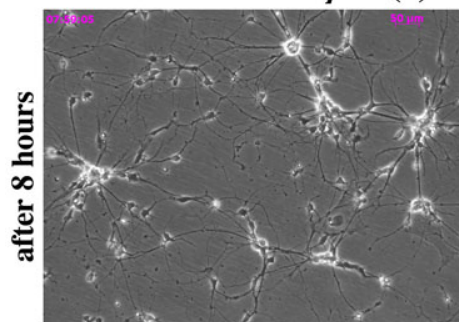
The completely opposite behaviour was observed after treatment with RA-conjugate **5**. A combined treatment of RA and **4** resulted in well-defined β III-tubulin level, which was confirmed by ELISA (6.2.4.1). However, decreased intensity of GFAP fluorescence was observed after combination of RA with **4** similar to effect after treatment with compound **4** alone. Contrary, an effect comparable to RA (positive control) was monitored with compound **5**, i.e., it helps neurons to develop well (Figure 6- 8B).

6.2.4.1 ELISA measurement of β III-tubulin

The levels of β III-tubulin after treatment with illudins **4** and **5** give a similar result (Figure 6- 8C). While compound **5** slightly promotes neuronal growth, illudin M is slightly toxic at 1 μ M concentration. In addition, illudin M does not preclude the effect of RA on neuronal growth.



B Neurons + 10 μ M (5)



C ELISA- level of β -tubulin

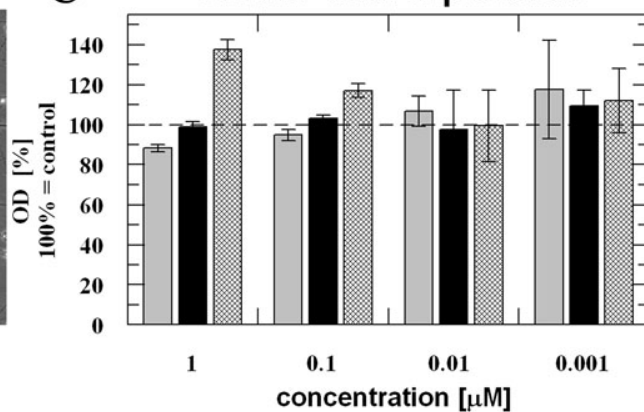


Figure 6- 8 Microscopic observation of murine neurons (DIV16/18) after 48 h incubation in the absence or presence of 4 or 5 (0.1-1 μ M). Primary neurons were visualized by specific immunostaining. Blue: nuclei stained with DAPI (4',6-diamidino-2-phenylindole); green: tubulin cytoskeleton stained with β III-tubulin specific antibody; red: glial fibrillary acidic proteins (GFAP). The pictures were taken with a fluorescence microscope (Zeiss Axiovert 200M). B: Time lapse recording of neurons incubated with 5 (10 μ M). The picture is taken after treatment for 8 hours. C: Levels of β III-tubulin after 24 h exposure to different concentrations of illudin M (4, grey columns), RA-illudin (5, black columns) or illudin M + RA (hatched columns). Control – untreated neurons (set to 100%). Values and standard deviations are means of three independent experiments.

6. Effects of the Illudin M (4) and its derivative RA-Illudin (5)

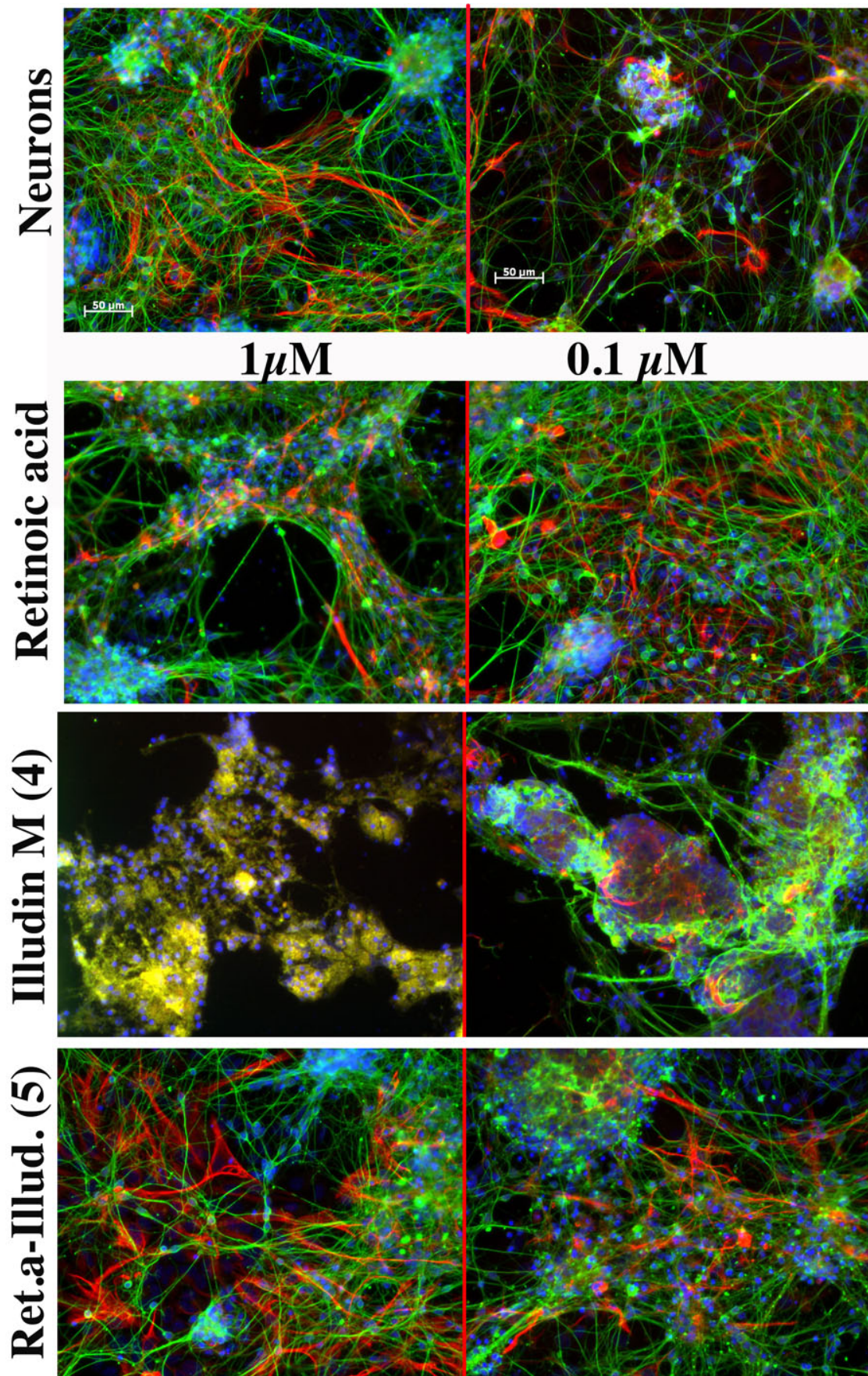


Figure 6- 9 Immunofluorescence staining of murine neurons (DIV16/18) after 48 h incubation with illudins 4 and 5.

6.3 Single cell DNA damage monitoring by comet-assay

A large number of agents bind to duplex DNA in a covalent or non-covalent fashion. An important technique for studying the interaction between a drug and DNA is the electrophoretic mobility shift assay (EMSA). However, no band shift was observed after incubation with **4**. McMorris et al. (1989) discovered that the extreme toxicity of illudin M is due to the alkylating ability in reaction with various nucleophiles at neutral or low pH (McMorris et al., 1989; McMorris et al., 1992; McMorris et al., 1996).

Recently, the comet assay has become a widely accepted and valuable method to determine DNA damage in cells and to reveal the nature of this damage. This was a reason to establish alkaline comet in this work (Figure 6- 10).

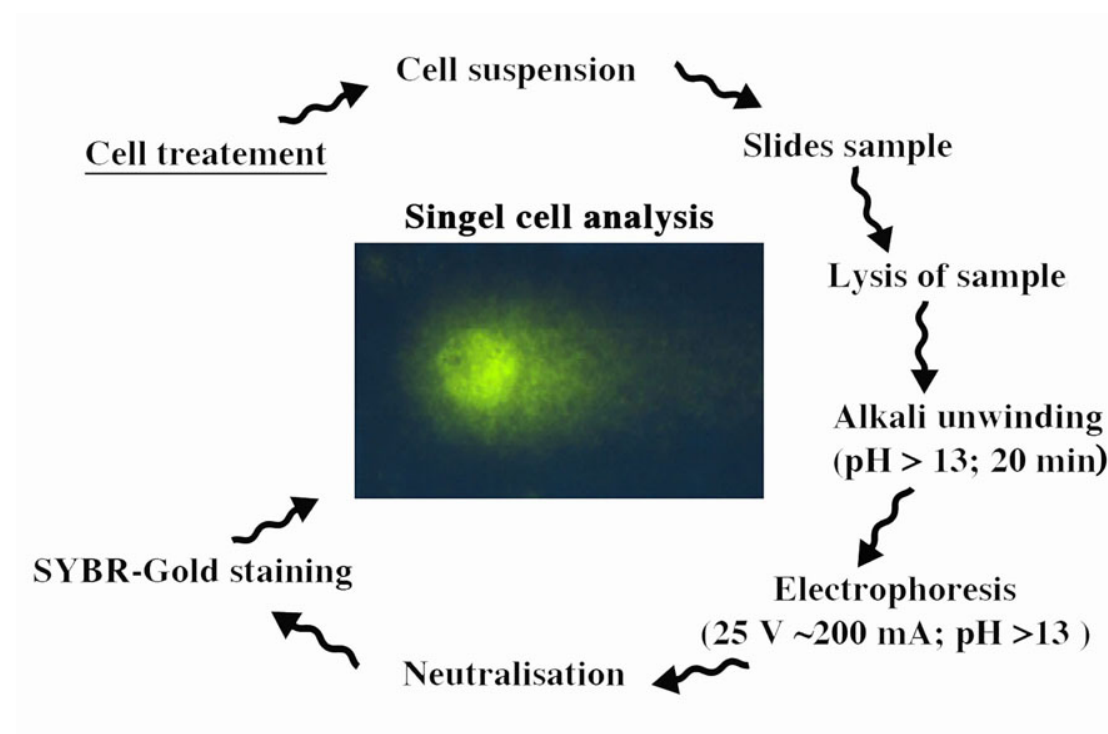


Figure 6- 10 Scheme of critical steps in the alkaline (pH >13) comet assay. The basic steps of the assay include single cell suspension, slide preparation, lysis of cells to liberate DNA, alkaline exposure to obtain single-stranded DNA and express alkali-labile sites as single strand breaks, electrophoresis, neutralisation, DNA staining, comet visualisation and scoring.

A suitable electrophoretic equipment was designed and an optimized comet assay was developed after various steps of improvements (Zoldakova and Rymarczyk, 2009). HL60 cells were incubated with 1 μ M of illudin M (**4**). The control sample was treated without compound **4**. The alkaline (pH >13) comet assay includes single cell investigations, which were analyzed in prepared gel-slides. The lysis of cells was performed under alkaline conditions to obtain single-stranded DNA. Gel-samples

6. Effects of the Illudin M (4) and its derivative RA-Illudin (5)

were neutralized followed by staining with SYBR-Gold dye. Comets were visualized by fluorescence microscopy and the free-software *TriTek CometScore™* version 1.5 was used for comet analysis.

Untreated (control) cells do not suffer from any DNA damage (Figure 6- 11). The DNA damage caused by illudin M was expressed in various DNA-tail lengths.

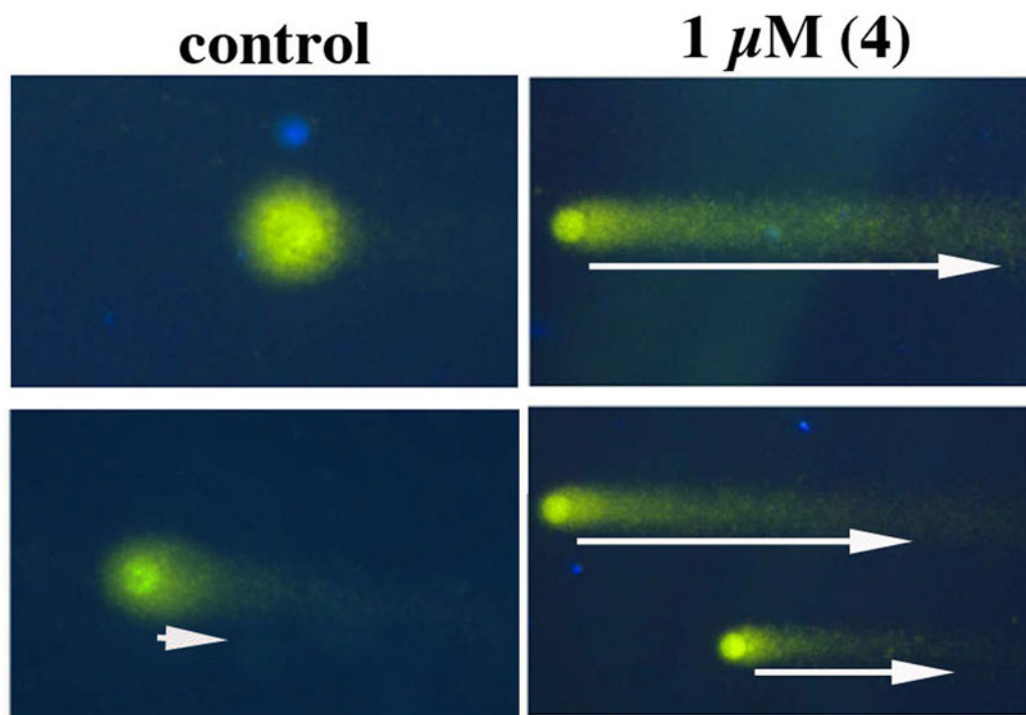


Figure 6- 11 Images of comets with various tail lengths. Control cells show no tail or only a very short tail (white arrow). Illudin M (4) treated cells gave single strand breaks (damaged DNA) in various stages, resulting into longer tails (arrows).

The fragments of damaged chromosomal DNA were released and pulled towards the anode and this affected the tail-length. Cells with DNA damage appeared as comets with small heads and very long tails. The total level of DNA fluorescence represented 100% and the part distributed within the tail was calculated. Thus, control cells were characterized by only $20 \pm 3\%$ of DNA in the tail. After 5 minutes of incubation with compound **4** ($1 \mu\text{M}$) $24 \pm 14\%$ single-strand breaks appeared, and already $50 \pm 18\%$ single-strand breaks appeared after 10 minutes.

6.4 Intracellular calcium concentration

The intracellular concentration of Ca^{2+} after treatment with illudin M (**4**) and RA conjugate **5** in 518A2 and HL60 cells was investigated as a sign for apoptosis induction in these cells (Table 6- 4). The level of the intracellular Ca^{2+} concentration in cells is usually maintained at about 10-100 nM by mechanisms including transport

via voltage-dependent and voltage-insensitive channels, controlled release from the endoplasmic reticulum (ER), and cytosolic Ca²⁺ buffering (Sergeev, 2005). Aside the regulation of vital cell functions, Ca²⁺ signalling was also found to play an important role in promoting cell death (Orrenius et al., 2003; Sergeev, 2005). A distinctly enhanced intracellular Ca²⁺ concentration was observed in the HL-60 leukemia cells after 24 h of exposure to compounds **4** and **5** reaching levels higher than 200 nM. This high Ca²⁺ level is very likely associated with apoptosis of these cells, which usually leads to increased Ca²⁺ levels (200-500 nM).

Table 6- 4 Intracellular Ca²⁺ concentration^a of 518A2 melanoma and HL-60 leukemia cells after incubation with compounds 4 and 5 (24 h). Concentrations in 518A2 cells: 4 = 0.05 µM, 5 = 5.00 µM; in HL-60 cells 4 = 0.1 µM, 5 = 7.0 µM.

Ca ²⁺ [nM]	518A2	HL60
Control cells	73.1 ± 8.1	52.3 ± 9.2
Illudin M (4)	111.0 ± 14.0	293.3 ± 4.7
RA-Illudin (5)	82.4 ± 8.9	239.6 ± 9.4

^a Values represent means and standard deviations of three independent experiments

6.5 Interference with ABC transporters

The role of efflux proteins in the detoxification of cancer cells represents one the main interests of pharmaceutical studies. The interaction of compounds **4** and **5** with pertinent drug efflux proteins like ABCB1 (P-gp) (Hyde et al., 1990; Simstein et al., 2003; Smith et al., 2001) or BCRP (Borst et al., 1997) was investigated in a substrate- or inhibitor-like fashion.

6.5.1 Illudin efflux via P-glycoproteins

P-gp expressing KBv1^{+Vbl} cervix carcinoma cells (Schwab et al., 2003) were treated with illudins **4** and **5** in the presence of calcein-AM (Figure 6- 12). Illudin M (**4**) did not surpass the fluorescence intensity of calcein in the negative control. In contrast, conjugate **5** was more effective and its relative fluorescence reached almost 80% of the activity of verapamil. Wild type KBv1 cells gave very similar results. Possibly, they possess different ways to eliminate calcein-AM or calcein, which is not without precedence (Marchan et al., 2008; Oku et al., 1995).

6. Effects of the Illudin M (4) and its derivative RA-Illudin (5)

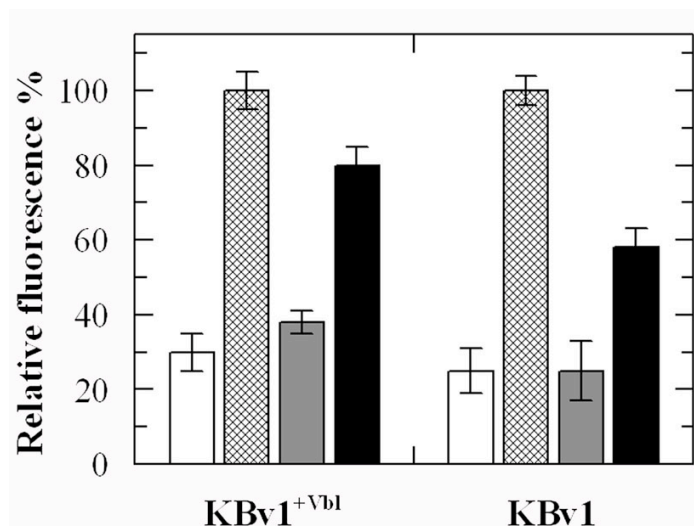


Figure 6- 12 Calcein-AM assay: % inhibition of P-gp drug transporters in KBv1^{+Vbl} and KBv1 cells by 50 μ M of illudin M 4 (grey bars) and RA-Illudin 5 (black bars) relative to the inhibition of P-gp by verapamil (hatched bars) after 15 min exposure. White bars: negative control.

6.5.2 Illudin efflux via BCRP proteins

MCF-7 breast carcinoma cells express BCRP drug transporters. Treatment with topotecan (550 nM over 40 generations) leads to overexpression of this protein (MCF-7^{+Top} cells). The mitoxantrone assay is based on the active export of the fluorescent anticancer drug mitoxantrone by BCRP transporters. The effects of illudins **4** and **5** compared with the specific BCRP inhibitor fumitremorgine C (Oku et al., 1995) and with a negative control treated only with mitoxantrone was investigated (Figure 6- 13). Similar to the calcein-AM assay, compound **4** did not reveal any inhibition. Here, conjugate **5** showed only a slight inhibition in comparison with the negative control.

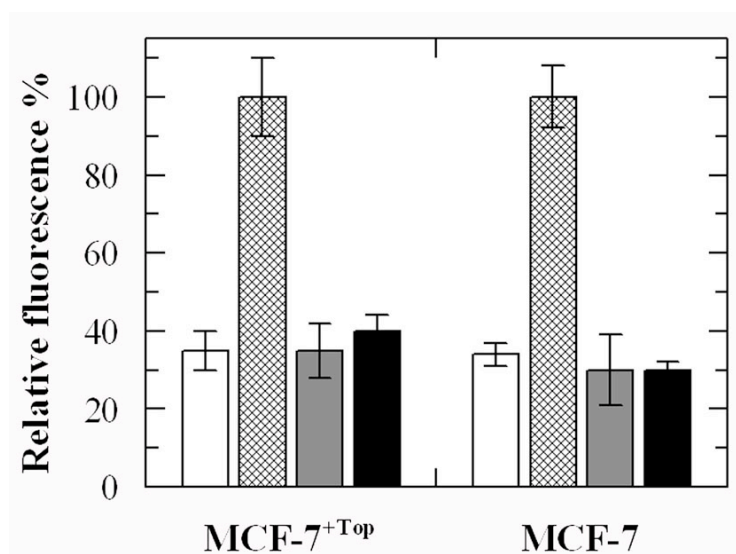


Figure 6- 13 Mitoxantrone assay: % inhibition of BCRP drug transporters in MCF-7^{+Top} and MCF-7 cells by 10 μ M of illudin M 4 (grey bars) and RA-illudin 5 (black bars) relative to fumitremorgine C (hatched bars) after 30 min exposure. White bars: fluorescence of cells treated with mitoxantrone (negative control).

6.6 Conclusion

All-trans retinoic acid (RA) shows antitumor effects against various cancers. For instance, exposure to 1 μM of retinoic acid caused effects progressing linearly in a time-dependent and dose-dependent fashion, and after treatment for 7 days cell growth was inhibited by approximately 65% (Lotan and Lotan, 1980). The new illudinyl retinoate **5** is much more effective and we were able to observe comparable effects already after 48 hours. Compound **5** is far less toxic to neurons, more cancer selective and more cell line-specific than the parent compound illudin M. Though illudins are highly efficacious against various tumors, their extreme toxicity precluded clinical applications (Kelner et al., 1987; Kelner et al., 1990). The toxicity of conjugate **5** against mouse neurons is 40-70 times lower compared with illudin M (**4**). Neural stem cells (NE-4C) are most sensitive; yet, the U87 glioma cells appeared to be more sensitive to compound **5** after prolonged exposure than primary neurons or astrocytes. These results are in line with the fact that RA is an inhibitor of Jun N-Terminal Kinase (JNK) (Lee et al., 1999). Illudin derivatives, such as irofulven, are known to induce apoptosis by a mechanism mediated *via* activated JNK and ERK (Lotan and Lotan, 1980). The putative inhibition of JNK-signaling in neurons treated with RA or derivative **5** could probably postpone eventual toxic effects of **4**. Compound **5** is at least 5 times more active against cancer cells than against neurons.

MDR cells expressing Pgp or BCRP proteins revealed an enhanced sensitivity towards **5** (48 hours $\sim 1,2/0.08 \mu\text{M}$). Indeed, an inhibition of P-gp drug transporters was confirmed only for conjugate **5**. Enhanced Ca^{2+} concentrations were observed in HL-60 leukemia cells treated with compound **5**. Together with the cell rounding and retraction of pseudopodes in KBv1^{+vbl} cervix carcinoma and in 518A2 melanoma cells visible *via* time-lapse microscopy, these are all hints at an induction of apoptotic cell death by conjugate **5** (Lotan and Lotan, 1980).

Summary

This thesis presents a study on novel chemotherapeutics based on naturally designed scaffolds. The cytotoxicity of promising pharmaceutical compounds was tested on various cells of neural and/or cancerous origin, monitoring their specificity, re-growth retardation and mechanism of apoptosis induction. The proposed drug uptake was analysed using specific inhibitors to disable certain transporters/carriers. Changes in the shapes of cellular and sub-cellular components resulting from drug treatment were observed by light microscopy, immune-fluorescence microscopy, time-lapse recording microscopy and transmission electron microscopy. The apoptotic signals, increased cellular activity of caspase-3 or redundant calcium level, were monitored during drug incubation. Because DNA-degradation plays an important role in apoptosis, DNA-drug interactions affecting chromosomal or plasmid DNA were investigated from various perspectives. Since resistance is a constricting factor for drug efficiency, the interaction of the drugs with glutathione and various efflux transporters were analysed.

Many of the methods in this thesis were not previously in use in the department of organic chemistry. Therefore, the methods were optimised or performed in international collaboration during a short-time fellowship in the *Laboratory of Cellular and Developmental Neurobiology, Institute of Experimental Medicine of the Hungarian Academy of Sciences, Budapest* (2 months) and in the *Institute of Biophysics, Academy of Sciences of the Czech Republic, Brno* (4 months).

7.1 Chalcone (1) and its Pt-derivatives (2, 3)

The combretastatin A4 analogs chalcone **1** and chalcone-Pt **2** were found to be highly active against a variety of cancer cell lines while differing in their apoptosis induction and long-term regrowth retardation (Schobert et al., 2009).

Chalcone-Pt **2** was more tumour-specific than parent chalcone **1** in neural cells. This was apparent from the IC₅₀ ratios (48 h) against primary astrocytes *vs.* human glioma cells U87 (>7000 for complex **2**; 55 μ M for compound **1**). The cellular uptake of chalcone-Pt **2**, like that of oxaliplatin, occurred mainly *via* organic cation transporters (OCT-1/2; ~32%) and copper transporter related proteins (Ctr1; ~24%), whereas that of chalcone **1** was dependent on endocytosis (~80%). In tubulin-rich neurons and 518A2 melanoma cells, complex **2** disrupted microtubules and actin filaments. Cancer cells treated with **2** could repair the cytoskeletal damage, but ceased

to proliferate and perished. Complex **2** was particularly cytotoxic against P-gp-rich cells. It acted as a substrate for ABC-transporters of types BCRP, MRP3, and MRP1 and was therefore less active against the corresponding cancer cell lines. Complex **2** arrested the cell cycle of the melanoma cells in G1 and G2/M phases. Massive fragmentation of the Golgi apparatus of these cells was observed using TEM during incubation with complex **2** but not with **1**. Unlike chalcone **1**, the platinum complex **2** is highly cell-line specific, and is taken up *via* cell-controlled transporters and induces apoptosis by triggering multiple targets.

Chalcone-DAP-Pt **3** was tested for antitumour activity, DNA binding, and glutathione binding. In MTT-tests against cells of melanoma 518A2, complex **3** inhibited leukemia HL-60 and colon carcinoma HCT-116 more efficiently than **2** and **1**. The morphology of tumor cells treated with the chalcones **1**, **2**, and **3** differed from that of cells exposed to colchicine. While complex **3** is only 70% water-soluble, it binds to the same DNA sites as cisplatin. In contrast to cisplatin, DNA binding of **3** caused a larger DNA unwinding angle and ten times more interstrand cross-links (~60%). These results were confirmed by a DNA-footprint experiment, where it was found that one chalcone-DAP-Pt molecule was coordinated to neighbouring guanine residues and formed a 1,2-d(GpG) intrastrand cross-link. In addition, DNA lesions due to binding of **3** were repaired by the melanoma cellular extract only half as efficiently as cisplatin-DNA adducts. Complex **3** also showed a much lower affinity towards the known platinum detoxifier glutathione.

7.2 Illudin M (**4**) and its retinoate (**5**)

The fungal metabolite illudin M **4** is indiscriminately cytotoxic in cancer and non-malignant cells. Its retinoate **5** showed a greater selectivity for the malignant cells, especially in a cerebral cortex. Illudin M killed malignant glioma cells as well as primary neurons and astrocytes at similarly low concentrations by destroying their microtubule and glial fibrillary acidic protein (GFAP) networks. In contrast, the ester **5** was distinctly more cytotoxic in highly dedifferentiated U87 glioma cells than in neurons, which were even stimulated to enhanced growth. This was also observed in co-cultures of normal neurons with U87 cells, where conjugate **5** singled out the latter and eventually killed them by induction of differentiation. Hence, illudin M retinoate **5** appears to be a promising drug candidate to treat glioma stem cells.

Zusammenfassung

Diese Arbeit stellt eine Studie über neue Chemotherapeutika dar, welche ausgehend von Naturstoff-basierenden Strukturen dargestellt worden sind. Die cytotoxische Wirkung der vielversprechendsten Verbindungen wurde an verschiedenen Zellen neuralen und/oder malignen Ursprungs getestet, und ihre Spezifität, Wachstumshemmung sowie Mechanismen der Apoptoseinduktion wurden analysiert. Mutmaßliche Wege der Wirkstoffaufnahme wurden durch Einsatz spezifischer Hemmer bestimmter Transport- und Carrierproteine untersucht. Wirkstoff-induzierte morphologische Veränderungen zellulärer und sub-zellulärer Strukturen wurden Licht-mikroskopisch, Immunfluoreszenz-mikroskopisch, Zeitraffer-mikroskopisch und Transmissionselektronen-mikroskopisch beobachtet. Durch einzelne Wirkstoffe hervorgerufene apoptotische Signale wie verstärkte Caspase-3-Aktivität oder erhöhter Calciumspiegel wurden analysiert. Da die DNA-Schädigung und der DNA-Abbau eine wichtige Rolle zur Apoptoseeinleitung und auch während der Apoptose spielt, wurden DNA-Wirkstoff-Wechselwirkungen bezüglich chromosomaler und Plasmid-DNA von verschiedenen Blickwinkeln aus untersucht. Schließlich stellt die Wirkstoffresistenz von Tumorzellen einen limitierenden Faktor dar, welche in entsprechenden Experimenten zur Interaktion der Wirkstoffe mit Glutathion oder mit verschiedenen Efflux-Transportern analysiert wurde.

Eine Vielzahl der in dieser Arbeit beschriebenen Methoden wurde vorher nicht am Lehrstuhl für Organische Chemie praktiziert. Deshalb wurde zum Methodenstudium und zur Methodenverfeinerung die Expertise anderer Forschungsinstitute im Rahmen kurzzeitiger Forschungsaufenthalte in Anspruch genommen, namentlich sind dies das *Laboratory of Cellular and Developmental Neurobiology, Institute of Experimental Medicine of the Hungarian Academy of Sciences* in Budapest (2 Monate) und das *Institute of Biophysics, Academy of Sciences of the Czech Republic* in Brünn (4 Monate).

7.3 Chalkon (1) und seine Pt-Derivate (2, 3)

Die Combretastatin-A4-Analoga Chalkon **1** und Chalkon-Pt **2** erwiesen sich als höchst wirksam gegen eine Vielzahl verschiedener Krebszell-Linien, während sie

sich in ihrer Fähigkeit, Apoptose zu induzieren und in ihrer Langzeitwirkung unterschieden (Schobert et al., 2009).

Chalkon-Pt **2** zeigte sich bei neuronalen Zellen Tumor-spezifischer als die Vorläuferverbindung Chalkon **1**. Dies wurde durch den Vergleich der IC₅₀-Werte (48 h) bei primären Astrocyten vs. humanen Gliomazellen U87 (>7000 µM für Komplex **2**; 55 µM für Verbindung **1**) ersichtlich. Die Aufnahme von Chalkon-Pt **2** in die Zelle vollzog sich wie im Falle von Oxaliplatin hauptsächlich über *organic cation transporters* (OCT-1/2; ~32%) und *copper transporter related proteins* (Ctr1; ~24%), wogegen Chalkon **1** sich stark Endocytose-abhängig (~80%) zeigte. In Tubulin-reichen Neuronen und in 518A2-Melanomzellen zerstörte der Komplex **2** effizient Mikrotubuli und Actinfilamente. Diese Krebszellen konnten zwar den cytoskeletalen Schaden wieder reparieren, hörten aber auf zu proliferieren und starben letztlich ab. Komplex **2** war besonders wirksam gegen P-gp-reiche Zellen. Es fungierte aber als Substrat für ABC-Transporter der Typen BCRP, MRP3 und MRP1 und war daher weniger aktiv gegen entsprechende Zelllinien. Komplex **2** stoppte den Zellzyklus von Melanomzellen in der G1- und G2/M-Phase. Eine massive Fragmentierung des Golgi-Apparates dieser Zellen wurde mittels TEM nur nach Behandlung mit Komplex **2** und nicht bei Chalkon **1** beobachtet. Im Gegensatz zu Chalkon **1** zeigte sich der Platinkomplex **2** hoch Zelllinien-spezifisch, wurde kontrolliert über geeignete Transportproteine aufgenommen und induzierte Apoptose über vielfältige Mechanismen.

Das Chalkon-Pt-Konjugat **3**, welches im Gegensatz zu Komplex **2** einen Diamin-Liganden besitzt, wurde auf seine Antitumorwirkung, DNA-Bindung und Glutathion-Bindung untersucht. In MTT-Tests inhibierte Komplex **3** Leukämiezellen HL-60 und Darmkrebszellen HCT-116 effektiver als die Analoga **2** und **1**. Die Morphologie der Tumorzellen, die mit den Chalkon-Derivaten **1**, **2** und **3** behandelt wurden, unterschied sich von der von Zellen, die mit Colchicin behandelt wurden. Obwohl Komplex **3** weniger wasserlöslich ist als Cisplatin, bindet es an die gleichen DNA-Bindungsstellen wie Cisplatin. Im Gegensatz zu Cisplatin verursachte Komplex **3** eine stärkere DNA-Entwindung und eine zehnmal größere Anzahl an Interstrang-Quervernetzungen (~60%). Diese Ergebnisse wurden durch ein DNA-Footprint-Experiment bestätigt, welches zeigte, dass nur ein einziges Molekül **3** die einzigen benachbarten Guaninreste koordinierte und die einzig mögliche 1,2-d(GpG)-

7. Zusammenfassung

Intrastrang-Quervernetzung bildete. Außerdem wurden durch Verbindung **3** hervorgerufene DNA-Schäden durch 518A2-Melanomextrakte nur halb so effizient repariert als entsprechende Cisplatin-DNA-Addukte. Komplex **3** zeigte zudem eine weit geringere Affinität zum bekannten Platin-Entgifter Glutathion.

7.4 Illudin M (4) und sein Retinoat (5)

Der Pilz-Metabolit Illudin M **4** ist eine hoch-cytotoxische Verbindung, tötet aber Krebszellen und non-maligne Zellen gleichermaßen ab und ist für einen klinischen Einsatz daher nicht geeignet. Sein Retinoat **5** dagegen zeigte eine höhere Selektivität gegenüber malignen Zellen, speziell im empfindlichen zerebralen Gewebe. Illudin M wirkte sowohl gegen Gliomazellen als auch primäre Neuronen und Astrocyten bei gleichermaßen geringen Dosen und zerstörte ihre Microtubuli- und GFAP(*glial fibrillary acidic protein*)-Netzwerke. Im Gegensatz dazu zeigte der Ester **5** eine deutlich höhere Cytotoxizität gegen U87 Gliomazellen als in Neuronen, bei letzteren wurde sogar das Wachstum stimuliert. Dieser Effekt wurde ebenfalls in Co-Kulturen normaler Neuronen mit U87-Zellen beobachtet, wo Konjugat **5** letztere selektiv abtötete. Das Retinoat **5** scheint folglich ein viel versprechender Wirkstoffkandidat gegen Hirntumore und deren Stammzellen zu sein.

8 References

- Aebi, S., Kroning, R., Cenni, B., Sharma, A., Fink, D., Los, G., Weisman, R., Howell, S.B., and Christen, R.D. (1997). all-trans retinoic acid enhances cisplatin-induced apoptosis in human ovarian adenocarcinoma and in squamous head and neck cancer cells. *Clin Cancer Res* 3, 2033-2038.
- Ahmed, Z., Deyama, Y., Yoshimura, Y., and Suzuki, K. (2009). Cisplatin sensitivity of oral squamous carcinoma cells is regulated by Na⁺,K⁺-ATPase activity rather than copper-transporting P-type ATPases, ATP7A and ATP7B. *Cancer Chemother Pharmacol* 63, 643-650.
- Alison Rodger, and Nordén, B. (1997). *Circular Dichroism and Linear Dichroism* (Oxford, Oxford Univeristy).
- Anchel, M., Hervey, A., and Robbins, W.J. (1950). Antibiotic substances from Basidiomycetes+. VII. Clitocybe illudens. *Proc Natl Acad Sci U S A* 36, 300-305.
- Andrews, P.A., Mann, S.C., Huynh, H.H., and Albright, K.D. (1991). Role of the Na⁺, K(+)-adenosine triphosphatase in the accumulation of cis-diamminedichloroplatinum(II) in human ovarian carcinoma cells. *Cancer Res* 51, 3677-3681.
- Arends, M.J., Morris, R.G., and Wyllie, A.H. (1990). Apoptosis. The role of the endonuclease. *Am J Pathol* 136, 593-608.
- Arnould, S., Hennebelle, I., Canal, P., Bugat, R., and Guichard, S. (2003). Cellular determinants of oxaliplatin sensitivity in colon cancer cell lines. *Eur J Cancer* 39, 112-119.
- Bach, A.M., Hann, L.E., Hadar, O., Shi, W., Yoo, H.H., Giess, C.S., Sheinfeld, J., and Thaler, H. (2001). Testicular microlithiasis: what is its association with testicular cancer? *Radiology* 220, 70-75.
- Balcarova, Z., Mrazek, J., Kleinwachter, V., and Brabec, V. (1992). Cleavage by restriction enzymes of DNA modified with the antitumour drug cis-diamminedichloroplatinum(II). *Gen Physiol Biophys* 11, 579-588.
- Batovska, D.I., and Todorova, I.T. (2010). Trends in utilization of the pharmacological potential of chalcones. *Curr Clin Pharmacol* 5, 1-29.
- Bernhardt, G., Biersack, B., Bollwein, S., Schobert, R., and Zoldakova, M. (2008). Terpene conjugates of diaminedichloridoplatinum(II) complexes: antiproliferative effects in HL-60 leukemia, 518A2 melanoma, and HT-29 colon cancer cells. *Chem Biodivers* 5, 1645-1659.
- Beuvink, I., Boulay, A., Fumagalli, S., Zilbermann, F., Ruetz, S., O'Reilly, T., Natt, F., Hall, J., Lane, H.A., and Thomas, G. (2005). The mTOR inhibitor RAD001 sensitizes tumor cells to DNA-damaged induced apoptosis through inhibition of p21 translation. *Cell* 120, 747-759.
- Biersack, B. (2009). *Naturstoff-basierte Cytostatika mit verbesserter Tumorselektivität un Potential zur Überwindung von Wirkstoffresistenzen* (Bayreuth).

8. References

- Biersack, B., Zoldakova, M., Effenberger, K., and Schobert, R. (2010). (Arene)Ru(II) complexes of epidermal growth factor receptor inhibiting tyrophostins with enhanced selectivity and cytotoxicity in cancer cells. *Eur J Med Chem* 45, 1972-1975.
- Binks, S.P., and Dobrota, M. (1990). Kinetics and mechanism of uptake of platinum-based pharmaceuticals by the rat small intestine. *Biochem Pharmacol* 40, 1329-1336.
- Borst, P., Kool, M., and Evers, R. (1997). Do cMOAT (MRP2), other MRP homologues, and LRP play a role in MDR? *Semin Cancer Biol* 8, 205-213.
- Bortner, C.D., Oldenburg, N.B., and Cidlowski, J.A. (1995). The role of DNA fragmentation in apoptosis. *Trends Cell Biol* 5, 21-26.
- Bowersox, J. (1993). Sphingolipids implicated in programmed cell death. *J Natl Cancer Inst* 85, 696-697.
- Brabec, V. (2002). DNA modifications by antitumor platinum and ruthenium compounds: their recognition and repair. *Prog Nucleic Acid Res Mol Biol* 71, 1-68.
- Brabec, V., and Balcarova, Z. (1993). Restriction-enzyme cleavage of DNA modified by platinum(II) complexes. *Eur J Biochem* 216, 183-187.
- Brabec, V., Christofis, P., Slamova, M., Kostrhunova, H., Novakova, O., Najajreh, Y., Gibson, D., and Kasparkova, J. (2007). DNA interactions of new cytotoxic tetrafunctional dinuclear platinum complex $\text{trans,trans-}[\{\text{PtCl}_2(\text{NH}_3)\}_2(\text{piperazine})]$. *Biochem Pharmacol* 73, 1887-1900.
- Brabec, V., and Kasparkova, J. (2002). Molecular aspects of resistance to antitumor platinum drugs. *Drug Resist Updat* 5, 147-161.
- Brabec, V., Kleinwachter, V., Butour, J.L., and Johnson, N.P. (1990). Biophysical studies of the modification of DNA by antitumour platinum coordination complexes. *Biophys Chem* 35, 129-141.
- Brabec, V., and Leng, M. (1993). DNA interstrand cross-links of trans-diamminedichloroplatinum(II) are preferentially formed between guanine and complementary cytosine residues. *Proc Natl Acad Sci U S A* 90, 5345-5349.
- Bursova, V., Kasparkova, J., Hofr, C., and Brabec, V. (2005). Effects of monofunctional adducts of platinum(II) complexes on thermodynamic stability and energetics of DNA duplexes. *Biophys J* 88, 1207-1214.
- Butour, J.L., Mazard, A.M., Vieussens, C., and Johnson, N.P. (1990). Kinetic studies of the hydrolysis of platinum-DNA complexes by nuclease S1. *Chem Biol Interact* 73, 195-205.
- Calliste, C.A., Le Bail, J.C., Trouillas, P., Pouget, C., Habrioux, G., Chulia, A.J., and Duroux, J.L. (2001). Chalcones: structural requirements for antioxidant, estrogenic and antiproliferative activities. *Anticancer Res* 21, 3949-3956.
- Carte, N., Legendre, F., Leize, E., Potier, N., Reeder, F., Chottard, J.C., and Van Dorsselaer, A. (2000). Determination by electrospray mass spectrometry of the outersphere association constants of DNA/platinum complexes using 20-mer oligonucleotides and $[\text{Pt}(\text{NH}_3)_4]^{2+}$, 2Cl^- or $[\text{Pt}(\text{py})_4]^{2+}$, 2Cl^- . *Anal Biochem* 284, 77-86.

- Castedo, M., Perfettini, J.L., Roumier, T., Andreau, K., Medema, R., and Kroemer, G. (2004). Cell death by mitotic catastrophe: a molecular definition. *Oncogene* 23, 2825-2837.
- Cetinkaya, I., Ciarimboli, G., Yalcinkaya, G., Mehrens, T., Velic, A., Hirsch, J.R., Gorboulev, V., Koepsell, H., and Schlatter, E. (2003). Regulation of human organic cation transporter hOCT2 by PKA, PI3K, and calmodulin-dependent kinases. *Am J Physiol Renal Physiol* 284, F293-302.
- Chambon, P. (1996). A decade of molecular biology of retinoic acid receptors. *FASEB J* 10, 940-954.
- Chan, D.C. (2006). Mitochondrial fusion and fission in mammals. *Annu Rev Cell Dev Biol* 22, 79-99.
- Chang, J., Reiner, J., and Xie, J. (2005). Progress on the chemistry of dibenzocyclooctadiene lignans. *Chem Rev* 105, 4581-4609.
- Chaplin, D.J., Pettit, G.R., Parkins, C.S., and Hill, S.A. (1996). Antivascular approaches to solid tumour therapy: evaluation of tubulin binding agents. *Br J Cancer Suppl* 27, S86-88.
- Chowdhury, M.A., Huq, F., Abdullah, A., Beale, P., and Fisher, K. (2005). Synthesis, characterization and binding with DNA of four planar platinum(II) complexes of the forms: trans-PtL₂Cl₂ and [PtL₃Cl]Cl, where L = 3-hydroxypyridine, 4-hydroxypyridine and imidazo(1,2- α)pyridine. *J Inorg Biochem* 99, 1098-1112.
- Coggiola, B., Pagliai, F., Allegrone, G., Genazzani, A.A., and Tron, G.C. (2005). Synthesis and biological activity of mustard derivatives of combretastatins. *Bioorg Med Chem Lett* 15, 3551-3554.
- Culotta, V.C., Lin, S.J., Schmidt, P., Klomp, L.W., Casareno, R.L., and Gitlin, J. (1999). Intracellular pathways of copper trafficking in yeast and humans. *Adv Exp Med Biol* 448, 247-254.
- Cummings, J., Zelcer, N., Allen, J.D., Yao, D., Boyd, G., Maliepaard, M., Friedberg, T.H., Smyth, J.F., and Jodrell, D.I. (2004). Glucuronidation as a mechanism of intrinsic drug resistance in colon cancer cells: contribution of drug transport proteins. *Biochem Pharmacol* 67, 31-39.
- Dark, G.G., Hill, S.A., Prise, V.E., Tozer, G.M., Pettit, G.R., and Chaplin, D.J. (1997). Combretastatin A-4, an agent that displays potent and selective toxicity toward tumor vasculature. *Cancer Res* 57, 1829-1834.
- de Bruin, M., Miyake, K., Litman, T., Robey, R., and Bates, S.E. (1999). Reversal of resistance by GF120918 in cell lines expressing the ABC half-transporter, MXR. *Cancer Lett* 146, 117-126.
- Dowlati, A., Robertson, K., Cooney, M., Petros, W.P., Stratford, M., Jesberger, J., Rafie, N., Overmoyer, B., Makkar, V., Stambler, B., *et al.* (2002). A phase I pharmacokinetic and translational study of the novel vascular targeting agent combretastatin a-4 phosphate on a single-dose intravenous schedule in patients with advanced cancer. *Cancer Res* 62, 3408-3416.
- Doyle, L.A., and Ross, D.D. (2003). Multidrug resistance mediated by the breast cancer resistance protein BCRP (ABCG2). *Oncogene* 22, 7340-7358.

8. References

- Ducki, S., Forrest, R., Hadfield, J.A., Kendall, A., Lawrence, N.J., McGown, A.T., and Rennison, D. (1998). Potent antimitotic and cell growth inhibitory properties of substituted chalcones. *Bioorg Med Chem Lett* 8, 1051-1056.
- Eliyahu, D., Raz, A., Gruss, P., Givol, D., and Oren, M. (1984). Participation of p53 cellular tumour antigen in transformation of normal embryonic cells. *Nature* 312, 646-649.
- Finlay, C.A., Hinds, P.W., and Levine, A.J. (1989). The p53 proto-oncogene can act as a suppressor of transformation. *Cell* 57, 1083-1093.
- Fredman, P. (1998). Sphingolipids and cell signalling. *J Inherit Metab Dis* 21, 472-480.
- Fuertes, M.A., Alonso, C., and Perez, J.M. (2003). Biochemical modulation of Cisplatin mechanisms of action: enhancement of antitumor activity and circumvention of drug resistance. *Chem Rev* 103, 645-662.
- Geimer, S., and Fischer, M. (2008). Transmission electron microscopy study of the chalcones. In *Laboratory of Electron Microscopy Laboratory, Biology (Bayreuth, University of Bayreuth)*.
- Gmeiner, A., Effenberger-Neidnicht, K., Zoldáková, M., and Schobert, R. (2010). A methyltitanocene complex of schisandrol A with high efficacy against multi-drug resistant cervix and breast carcinoma cells.
- Goldstein, L.J. (1996). MDR1 gene expression in solid tumours. *Eur J Cancer* 32A, 1039-1050.
- Grotemeier, A.S. (2006). Bioevaluation and Mode of Action of New cis-Pt(II)Complexconjugates. In *Department of Biology, Chemistry and Geo-science (Bayreuth, University of Bayreuth)*, pp. 21-23.
- Hadfield, J.A., Ducki, S., Hirst, N., and McGown, A.T. (2003). Tubulin and microtubules as targets for anticancer drugs. *Prog Cell Cycle Res* 5, 309-325.
- Halamikova, A., Vrana, O., Kasparkova, J., and Brabec, V. (2007). Biochemical studies of the thermal effects on DNA modifications by the antitumor cisplatin and their repair. *Chembiochem* 8, 2008-2015.
- Hardcastle, I.R., Rowlands, M.G., Barber, A.M., Grimshaw, R.M., Mohan, M.K., Nutley, B.P., and Jarman, M. (1999). Inhibition of protein prenylation by metabolites of limonene. *Biochem Pharmacol* 57, 801-809.
- Hasaka, T.P., Myers, K.A., and Baas, P.W. (2004). Role of actin filaments in the axonal transport of microtubules. *J Neurosci* 24, 11291-11301.
- Hegedus, B., Czirik, A., Fazekas, I., B'Abel, T., Madar'asz, E., and Vicsek, T. (2000). Locomotion and proliferation of glioblastoma cells in vitro: statistical evaluation of videomicroscopic observations. *J Neurosurg* 92, 428-434.
- Henderson, D.S. (1999). *DNA repair protocols - Eucarytic System* (New Jersey, Humana Press).
- Higgins, C.F. (1995). The ABC of channel regulation. *Cell* 82, 693-696.

- Higgins, C.F. (2007). Multiple molecular mechanisms for multidrug resistance transporters. *Nature* *446*, 749-757.
- Hinnen, P., and Eskens, F.A. (2007). Vascular disrupting agents in clinical development. *Br J Cancer* *96*, 1159-1165.
- Hirschmann-Jax, C., Foster, A.E., Wulf, G.G., Nuchtern, J.G., Jax, T.W., Gobel, U., Goodell, M.A., and Brenner, M.K. (2004). A distinct "side population" of cells with high drug efflux capacity in human tumor cells. *Proc Natl Acad Sci U S A* *101*, 14228-14233.
- Hoekstra, D., Maier, O., van der Wouden, J.M., Slimane, T.A., and van, I.S.C. (2003). Membrane dynamics and cell polarity: the role of sphingolipids. *J Lipid Res* *44*, 869-877.
- Hori, Y., Kawamoto, K., Yamazaki, N., Kumazawa, H., Yamashita, T., and Kumazawa, T. (1993). Establishment of a cisplatin-resistant KB cell line and its characterization. *Acta Otolaryngol Suppl* *500*, 142-148.
- Hua, S., Kittler, R., and White, K.P. (2009). Genomic antagonism between retinoic acid and estrogen signaling in breast cancer. *Cell* *137*, 1259-1271.
- Hughes, F.M., Jr., and Cidlowski, J.A. (2000). Apoptotic nuclease assays. *Methods Enzymol* *322*, 47-62.
- Huszti, Z., and Madarasz, E. (2002). Histamine (HA) suppresses the production of tumor necrosis factor alpha (TNFalpha) in cultured astroglial cells. *Inflamm Res* *51 Suppl 1*, S61-62.
- Hyde, S.C., Emsley, P., Hartshorn, M.J., Mimmack, M.M., Gileadi, U., Pearce, S.R., Gallagher, M.P., Gill, D.R., Hubbard, R.E., and Higgins, C.F. (1990). Structural model of ATP-binding proteins associated with cystic fibrosis, multidrug resistance and bacterial transport. *Nature* *346*, 362-365.
- Ishida, S., Lee, J., Thiele, D.J., and Herskowitz, I. (2002). Uptake of the anticancer drug cisplatin mediated by the copper transporter Ctr1 in yeast and mammals. *Proc Natl Acad Sci U S A* *99*, 14298-14302.
- Ishikawa, T., and Ali-Osman, F. (1993). Glutathione-associated cis-diamminedichloroplatinum(II) metabolism and ATP-dependent efflux from leukemia cells. Molecular characterization of glutathione-platinum complex and its biological significance. *J Biol Chem* *268*, 20116-20125.
- Ivanov, A.I., Nusrat, A., and Parkos, C.A. (2004). Endocytosis of epithelial apical junctional proteins by a clathrin-mediated pathway into a unique storage compartment. *Mol Biol Cell* *15*, 176-188.
- Ivanov, V.I., Minchenkova, L.E., Schyolkina, A.K., and Poletayev, A.I. (1973). Different conformations of double-stranded nucleic acid in solution as revealed by circular dichroism. *Biopolymers* *12*, 89-110.
- Jennerwein, M., and Andrews, P.A. (1995). Effect of intracellular chloride on the cellular pharmacodynamics of cis-diamminedichloroplatinum(II). *Drug Metab Dispos* *23*, 178-184.

8. References

- Jones, J.C., Zhen, W.P., Reed, E., Parker, R.J., Sancar, A., and Bohr, V.A. (1991). Gene-specific formation and repair of cisplatin intrastrand adducts and interstrand cross-links in Chinese hamster ovary cells. *J Biol Chem* *266*, 7101-7107.
- Kanthou, C., and Tozer, G.M. (2002). The tumor vascular targeting agent combretastatin A-4-phosphate induces reorganization of the actin cytoskeleton and early membrane blebbing in human endothelial cells. *Blood* *99*, 2060-2069.
- Kanthou, C., and Tozer, G.M. (2009). Microtubule depolymerizing vascular disrupting agents: novel therapeutic agents for oncology and other pathologies. *Int J Exp Pathol* *90*, 284-294.
- Kapp, T., Muller, S., and Gust, R. (2006). Dinuclear alkylamine platinum(II) complexes of [1,2-bis(4-fluorophenyl)ethylenediamine]platinum(II): influence of endocytosis and copper and organic cation transport systems on cellular uptake. *ChemMedChem* *1*, 560-564.
- Keck MV, and SJ, L. (1992). Unwinding of supercoiled DNA by platinum ethidium and related complexes. *Journal of American Chemistry Society* *114*, 3386-3390.
- Kelner, M.J., McMorris, T.C., Beck, W.T., Zamora, J.M., and Taetle, R. (1987). Preclinical evaluation of illudins as anticancer agents. *Cancer Res* *47*, 3186-3189.
- Kishimoto, S., Kawazoe, Y., Ikeno, M., Saitoh, M., Nakano, Y., Nishi, Y., Fukushima, S., and Takeuchi, Y. (2006). Role of Na⁺, K⁺-ATPase alpha1 subunit in the intracellular accumulation of cisplatin. *Cancer Chemother Pharmacol* *57*, 84-90.
- Knauer, S., Biersack, B., Zoldakova, M., Effenberger, K., Milius, W., and Schobert, R. (2009). Melanoma-specific ferrocene esters of the fungal cytotoxin illudin M. *Anticancer Drugs* *20*, 676-681.
- Koepsell, H. (2011). Substrate recognition and translocation by polyspecific organic cation transporters. *Biol Chem* *392*, 95-101.
- Koepsell, H., Lips, K., and Volk, C. (2007). Polyspecific organic cation transporters: structure, function, physiological roles, and biopharmaceutical implications. *Pharm Res* *24*, 1227-1251.
- Kohno, K., Kikuchi, J., Sato, S., Takano, H., Saburi, Y., Asoh, K., and Kuwano, M. (1988). Vincristine-resistant human cancer KB cell line and increased expression of multidrug-resistance gene. *Jpn J Cancer Res* *79*, 1238-1246.
- Koivusalo, M., Welch, C., Hayashi, H., Scott, C.C., Kim, M., Alexander, T., Touret, N., Hahn, K.M., and Grinstein, S. (2010). Amiloride inhibits macropinocytosis by lowering submembranous pH and preventing Rac1 and Cdc42 signaling. *J Cell Biol* *188*, 547-563.
- Kok, J.W., Veldman, R.J., Klappe, K., Koning, H., Filipeanu, C.M., and Muller, M. (2000). Differential expression of sphingolipids in MRP1 overexpressing HT29 cells. *Int J Cancer* *87*, 172-178.
- Komatsu, M., Sumizawa, T., Mutoh, M., Chen, Z.S., Terada, K., Furukawa, T., Yang, X.L., Gao, H., Miura, N., Sugiyama, T., *et al.* (2000). Copper-transporting P-type adenosine triphosphatase (ATP7B) is associated with cisplatin resistance. *Cancer Res* *60*, 1312-1316.

- Korneyi, Z., Czirok, A., Vicsek, T., and Madarasz, E. (2000). Proliferative and migratory responses of astrocytes to in vitro injury. *J Neurosci Res* 61, 421-429.
- Korneyi, Z., Szlavik, V., Szabo, B., Gocza, E., Czirok, A., and Madarasz, E. (2005). Humoral and contact interactions in astroglia/stem cell co-cultures in the course of glia-induced neurogenesis. *Glia* 49, 430-444.
- Krishan, A. (1975). Rapid flow cytofluorometric analysis of mammalian cell cycle by propidium iodide staining. *J Cell Biol* 66, 188-193.
- Kuhnle, M., Egger, M., Muller, C., Mahringer, A., Bernhardt, G., Fricker, G., Konig, B., and Buschauer, A. (2009). Potent and selective inhibitors of breast cancer resistance protein (ABCG2) derived from the p-glycoprotein (ABCB1) modulator tariquidar. *J Med Chem* 52, 1190-1197.
- Lawrence, N.J., Patterson, R.P., Ooi, L.L., Cook, D., and Ducki, S. (2006). Effects of alpha-substitutions on structure and biological activity of anticancer chalcones. *Bioorg Med Chem Lett* 16, 5844-5848.
- Lee, J.J., Kim, B.C., Park, M.J., Lee, Y.S., Kim, Y.N., Lee, B.L., and Lee, J.S. (2010). PTEN status switches cell fate between premature senescence and apoptosis in glioma exposed to ionizing radiation. *Cell Death Differ*.
- Lemaire, M.A., Schwartz, A., Rahmouni, A.R., and Leng, M. (1991). Interstrand cross-links are preferentially formed at the d(GC) sites in the reaction between cis-diamminedichloroplatinum (II) and DNA. *Proc Natl Acad Sci U S A* 88, 1982-1985.
- Leng, M., and Brabec, V. (1994). DNA adducts of cisplatin, transplatin and platinum-intercalating drugs. *IARC Sci Publ*, 339-348.
- Lester, R.L., Wells, G.B., Oxford, G., and Dickson, R.C. (1993). Mutant strains of *Saccharomyces cerevisiae* lacking sphingolipids synthesize novel inositol glycerophospholipids that mimic sphingolipid structures. *J Biol Chem* 268, 845-856.
- Lippert, B. (1999). *Cisplatin*, Pekka Jäckli, Dr. Oliver Renn edn (Würzburg, Verlag Helvetica Chimica Acta, WILEY-VCH).
- Lippert, J.W., 3rd (2007). Vascular disrupting agents. *Bioorg Med Chem* 15, 605-615.
- Liu, X.L., Tee, H.W., and Go, M.L. (2008). Functionalized chalcones as selective inhibitors of P-glycoprotein and breast cancer resistance protein. *Bioorg Med Chem* 16, 171-180.
- Maden, M. (2007). Retinoic acid in the development, regeneration and maintenance of the nervous system. *Nat Rev Neurosci* 8, 755-765.
- Mancini, M., Anderson, B.O., Caldwell, E., Sedghinasab, M., Paty, P.B., and Hockenbery, D.M. (1997). Mitochondrial proliferation and paradoxical membrane depolarization during terminal differentiation and apoptosis in a human colon carcinoma cell line. *J Cell Biol* 138, 449-469.
- Mao, Q. (2008). BCRP/ABCG2 in the placenta: expression, function and regulation. *Pharm Res* 25, 1244-1255.
- Mao, Q., and Unadkat, J.D. (2005). Role of the breast cancer resistance protein (ABCG2) in drug transport. *AAPS J* 7, E118-133.

8. References

- Marchan, R., Hammond, C.L., and Ballatori, N. (2008). Multidrug resistance-associated protein 1 as a major mediator of basal and apoptotic glutathione release. *Biochim Biophys Acta* 1778, 2413-2420.
- Matthay, K.K., Reynolds, C.P., Seeger, R.C., Shimada, H., Adkins, E.S., Haas-Kogan, D., Gerbing, R.B., London, W.B., and Villablanca, J.G. (2009). Long-term results for children with high-risk neuroblastoma treated on a randomized trial of myeloablative therapy followed by 13-cis-retinoic acid: a children's oncology group study. *J Clin Oncol* 27, 1007-1013.
- Maxam, A.M., and Gilbert, W. (1980). Sequencing end-labeled DNA with base-specific chemical cleavages. *Methods Enzymol* 65, 499-560.
- McIlwain, C.C., Townsend, D.M., and Tew, K.D. (2006). Glutathione S-transferase polymorphisms: cancer incidence and therapy. *Oncogene* 25, 1639-1648.
- McMorris, T.C., Kelner, M.J., Wang, W., Moon, S., and Taetle, R. (1990). On the mechanism of toxicity of illudins: the role of glutathione. *Chem Res Toxicol* 3, 574-579.
- McMorris, T.C., and M., A. (1963). The structures of the basidiomycete metabolites illudin S and illudin M. *J Amer Chem Soc* 85, 831-832.
- Meier, O., Boucke, K., Hammer, S.V., Keller, S., Stidwill, R.P., Hemmi, S., and Greber, U.F. (2002). Adenovirus triggers macropinocytosis and endosomal leakage together with its clathrin-mediated uptake. *J Cell Biol* 158, 1119-1131.
- Merrill, A.H., Jr., Hannun, Y.A., and Bell, R.M. (1993). Introduction: sphingolipids and their metabolites in cell regulation. *Adv Lipid Res* 25, 1-24.
- Mey, J. (2006). New therapeutic target for CNS injury? The role of retinoic acid signaling after nerve lesions. *J Neurobiol* 66, 757-779.
- Mosmann, T. (1983). Rapid colorimetric assay for cellular growth and survival: application to proliferation and cytotoxicity assays. *J Immunol Methods* 65, 55-63.
- Mukherjee, S., Chiu, R., Leung, S.M., and Shields, D. (2007). Fragmentation of the Golgi apparatus: an early apoptotic event independent of the cytoskeleton. *Traffic* 8, 369-378.
- Muller, J., Lips, K.S., Metzner, L., Neubert, R.H., Koepsell, H., and Brandsch, M. (2005). Drug specificity and intestinal membrane localization of human organic cation transporters (OCT). *Biochem Pharmacol* 70, 1851-1860.
- Nawa, M., Takasaki, T., Yamada, K., Kurane, I., and Akatsuka, T. (2003). Interference in Japanese encephalitis virus infection of Vero cells by a cationic amphiphilic drug, chlorpromazine. *J Gen Virol* 84, 1737-1741.
- Neidle, S. (1979). The molecular basis for the action of some DNA-binding drugs. *Prog Med Chem* 16, 151-221.
- Nobre-Junior, H.V., Oliveira, R.A., Maia, F.D., Nogueira, M.A., de Moraes, M.O., Bandeira, M.A., Andrade, G.M., and Viana, G.S. (2009). Neuroprotective effects of chalcones from *Myracrodruon urundeuva* on 6-hydroxydopamine-induced cytotoxicity in rat mesencephalic cells. *Neurochem Res* 34, 1066-1075.

- Ochoa, M. (1969). ALKYLATING AGENTS IN CLINICAL CANCER CHEMOTHERAPY*. *Ann NY Acad Sci* 163, 921-930.
- Oku, N., Saito, N., Okada, S., Watanabe, N., and Kobayashi, Y. (1995). Permeability change of liposomal membrane induced by interleukin-1 alpha. *J Biochem* 118, 832-835.
- Padhye, S., Ahmad, A., Oswal, N., Dandawate, P., Rub, R.A., Deshpande, J., Swamy, K.V., and Sarkar, F.H. (2010). Fluorinated 2'-hydroxychalcones as garcinol analogs with enhanced antioxidant and anticancer activities. *Bioorg Med Chem Lett* 20, 5818-5821.
- Peitsch, M.C., Muller, C., and Tschopp, J. (1993). DNA fragmentation during apoptosis is caused by frequent single-strand cuts. *Nucleic Acids Res* 21, 4206-4209.
- Petris, M.J. (2004). The SLC31 (Ctr) copper transporter family. *Pflugers Arch* 447, 752-755.
- Pettit, G.R., Singh, S.B., Hamel, E., Lin, C.M., Alberts, D.S., and Garcia-Kendall, D. (1989). Isolation and structure of the strong cell growth and tubulin inhibitor combretastatin A-4. *Experientia* 45, 209-211.
- Pettit, G.R., Temple, C., Jr., Narayanan, V.L., Varma, R., Simpson, M.J., Boyd, M.R., Rener, G.A., and Bansal, N. (1995). Antineoplastic agents 322. synthesis of combretastatin A-4 prodrugs. *Anticancer Drug Des* 10, 299-309.
- Poirier, M.C., Reed, E., Litterst, C.L., Katz, D., and Gupta-Burt, S. (1992). Persistence of platinum-ammine-DNA adducts in gonads and kidneys of rats and multiple tissues from cancer patients. *Cancer Res* 52, 149-153.
- Pompella, A., Corti, A., Paolicchi, A., Giommarelli, C., and Zunino, F. (2007). Gamma-glutamyltransferase, redox regulation and cancer drug resistance. *Curr Opin Pharmacol* 7, 360-366.
- Puli, S., Jain, A., Lai, J.C., and Bhushan, A. (2010). Effect of combination treatment of rapamycin and isoflavones on mTOR pathway in human glioblastoma (U87) cells. *Neurochem Res* 35, 986-993.
- Punnonen, E.L., Ryhanen, K., and Marjomaki, V.S. (1998). At reduced temperature, endocytic membrane traffic is blocked in multivesicular carrier endosomes in rat cardiac myocytes. *Eur J Cell Biol* 75, 344-352.
- Rabik, C.A., and Dolan, M.E. (2007). Molecular mechanisms of resistance and toxicity associated with platinating agents. *Cancer Treat Rev* 33, 9-23.
- Rakowski, R.F., Gadsby, D.C., and De Weer, P. (1989). Stoichiometry and voltage dependence of the sodium pump in voltage-clamped, internally dialyzed squid giant axon. *J Gen Physiol* 93, 903-941.
- Reynolds, E.S. (1963). The use of lead citrate at high pH as an electron-opaque stain in electron microscopy. *The Journal of cell biology* 17, 208-212.
- Robey, R.W., Polgar, O., Deeken, J., To, K.W., and Bates, S.E. (2007). ABCG2: determining its relevance in clinical drug resistance. *Cancer Metastasis Rev* 26, 39-57.
- Robinson, J.D., and Flashner, M.S. (1979). The (Na⁺ + K⁺)-activated ATPase. Enzymatic and transport properties. *Biochim Biophys Acta* 549, 145-176.

8. References

- Rocchi, E., Khodjakov, A., Volk, E.L., Yang, C.H., Litman, T., Bates, S.E., and Schneider, E. (2000). The product of the ABC half-transporter gene ABCG2 (BCRP/MXR/ABCP) is expressed in the plasma membrane. *Biochem Biophys Res Commun* 271, 42-46.
- Safaei, R., and Howell, S.B. (2005). Copper transporters regulate the cellular pharmacology and sensitivity to Pt drugs. *Crit Rev Oncol Hematol* 53, 13-23.
- Sandvig, K., Torgersen, M.L., Raa, H.A., and van Deurs, B. (2008). Clathrin-independent endocytosis: from nonexistent to an extreme degree of complexity. *Histochem Cell Biol* 129, 267-276.
- Schlett, K., Herberth, B., and Madarasz, E. (1997). In vitro pattern formation during neurogenesis in neuroectodermal progenitor cells immortalized by p53-deficiency. *Int J Dev Neurosci* 15, 795-804.
- Schlett, K., and Madarasz, E. (1997). Retinoic acid induced neural differentiation in a neuroectodermal cell line immortalized by p53 deficiency. *J Neurosci Res* 47, 405-415.
- Schobert, R., and Biersack, B. (2005). cis-Dichloroplatinum (II) complexes with aminomethylnicotinate and -isonicotinate ligands. *Inorg Chim Acta* 358, 3369-3376.
- Schobert, R., Biersack, B., Dietrich, A., Grotemeier, A., Muller, T., Kalinowski, B., Knauer, S., Voigt, W., and Paschke, R. (2007). Monoterpenes as drug shuttles: cytotoxic (6-aminomethylnicotinate)dichloridoplatinum(II) complexes with potential to overcome cisplatin resistance. *J Med Chem* 50, 1288-1293.
- Schobert, R., Biersack, B., Dietrich, A., Knauer, S., Zoldakova, M., Fruehauf, A., and Mueller, T. (2009). Pt(II) complexes of a combretastatin A-4 analogous chalcone: effects of conjugation on cytotoxicity, tumor specificity, and long-term tumor growth suppression. *J Med Chem* 52, 241-246.
- Schobert, R., Biersack, B., Knauer, S., and Ocker, M. (2008a). Conjugates of the fungal cytotoxin illudin M with improved tumour specificity. *Bioorg Med Chem* 16, 8592-8597.
- Schobert, R., Kern, W., Milius, W., Ackermann, T., and Zoldakova, M. (2008b). Synthesis of the first unnatural schisantherins and their effects in multidrug-resistant cancer cells. *Tetrahedron Letters* 49, 3359-3362.
- Schobert, R., Knauer, S., Seibt, S., and Biersack, B. (2011). Anticancer active illudins: recent developments of a potent alkylating compound class. *Curr Med Chem* 18, 790-807.
- Schwab, D., Fischer, H., Tabatabaei, A., Poli, S., and Huwyler, J. (2003). Comparison of in vitro P-glycoprotein screening assays: recommendations for their use in drug discovery. *J Med Chem* 46, 1716-1725.
- Scovell, W.M., and Collart, F. (1985). Unwinding of supercoiled DNA by cis- and trans-diamminedichloroplatinum(II): influence of the torsional strain on DNA unwinding. *Nucleic Acids Res* 13, 2881-2895.
- Shah, A., Khan, A.M., Qureshi, R., Ansari, F.L., Nazar, M.F., and Shah, S.S. (2008). Redox behavior of anticancer chalcone on a glassy carbon electrode and evaluation of its interaction parameters with DNA. *Int J Mol Sci* 9, 1424-1434.
- Sharom, F.J. (1997). The P-glycoprotein efflux pump: how does it transport drugs? *J Membr Biol* 160, 161-175.

- Shen, K.H., Chang, J.K., Hsu, Y.L., and Kuo, P.L. (2007). Chalcone arrests cell cycle progression and induces apoptosis through induction of mitochondrial pathway and inhibition of nuclear factor kappa B signalling in human bladder cancer cells. *Basic Clin Pharmacol Toxicol* *101*, 254-261.
- Simstein, R., Burow, M., Parker, A., Weldon, C., and Beckman, B. (2003). Apoptosis, chemoresistance, and breast cancer: insights from the MCF-7 cell model system. *Exp Biol Med (Maywood)* *228*, 995-1003.
- Singh, N.P., McCoy, M.T., Tice, R.R., and Schneider, E.L. (1988). A simple technique for quantitation of low levels of DNA damage in individual cells. *Exp Cell Res* *175*, 184-191.
- Smith, B.J., Doran, A.C., McLean, S., Tingley, F.D., 3rd, O'Neill, B.T., and Kajiji, S.M. (2001). P-glycoprotein efflux at the blood-brain barrier mediates differences in brain disposition and pharmacodynamics between two structurally related neurokinin-1 receptor antagonists. *J Pharmacol Exp Ther* *298*, 1252-1259.
- Soloz, M., and Vulpe, C. (1996). CPx-type ATPases: a class of P-type ATPases that pump heavy metals. *Trends Biochem Sci* *21*, 237-241.
- Stirling, L., Williams, M.R., and Morielli, A.D. (2009). Dual roles for RHOA/RHO-kinase in the regulated trafficking of a voltage-sensitive potassium channel. *Mol Biol Cell* *20*, 2991-3002.
- Takahashi, N. (2002). [Induction of cell differentiation and development of new anticancer drugs]. *Yakugaku Zasshi* *122*, 547-563.
- Tang, X.H., and Gudas, L.J. (2011). Retinoids, retinoic Acid receptors, and cancer. *Annu Rev Pathol* *6*, 345-364.
- Tavares, T.S., Nanus, D., Yang, X.J., and Gudas, L.J. (2008). Gene microarray analysis of human renal cell carcinoma: the effects of HDAC inhibition and retinoid treatment. *Cancer Biol Ther* *7*, 1607-1618.
- Thornberry, N.A. (1994). Interleukin-1 beta converting enzyme. *Methods Enzymol* *244*, 615-631.
- Thornberry, N.A., Rano, T.A., Peterson, E.P., Rasper, D.M., Timkey, T., Garcia-Calvo, M., Houtzager, V.M., Nordstrom, P.A., Roy, S., Vaillancourt, J.P., *et al.* (1997). A combinatorial approach defines specificities of members of the caspase family and granzyme B. Functional relationships established for key mediators of apoptosis. *J Biol Chem* *272*, 17907-17911.
- Townsend, D.M., and Tew, K.D. (2003). The role of glutathione-S-transferase in anti-cancer drug resistance. *Oncogene* *22*, 7369-7375.
- Trombetta, D., Castelli, F., Sarpietro, M.G., Venuti, V., Cristani, M., Daniele, C., Saija, A., Mazzanti, G., and Bisignano, G. (2005). Mechanisms of antibacterial action of three monoterpenes. *Antimicrob Agents Chemother* *49*, 2474-2478.
- Tsuchida, S., and Sato, K. (1992). Glutathione transferases and cancer. *Crit Rev Biochem Mol Biol* *27*, 337-384.

8. References

- Vaillant, A.R., Zanassi, P., Walsh, G.S., Aumont, A., Alonso, A., and Miller, F.D. (2002). Signaling mechanisms underlying reversible, activity-dependent dendrite formation. *Neuron* 34, 985-998.
- Vantard, M., Cowling, R., and Delichere, C. (2000). Cell cycle regulation of the microtubular cytoskeleton. *Plant Mol Biol* 43, 691-703.
- Vitale, I., Antocchia, A., Cenciarelli, C., Crateri, P., Meschini, S., Arancia, G., Pisano, C., and Tanzarella, C. (2007). Combretastatin CA-4 and combretastatin derivative induce mitotic catastrophe dependent on spindle checkpoint and caspase-3 activation in non-small cell lung cancer cells. *Apoptosis* 12, 155-166.
- Vrana, O., and Brabec, V. (1986). The effect of combined treatment with platinum complexes and ionizing radiation on DNA in vitro. *Int J Radiat Biol Relat Stud Phys Chem Med* 50, 995-1007.
- Wada, H., Saikawa, Y., Niida, Y., Nishimura, R., Noguchi, T., Matsukawa, H., Ichihara, T., and Koizumi, S. (1999). Selectively induced high MRP gene expression in multidrug-resistant human HL60 leukemia cells. *Exp Hematol* 27, 99-109.
- Wang, D., and Lippard, S.J. (2005). Cellular processing of platinum anticancer drugs. *Nat Rev Drug Discov* 4, 307-320.
- Waring, M. (2006). *Sequence-specific DNA Binding Agents*, Stephen Neidle edn (Cambridge, The Royal Society of Chemistry).
- Westermann, B. (2008). Molecular machinery of mitochondrial fusion and fission. *J Biol Chem* 283, 13501-13505.
- Wright, S.H. (2005). Role of organic cation transporters in the renal handling of therapeutic agents and xenobiotics. *Toxicol Appl Pharmacol* 204, 309-319.
- Yuri, T., Danbara, N., Tsujita-Kyutoku, M., Kiyozuka, Y., Senzaki, H., Shikata, N., Kanzaki, H., and Tsubura, A. (2004). Perillyl alcohol inhibits human breast cancer cell growth in vitro and in vivo. *Breast Cancer Res Treat* 84, 251-260.
- Zhang, J., Li, Y., and Shen, B. (2003). PI3-K/Akt pathway contributes to IL-6-dependent growth of 7TD1 cells. *Cancer Cell Int* 3, 1.
- Zhang, S., Lovejoy, K.S., Shima, J.E., Lagpacan, L.L., Shu, Y., Lapuk, A., Chen, Y., Komori, T., Gray, J.W., Chen, X., *et al.* (2006). Organic cation transporters are determinants of oxaliplatin cytotoxicity. *Cancer Res* 66, 8847-8857.
- Zoldakova, M., and Albrecht, A. (2009). Cell viability and analysis of efflux inhibition of chalcone and Pt-complexes on MDR cells. In *Organic Chemistry Department (University Bayreuth)*, Advisor: Miroslava Zoldakova.
- Zoldakova, M., and Beneke, J. (2008). Synthese von Combretastatinderivaten und deren Wirkung auf Zellen des Melanoms 518A2. In *Organic CHEMistry Department (University Bayreuth)*, Advisor: Bernhard Biersack, Miroslava Zoldakova.
- Zoldakova, M., Biersack, B., Kostrhunova, H., Ahmad, A., Padhye, S., Sarkar, F.H., Schobert, R., and Brabec, V. (2011). (Carboxydiamine)Pt(ii) complexes of a combretastatin A-4 analogous chalcone: the influence of the diamine ligand on DNA binding and anticancer effects. *MedChemComm* 2, 493-499.

- Zoldakova, M., and Boos, I. (2010). New anticancer drugs study. In Department of Organic Chemistry (Bayreuth, University of Bayreuth) (University of Bayreuth), Advisor: Miroslava Zoldakova.
- Zoldakova, M., and Doblhofer, E. (2008). Biochemie von Illudinderivaten. In Organic Chemistry Department (University of Bayreuth), Advisor: Sebastian Knauer, Bernhard Biersack, Miroslava Zoldakova.
- Zoldakova, M., and Fessler, J.M. (2008). Synthese von neuen Platin-Verbindungen und Ru(Aren)-Komplexkonjugaten, sowie deren Wirkung auf humane Krebszellen Bearbeitungszeitraum: . In Organic Chemistry Department (University of Bayreuth), pp. Advisor: Bernhard Biersack, Miroslava Zoldakova.
- Zoldakova, M., Kornyei, Z., Brown, A., Biersack, B., Madarász, E., and Schobert, R. (2010). Effects of a combretastatin A4 analogous chalcone and its Pt-complex on cancer cells: a comparative study of uptake, cell cycle and damage to cellular compartments. In Biochemical Pharmacology.
- Zoldakova, M., and Mauerer, C. (2009). ABC proteins in cancer cells as a target for Illudins. In Organic Chemistry Department (University of Bayreuth), pp. Advisor: Miroslava Zoldakova.
- Zoldakova, M., and Mauerer, C. (2010). Effect of Chalcones at HT29 overexpressing MRP1/MRP3 and 518A2 cells. In Department of Organic Chemistry I (Bayreuth, University of Bayreuth). Advisor: Miroslava Zoldakova.
- Zoldakova, M., and Münzner, J.K. (2008). Die Aufnahme von Chalkone-Konjugation in humane Krebszellen und ihr Potential als Inhibitoren der Multi-Drug-Resistance Proteine P-gp und MDR. In Department of Organic Chemistry I (Bayreuth, University of Bayreuth). Advisor: Miroslava Zoldakova.
- Zoldakova, M., and Münzner, J.K. (2009). Apoptosis and its signaling pathway induced by newly synthesized Illudin complexes in comparison with Illudin M in melanoma 518A2 and leukemic HL-60 cells. In Organic Chemistry Department (Bayreuth, University of Bayreuth), Advisor: Miroslava Zoldakova.
- Zoldakova, M., and Rymarczyk, B. (2008). Neuartige zytotoxische Chalcone und Ru(Aren) Komplexkonjugate, ihre Transportwege in humane Krebszellen, sowie ihre inhibitorische Wirkung auf ABC-Transporter. In Department of Organic Chemistry I (Bayreuth, University of Bayreuth). Advisor: Miroslava Zoldakova.
- Zoldakova, M., and Rymarczyk, B. (2009). Method Optimisation & Analysis of Illudin M Effect on Single-cell DNA. In Organic Chemistry Department (Bayreuth, University of Bayreuth), Advisor: Miroslava Zoldakova.
- Zoldakova, M., and Schreder, A. (2009a). ABC proteins in cancer cells as a target for chalcones. In Organic Chemistry Department (University of Bayreuth), Advisor: Miroslava Zoldakova.
- Zoldakova, M., and Schreder, A. (2009b). Active Estron derivative of carboplatin targeted for MCF-7 cancer cells. In Organic Chemistry Department (University of Bayreuth), pp. Advisor: Miroslava Zoldakova.

8. References

- Zoldakova, M., and Schreder, A. (2009c). UV spectral analysis of Glutathione-Chalcones complex formation. In Organic Chemistry Department (University Bayreuth), pp. Advisor: Miroslava Zoldakova.
- Zoldakova, M., Shehata, S., and Obenauf, J. (2009). Specificity of platinated estrons and Ruthenium complexes on different cell lines. In Organic Chemistry Department (University Bayreuth), Advisor: Miroslava Zoldakova.
- Zoldakova, M., and Suchy, T. (2010). Altered cell shapes of melanoma cells after chalcone treatment In Organic Chemistry Department (Univeristy of Bayreuth), Advisor: Miroslava Zoldakova.

9 Publications and conference activities

- Bernhardt, G., Biersack, B., Bollwein, S., Schobert, R., and Zoldakova, M. (2008). Terpene conjugates of diaminedichloridoplatinum(II) complexes: antiproliferative effects in HL-60 leukemia, 518A2 melanoma, and HT-29 colon cancer cells. *Chem Biodivers* 5, 1645-1659.
- Biersack, B., Zoldakova, M., Effenberger, K., and Schobert, R. (2010). (Arene)Ru(II) complexes of epidermal growth factor receptor inhibiting tyrphostins with enhanced selectivity and cytotoxicity in cancer cells. *Eur J Med Chem* 45, 1972-1975.
- Gmeiner, A., Effenberger-Neidnicht, K., Zoldáková, M., and Schobert, R. (2010). A methyltitanocene complex of schisandrol A with high efficacy against multi-drug resistant cervix and breast carcinoma cells.
- Knauer, S., Biersack, B., Zoldakova, M., Effenberger, K., Milius, W., and Schobert, R. (2009). Melanoma-specific ferrocene esters of the fungal cytotoxin illudin M. *Anticancer Drugs* 20, 676-681.
- Schobert, R., Biersack, B., Dietrich, A., Knauer, S., Zoldakova, M., Fruehauf, A., and Mueller, T. (2009). Pt(II) complexes of a combretastatin A-4 analogous chalcone: effects of conjugation on cytotoxicity, tumor specificity, and long-term tumor growth suppression. *J Med Chem* 52, 241-246.
- Schobert, R., Kern, W., Milius, W., Ackermann, T., and Zoldakova, M. (2008). Synthesis of the first unnatural schisantherins and their effects in multidrug-resistant cancer cells. *Tetrahedron Letters* 49, 3359-3362.
- Zoldakova, M., Biersack, B., Kostrhunova, H., Ahmad, A., Padhye, S., Sarkar, F.H., Schobert, R., and Brabec, V. (2011). (Carboxydiamine)Pt(ii) complexes of a combretastatin A-4 analogous chalcone: the influence of the diamine ligand on DNA binding and anticancer effects. *MedChemComm* 2, 493-499.
- Zoldakova, M., Kornyei, Z., Brown, A., Biersack, B., Madarász, E., and Schobert, R. (2010). Effects of a combretastatin A4 analogous chalcone and its Pt-complex on cancer cells: a comparative study of uptake, cell cycle and damage to cellular compartments. In *Biochemical Pharmacology*.

Posters and short lecture

- Žoldáková, M., Biersack, B., and Schobert, R. (2007). In vitro studies of steroid–cisplatin complex conjugates. In *Structure and Stability of Biomacromolecules* (Kosice, Slovakia). *Poster*.
- Zoldakova, M., Biersack, B., Kornyei, Z., and Schobert, R. (2009). Enhancement of specificity, uptake and breach of resistance of a combretastatin A4 analogous chalcone by platination. In *Structure and stability of Biomacromolecules, t.i. Conference*, ed. (Kosice, Slovakia). *Short lecture*.

Zoldakova, M., Biersack, B., and Schobert, R. (2010). Mechanism of accumulation of an antitumoral chalcone and its platinum (II) complex by cancer cells. In 7th Transport Colloquium E. Petzinger, G. Buckhardt, and R. Tampé, eds. (Castle Rauischholzhausen, Germany, German society of Experimental and Clinical Pharmacology and Toxicology). *Poster*.